Periodic Motions of a Periodically Forced, Nonlinear Spring Pendulum

by Yaoguang Yuan, Bachelor of Science

A Thesis Submitted in Partial
Fulfillment of the Requirements
for the Degree of
Master of Science
in the field of Mechanical Engineering

Advisory Committee:

Albert C.J. Luo, Chair

Xin Chen

Fengxia Wang

Graduate School
Southern Illinois University Edwardsville
Dec, 2018

ACKNOWLEDGMENTS

Foremost, I want to express my sincere gratitude to my advisor Dr Albert C. J. Luo. Thank you to letting me join this amazing group and giving me this chance to further improve my ability in my chosen field. Your persistent support on my master thesis and research, and your pure motivation on research strongly inspire me to farther forward in the scientific research. Your theory and research showed me a bright new field to explore. Thank you Dr. Luo for being my advisor and for all of your guidance. Your immense knowledge will always been my great fortune.

Furthermore, I would like to thank the other committee members of my thesis: Dr. Xin Chen, and Dr. Fengxia Wang for their most inspiring comments and suggestions. Also, I would like to thank my group members. Bo Yu, Haolin Ma, Yeyin Xu, Chuan Guo, Siyu Guo, Siyuan Xin and Chuanping Liu. Thank you for your supports and suggestions in my research and study.

Last but not the least, I would like to thank my parents Hongyuan Yuan and Yongfang Zhang. Thanks for your consistent support and all the plan you made for me. Nothing is comparable to your love.

ABSTRACT

PERIODIC MOTIONS AND BIFURCATION OF A PERIODICALLY FORCED, NONLINEAR SPRING PENDULUM

by

YAOGUANG YUAN

Chairperson: Professor Albert C. J. Luo

In this thesis, the bifurcation trees of period-1 to period-2 motions in a periodically forced, nonlinear spring pendulum system are predicted by a semi-analytic method. The differential equations of periodically forced, nonlinear spring pendulum system are discretized for the predication of the semi-analytic method. To obtain the periodic solutions, the corresponding mapping structure of the implicit mapping is presented. Based on the eigenvalue analysis, the corresponding stability of the periodical solutions are shown on the bifurcation trees as well. The harmonic frequency-amplitude for periodical motions are analyzed from the finite discrete Fourier series. From the harmonic amplitudes, the bifurcation trees of periodic motions are presented as well. From the analytical prediction, numerical illustrations of periodic motions are completed, the comparison of numerical solution and analytical solution are given. Through the numerical illustration, the spring possess dynamical behavior of a parametric nonlinear systems, which is different from the pendulum. The method presented in this paper can be applied to other nonlinear dynamical systems to obtain the bifurcation trees of periodic motions to chaos.

TABLE OF CONTENT

LIST OF FIGURES

Figure Page

LIST OF TABLES

Table Page

CHAPTER I

INTRODUCTION

Literature Review:

In recent years, there are many researches about parametric nonlinear systems in engineering, as they perform different dynamical behaviors from periodically forced nonlinear systems. However, not all periodic solutions can be predict by the traditional analysis method. In this paper, a semi-analytical method will be introduce to find more accurate periodic motions in such nonlinear system, the corresponding bifurcation trees and frequency-amplitudes of predicted periodic motions will be given as well.

The analytical methods for periodic motions are discussed first. In 1788, Lagrange [1] used the method of averaging for the periodic motion in the three-body problem as a perturbation of the two-body problem. In 1890, Poincare [2] developed the perturbation theory for the periodic motions of celestial bodies. In 1920, van der Pol [3] employed the method of averaging for the periodic solutions of oscillation systems in circuits. In 1928, Fatou [4] gave the proof of the asymptotic validity through the solution existence theorems of differential equations. In 1935, Krylov and Bogoliubov [5] further developed the method of averaging for nonlinear oscillations in nonlinear vibration systems. In 1964, Hayashi [6] presented the perturbation methods including averaging method and principle of harmonic balance. In 1969, Barkham and Soudack [7] extended the Krylov-Bogoliubov method for the approximate solutions of nonlinear autonomous second-order differential equations (also see, Barkham and Soudack [8]). In 1987, a harmonic balance approach was used by Garcia-Margallo and Bejarano [9] for approximate solutions of nonlinear oscillations with strong nonlinearity. Rand and Armbruster [10] used the perturbation method and bifurcation theory

for the stability of periodic solutions. In 1989, Yuste and Bejarano [11] used the elliptic functions rather than trigonometric functions for improvement of the Krylov-Bogoliubov method. In 1990, Coppola and Rand [12] used the averaging method with elliptic functions to determine approximation of limit cycle. In 2012, Luo [13] developed an analytical method for analytical solutions of periodic motions in nonlinear dynamical systems. Luo and Huang [14] applied such a method to a Duffing oscillator for approximate solutions of periodic motions, and Luo and Huang [15] gave the analytical bifurcation trees of period-m motions to chaos in the Duffing oscillator. The analytical bifurcation trees of period-m motion to chaos in the Duffing oscillator with twin-well potentials were presented in Luo and Huang [16,17]. In 2015, Luo [18] developed a semi-analytical method for the analytical prediction of periodic motions in nonlinear dynamic systems. Luo and Guo [19] discovered the bifurcation trees of periodic motions in the twin-well Duffing oscillator through the semi-analytical method. The rich dynamic characteristics of periodic motions to chaos in such a twin-well Duffing oscillator were also observed in Guo and Luo [20]. This semi-analytical method can provide the analytical prediction of periodic motions with high accuracy, and can predict the stability and bifurcation to chaos. In 2017, Luo and Xing [21] used this technique doe determining the time-delay effects on periodic motions of the time-delayed Duffing oscillator.

In this paper, periodic motions in a periodically forced nonlinear spring pendulum will be investigated through the discrete implicit maps, and the corresponding stability and bifurcation analysis of periodic motions will be performed. From the analytical prediction, numerical simulation results of periodic motions are performed. The harmonic amplitude spectrums will be presented.

Objectives:

In this paper, bifurcation trees of period-1 to period-2 motions in this periodically forced, nonlinear spring pendulum will be predicted analytically by a semi-analytic method. For the semi-analytical approach. The discrete implicit maps will be obtained from differential equation of this periodically forced, nonlinear spring pendulum, and based on the implicit maps, a mapping structure will be employed to predict the periodic motions analytically. From mapping structure, bifurcation trees of period-1 to period-2 motions will be obtained analytically, and the corresponding stability and bifurcations of the periodic motions will be discussed. From the finite Fourier series, the bifurcation trees of the harmonic amplitude will also be presented. From the analytical prediction, numerical simulations of periodic motions will be completed to perform the comparison of numerical solution and analytical solution.

Significance:

By the semi-analytical approach, for the first time we obtain the analytical solution of periodic motions in spring pendulum dynamical system. From the finite discrete Fourier series, the frequency-amplitudes for symmetric and asymmetric period-1 to period-2 motions are analyzed and the bifurcation trees from harmonic amplitude are presented. From the analytical prediction, numerical results of periodic motions are completed to verify the analytical predication. Through the numerical simulations, the periodic motions of the spring in this periodically forced, nonlinear spring pendulum system possess dynamical behavior of a parametric nonlinear system. The semi-analytic method used in this research can be applied to other nonlinear dynamical systems for possible bifurcation trees of periodic motions to chaos.

CHAPTER II

METHODOLOGY

Here the method to determine the periodic motions in dynamical system will be discussed. From Luo (2014), we have the following theorem.

Theorem 1. *Consider a nonlinear dynamical system*

$$\dot{x} = \mathbf{f}\left(\mathbf{x}, t, \mathbf{p}\right) \in \mathbf{R}^{n} \tag{1}$$

Where $\mathbf{f}(\mathbf{x}, t, \mathbf{p})$ *is a* C^{r} *-continuous nonlinear vector function (*$r \geq 1$*) .If such a dynamical system has a periodic motion* $\mathbf{x}(t)$ *with finite norm* $\|\mathbf{x}\|$ *and period* $T = 2\pi / \Omega$*, then there are a set of values of time* $t_k \left(k = 0, 1, \ldots, N\right)$ *with* $\left(N \geq 1\right)$ *on a time interval* $\left(t_0, T + t_0\right)$ *and a set of points* $\mathbf{x}_k$*, such that* $\left\|x\left(t_k\right) - x_k\right\| \leq \varepsilon_k$ *with a small* $\varepsilon_k \geq 0$ *and*

$$\left\|\mathbf{f}\left(\mathbf{x}\left(t_k\right), t_k, \mathbf{p}\right) - \mathbf{f}\left(\mathbf{x}_k, t_k, \mathbf{p}\right)\right\| \leq \delta_k \tag{2}$$

With a small $\delta_k \geq 0$*. Furthermore, there exists a vector function* $\mathbf{g}_k$ *with*

$$\mathbf{g}_k\left(\mathbf{x}_{k-1}, \mathbf{x}_k, \mathbf{p}\right) = \mathbf{0}\left(k = 1, 2, \ldots N\right) \tag{3}$$

that determines a general mapping $P_k : \mathbf{x}_{k-1} \to \mathbf{x}_k \left(k = 1, 2, \ldots, N\right)$*. The particular form of the function* $\mathbf{g}_k$ *is determined by a particular computational scheme which one uses to study the system in Eq. (1). Consider a mapping structure as*

$$\begin{gathered} P = P_N \circ P_{N-1} \circ \cdots \circ P_2 \circ P_1 : \mathbf{x}_0 \to \mathbf{x}_N; \\ \text{with } P_k : \mathbf{x}_{k-1} \to \mathbf{x}_k \left(k = 1, 2, \ldots, N\right). \end{gathered} \tag{4}$$

For $\mathbf{x}_N = P\mathbf{x}_0$*, if there is a set of nodes points* $\mathbf{x}_k^{*}\left(k = 1, 2, \ldots, N\right)$ *computed by*

$$\mathbf{g}_k\left(\mathbf{x}_{k-1}^{*}, \mathbf{x}_k^{*}, \mathbf{p}\right) = \mathbf{0}, \left(k = 1, 2, \ldots, N\right) \tag{5}$$

$$\mathbf{x}_0^* = \mathbf{x}_N^*,$$

then the points $\mathbf{x}_k^*\left(k=1,2,\ldots,N\right)$ *are approximations of points* $\mathbf{x}\left(t_k\right)$ *of the periodic solution. In the neighborhood of* $\mathbf{x}_k^*$, *with* $\mathbf{x}_k = \mathbf{x}_k^* + \Delta\mathbf{x}_k$, *the linearized equation is given by*

$$\begin{gathered}\Delta\mathbf{x}_k = DP_k \Delta\mathbf{x}_{k-1}, \\ \text{with} \quad \mathbf{g}_k\left(\mathbf{x}_{k-1}^* + \Delta\mathbf{x}_{k-1}, \mathbf{x}_k^* + \Delta\mathbf{x}_k, \mathbf{p}\right) = \mathbf{0}, \\ \left(k=1,2,\ldots,N\right).\end{gathered} \tag{6}$$

The resultant Jacobian matrices of the periodic motion are

$$\begin{gathered}DP_{k(k-1)\cdots 1} = DP_k \cdot DP_{k-1} \cdots DP_1, \left(k=1,2,\ldots,N\right); \\ DP \equiv DP_{N(N-1)\cdots 1} = DP_N \cdot DP_{N-1} \cdots\cdots DP_1,\end{gathered} \tag{7}$$

Where

$$DP_k = \left[\frac{\partial \mathbf{x}_k}{\partial \mathbf{x}_{k-1}}\right]_{(\mathbf{x}_{k-1}^*, \mathbf{x}_k^*)} = -\left[\frac{\partial \mathbf{g}_k}{\partial \mathbf{x}_k}\right]^{-1}_{(\mathbf{x}_{k-1}^*, \mathbf{x}_k^*)} \left[\frac{\partial \mathbf{g}_k}{\partial \mathbf{x}_{k-1}}\right]_{(\mathbf{x}_{k-1}^*, \mathbf{x}_k^*)} \tag{8}$$

The eigenvalues of DP and $DP_{k(k-1)\ldots 1}$ *for such a periodic motion are determined by*

$$\begin{gathered}\left|DP_{k(k-1)\ldots 1} - \bar{\lambda}\mathbf{I}_{n\times n}\right| = 0, \left(k=1,2,\ldots,N\right); \\ \left|DP - \lambda\mathbf{I}_{n\times n}\right| = 0.\end{gathered} \tag{9}$$

Thus, the stability and bifurcation of the periodic motion can be classified by the eigenvalues of $DP\left(\mathbf{x}_0^*\right)$ *with*

$$([n_1^m, n_1^o]:[n_2^m, n_2^o]:[n_3, \kappa_3]:[n_4, \kappa_4]\,|\,n_5 : n_6 : [n_7, l, \kappa_7]). \tag{10}$$

Where n_1 *is the total number of real eigenvalues with magnitudes less than one* $\left(n_1 = n_1^m + n_1^0\right)$, n_2 *is the total number of real eigenvalues with magnitude greater than*

one $\left(n_2 = n_2^m + n_2^0\right)$, n_3 *is the total number of real eigenvalues equal to* $+1$*;* n_4 *is the total number of real eigenvalues equal to* -1*;* n_5 *is the total pair number of complex eigenvalues with magnitudes less than one,* n_6 *is the total pair number of complex eigenvalues with magnitudes less than one,* n_7 *is the total pair number of complex eigenvalues with magnitudes equal to one.*

(i) If the magnitudes of all eigenvalues of DP are less than one, the approximate periodic solution is stable.

(ii) If at least the magnitude of one eigenvalue of DP is greater than one, the approximate periodic solution is unstable.

(iii) The boundaries between stable and unstable periodic motion give bifurcation and stability conditions.

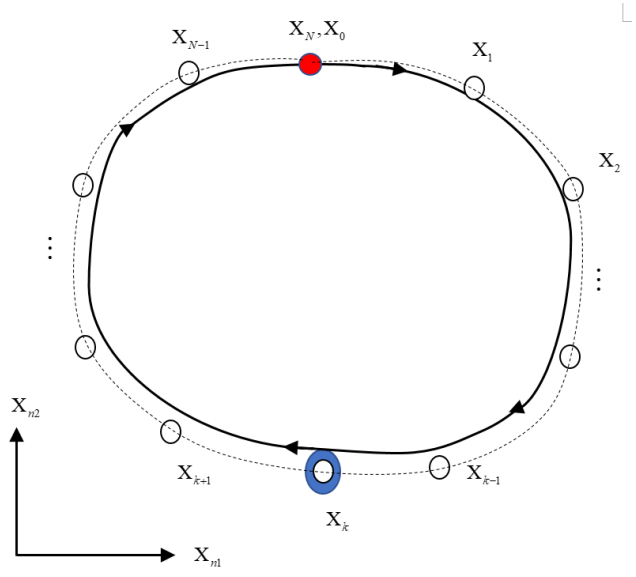

Fig. 1. Period-1 motion with N-node points. The solid curve represents the numerical results with N-nodes. The dashed curve represents the predicted solution with N-nodes marked by

circle symbols. The shaded circle symbol is the initial and the n^{th} node. The local shaded area is a small neighborhood of the exact solution at k^{th} node

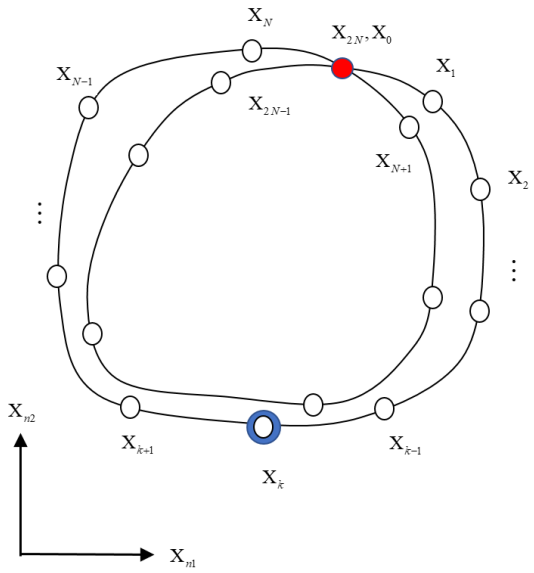

Fig. 2. Period- motion with 2N-node points. solid curve: numerical results.

To explain how to approximate the periodic motion in an n-dimensional nonlinear dynamical system, consider an $n_1 \times n_2$ *plane* $(n_1 + n_2 = n)$, *as shown in Fig. 1. N-nodes of the periodic motion are chosen for an approximate solution with a certain accuracy* $\|\mathbf{x}(t_k) - \mathbf{x}_k\| \le \varepsilon_k \ (\varepsilon_k \ge 0)$ *and* $\|\mathbf{f}(\mathbf{x}(t_k), t_k, \mathbf{p}) - \mathbf{f}(\mathbf{x}_k, t_k, \mathbf{p})\| \le \delta_k \ (\delta_k \ge 0)$ *.Letting* $\delta = \max\{\delta_k\}_{k\in\{1,2,\ldots,N\}}$ *and* $\varepsilon = \max\{\varepsilon_k\}_{k\in\{1,2,\ldots,N\}}$ *be small positive quantities prescribed, the periodic motion can be approximately described by a set of specific implicit mappings* P_k *with* $\mathbf{g}_k(\mathbf{x}_{k-1}, \mathbf{x}_k, \mathbf{p}) = \mathbf{0}(k = 1, 2, \ldots, N)$ *with periodicity condition* $\mathbf{x}_N = \mathbf{x}_0$. *Based on the approximate mapping functions, the nodes of the trajectory of periodic motion are computed approximately, which is depicted by a solid curve. The exact solution of the periodic motion is described by a dashed curve. The node points on the periodic motion are depicted with short lines. The symbols are node points on the exact solution of the periodic motion. The discrete mapping* P_k *is developed from the differential equation. With the control of computational accuracy, the nodes of the periodic motion can be obtained with a good*

approximation.

From the stability and bifurcation analysis, the period-1 motion under period $T = 2\pi/\Omega$ *, based on the set of discrete implicit mapping* P_k *with* $\mathbf{g}_k\left(\mathbf{x}_{k-1}, \mathbf{x}_k, \mathbf{p}\right) = \mathbf{0}\left(k = 1, 2, \ldots, N\right)$ *, is stable or unstable. If the period-doubling bifurcation occurs, the periodic motion will become a periodic motion under period* $T' = 2T$ *, and such a periodic motion is called the period-2 motion. Due to the period-doubling, 2N nodes of the period-2 motion will be employed to describe the period-2 motion. Thus, consider a mapping structure of the period-2 motion with 2N implicit mappings.*

$$\begin{aligned} &P = P_{2N} \circ P_{2N-1} \circ \cdots \circ P_2 \circ P_1 : \mathbf{x}_0 \to \mathbf{x}_{2N}; \\ &\text{with} \quad P_k : \mathbf{x}_{k-1} \to \mathbf{x}_k \left(k = 1, 2, \ldots, 2N\right). \end{aligned} \tag{11}$$

For $\mathbf{x}_{2N} = P\mathbf{x}_0$ *, there is a set of points* $\mathbf{x}_k^*\left(k = 1, 2, \ldots, 2N\right)$ *computed by the following implicit vector functions*

$$\begin{aligned} &\mathbf{g}_k\left(\mathbf{x}_{k-1}^*, \mathbf{x}_k^*, \mathbf{p}\right) = \mathbf{0}, \left(k = 1, 2, \ldots, 2N\right) \\ &\mathbf{x}_0^* = \mathbf{x}_{2N}^*. \end{aligned} \tag{12}$$

After period-doubling, the period-1 motion becomes period-2 motion. The nodes points increase to 2N points during two periods (2T). The period-2 motion can be sketched in Fig. 2. The node points are determined through the discrete implicit mapping with a mathematical relation in Eq.(12). On the other hand,

$$T' = 2T = \frac{2\left(2\pi\right)}{\Omega} = \frac{2\pi}{\omega} \Rightarrow \omega = \frac{\Omega}{2} \tag{13}$$

During the period of T' *, there is a periodic motion, which can be described by node points* $\mathbf{x}_k\left(k = 1, 2, \ldots, N'\right)$ *. Since the period-1 motion is described by node points* $\mathbf{x}_k\left(k = 1, 2, \ldots, N\right)$ *during the period T, due to* $T' = 2T$ *, the period-2 motion can be described by* $N' \geq 2N$ *nodes. Thus the corresponding mapping* P_k *is defined as*

$$p_k : \mathbf{x}_{k-1}^{(2)} \to \mathbf{x}_k^{(2)} \left(k = 1, 2, \ldots, 2N\right), \tag{14}$$

and

$$\begin{gathered} \mathbf{g}_k \left(\mathbf{x}_{k-1}^{(2)*}, \mathbf{x}_k^{(2)*}, \mathbf{p}\right) = \mathbf{0}, \left(k = 1, 2, \ldots, 2N\right), \\ \mathbf{x}_0^{(2)*} = \mathbf{x}_{2N}^{(2)*}. \end{gathered} \tag{15}$$

In general, for period $T' = mT$, *there is a period-m motion which can be described by* $N' \geq mN$. *The corresponding mapping* P_k

$$p_k : \mathbf{x}_{k-1}^{(m)} \to \mathbf{x}_k^{(m)} \left(k = 1, 2, \ldots, mN\right), \tag{16}$$

and

$$\begin{gathered} \mathbf{g}_k \left(\mathbf{x}_{k-1}^{(m)*}, \mathbf{x}_k^{(m)*}, \mathbf{p}\right) = \mathbf{0}, \left(k = 1, 2, \ldots, mN\right), \\ \mathbf{x}_0^{(m)*} = \mathbf{x}_{2N}^{(m)*}. \end{gathered} \tag{17}$$

From the above discussion, the period-m motion in a nonlinear dynamical system can be described through (mN+1) nodes for period mT. As in Luo (2014), the corresponding theorem is presented as follows.

Theorem 2. *Consider a nonlinear dynamical system in Eq. (1). If such a dynamical system has a period-m motion* $\mathbf{x}^{(m)}\left(t\right)$ *with finite norm* $\left\|\mathbf{x}^{(m)}\right\|$ *and period* $mT\left(T = 2\pi/\Omega\right)$, *then there are a set of values of time* $t_k \left(k = 0, 1, \ldots, mN\right)$ *with* $\left(N \geq 1\right)$ *on a time interval* $\left[t_0, mT + t_0\right]$ *and a set of points* $\mathbf{x}_k^{(m)}$, *such that* $\left\|\mathbf{x}^m\left(t_k\right) - \mathbf{x}_k^{(m)}\right\| \leq \varepsilon_k$ *with a small* $\varepsilon_k \geq 0$ *and*

$$\left\|\mathbf{f}\left(\mathbf{x}^{(m)}\left(t_k\right), t_k, \mathbf{p}\right) - \mathbf{f}\left(\mathbf{x}_k^{(m)}, t_k, \mathbf{p}\right)\right\| \leq \delta_k, \tag{18}$$

with a small $\delta_k \geq 0$. *Furthermore, there exists a vector function* $\mathbf{g}_k$ *with*

$$\mathbf{g}_k \left(\mathbf{x}_{k-1}^{(m)*}, \mathbf{x}_k^{(m)*}, \mathbf{p}\right) = \mathbf{0}, \left(k = 1, 2, \ldots, mN\right), \tag{19}$$

that determines a general implicit mapping $p_k : \mathbf{x}_{k-1}^{(m)} \to \mathbf{x}_k^{(m)} \left(k = 1, 2, \ldots, mN\right)$. *The particular*

form of the function $\mathbf{g}_k$ *is determined by a particular computational scheme which one used to study the system in Eq. (1). Consider a mapping structure as*

$$\begin{aligned} &P = P_{mN} \circ P_{mN-1} \circ \cdots \circ P_2 \circ P_1 : \mathbf{x}_0^{(m)} \to \mathbf{x}_{mN}^{(m)}; \\ &\text{with} \quad p_k : \mathbf{x}_{k-1}^{(m)} \to \mathbf{x}_k^{(m)} \left(k = 1, 2, \ldots, mN\right). \end{aligned} \tag{20}$$

For $\mathbf{x}_{mN}^{(m)} = P\mathbf{x}_0^{(m)}$*., if there is a set of points* $\mathbf{x}_k^{(m)*} \left(k = 0, 1, \ldots, mN\right)$ *computed by*

$$\begin{aligned} &\mathbf{g}_k \left(\mathbf{x}_{k-1}^{(m)*}, \mathbf{x}_k^{(m)*}, \mathbf{p}\right) = \mathbf{0}, \left(k = 1, 2, \ldots, mN\right), \\ &\mathbf{x}_0^{(m)*} = \mathbf{x}_{mN}^{(m)*}. \end{aligned} \tag{21}$$

then the points $\mathbf{x}_k^{(m)*} \left(k = 0, 1, \ldots, mN\right)$ *are approximations of points* $\mathbf{x}^{(m)} \left(t_k\right)$ *of the periodic solution. In the neighborhood of* $\mathbf{x}_k^{(m)*}$*, with* $\mathbf{x}_k^{(m)} = \mathbf{x}_k^{(m)*} + \Delta\mathbf{x}_k^{(m)}$*, the linearized equation is given by*

$$\begin{aligned} &\Delta\mathbf{x}_k^{(m)} = DP_k \Delta\mathbf{x}_{k-1}^{(m)}, \\ &\text{with} \quad \mathbf{g}_k \left(\mathbf{x}_{k-1}^{(m)*} + \Delta\mathbf{x}_{k-1}^{(m)}, \mathbf{x}_k^{(m)*} + \Delta\mathbf{x}_k^{(m)}, \mathbf{p}\right) = \mathbf{0}, \\ &\left(k = 1, 2, \ldots, mN\right). \end{aligned} \tag{22}$$

The resultant Jacobian matrices of the periodic motion are

$$\begin{aligned} &DP_{k(k-1)\cdots 1} = DP_k \cdot DP_{k-1} \cdots DP_1, \left(k = 1, 2, \ldots, mN\right); \\ &DP \equiv DP_{mN(mN-1)\cdots 1} = DP_{mN} \cdot DP_{mN-1} \cdots\cdots DP_1, \end{aligned} \tag{23}$$

Where

$$DP_k = \left[\frac{\partial \mathbf{x}_k^{(m)}}{\partial \mathbf{x}_{k-1}^{(m)}}\right]_{(\mathbf{x}_{k-1}^{(m)*}, \mathbf{x}_k^{(m)*})} = -\left[\frac{\partial \mathbf{g}_k}{\partial \mathbf{x}_k^{(m)}}\right]^{-1}_{(\mathbf{x}_{k-1}^{*}, \mathbf{x}_k^{*})} \left[\frac{\partial \mathbf{g}_k}{\partial \mathbf{x}_{k-1}^{(m)}}\right]\Bigg|_{(\mathbf{x}(m)_{k-1}^{*}, \mathbf{x}_k^{(m)*})} \tag{24}$$

The eigenvalues of $DP\left(\mathbf{x}_0^{(m)*}\right)$ *and* $DP_{k(k-1)\ldots 1}$ *for such a periodic motion are determined by*

$$\left|DP_{k(k-1)\ldots 1}-\bar{\lambda}\mathbf{I}_{n\times n}\right|=0,\left(k=1,2,\ldots,mN\right);$$
$$\left|DP-\lambda\mathbf{I}_{n\times n}\right|=0. \tag{25}$$

Thus, the stability and bifurcation of the periodic motion can be classified by the eigenvalues of $DP\left(\mathbf{x}_0^{(m)*}\right)$ *with*

$$([n_1^m,n_1^o]:[n_2^m,n_2^o]:[n_3,\kappa_3]:[n_4,\kappa_4]\,|\,n_5:n_6:[n_7,l,\kappa_7]). \tag{26}$$

(i) If the magnitudes of all eigenvalues of $DP\left(\mathrm{m}\right)$ *are less than one (i.e.,* $\left|\lambda_i\right|<1,i=1,2,\ldots,n$*), the approximate period-m solution is stable.*

(ii) If at least the magnitude of one eigenvalue of $DP\left(\mathrm{m}\right)$ *is greater than one (i.e.,* $\left|\lambda_i\right|>1,i\in\left\{1,2,\ldots,n\right\}$*), the approximate period-m solution is unstable.*

(iii) The boundaries between stable and unstable period-m motions give bifurcation and stability conditions.

CHAPTER III

DISCRETIZATION OF DYNAMICAL SYSTEMS

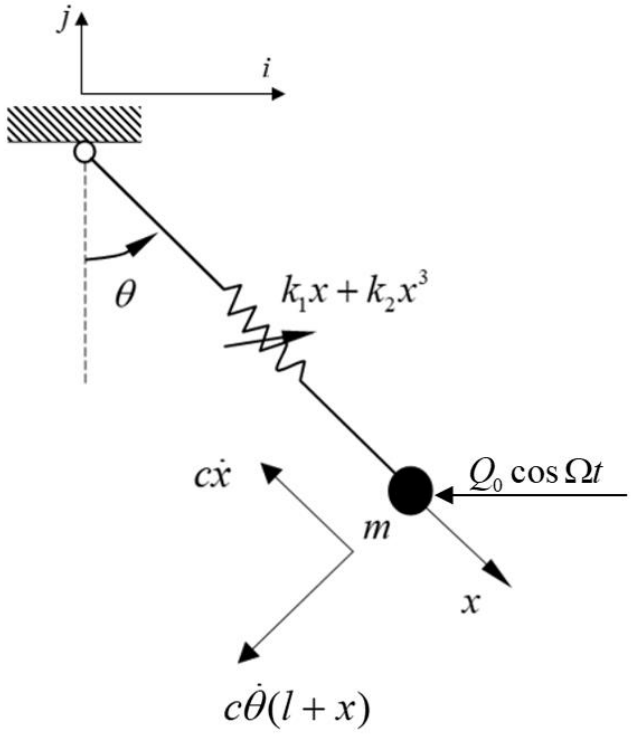

Fig. 3. The basic model of the periodically forced, nonlinear spring pendulum.

Equation of Motion

A nonlinear spring pendulum system with air resistance is shown in Fig.3. The length of the nonlinear spring is l. The spring-pendulum possesses a nonlinear spring with $k_1x + k_2x^3$ and a damping of $c\dot{x}$ and $c\dot{\theta}(l+x)$. The excitation force of $Q_0 \cos \Omega t$ is on the horizontal direction. The kinetic energy can be determined as:

$$T = \frac{1}{2} m \left\{ \left[\dot{x} \sin\theta + \dot{\theta}(l+x)\cos\theta \right]^2 + \left[-\dot{x}\cos\theta + \dot{\theta}(l+x)\sin\theta \right]^2 \right\}$$
$$= \frac{1}{2} m \left[\dot{x}^2 + \dot{\theta}^2 (l+x)^2 \right] \tag{27}$$

The potential energy can be determined as:

$$V = mgh + \frac{1}{2}k_1x^2 + \frac{1}{4}k_2x^4 = -mg\left(l+x\right)\cos\theta + \frac{1}{2}kx^2 + \frac{1}{4}k_2x^4 \tag{28}$$

Then we have Lagrangian:

$$L = T - V = \frac{1}{2}m\left[\dot{x}^2 + \dot{\theta}^2\left(L+x\right)^2\right] + mg\left(l+x\right)\cos\theta - \frac{1}{2}kx^2 - \frac{1}{4}k_2x^4 \tag{29}$$

From the Langrange equation, the equation of motions can be obtained as:

$$\begin{aligned} m\ddot{x} &= m(l+x)\dot{\theta}^2 + mg\cos\theta - k_1x - k_2x^3 \\ &\quad - c\dot{x} - Q_0\cos\Omega t\sin\theta \\ m\ddot{\theta} &= \frac{1}{(l+x)^2}[-2\dot{x}(l+x)m\dot{\theta} - mg(l+x)\sin\theta \\ &\quad - c\dot{\theta}(l+x)^2 - Q_0(l+x)\cos\Omega t\cos\theta] \end{aligned} \tag{30}$$

Let $x_1 = x$, $y_1 = \dot{x}$, $x_2 = \theta$, $y_2 = \dot{\theta}$. Equation (27) becomes:

$$\begin{aligned} \dot{x}_1 &= y_1 \\ \dot{y}_1 &= -\frac{1}{m}cy_1 + (l+x_1)y_2^2 + g\cos x_2 \\ &\quad -\frac{1}{m}k_1x_1 - \frac{1}{m}k_2x_1^3 - \frac{1}{m}Q_0\cos\Omega t\sin x_2 \\ \dot{x}_2 &= y_2 \\ \dot{y}_2 &= -\frac{1}{m}cy_2 - \frac{2}{(l+x_1)}y_1y_2 - \frac{1}{(l+x_1)}g\sin x_2 \\ &\quad -\frac{1}{m(l+x_1)}Q_0\cos\Omega t\cos x_2 \end{aligned} \tag{31}$$

The differential equation can be discretized by a midpoint scheme for the time interval $t \in [t_{k-1}, t_k]$ to form a map P_k ($k = 1, 2, \cdots$) as

$$\begin{aligned} &P_k : \mathbf{x}_{k-1} \to \mathbf{x}_k \\ &\Rightarrow \ \mathbf{x}_k = P_k\mathbf{x}_{k-1} \end{aligned} \tag{32}$$

where $\mathbf{x}_k = (x_1, y_1, x_2, y_2)^{\mathrm{T}}$.

By the midpoint discrete approximation, the implicit relation can be described as:

$$
\begin{aligned}
x_{1k} &= x_{1(k-1)} + \tfrac{1}{2}h(y_{1(k-1)} + y_{1k}),\\
y_{1k} &= y_{1(k-1)} - h\{\tfrac{1}{2m}c(y_{1(k-1)} + y_{1k})\\
&\quad -\tfrac{1}{4}[l + \tfrac{1}{2}(x_{1(k-1)} + x_{1k})](y_{2(k-1)} + y_{2k})^2\\
&\quad -g\cos[\tfrac{1}{2}(x_{2(k-1)} + x_{2k})] + \tfrac{1}{2m}k_1(x_{1(k-1)} + x_{1k})\\
&\quad +\tfrac{1}{8m}k_2(x_{1(k-1)} + x_{1k})^3\\
&\quad +\tfrac{1}{m}Q_0\cos\Omega(t_{k-1} + \tfrac{1}{2}h)\sin[\tfrac{1}{2}(x_{2(k-1)} + x_{2k})]\},\\
x_{2(k)} &= x_{2(k-1)} + \tfrac{1}{2}h(y_{2(k-1)} + y_{2k}),\\
y_{2(k)} &= y_{2(k-1)} - \tfrac{1}{2m}ch(y_{2(k-1)} + y_{2k})\\
&\quad -\tfrac{h}{[l + \frac{1}{2}(x_{1(k-1)} + x_{1k})]}\{\tfrac{1}{2}(y_{1(k-1)} + y_{1k})(y_{2(k-1)} + y_{2k})\\
&\quad +g\sin[\tfrac{1}{2}(x_{2(k-1)} + x_{2k})]\\
&\quad +\tfrac{1}{m}Q_0\cos\Omega(t_{k-1} + \tfrac{1}{2}h)\cos[\tfrac{1}{2}(x_{2(k-1)} + x_{2k})]\}.
\end{aligned}
\tag{33}
$$

So discretization of the differential equation (2) is completed.

CHAPTER IV

PERIOD-1 MOTIONS AND STABILITY

The period-1 motion can be discretized into N points. A discrete mapping structure of a period-1 motion can be constructed as:

$$P = \underbrace{P_N \circ P_{N-1} \circ \cdots \circ P_1}_{N-actions} : \mathbf{x}_0 \to \mathbf{x}_N \tag{34}$$

with

$$\begin{aligned} & P_1 : \mathbf{x}_0 \to \mathbf{x}_1 \\ & \Rightarrow \mathbf{x}_1 = P_1 \mathbf{x}_0 \\ & P_2 : \mathbf{x}_1 \to \mathbf{x}_2 \\ & \Rightarrow \mathbf{x}_2 = P_2 \mathbf{x}_1 \\ & \vdots \\ & P_N : \mathbf{x}_{N-1} \to \mathbf{x}_N \\ & \Rightarrow \mathbf{x}_N = P_N \mathbf{x}_{N-1} \end{aligned} \tag{35}$$

From Eq.(30), the algebraic equations for period-1 motion can be obtained. For P_k, let

$$\mathbf{g}_k = (g_{k1}, g_{k2}, g_{k3}, g_{k4})^{\mathrm{T}} = \mathbf{0} \tag{36}$$

where

$$
\begin{aligned}
g_{k1} &= x_{1(k)} - [x_{1(k-1)} + \tfrac{1}{2}h(y_{1(k-1)} + y_{1k})], \\
g_{k2} &= y_{1(k)} - (y_{1(k-1)} - h\{\tfrac{1}{2m}c(y_{1(k-1)} + y_{1k}) \\
&\quad -\tfrac{1}{4}[l + \tfrac{1}{2}(x_{1(k-1)} + x_{1(k)})](y_{2(k-1)} + y_{2k})^2 \\
&\quad -g\cos[\tfrac{1}{2}(x_{2(k-1)} + x_{2k})] + \tfrac{1}{2m}k_1(x_{1(k-1)} + x_{1k}) \\
&\quad +\tfrac{1}{8m}k_2(x_{1(k-1)} + x_{1k})^3 \\
&\quad +\tfrac{1}{m}Q_0\cos\Omega(t_{k-1} + \tfrac{1}{2}h)\sin[\tfrac{1}{2}(x_{2(k-1)} + x_{2k})]\}), \\
g_{k3} &= x_{2(k)} - [x_{2(k-1)} + \tfrac{1}{2}h(y_{2(k-1)} + y_{2k})], \\
g_{k4} &= y_{2(k)} - (y_{2(k-1)} - h\tfrac{1}{2m}c(y_{2(k-1)} + y_{2k}) \\
&\quad -\tfrac{h}{[l + \frac{1}{2}(x_{1(k-1)} + x_{1k})]}\{\tfrac{1}{2}(y_{1(k-1)} + y_{1k})(y_{2(k-1)} + y_{2k}) \\
&\quad +g\sin[\tfrac{1}{2}(x_{2(k-1)} + x_{2k})] \\
&\quad +\tfrac{1}{m}Q_0\cos\Omega(t_{k-1} + \tfrac{1}{2}h)\cos[\tfrac{1}{2}(x_{2(k-1)} + x_{2k})]\}).
\end{aligned}
\tag{37}
$$

The periodicity gives

$$
\begin{aligned}
x_{1N} &= x_{10} \\
y_{1N} &= y_{10} \\
x_{2N} &= x_{20} + 2n\pi,\ n = 0,1,2,\cdots \\
y_{2N} &= y_{20}
\end{aligned}
\tag{38}
$$

From Eqs.(36)-(38), the discrete nodes of periodic motions can be determined by $4(N+1)$ equations. If the discrete nodes $(\mathbf{x}_k^*, \mathbf{y}_k^*)$ $(k = 1,2,\cdots,N)$ of the period-1 motion is obtained, the corresponding stability of the periodic motion can be discussed by the eigenvalue analysis of the implicit mappings of the periodic motion.

If $\mathbf{x}_k^*$ $(k = 1,2,\cdots,N)$ are obtained, in the neighborhood of $\mathbf{x}_k^*$, with $\mathbf{x}_k = \mathbf{x}_k^* + \Delta\mathbf{x}_k$, the linearized equation is

$$
\Delta\mathbf{x}_k = DP_k\Delta\mathbf{x}_{k-1} \tag{39}
$$

where

$$
DP_k = \frac{\partial\mathbf{x}_k}{\partial\mathbf{x}_{k-1}}|_{(\mathbf{x}_{k-1}^*, \mathbf{x}_k^*)} = -(\frac{\partial\mathbf{g}_k}{\partial\mathbf{x}_k})^{-1}\frac{\partial\mathbf{g}_k}{\partial\mathbf{x}_{k-1}}|_{(\mathbf{x}_{k-1}^*, \mathbf{x}_k^*)} \tag{40}
$$

where $k = 1,2,\cdots,N$ and the formulation of $(\partial\mathbf{g}_k / \partial\mathbf{x}_k)^{-1}$ and $\partial\mathbf{g}_k / \partial\mathbf{x}_{k-1}$ is given in Appendix.

The resultant Jacobian matrices of the periodic motion are

$$DP = DP_{N(N-1)\cdots 1} = DP_N \cdot DP_{N-1} \cdot \ldots \cdot DP_1 \tag{41}$$

The eigenvalues of DP matrices for the periodic motion are computed by

$$| DP - \lambda \mathbf{I}_{4\times 4} | = 0 \tag{42}$$

If the magnitudes of all eigenvalues of DP are less than one (i.e., $|\lambda_i| < 1,\ i = 1,2$), the approximate periodic solution is stable.

If at least the magnitude of one eigenvalue of DP is greater than one (i.e., $|\lambda_i| > 1,\ i \in \{1,2,\cdots, n(s+1)\}$), the approximate periodic solution is unstable.

The boundaries between stable and unstable periodic flow with higher order singularity give bifurcation and stability conditions with higher order singularity.

The bifurcation conditions of period -1 motion are presented as follows.

If one eigenvalue is equal to +1 and the other eigenvalues are within the unit circle, the saddle-node bifurcation (SN) occurs.

If one eigenvalue is equal to -1 and the other eigenvalues are within the unit circle, the period-doubling bifurcation (PD) occurs.

If the magnitude of a pair of complex eigenvalues is equal to 1, and the other eigenvalues are within the unit circle, Neimark bifurcation (NB) occurs.

CHAPTER V

PERIOD-M MOTIONS AND STABILITY

If the period-doubling bifurcation condition has been observed on the bifurcation trees of period-1 motions, then the period-2 motions will appear as well. Similarly if the period-doubling bifurcation condition occurs on the bifurcation trees of period-2 motions, the period-4 motion will appear as well. To predict the period-m motions in such a duffing oscillator analytically, consider a mapping structure as follows:

$$\begin{aligned} P &= \underbrace{P_{mN} \circ P_{mN-1} \circ \cdots \circ P_2 \circ P_1}_{mN-\text{actions}} : (\mathbf{x}_0^{(m)}) \to (\mathbf{x}_{mN}^{(m)}) \\ (\mathbf{x}_{mN}^{(m)}) &= P(\mathbf{x}_0^{(m)}) \end{aligned} \tag{43}$$

With

$$P_k : (\mathbf{x}_{k-1}^{(m)}) \to (\mathbf{x}_k^{(m)}) \quad (k = 1, 2, \cdots, mN). \tag{44}$$

From Eq.(33), the corresponding algebraic equations are

$$\begin{aligned} x_{1k}^{(m)} &= x_{1(k-1)}^{(m)} + \tfrac{1}{2} h (y_{1(k-1)}^{(m)} + y_{1k}^{(m)}), \\ y_{1k}^{(m)} &= y_{1(k-1)}^{(m)} - h\{ \tfrac{1}{2m} c (y_{1(k-1)}^{(m)} + y_{1k}^{(m)}) \\ &\quad - \tfrac{1}{4}[l + \tfrac{1}{2}(x_{1(k-1)}^{(m)} + x_{1k}^{(m)})](y_{2(k-1)}^{(m)} + y_{2k}^{(m)})^2 \\ &\quad - g\cos[\tfrac{1}{2}(x_{2(k-1)}^{(m)} + x_{2k}^{(m)})] + \tfrac{1}{2m} k_1 (x_{1(k-1)}^{(m)} + x_{1k}^{(m)}) \\ &\quad + \tfrac{1}{8m} k_2 (x_{1(k-1)}^{(m)} + x_{1k}^{(m)})^3 \\ &\quad + \tfrac{1}{m} Q_0 \cos\Omega(t_{k-1} + \tfrac{1}{2}h) \sin[\tfrac{1}{2}(x_{2(k-1)}^{(m)} + x_{2k}^{(m)})]\}, \\ x_{2(k)}^{(m)} &= x_{2(k-1)}^{(m)} + \tfrac{1}{2} h (y_{2(k-1)}^{(m)} + y_{2k}^{(m)}), \\ y_{2(k)}^{(m)} &= y_{2(k-1)}^{(m)} - \tfrac{1}{2m} ch (y_{2(k-1)}^{(m)} + y_{2k}^{(m)}) \\ &\quad - \frac{h}{[l + \frac{1}{2}(x_{1(k-1)}^{(m)} + x_{1k}^{(m)})]} \{ \tfrac{1}{2}(y_{1(k-1)}^{(m)} + y_{1k}^{(m)})(y_{2(k-1)}^{(m)} + y_{2k}^{(m)}) \\ &\quad + g\sin[\tfrac{1}{2}(x_{2(k-1)}^{(m)} + x_{2k}^{(m)})] \\ &\quad + \tfrac{1}{m} Q_0 \cos\Omega(t_{k-1} + \tfrac{1}{2}h) \cos[\tfrac{1}{2}(x_{2(k-1)}^{(m)} + x_{2k}^{(m)})]\}. \end{aligned} \tag{45}$$

The periodicity gives

$$\begin{aligned} x_{1mN}^{(m)} &= x_{10}^{(m)} \\ y_{1mN}^{(m)} &= x_{10}^{(m)} \\ x_{2mN}^{(m)} &= x_{20}^{(m)} + 2n\pi, n = 0,1,2\ldots \\ y_{2mN}^{(m)} &= y_{20}^{(m)} \end{aligned} \tag{46}$$

From Eqs.(45)-(46), the discrete nodes of periodic motions can be determined by $4(mN+1)$ equations. If the discrete nodes $(\mathbf{x}_k^{(m)*}, \mathbf{y}_k^{(m)*})$ ($k = 1,2,\cdots,mN$) of the period-m motion is obtained, the corresponding stability of the periodic motions can be discussed by the eigenvalue analysis of the implicit mappings of the periodic motion.

If $\mathbf{x}_k^{(m)*}$ ($k = 1,2,\cdots,mN$) are obtained, in the neighborhood of $\mathbf{x}_k^{(m)*}$, with $\mathbf{x}_k^{(m)} = \mathbf{x}_k^{(m)*} + \Delta\mathbf{x}_k^{(m)}$, the linearized equation is

$$\Delta\mathbf{x}_k^{(m)} = DP_k \Delta\mathbf{x}_{k-1}^{(m)} \tag{47}$$

where

$$DP_k = \frac{\partial \mathbf{x}_k^{(m)}}{\partial \mathbf{x}_{k-1}^{(m)}}\Big|_{(\mathbf{x}_{k-1}^{(m)*}, \mathbf{x}_k^{(m)*})} = -\left(\frac{\partial \mathbf{g}_k^{(m)}}{\partial \mathbf{x}_k^{(m)}}\right)^{-1} \frac{\partial \mathbf{g}_k^{(m)}}{\partial \mathbf{x}_{k-1}^{(m)}}\Big|_{(\mathbf{x}_{k-1}^{(m)*}, \mathbf{x}_k^{(m)*})} \tag{48}$$

where $k = 1,2,\cdots,mN$ and the formulation of $(\partial \mathbf{g}_k^{(m)} / \partial \mathbf{x}_k^{(m)})^{-1}$ and $\partial \mathbf{g}_k^{(m)} / \partial \mathbf{x}_{k-1}^{(m)}$ is given in Appendix.

The resultant Jacobian matrices of the periodic motion are

$$DP = DP_{mN(N-1)\cdots 1} = DP_{mN} \cdot DP_{mN-1} \cdot \ldots \cdot DP_1 \tag{49}$$

The eigenvalues of DP matrices for the periodic motion are computed by

$$| DP - \lambda \mathbf{I}_{4\times 4} | = 0 \tag{50}$$

The stability and bifurcation conditions are the same as for the period-1 motion.

CHAPTER VI

FINITE FOURIER SERIES ANALYSIS

Consider the node points of period-m motions as $\mathbf{x}_k^{(m)} = (x_k^{(m)}, y_k^{(m)})^{\mathrm{T}}$ for $k = 0,1,2,\cdots, mN$ in the time-delayed, hardening Duffing oscillator. The approximate expression of a period-m motion is determined by the finite Fourier series as

$$\mathbf{x}^{(m)}(t) \approx \mathbf{a}_0^{(m)} + \sum_{j=1}^{M} \mathbf{b}_{j/m} \cos(\frac{j}{m}\Omega t) + \mathbf{c}_{j/m} \sin(\frac{j}{m}\Omega t). \tag{51}$$

There are $(2M+1)$ unknown vector coefficients of $\mathbf{a}_0^{(m)}, \mathbf{b}_{j/m}, \mathbf{c}_{j/m}$ ($j = 1,2,\cdots, M$). To determine, from the given nodes $\mathbf{x}_k^{(m)}$ ($k = 0,1,2,\cdots, mN$), such unknowns ($2M+1 \le mN+1$) can be determined. In other words, $M \le mN/2$. The node points $\mathbf{x}_k^{(m)}$ on the period-m motion can be expressed by the finite Fourier series as for $t_k \in [0, mT]$

$$\begin{aligned} \mathbf{x}^{(m)}(t_k) \equiv \mathbf{x}_k^{(m)} &= \mathbf{a}_0^{(m)} + \sum_{j=1}^{mN/2} \mathbf{b}_{j/m} \cos(\frac{j}{m}\Omega t_k) + \mathbf{c}_{j/m} \sin(\frac{j}{m}\Omega t_k) \\ &= \mathbf{a}_0^{(m)} + \sum_{j=1}^{mN/2} \mathbf{b}_{j/m} \cos(\frac{j}{m}\frac{2k\pi}{N}) + \mathbf{c}_{j/m} \sin(\frac{j}{m}\frac{2k\pi}{N}) \\ (k &= 0,1,\cdots, mN-1) \end{aligned} \tag{52}$$

where

$$\begin{aligned} &T = \frac{2\pi}{\Omega} = N\Delta t;\ \Omega t_k = \Omega k \Delta t = \frac{2k\pi}{N}, \\ &\mathbf{a}_0^{(m)} = (a_{01}^{(m)}, a_{02}^{(m)})^{\mathrm{T}}, \mathbf{b}_{j/m} = (b_{j/m1}, b_{j/m2})^{\mathrm{T}}, \mathbf{c}_{j/m} = (c_{j/m1}, c_{j/m2})^{\mathrm{T}}. \end{aligned} \tag{53}$$

From discrete nodes on the period-m motion, equation (37) gives

$$\left.\begin{aligned} \mathbf{a}_0^{(m)} &= \frac{1}{N}\sum_{k=0}^{mN-1} \mathbf{x}_k^{(m)}, \\ \mathbf{b}_{j/m} &= \frac{2}{mN}\sum_{k=1}^{mN-1} \mathbf{x}_k^{(m)} \cos(k\frac{2j\pi}{mN}), \\ \mathbf{c}_{j/m} &= \frac{2}{mN}\sum_{k=1}^{mN-1} \mathbf{x}_k^{(m)} \sin(k\frac{2j\pi}{mN}) \end{aligned}\right\} \ (j = 1,2,\cdots, mN/2) \tag{54}$$

Thus the approximate expression for period-m motion in Eq.(19) is determined by

$$\mathbf{x}^{(m)}(t) \approx \mathbf{a}_0^{(m)} + \sum_{j=1}^{mN/2} \mathbf{b}_{j/m} \cos(\frac{j}{m}\Omega t) + \mathbf{c}_{j/m} \sin(\frac{j}{m}\Omega t). \tag{55}$$

The foregoing equation can be rewritten as

$$\begin{Bmatrix} x^{(m)}(t) \\ y^{(m)}(t) \end{Bmatrix} \equiv \begin{Bmatrix} x_1^{(m)}(t) \\ x_2^{(m)}(t) \end{Bmatrix} \approx \begin{Bmatrix} a_{01}^{(m)} \\ a_{02}^{(m)} \end{Bmatrix} + \sum_{j=1}^{mN/2} \begin{Bmatrix} A_{j/m1} \cos(\frac{j}{m}\Omega t - \varphi_{j/m1}) \\ A_{j/m1} \cos(\frac{j}{m}\Omega t - \varphi_{j/m2}) \end{Bmatrix} \tag{56}$$

where the harmonic amplitudes and harmonic phases for period-*m* motion are

$$\begin{aligned} A_{j/m1} &= \sqrt{b_{j/m1}^2 + c_{j/m1}^2},\ \varphi_{j/m1} = \arctan\frac{c_{j/m1}}{b_{j/m1}}, \\ A_{j/m2} &= \sqrt{b_{j/m2}^2 + c_{j/m2}^2},\ \varphi_{j/m2} = \arctan\frac{c_{j/m2}}{b_{j/m2}}. \end{aligned} \tag{57}$$

For simplicity, harmonic amplitudes of displacement $x^{(m)}(t)$ for period-m motions will be presented. Similarly, the harmonic amplitudes of velocity $y^{(m)}(t)$ for periodic motions can also be determined. Thus the displacement can be expressed as

$$x^{(m)}(t) \approx a_0^{(m)} + \sum_{j=1}^{mN/2} b_{j/m} \cos(\frac{j}{m}\Omega t) + c_{j/m} \sin(\frac{j}{m}\Omega t) \tag{58}$$

and

$$x^{(m)}(t) \approx a_0^{(m)} + \sum_{j=1}^{mN/2} A_{j/m} \cos(\frac{j}{m}\Omega t - \varphi_{j/m}) \tag{59}$$

where

$$A_{j/m} = \sqrt{b_{j/m}^2 + c_{j/m}^2},\ \varphi_{j/m} = \arctan\frac{c_{j/m}}{b_{j/m}}. \tag{60}$$

CHAPTER VII

NUMERICAL ILLUSTRATION

In this section, through the analytical predictions of period-1 to period-2 motions, the bifurcation trees of period-1 and period-2 motions for this periodically forced, nonlinear spring pendulum system will be present. Illustration of period-1 and period-2 motions for such system will be illustrated as well. Without loss of generality, a set of arbitrary parameters are chosen as

$$\begin{aligned} &k_1 = 5, k_2 = 100,\ c = 0.1,\ Q_0 = 20.0 \\ &L = 2, T = 2\pi / \Omega. \end{aligned} \tag{61}$$

and the excitation period $T = 2\pi / \Omega.$. In order to keep the computational accuracy of $\varepsilon = 10^{-9}$, then $h \sim 10^{-3}$ as the discretization with $\varepsilon \sim O(h^3)$. Now $N = T / h = T / \Delta t$, so we have $N = 1024$ for $\Omega \geq 4$, $N = 2048$ for $0 < \Omega < 4$. However for $0 < \Omega < 2$ the computational accuracy is not higher, as it will cost too much time to compute. For the stability analysis of periodic motions, the corresponding eigenvalues of the resultant Jacobian matrix are computed through the QR method in the following numerical illustrations. The bifurcation tree of period-1 to period-2 motion will be discussed in sequel.

Analytical Bifurcation Trees of Periodic Motions

The bifurcation trees of period-1 to period-2 motions for this periodically forced, nonlinear spring pendulum system are predicted analytically through the implicit mapping. The bifurcation trees are illustrated by displacement, velocity, angle, angular velocity of the periodic nodes, as shown in Fig.4-23. The solid line represent the stable motions and the dashed line represent the unstable motions. The acronyms ‘SN’, ‘PD’ and ‘NB’ represent the

saddle node, period doubling, and Neimark bifurcations, respectively. The period-1, period-2, motions are labeled by P-1, P-2, respectively. The period-2 motions appear from the PD bifurcations of the asymmetric period-1 motions. The global view of the bifurcation trees is presented in Fig.4, as is shown in the figure, the entire bifurcation trees consist four separate bifurcation trees which do not connect with each other. The zoom views of the first bifurcation trees for frequency ranges in $\Omega \in (4.59,18)$ are presented in Fig.5-10. The zoom view of the period-2 motion lie in the second bifurcation tree are shown in Fig.11. The asymmetric period-1 motions and period-2 motions of the last two bifurcation trees can be observed in Fig.12. Fig.13 contained the zoom view of the asymmetric period-1 motions and period-2 motions in the third bifurcation tree. The zoom view of the asymmetric period-1 motion and period-2 motions in the last bifurcation tree are presented in Fig.14-23. To make the bifurcation conditions at each bifurcation trees more clearly. The bifurcation points and bifurcation conditions on each bifurcation trees are listed in Tables 1-3 respectively.

In Fig.4, the global view of the bifurcation trees of period-1 to period-2 motion are presented. The periodic motions in the frequency range $\Omega > 18$ are simple, only symmetric period-1 motion occur at that range, so the global view only contain bifurcation trees in the frequency range of $\Omega \in (0,18)$. The bifurcation trees consist of four independent parts which does not connect with each other. The Frequency range for these bifurcation trees are $\Omega \in (4.59,18)$, $(0.3001,18)$, $(1.458,2.396)$, $(0,1.266)$. For the first bifurcation tress at frequency range of $\Omega \in (4.59,18)$, there are three bifurcation trees from symmetric to asymmetric at this range, the asymmetric condition started at saddle-node $\Omega = (7.17,7.512,4.744)$, two asymmetric period-1 motion stopped at $\Omega = 17.03,17.276$ as

the periodic motions at bigger excitation frequency can't be predicted due to the parameter chosen in eq.(61). The two bifurcation trees at frequency range of $\Omega \in (4.598, 4.744)$, $(6.14,17.276)$ only possess symmetric to asymmetric period-1 motion. Three bifurcation trees of period-1 to period-2 motions can be observed at frequency range of $\Omega \in (4.3,17.03)$. The asymmetric period-1 motions in $\Omega \in (4.598, 4.744)$ are presented in Fig.6, meanwhile Fig.7 provide zoom view for Fig.6(ii) and Fig.6(iv). The asymmetric period-1 motions in $\Omega \in (6.14,17.276)$ are shown in Fig.8-10, and the period-1 to period-2 motions in $\Omega \in (4.3,17.03)$ are presented in Fig 5-10. Fig.9 is a zoom view for Fig.8(ii) and Fig.8(iv), Fig 10 is another zoom view for Fig.8(iv) .The second bifurcation tree at frequency range of $(0.3001,18)$ contain only asymmetric period-1 motions and one period-2 motion coexist with asymmetric period-1 motion at frequency range of $\Omega \in (3.3842, 3.8064)$. Which is presented in Fig.4 and Fig.11 respectively. A general look of last two bifurcation trees can be observed in Fig.12. The third bifurcation tree is in the frequency range of $\Omega \in (1.458, 2.396)$. It is a close-loop and contains one asymmetric period-1 motion in the frequency range of $\Omega \in (1.754,1.851)$, there is one period-2 motion in $\Omega \in (1.774,1.85)$ as well. Which are shown in Fig.13. For the last bifurcation tree in the frequency range of $(0,1.266)$. In total, there are 12 branches contain symmetric to asymmetric period-1 motion, among them, four bifurcation trees exits in the frequency range of $\Omega \in (1.2296,1.2414)$, $(0.868,1.0143)$, $(0.4669, 0.4748)$, and $(0.8896, 0.9325)$. They only possess from symmetric to asymmetric period-1 motion. Eight asymmetric bifurcation trees exits in the frequency range of $\Omega \in (0.9923,1.141)$, $(0.4678, 0.4882)$, $(0.703, 0.762)$, $(0.7272, 0.9046)$,

$(0.6871, 0.6942)$, $(0.9003, 0.919)$, $(0.6637, 0.7126)$ contain one period-1 to period-2 motion for each one of them respectively, and four bifurcation trees of period-1 to period-2 motions occurred at frequency range of $\Omega \in (1.04, 1.3732)$. All of them are presented in Fig.14-23 respectively. Fig.20 and Fig.21 are zoom views of Fig.19 for a better look on the period-2 motions, Fig. 23 is a zoom view of Fig.22 as well. The saddle-node bifurcations for jumping phenomena and Neimark bifurcations can be easily observed, besides bifurcation points of symmetric period-1 motions are listed in Table 1, the bifurcation points for asymmetric period-1 motions are placed in Table 2, the bifurcation points for period-2 motions are placed in Table 3.

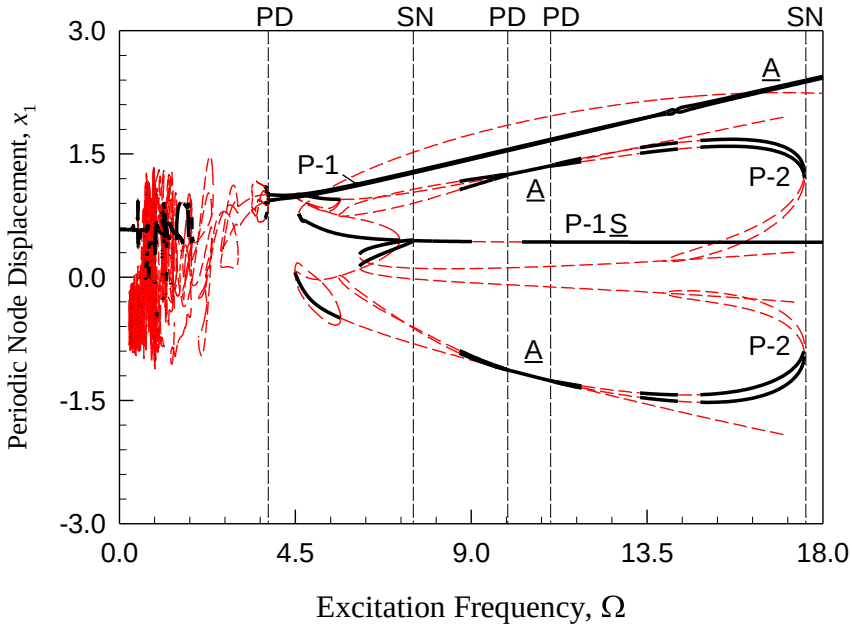

(i)

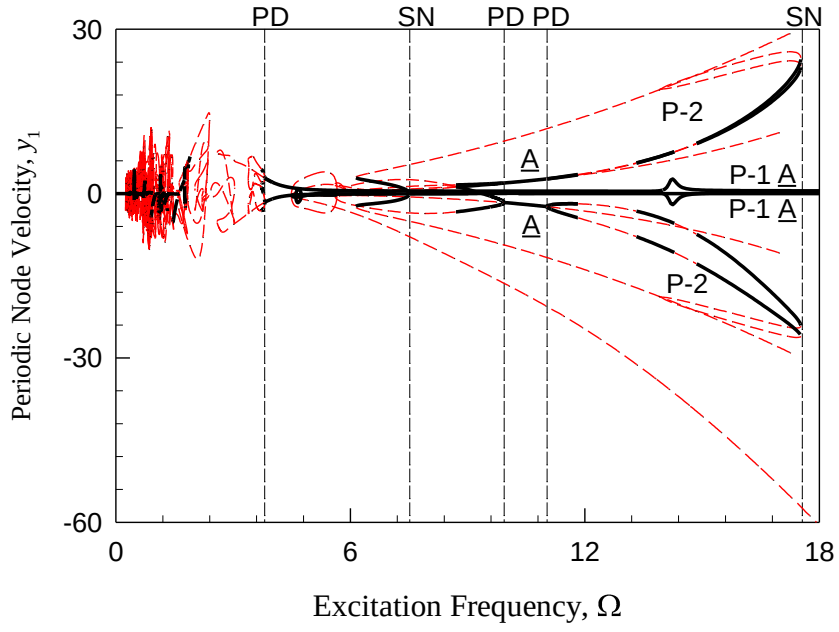

(ii)

Fig. 4. The global view of bifurcation tree of period-1 to period-2 motions varying with excitation frequency ($\Omega \in (0,18)$). (i) node displacement x_1, (ii) node velocity y_1, (iii) node angle x_2, (iv) node angular velocity y_2. ($k_1 = 5$, $k_2 = 100$, $c = 0.1$, $Q_0 = 20.0$, $L = 2$, $T = 2\pi / \Omega$).

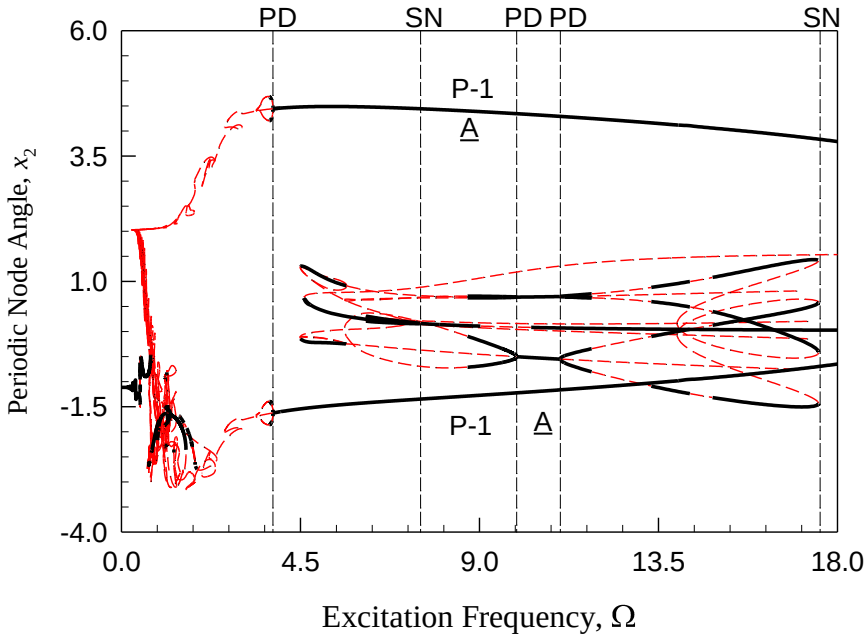

(iii)

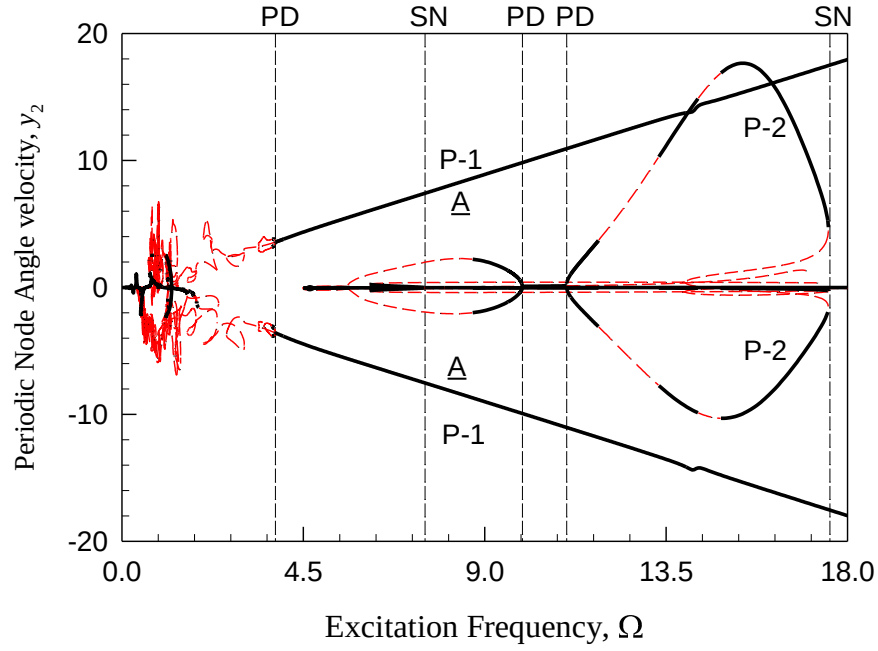

(iv)

Fig. 4 **(**continued)

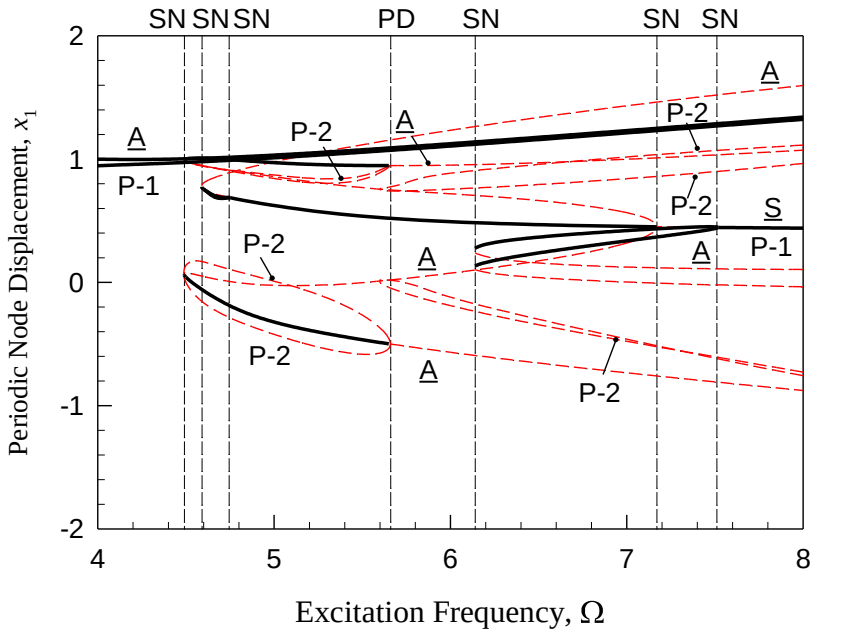

(i)

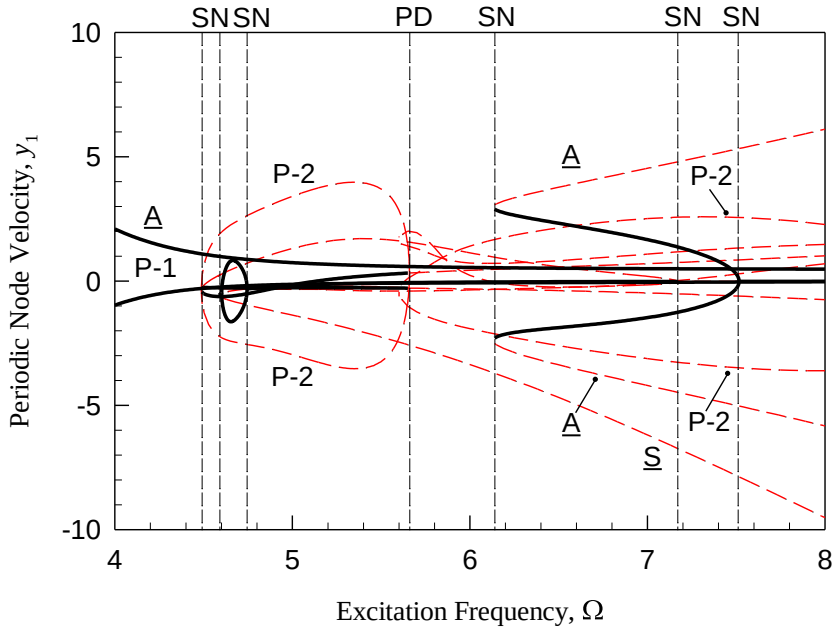

(ii)

Fig. 5. The zoom view of bifurcation tree of period-1 to period-2 motions varying with excitation frequency ($\Omega \in (4.59,18)$). (i) node displacement x_1, (ii) node velocity y_1, (iii) node angle x_2, (iv) node angular velocity y_2. ($k_1 = 5$, $k_2 = 100$, $c = 0.1$, $Q_0 = 20.0$, $L = 2$, $T = 2\pi / \Omega$).

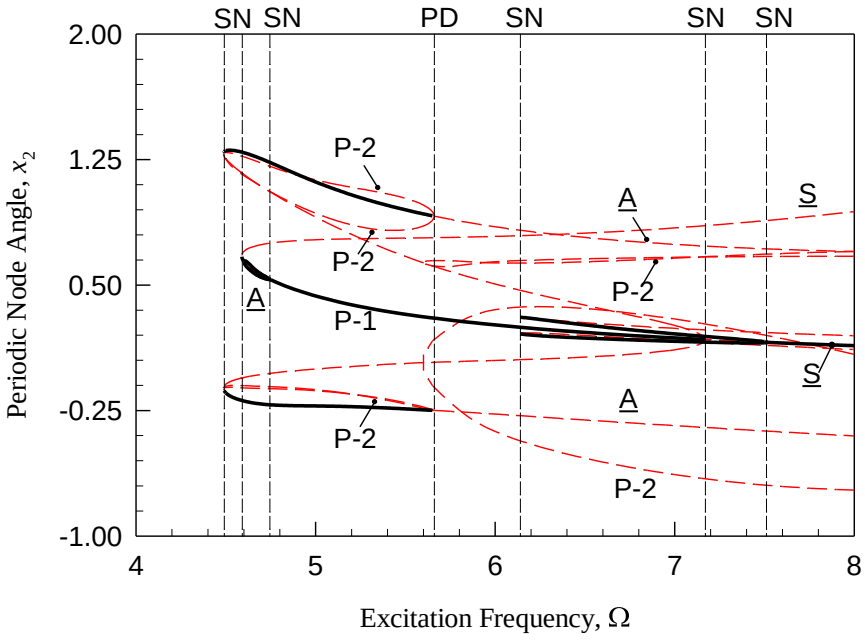

(iii)

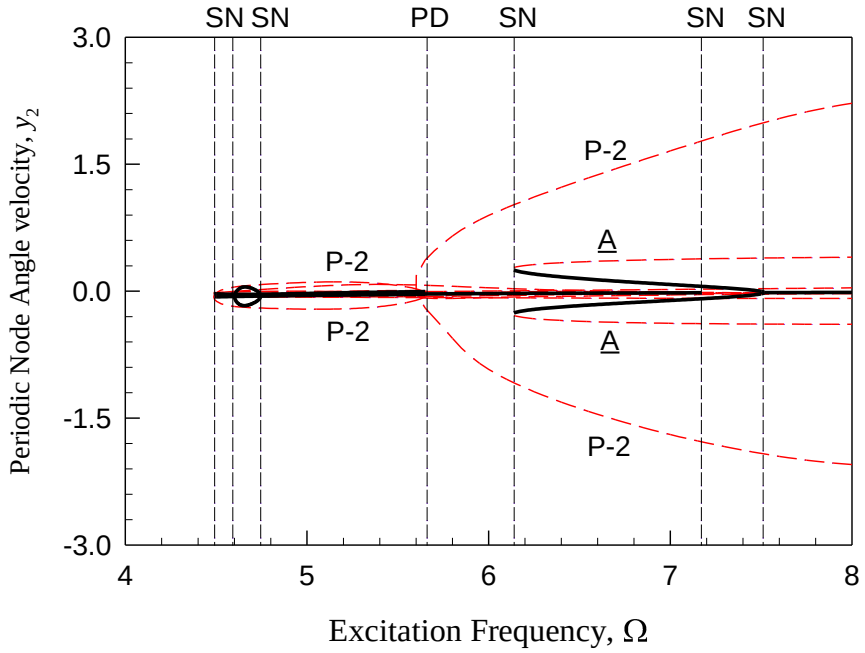

(iv)

Fig. 5 (continued)

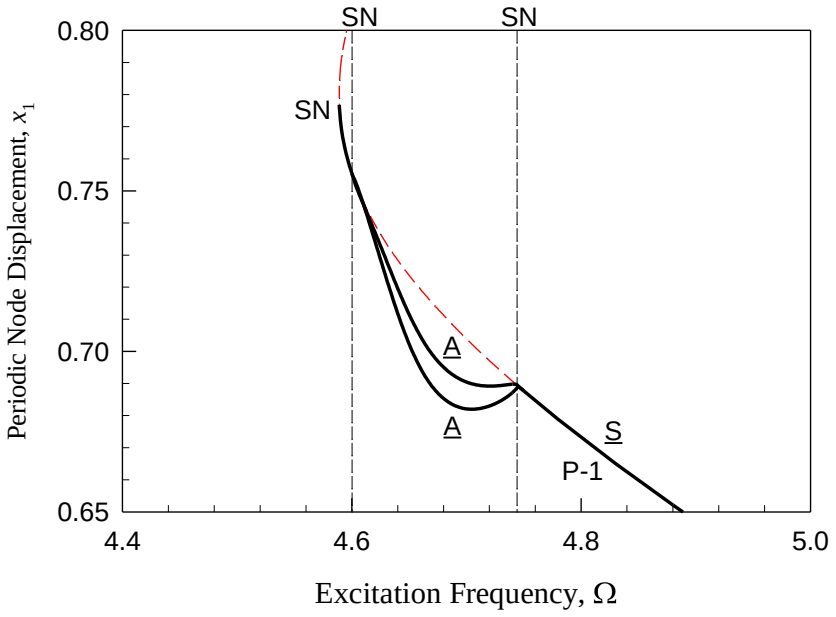

(i)

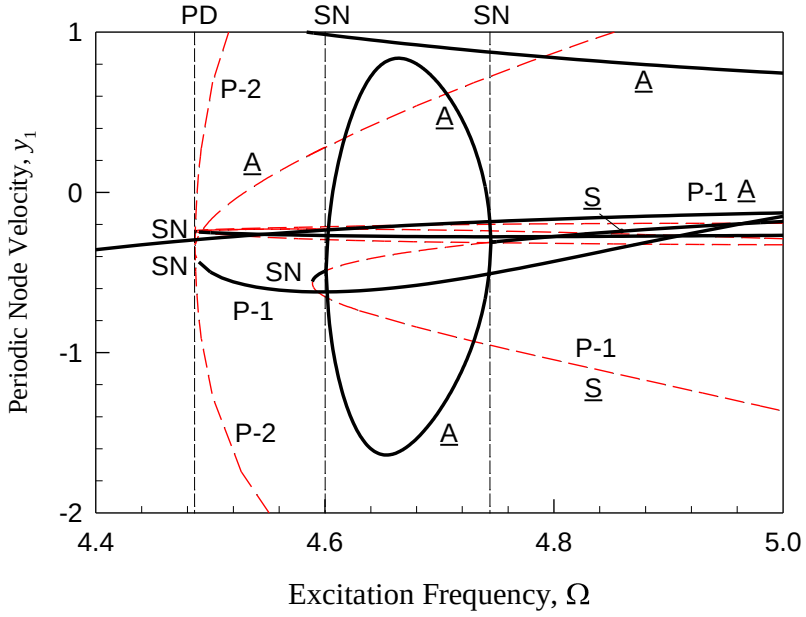

(ii)

Fig. 6. The zoom view of bifurcation tree of period-1 to period-2 motions varying with frequency ($\Omega \in (4.4, 5)$). (i) node displacement x_1, (ii) node velocity y_1, (iii) node angle x_2, (iv) node angular velocity y_2. ($k_1 = 5$, $k_2 = 100$, $c = 0.1$, $Q_0 = 20.0$, $L = 2$, $T = 2\pi / \Omega$).

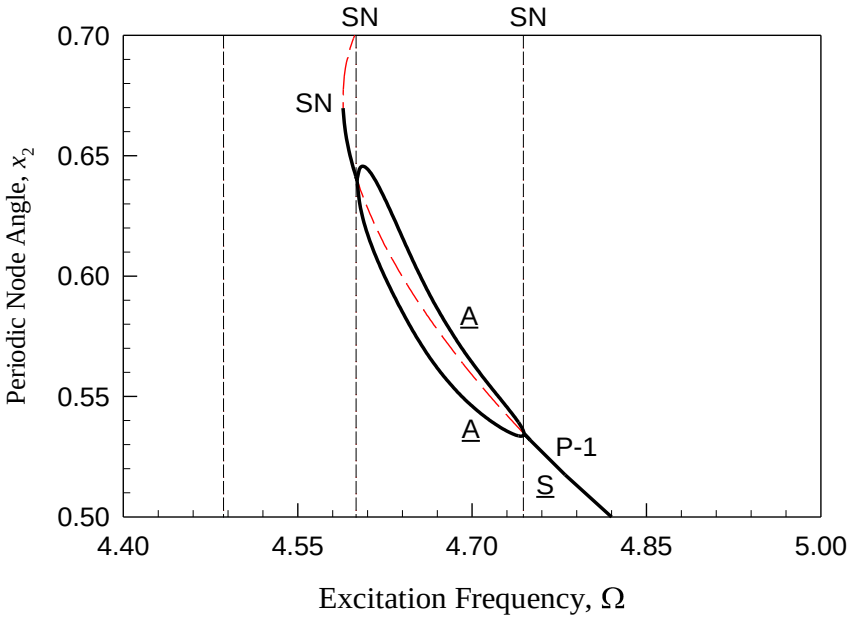

(iii)

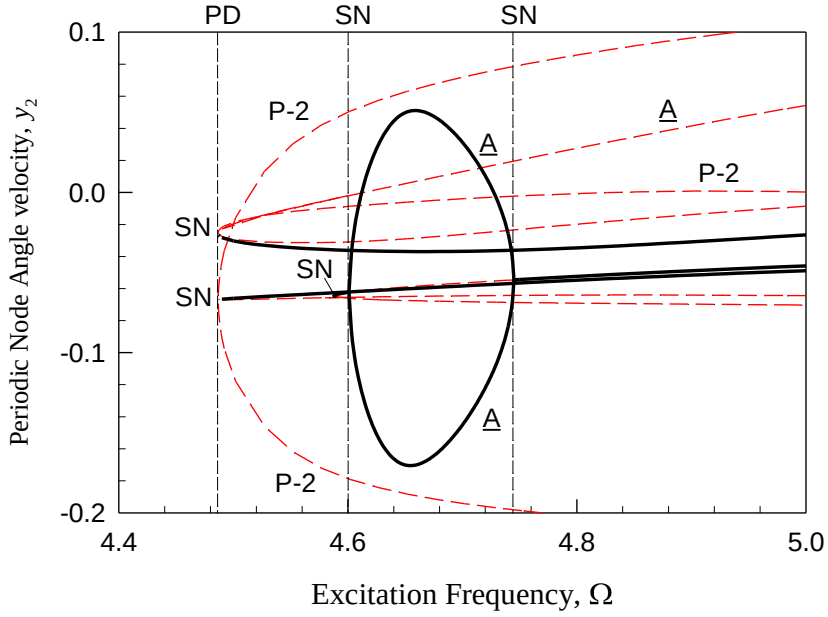

(iv)

Fig. 6 (continued)

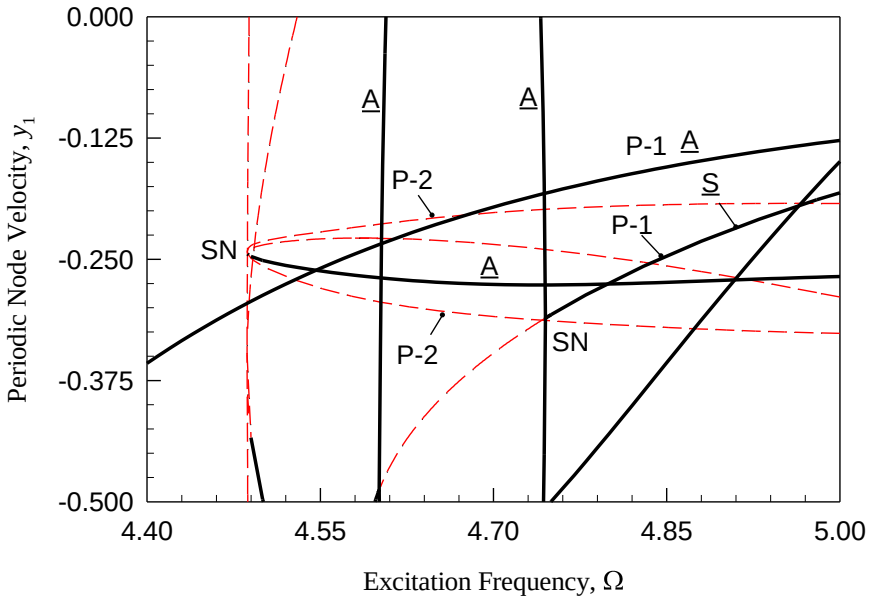

(i)

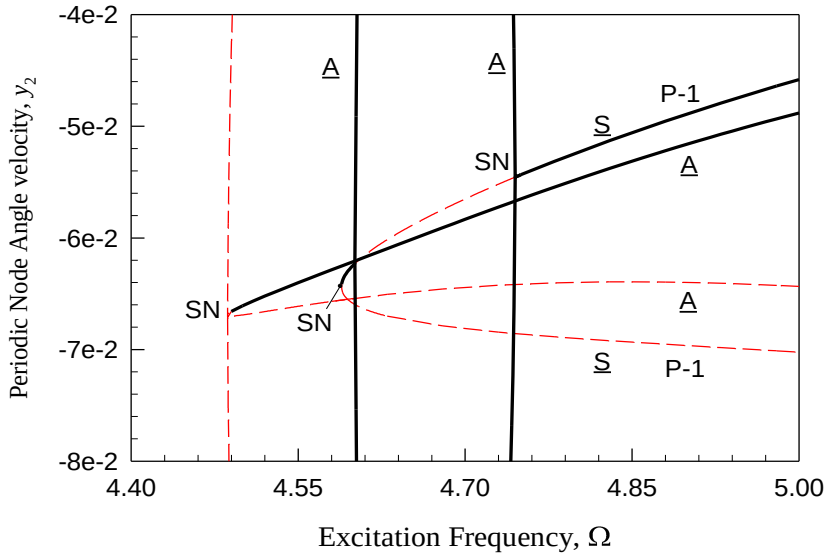

(ii)

Fig. 7. The zoom view of bifurcation tree of period-1 to period-2 motions varying with frequency ($\Omega \in (4.4, 5)$). (i) node velocity y_1, (ii) node angular velocity y_2. ($k_1 = 5$, $k_2 = 100$, $c = 0.1$, $Q_0 = 20.0$, $L = 2$, $T = 2\pi / \Omega$).

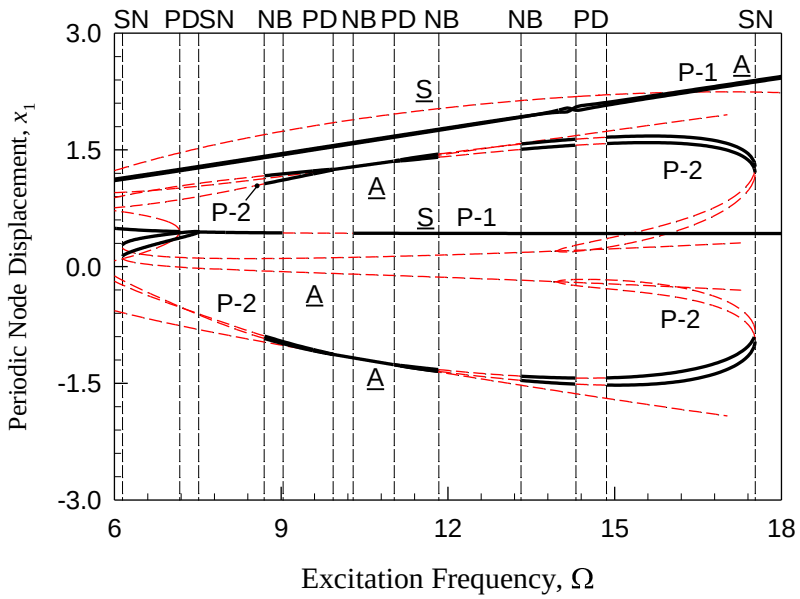

(i)

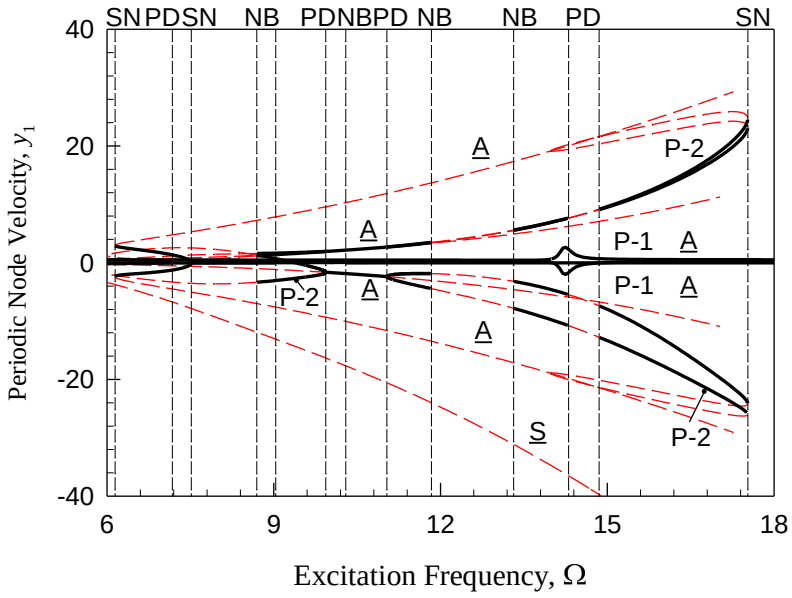

(ii)

Fig. 8. The zoom view of bifurcation tree of period-1 to period-2 motions varying with frequency ($\Omega \in (6,18)$). (i) node displacement x_1, (ii) node velocity y_1, (iii) node angle x_2, (iv) node angular velocity y_2. ($k_1 = 5$, $k_2 = 100$, $c = 0.1$, $Q_0 = 20.0$, $L = 2$, $T = 2\pi / \Omega$).

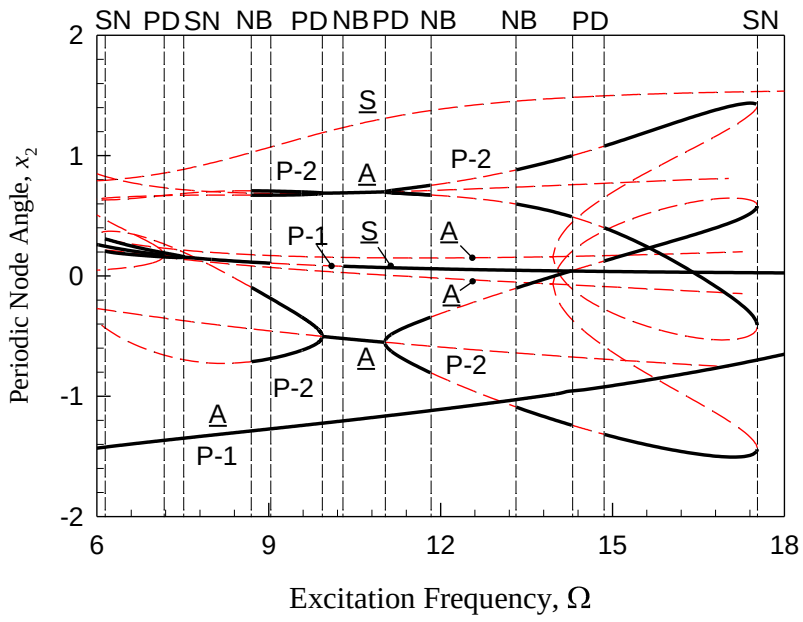

(iii)

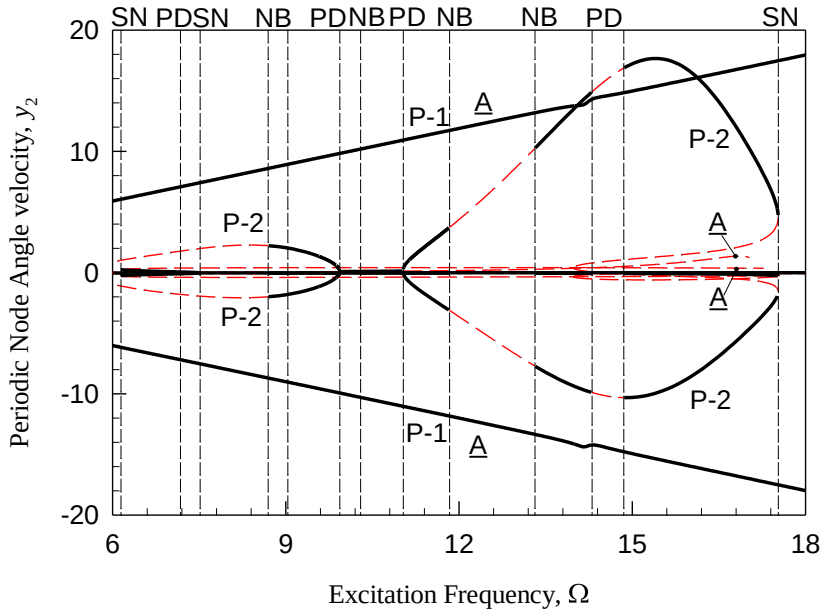

(iv)

Fig. 8 (continued)

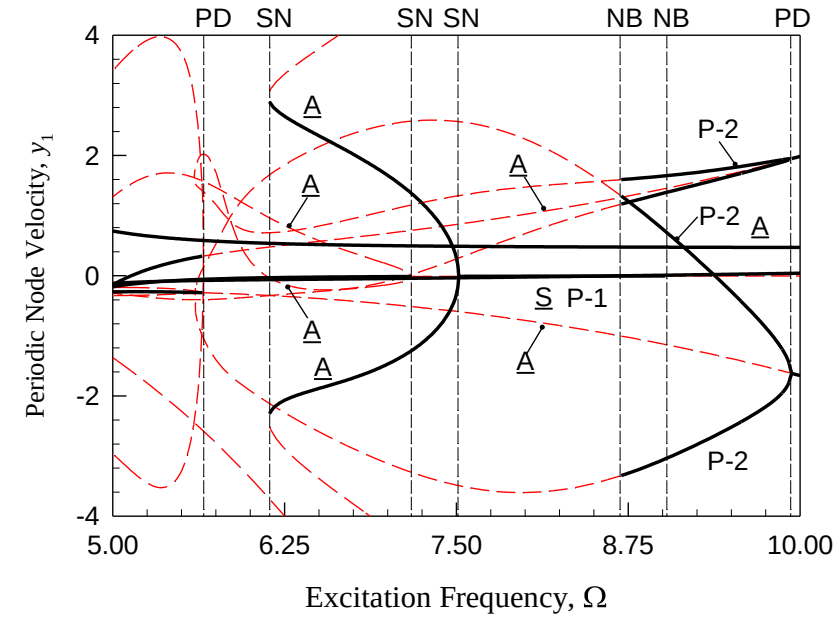

(i)

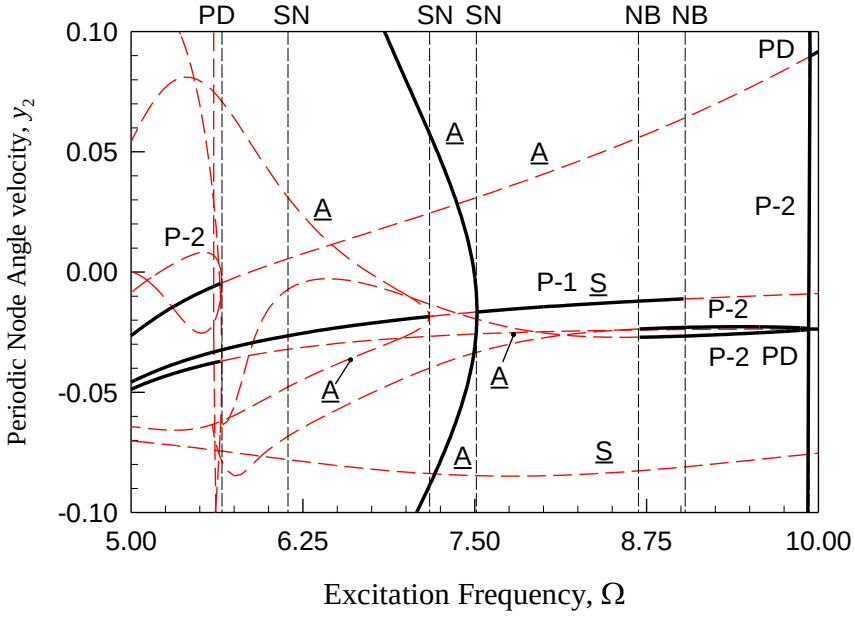

(ii)

Fig. 9. The zoom view of bifurcation tree of period-1 to period-2 motions varying with frequency ($\Omega \in (5,10)$).(i) node velocity y_1, (ii) node angular velocity y_2. ($k_1 = 5$, $k_2 = 100$, $c = 0.1$, $Q_0 = 20.0$, $L = 2$, $T = 2\pi / \Omega$).

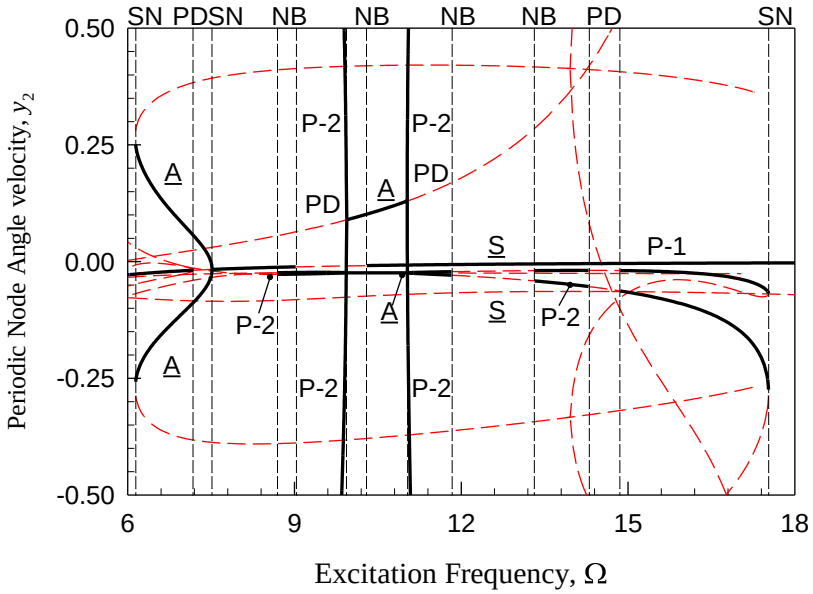

Fig. 10. The zoom view of bifurcation tree of period-1 to period-2 motions varying with frequency ($\Omega \in (6,18)$). Node angular velocity y_2. ($k_1 = 5$, $k_2 = 100$, $c = 0.1$, $Q_0 = 20.0$, $L = 2$, $T = 2\pi / \Omega$).

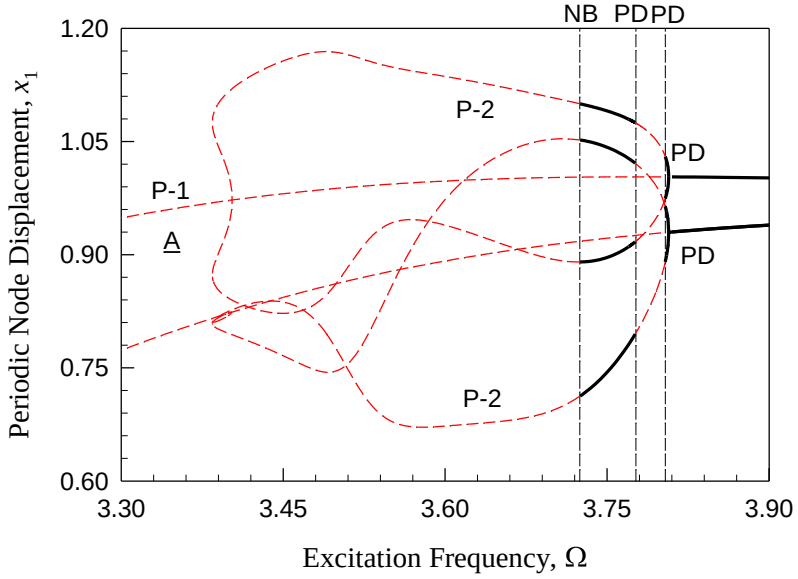

(i)

Fig. 11. The zoom view of bifurcation tree of period-1 to period-2 motions varying with frequency ($\Omega \in (3.30, 3.90)$). (i) node displacement x_1, (ii) node velocity y_2. (iii) node angle x_2, (iv) node angular velocity y_2 ($k_1 = 5$, $k_2 = 100$, $c = 0.1$, $Q_0 = 20.0$, $L = 2$, $T = 2\pi / \Omega$).

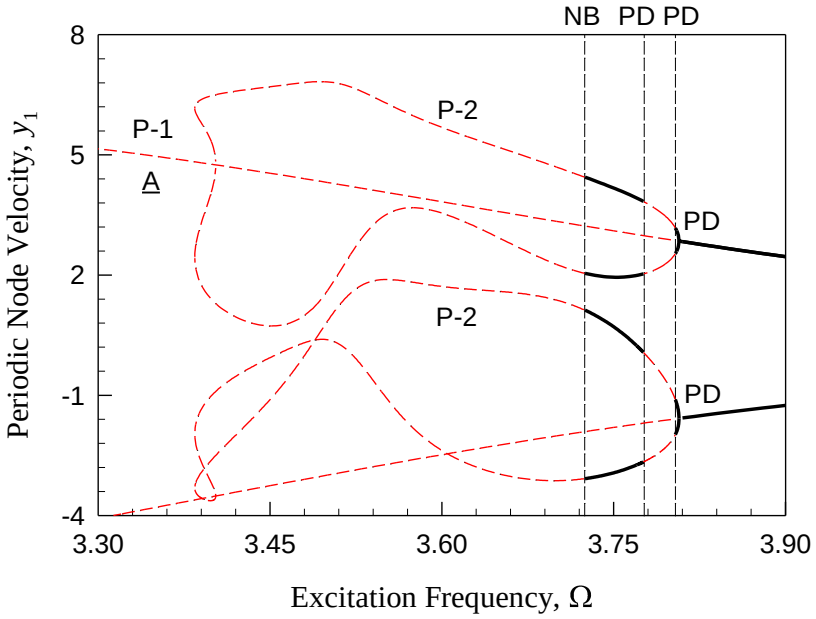

(ii)

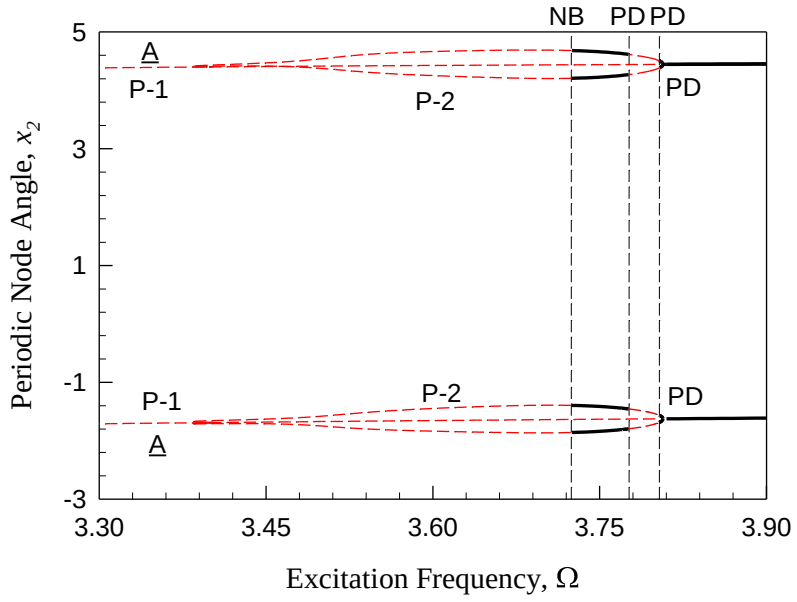

(iii)

Fig. 11. (continued)

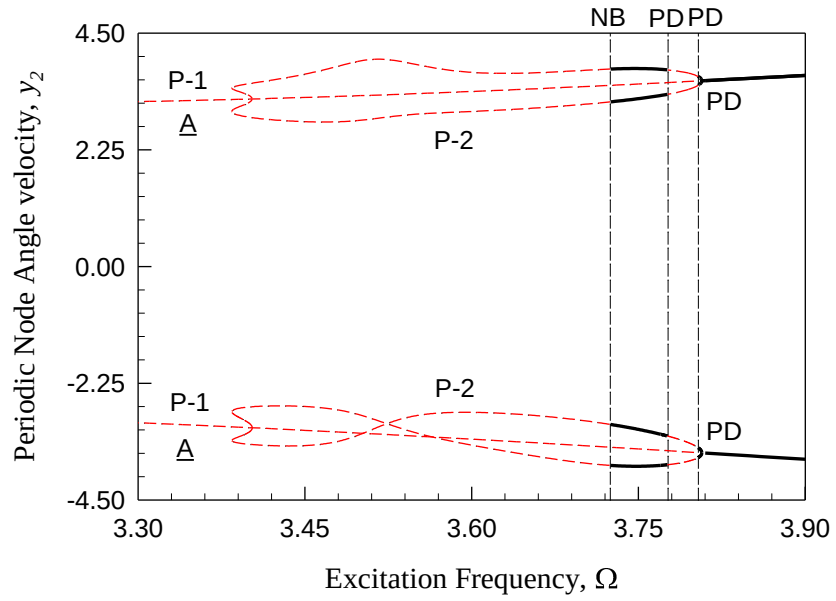

(iv)

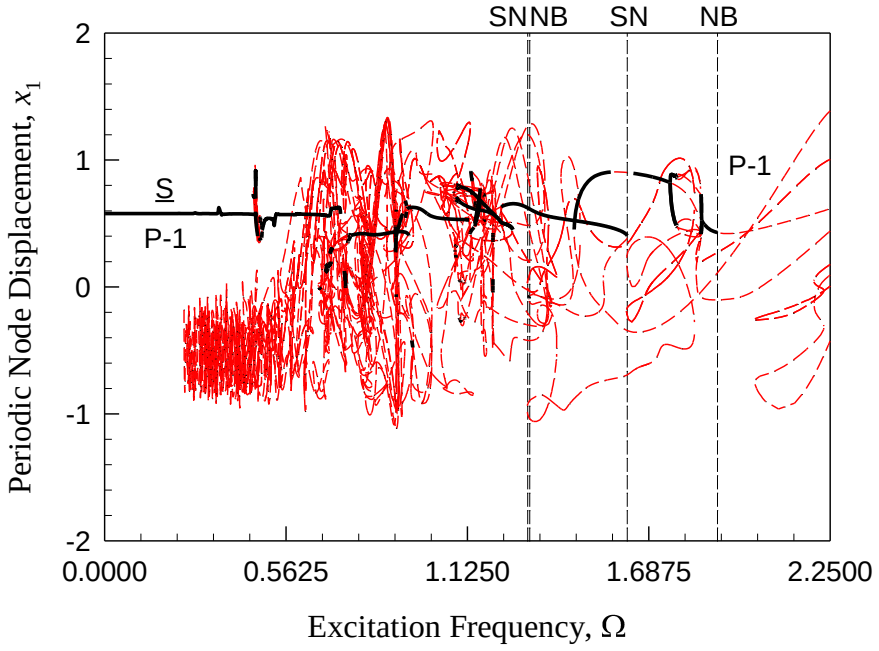

(i)

Fig. 12. The zoom view of bifurcation tree of period-1 to period-2 motions varying with frequency ($\Omega \in (0, 2.25)$). (i) node displacement x_1, (ii) node velocity y_2. (iii) node angle x_2, (iv) node angular velocity y_2 ($k_1 = 5$, $k_2 = 100$, $c = 0.1$, $Q_0 = 20.0$, $L = 2$, $T = 2\pi / \Omega$).

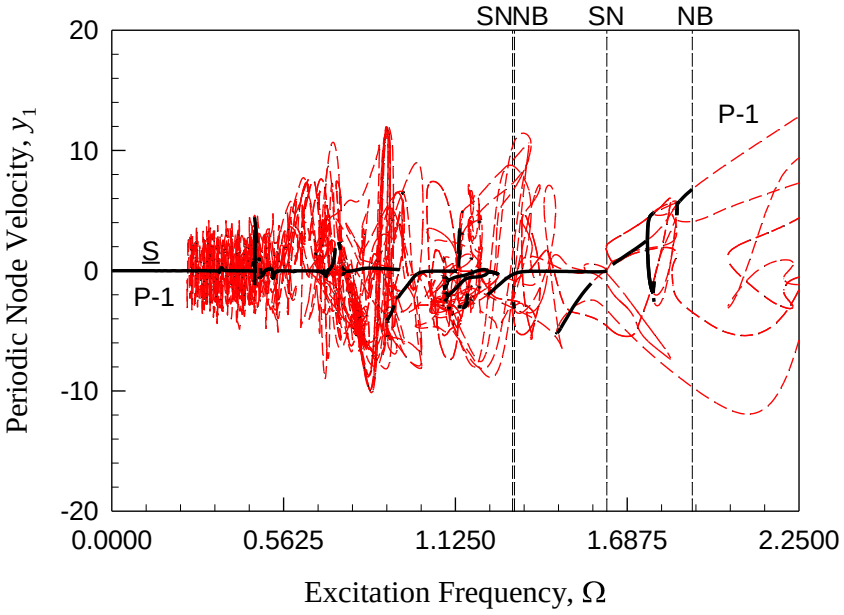

(ii)

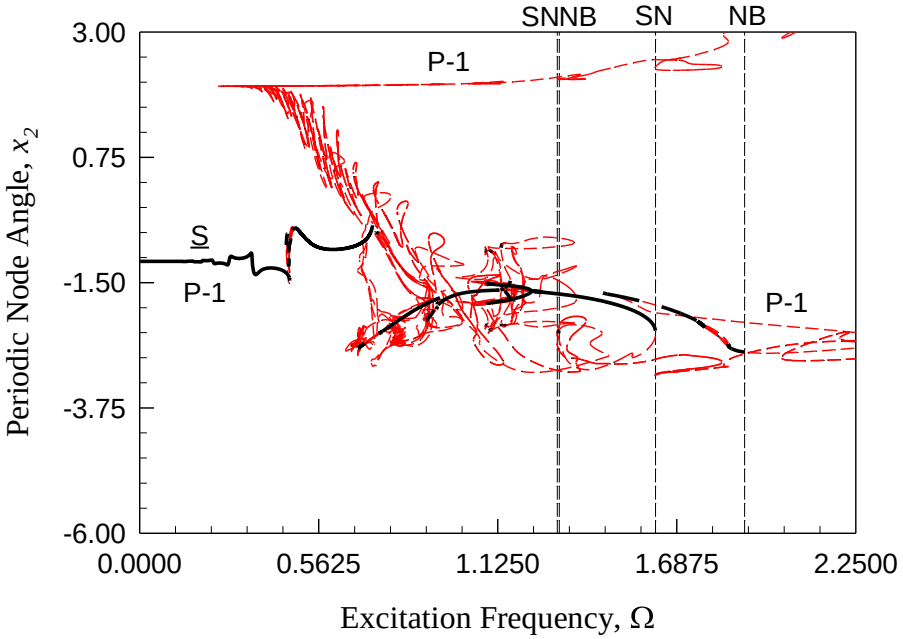

(iii)

Fig. 12. (continued)

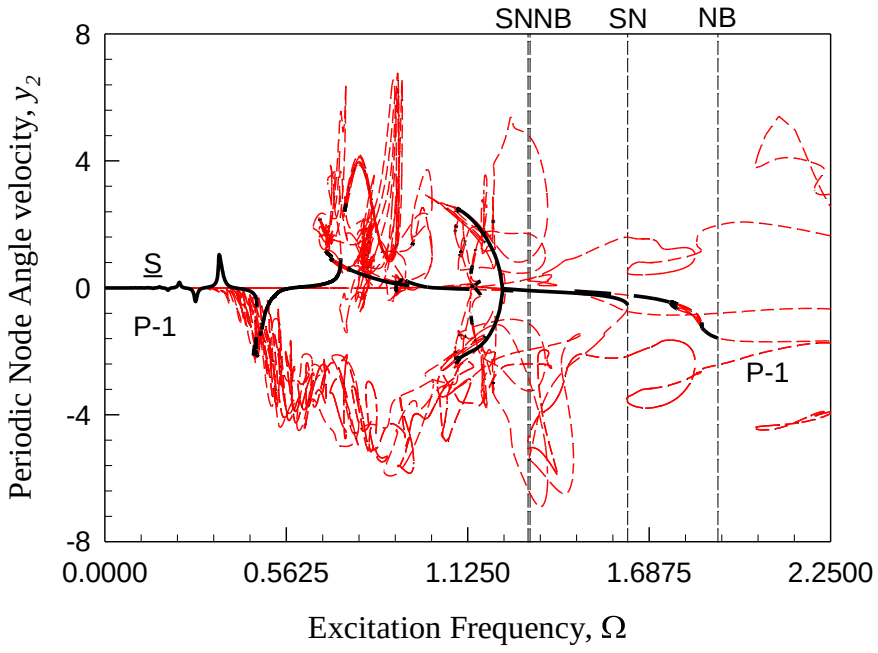

(iv)

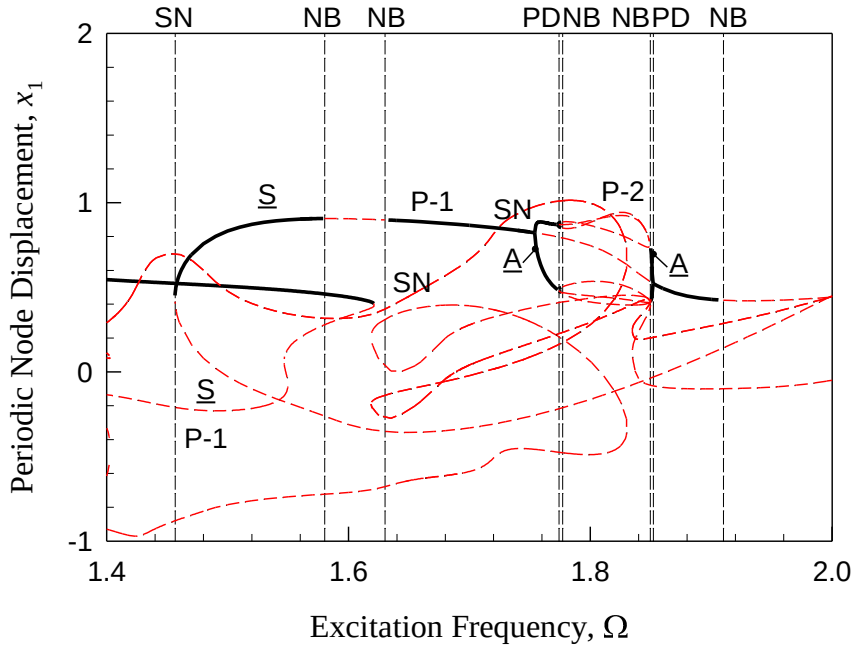

(i)

Fig. 13. The zoom view of bifurcation tree of period-1 to period-2 motions varying with frequency ($\Omega \in (1.4, 2)$). (i) node displacement x_1, (ii) node velocity y_2. (iii) node angle x_2, (iv) node angular velocity y_2 ($k_1 = 5$, $k_2 = 100$, $c = 0.1$, $Q_0 = 20.0$, $L = 2$, $T = 2\pi / \Omega$).

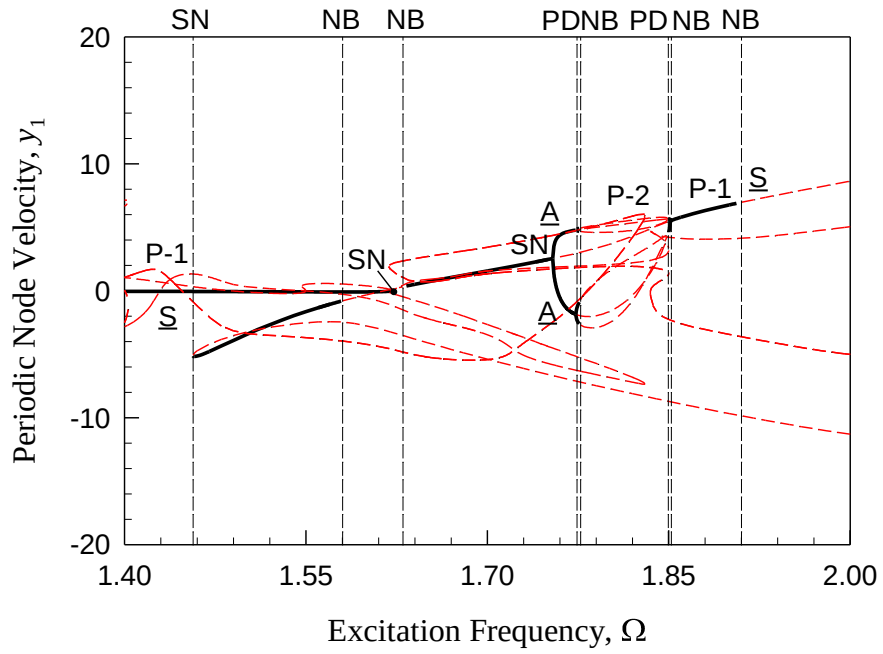

(ii)

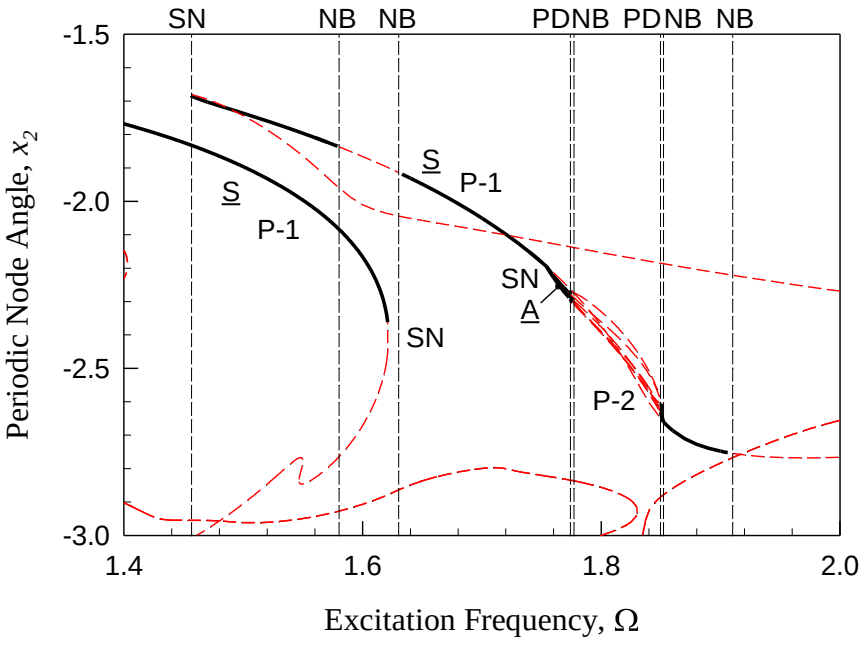

(iii)

Fig. 13. (continued)

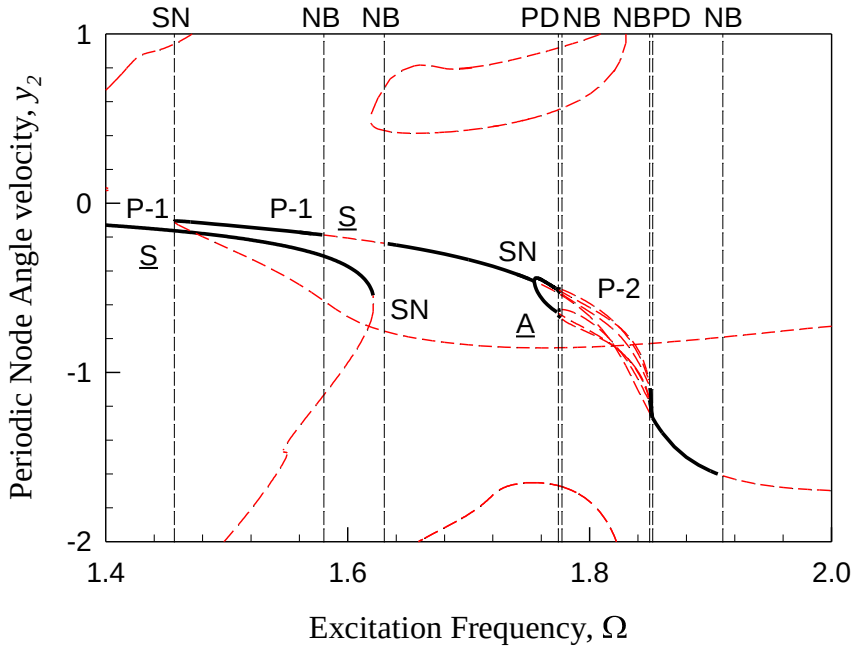

(iv)

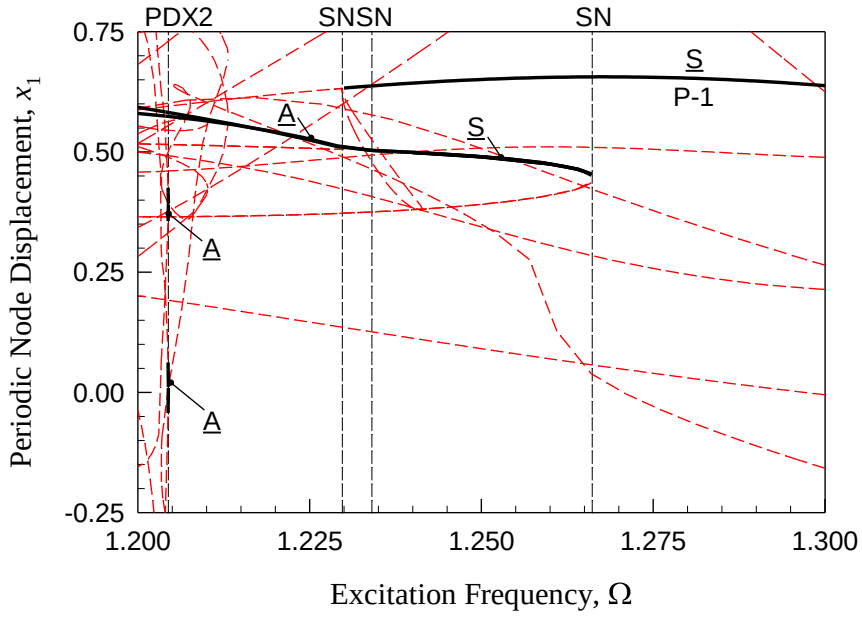

(i)

Fig. 14. The zoom view of bifurcation tree of period-1 to period-2 motions varying with frequency ($\Omega \in (1.2,1.3)$). (i) node displacement x_1, (ii) node velocity y_2. (iii) node angle x_2, (iv) node angular velocity y_2 ($k_1 = 5$, $k_2 = 100$, $c = 0.1$, $Q_0 = 20.0$, $L = 2$, $T = 2\pi/\Omega$).

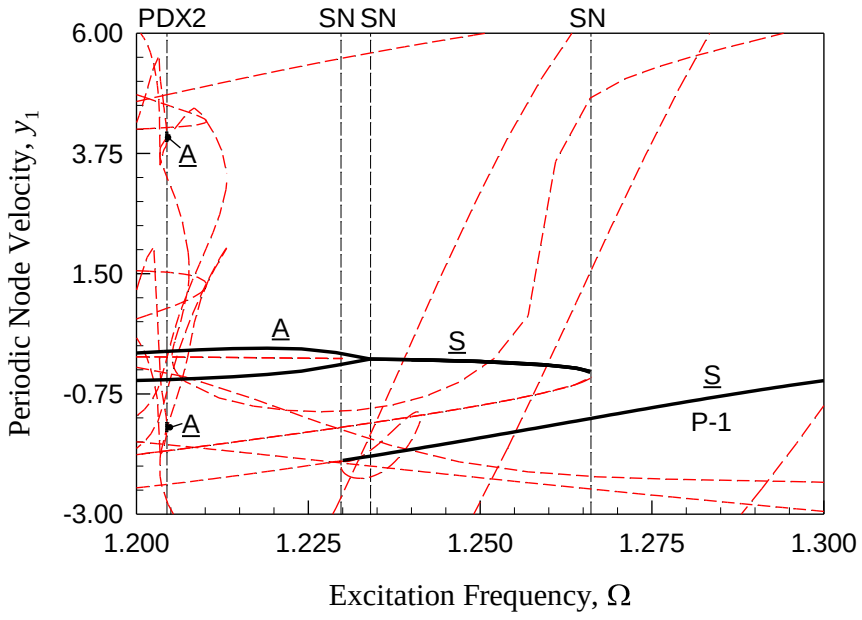

(ii)

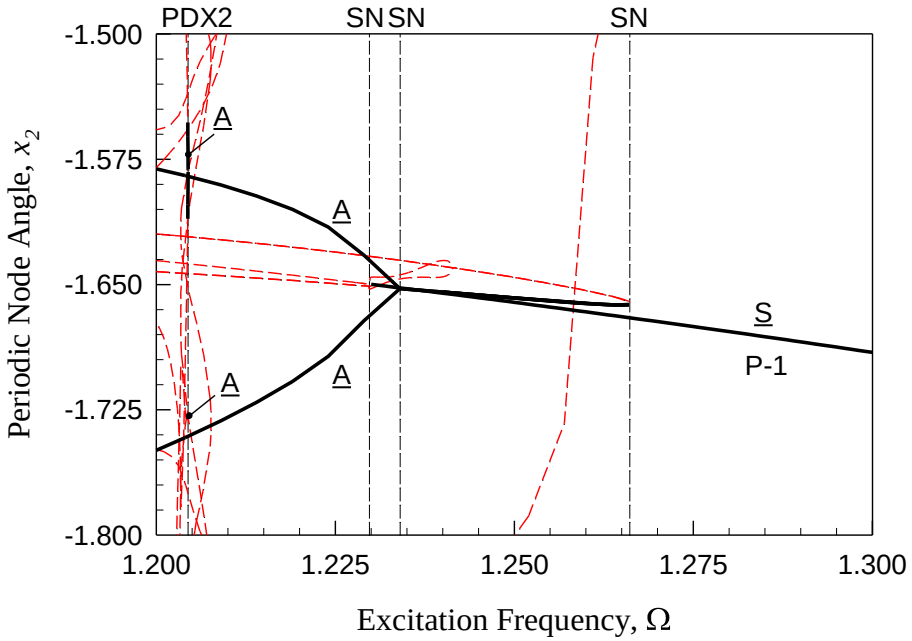

(iii)

Fig. 14. (continued)

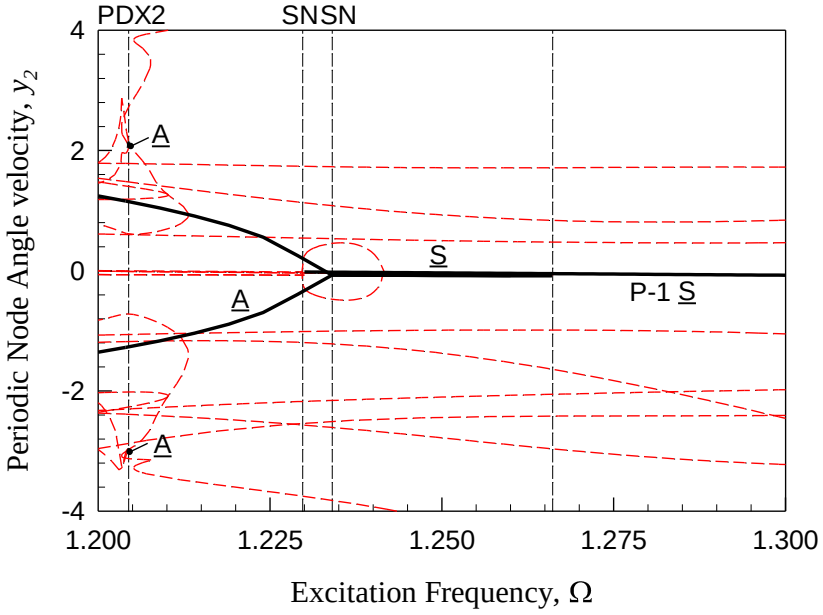

(iv)

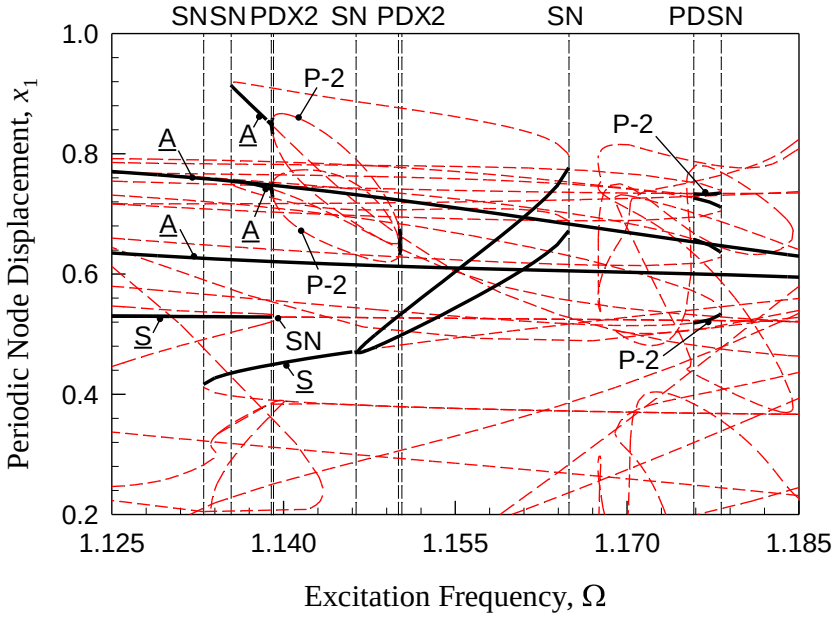

(i)

Fig. 15. The zoom view of bifurcation tree of period-1 to period-2 motions varying with frequency ($\Omega \in (1.125,1.185)$). (i) node displacement x_1, (ii) node velocity y_2. (iii) node angle x_2, (iv) node angular velocity y_2 ($k_1 = 5$, $k_2 = 100$, $c = 0.1$, $Q_0 = 20.0$, $L = 2$, $T = 2\pi/\Omega$).

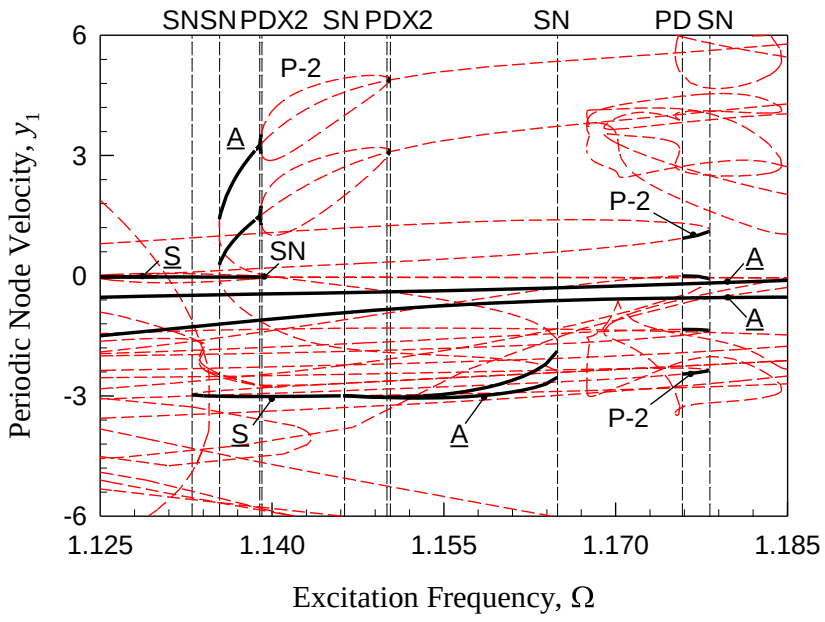

(ii)

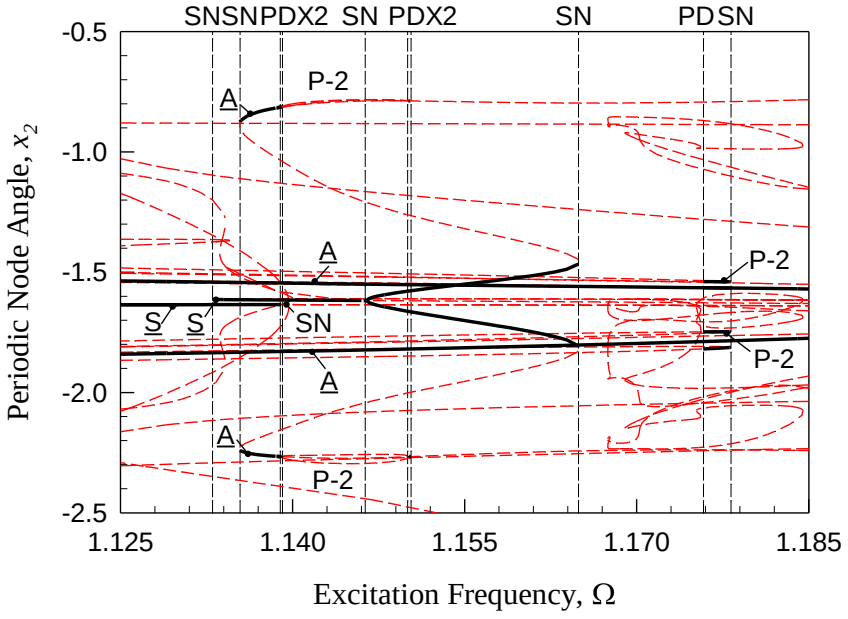

(iii)

Fig. 15. (continued)

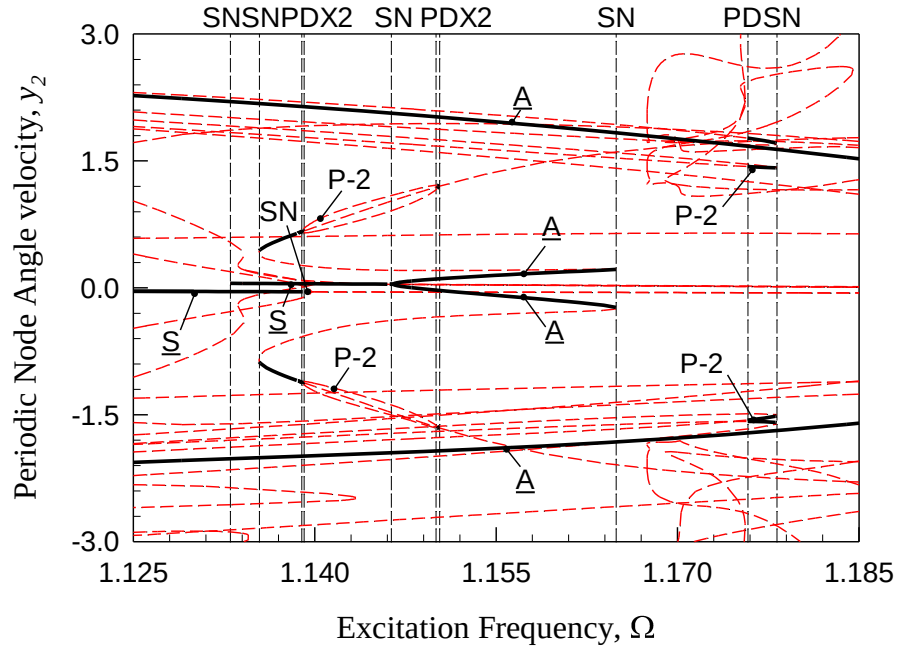

(iv)

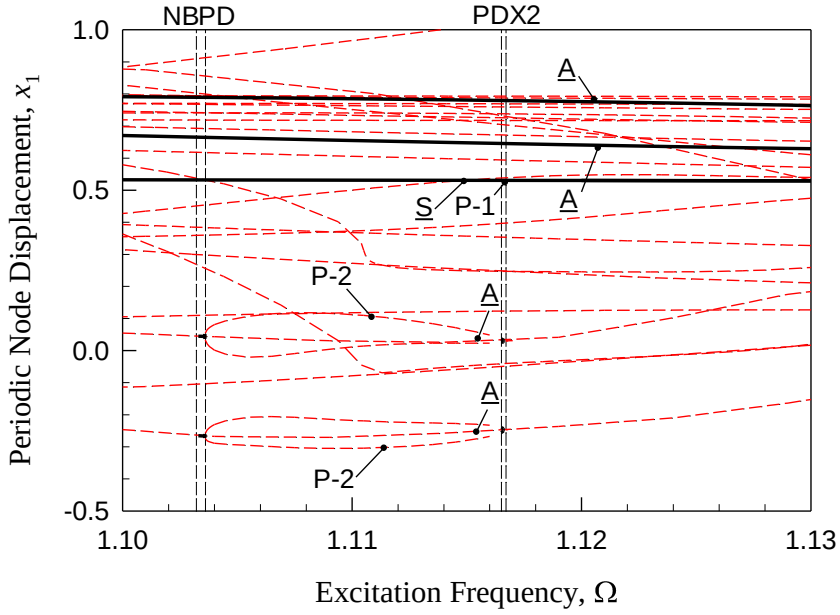

(i)

Fig. 16. The zoom view of bifurcation tree of period-1 to period-2 motions varying with frequency ($\Omega \in (1.10, 1.13)$). (i) node displacement x_1, (ii) node velocity y_2. (iii) node angle x_2, (iv) node angular velocity y_2 ($k_1 = 5$, $k_2 = 100$, $c = 0.1$, $Q_0 = 20.0$, $L = 2$, $T = 2\pi / \Omega$).

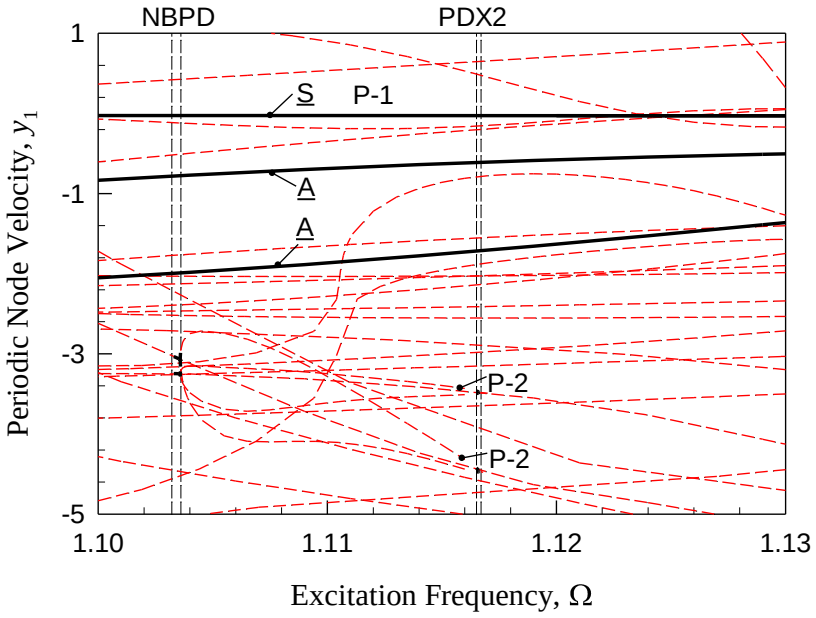

(ii)

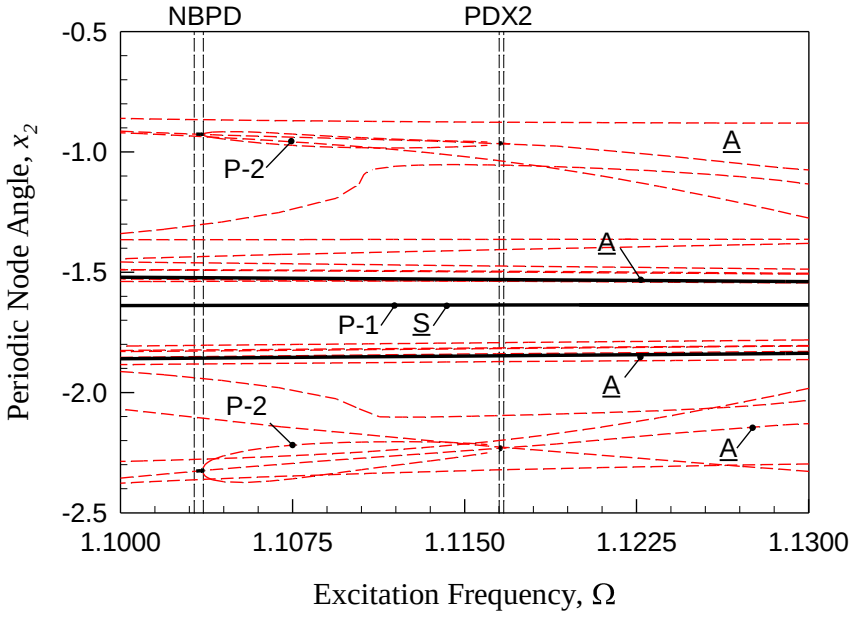

(iii)

Fig.16 (continued)

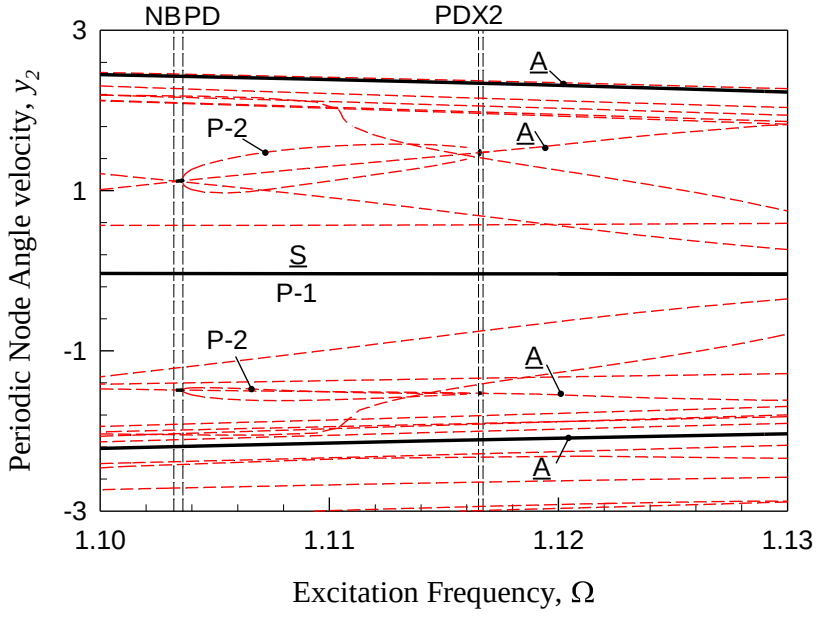

(iv)

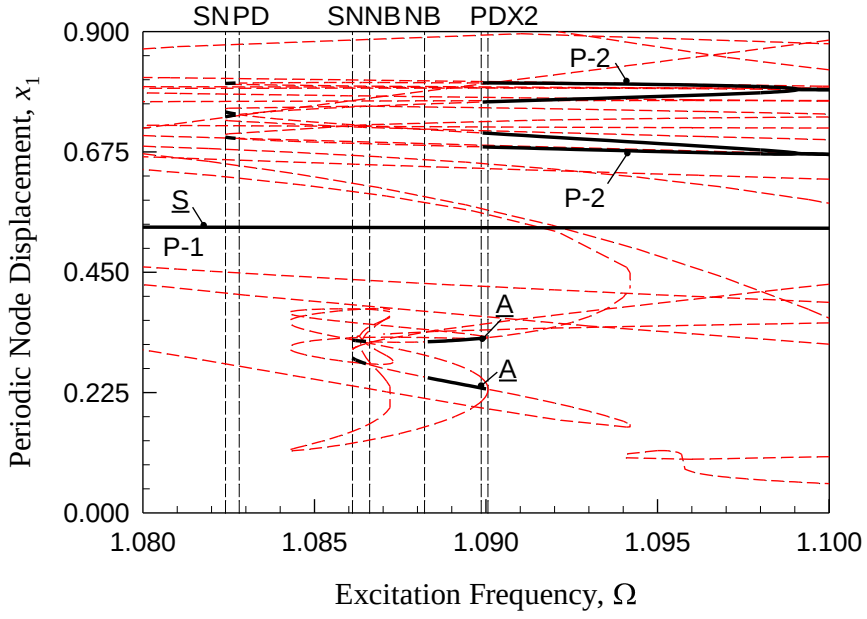

(i)

Fig. 17. The zoom view of bifurcation tree of period-1 to period-2 motions varying with frequency ($\Omega \in (1.08, 1.1)$). (i) node displacement x_1, (ii) node velocity y_2. (iii) node angle x_2, (iv) node angular velocity y_2 ($k_1 = 5$, $k_2 = 100$, $c = 0.1$, $Q_0 = 20.0$, $L = 2$, $T = 2\pi / \Omega$).

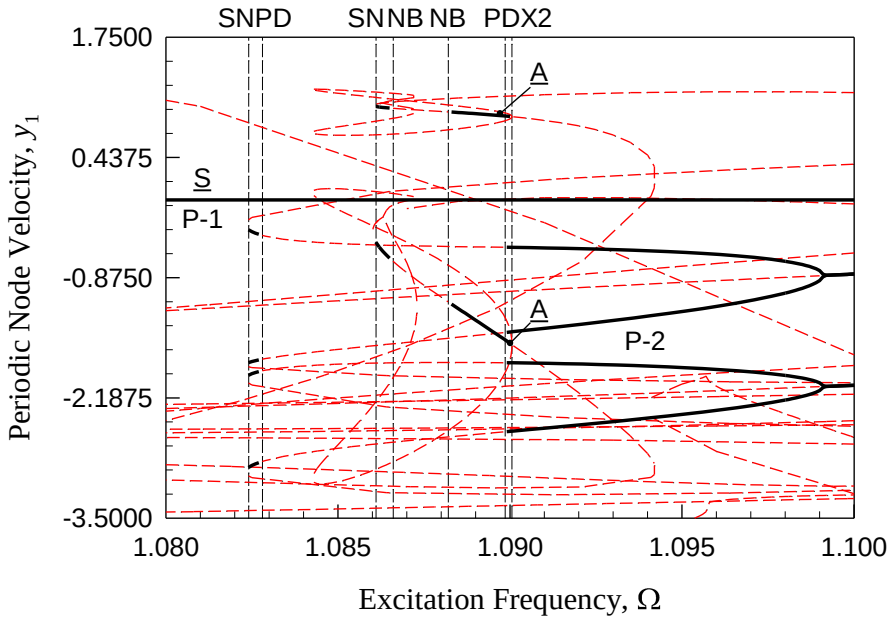

(ii)

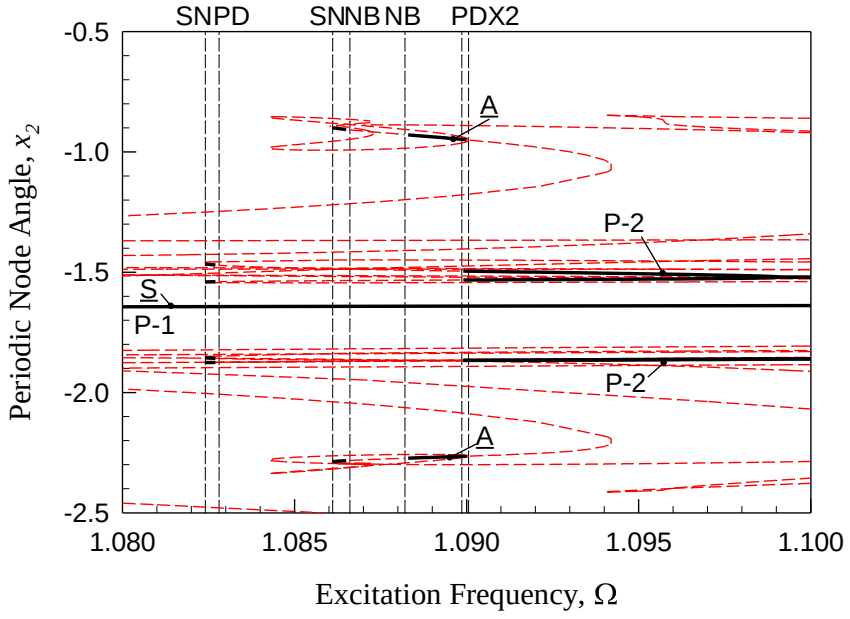

(iii)

Fig. 17. (continued)

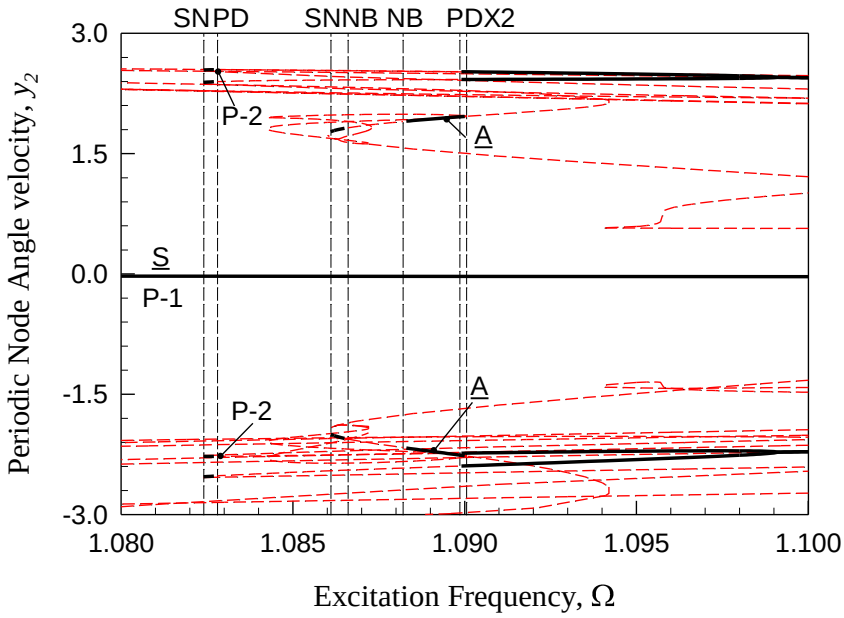

(iv)

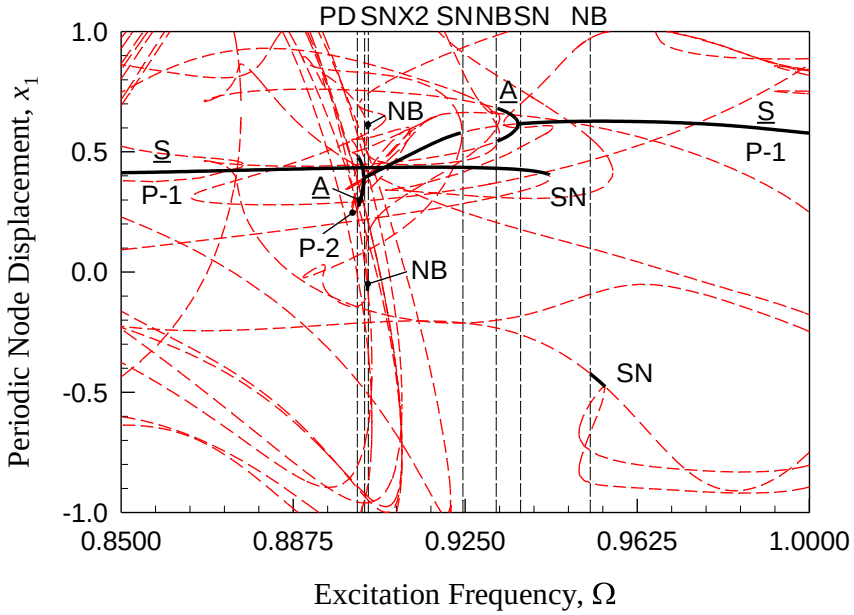

(i)

Fig. 18. The zoom view of bifurcation tree of period-1 to period-2 motions varying with frequency ($\Omega \in (0.85,1)$). (i) node displacement x_1 , (ii) node velocity y_2. (iii) node angle x_2, (iv) node angular velocity y_2 ($k_1 = 5$, $k_2 = 100$, $c = 0.1$, $Q_0 = 20.0$, $L = 2$, $T = 2\pi / \Omega$).

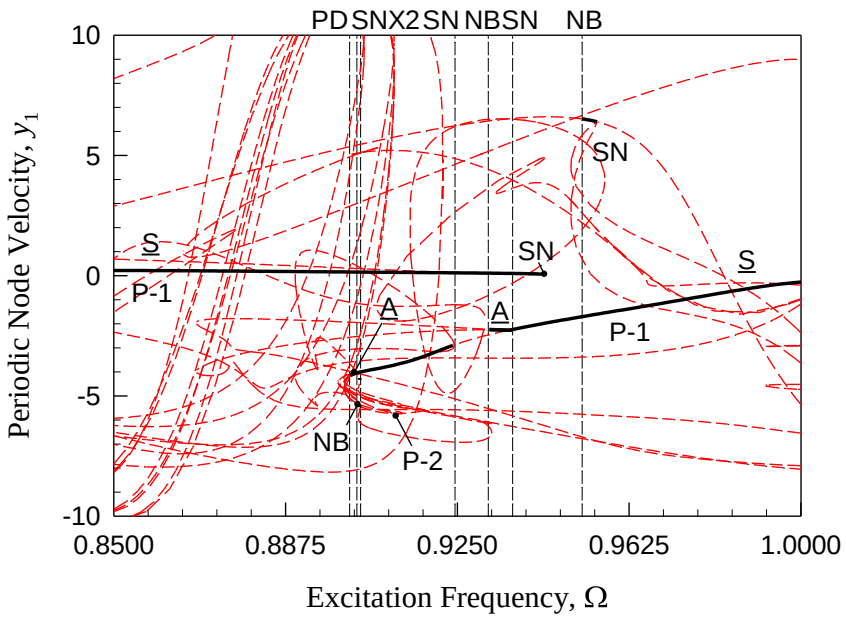

(ii)

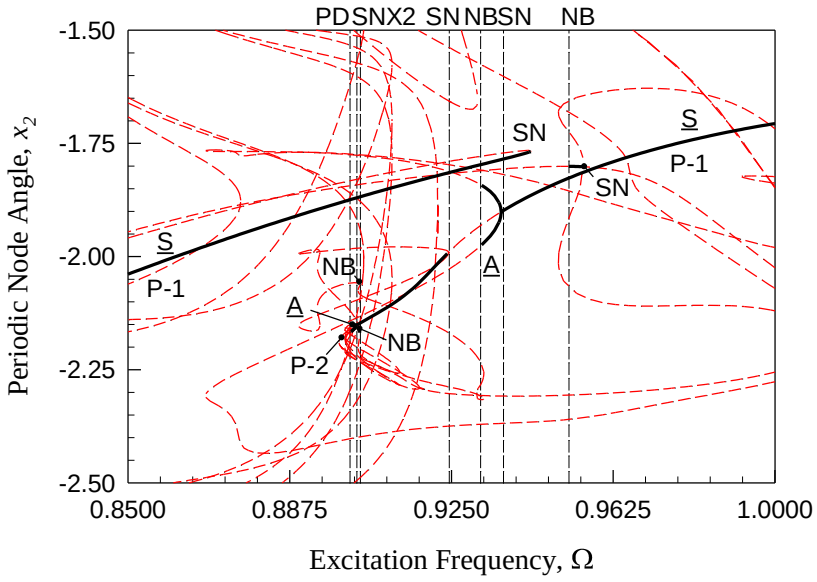

(iii)

Fig. 18. (continued)

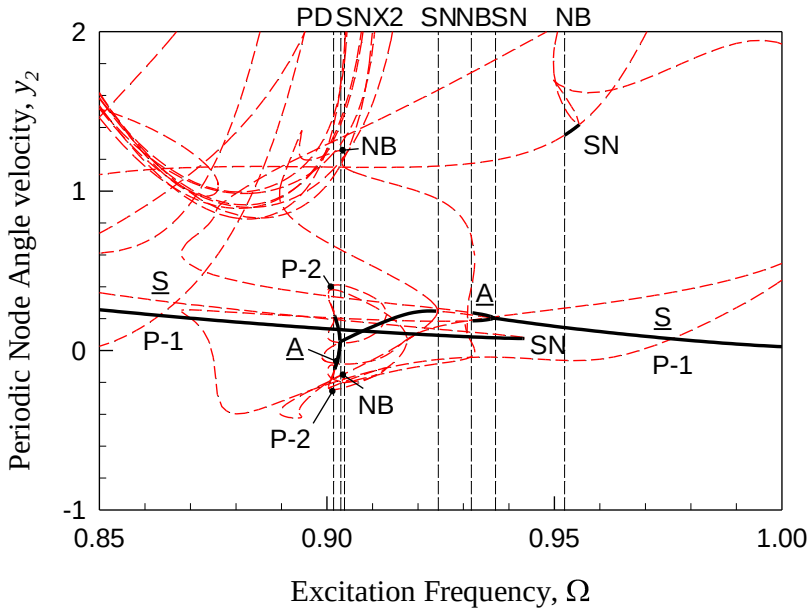

(iv)

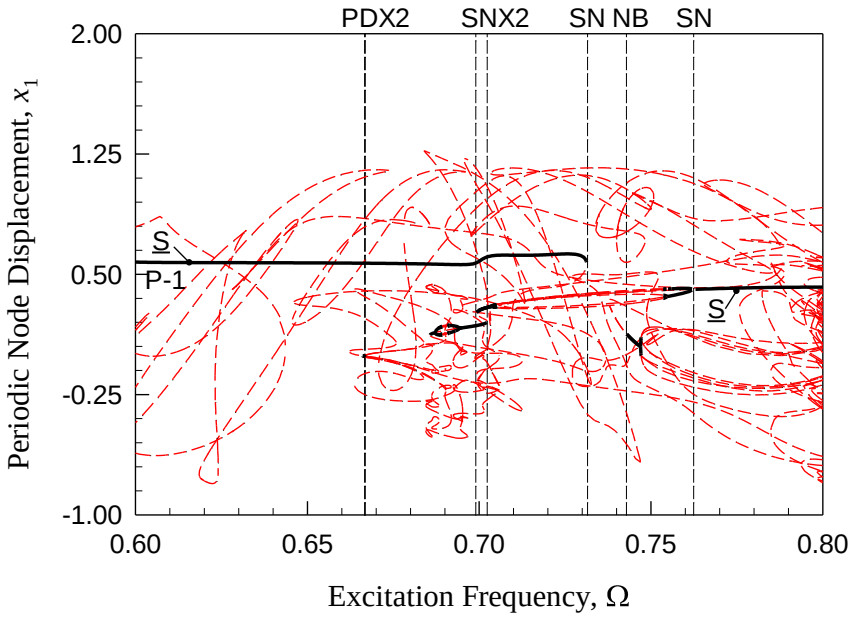

(i)

Fig. 19. The zoom view of bifurcation tree of period-1 to period-2 motions varying with frequency ($\Omega \in (0.6, 0.8)$). (i) node displacement x_1, (ii) node velocity y_2. (iii) node angle x_2, (iv) node angular velocity y_2 ($k_1 = 5$, $k_2 = 100$, $c = 0.1$, $Q_0 = 20.0$, $L = 2$, $T = 2\pi / \Omega$).

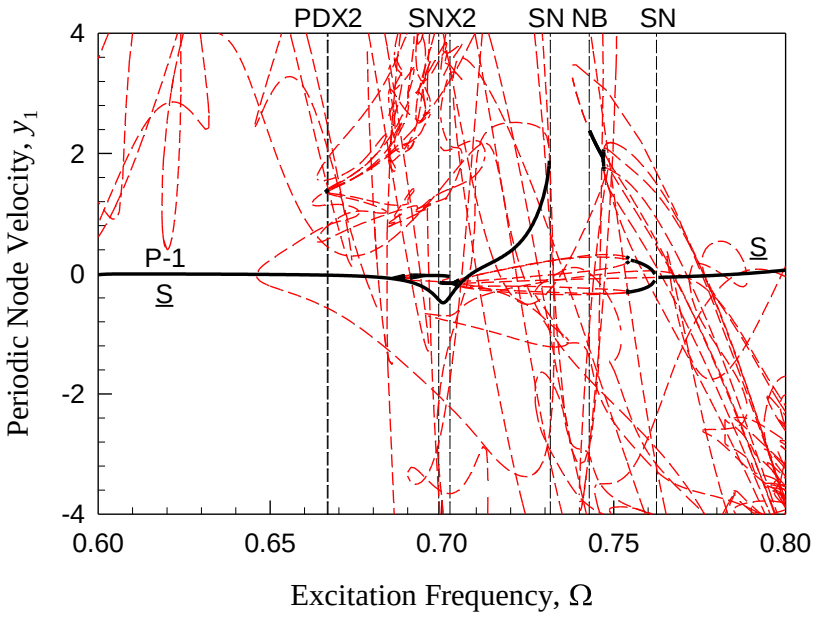

(ii)

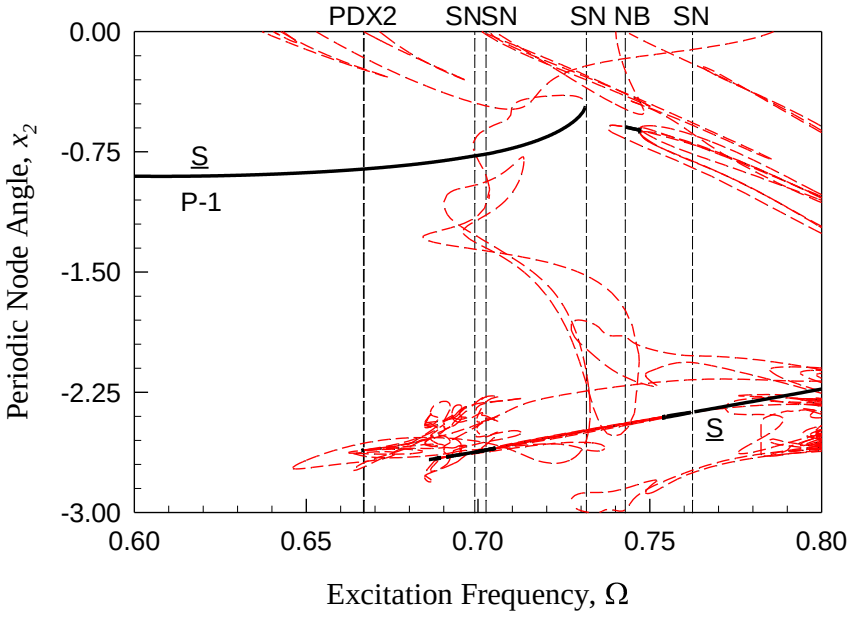

(iii)

Fig. 19. (continued)

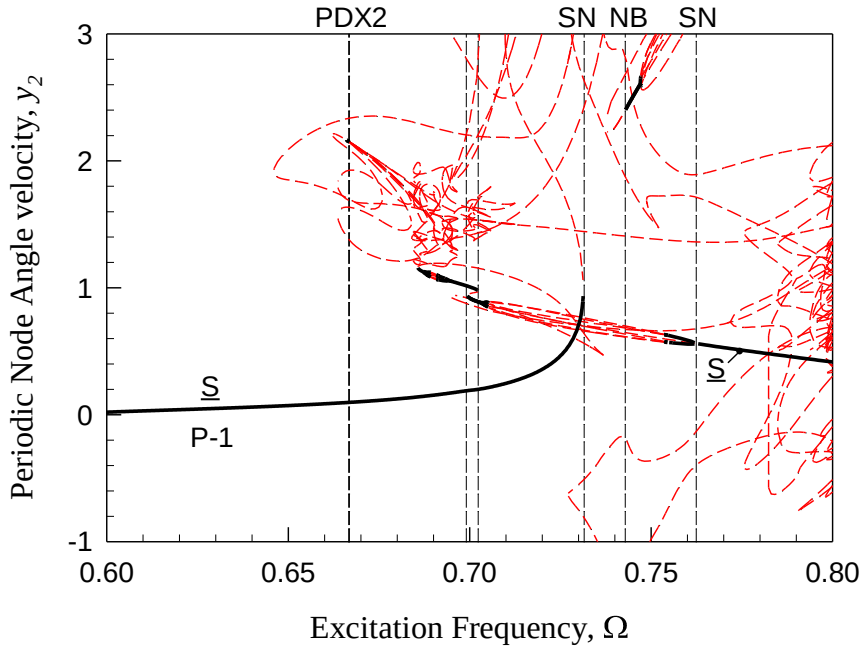

(iv)

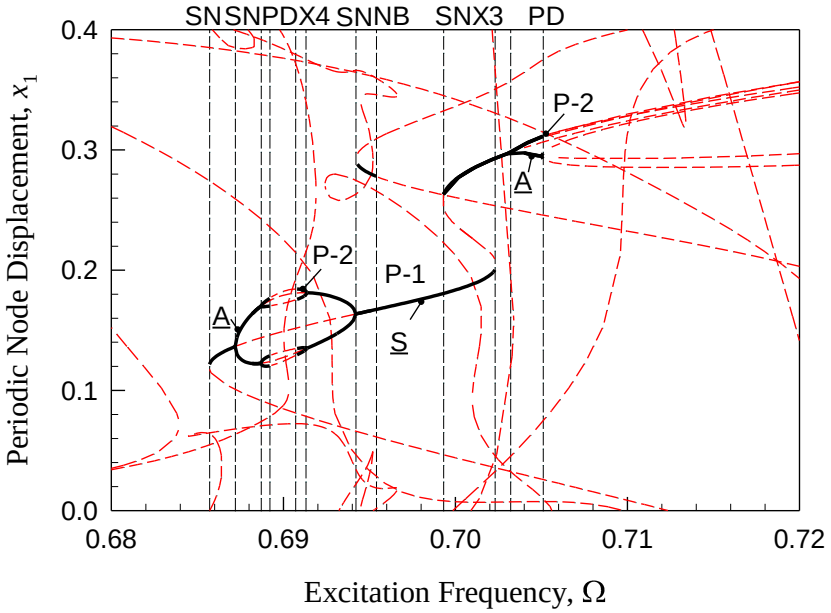

(i)

Fig. 20. The zoom view of bifurcation tree of period-1 to period-2 motions varying with frequency ($\Omega \in (0.68, 0.72)$). (i) node displacement x_1 , (ii) node velocity y_2. (iii) node angle x_2 , (iv) node angular velocity y_2 ($k_1 = 5$, $k_2 = 100$, $c = 0.1$, $Q_0 = 20.0$, $L = 2$, $T = 2\pi / \Omega$).

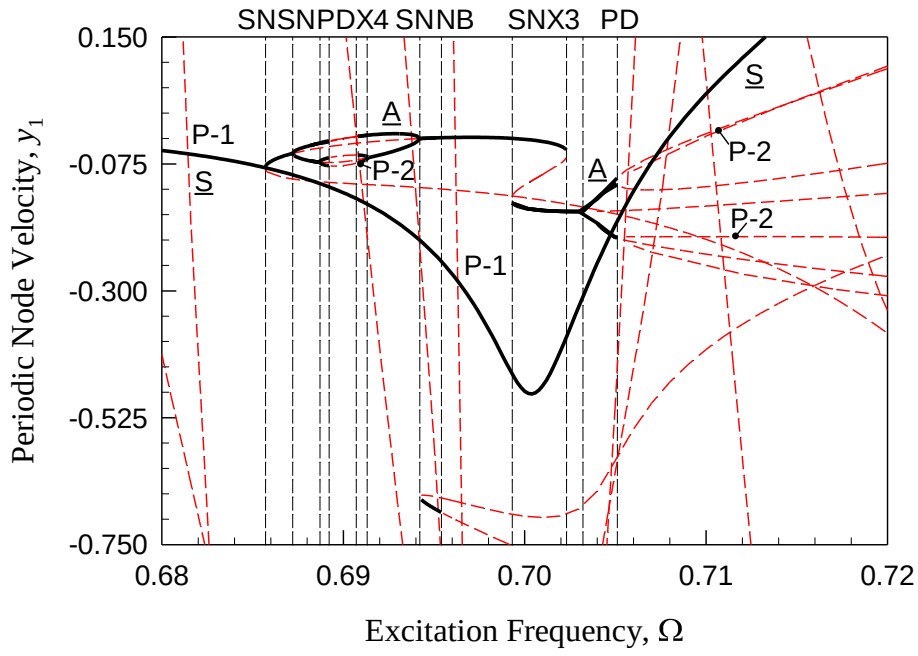

(ii)

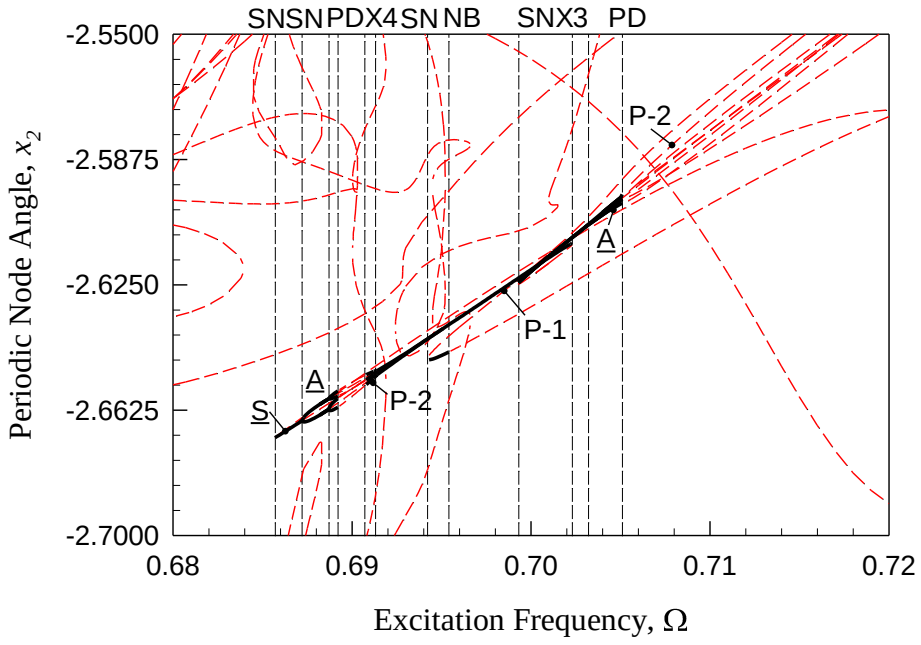

(iii)

Fig. 20. (continued)

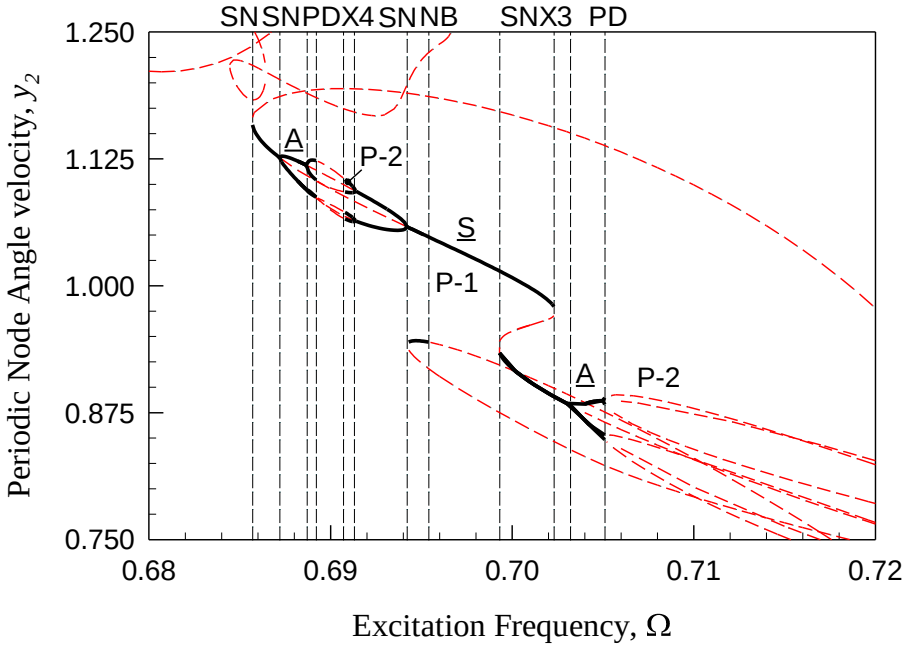

(iv)

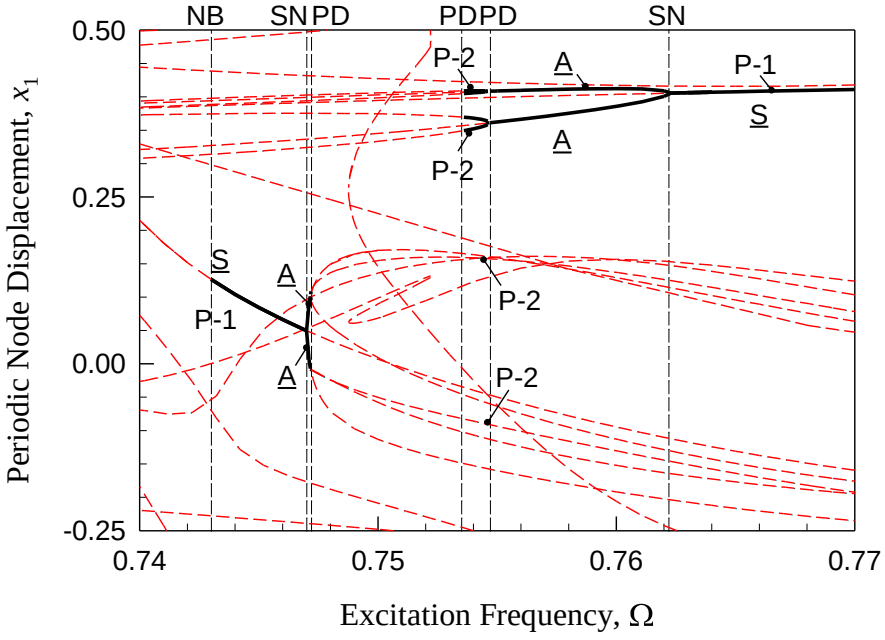

(i)

Fig. 21. The zoom view of bifurcation tree of period-1 to period-2 motions varying with frequency ($\Omega \in (0.74, 0.77)$). (i) node displacement x_1 , (ii) node velocity y_2. (iii) node angle x_2 , (iv) node angular velocity y_2 ($k_1 = 5$, $k_2 = 100$, $c = 0.1$, $Q_0 = 20.0$, $L = 2$, $T = 2\pi / \Omega$).

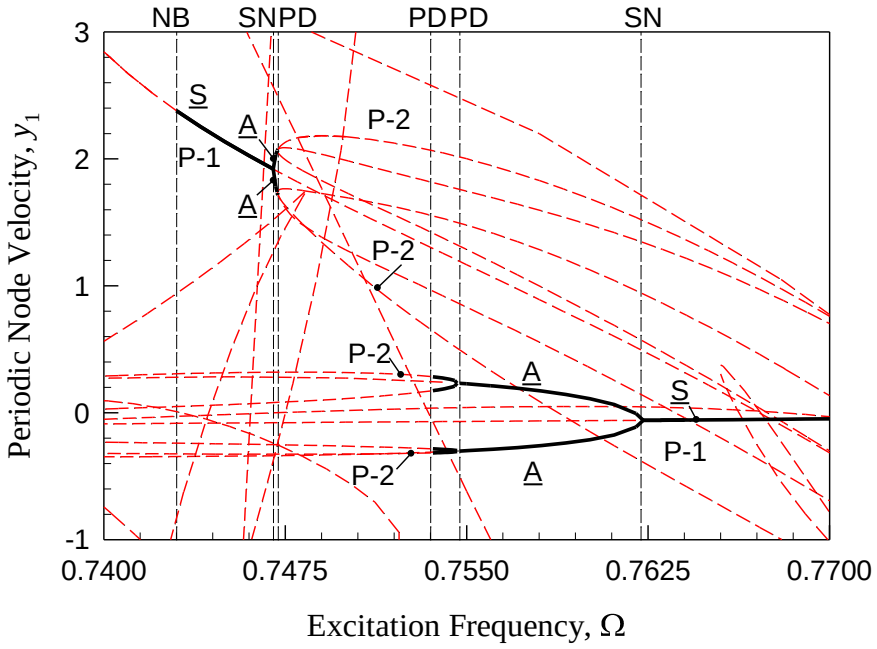

(ii)

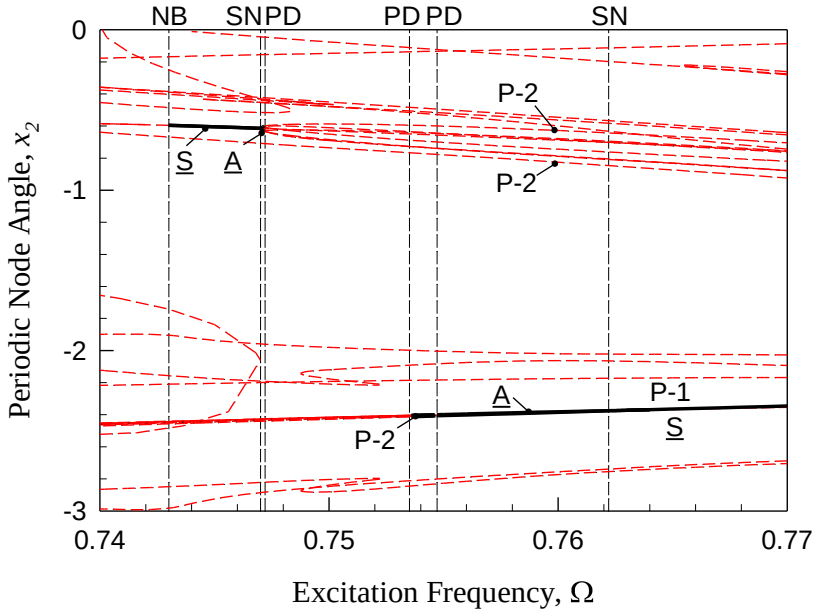

(iii)

Fig. 21. (continued)

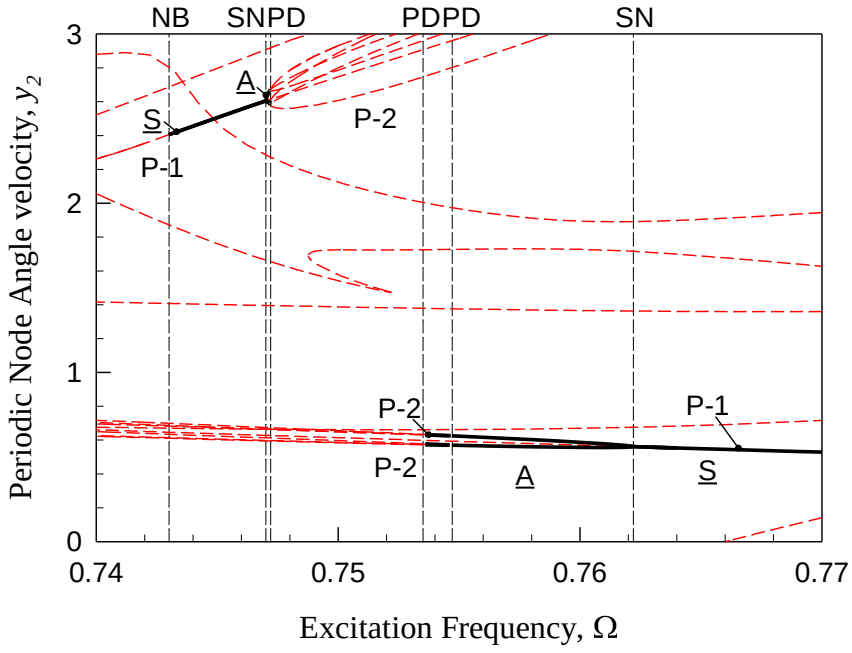

(iv)

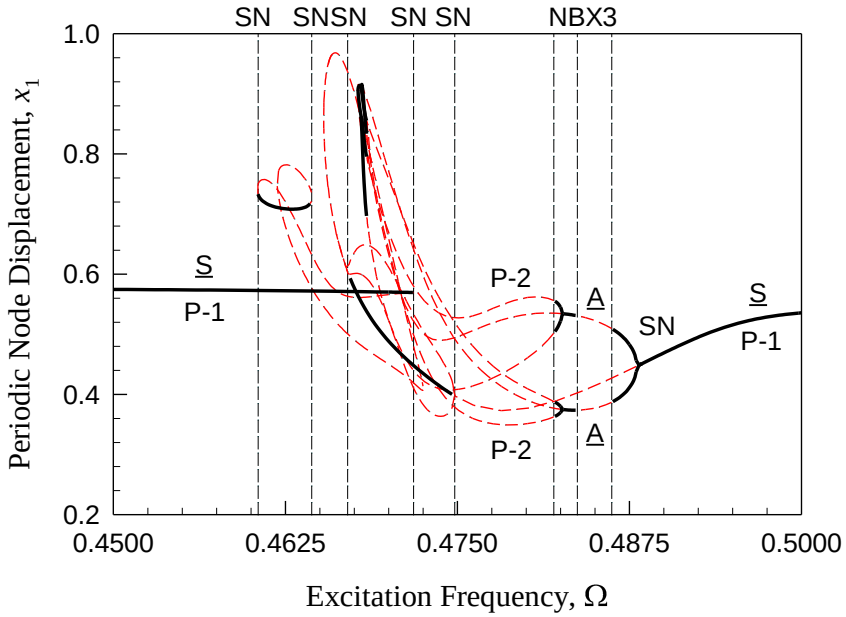

(i)

Fig. 22. The zoom view of bifurcation tree of period-1 to period-2 motions varying with frequency ($\Omega \in (0.45, 0.5)$). (i) node displacement x_1, (ii) node velocity y_2. (iii) node angle x_2, (iv) node angular velocity y_2 ($k_1 = 5$, $k_2 = 100$, $c = 0.1$, $Q_0 = 20.0$, $L = 2$, $T = 2\pi / \Omega$).

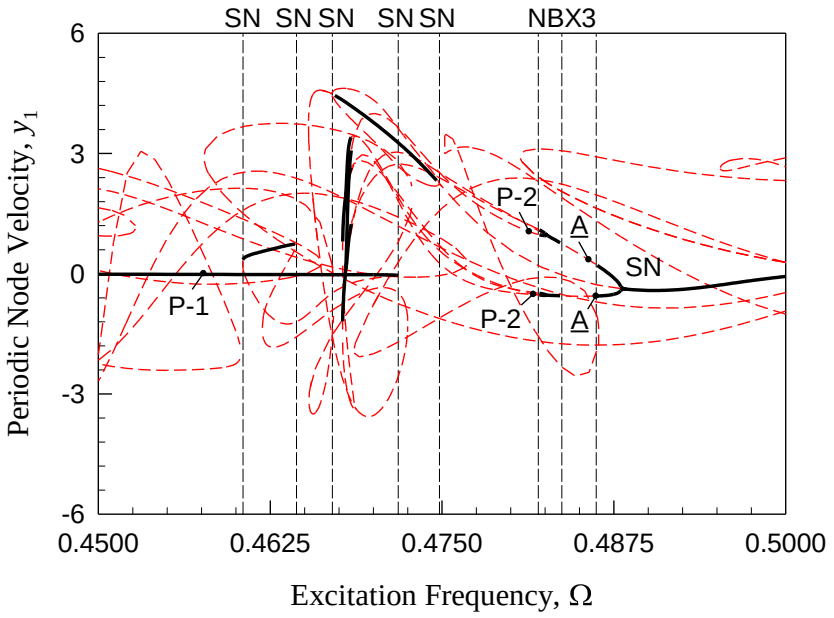

(ii)

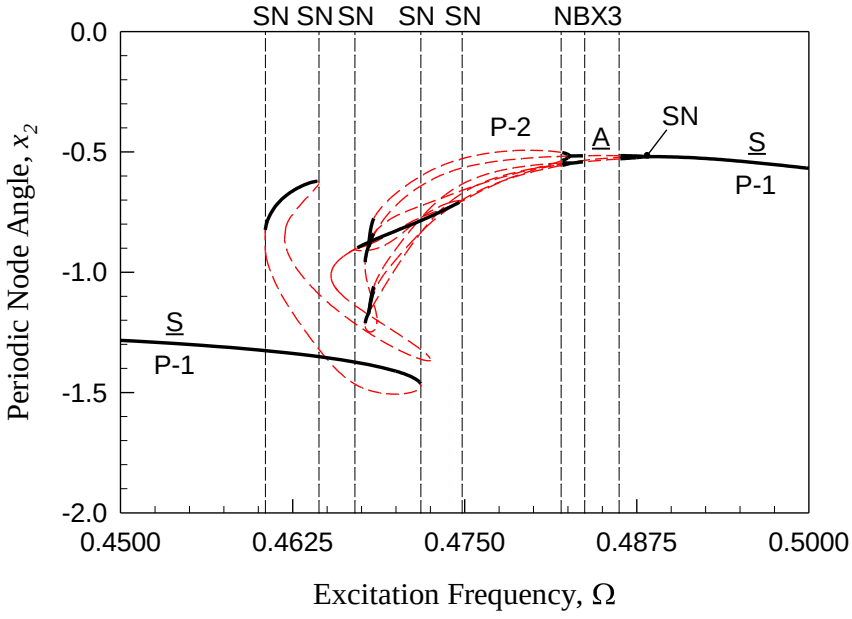

(iii)

Fig. 22. (continued)

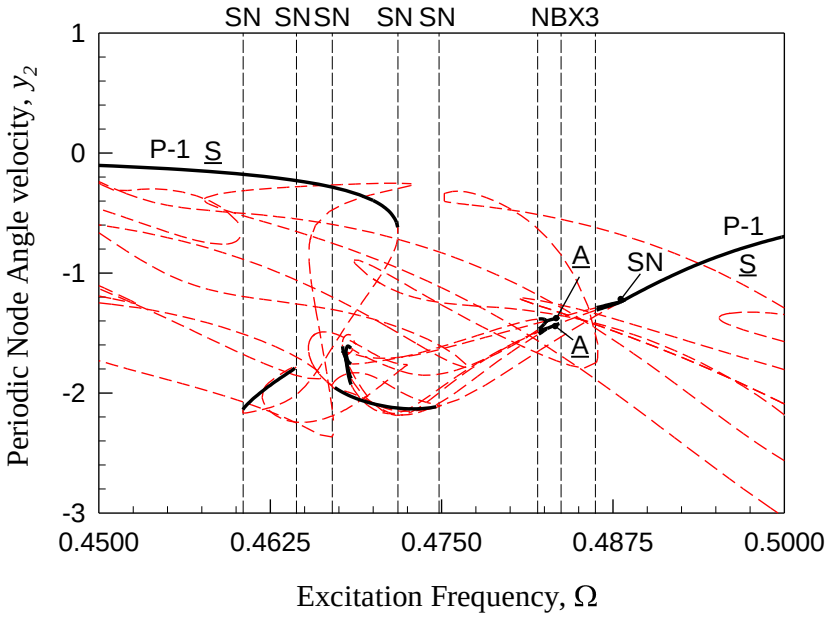

(iv)

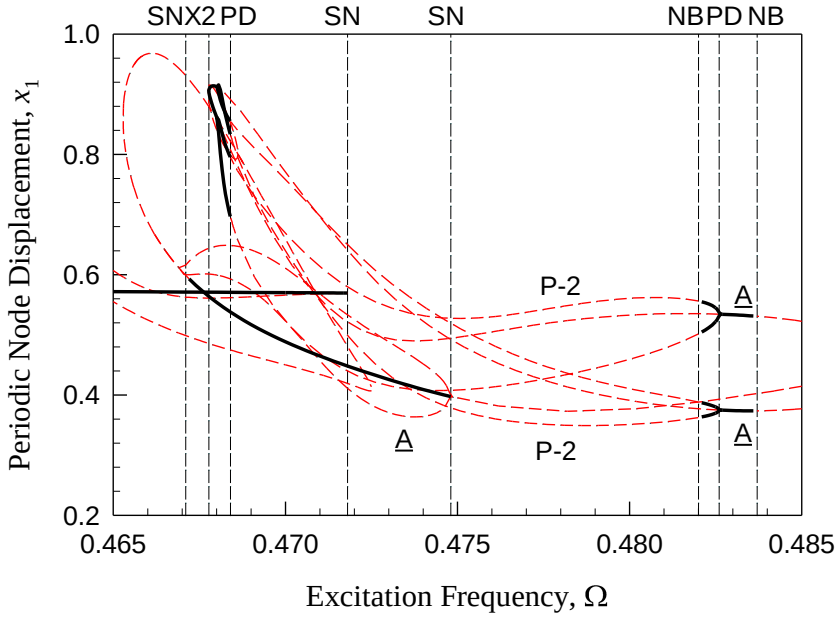

(i)

Fig. 23. The zoom view of bifurcation tree of period-1 to period-2 motions varying with frequency ($\Omega \in (0.465, 0.485)$). (i) node displacement x_1 , (ii) node velocity y_2. (iii) node angle x_2 , (iv) node angular velocity y_2 ($k_1 = 5$, $k_2 = 100$, $c = 0.1$, $Q_0 = 20.0$, $L = 2$, $T = 2\pi / \Omega$).

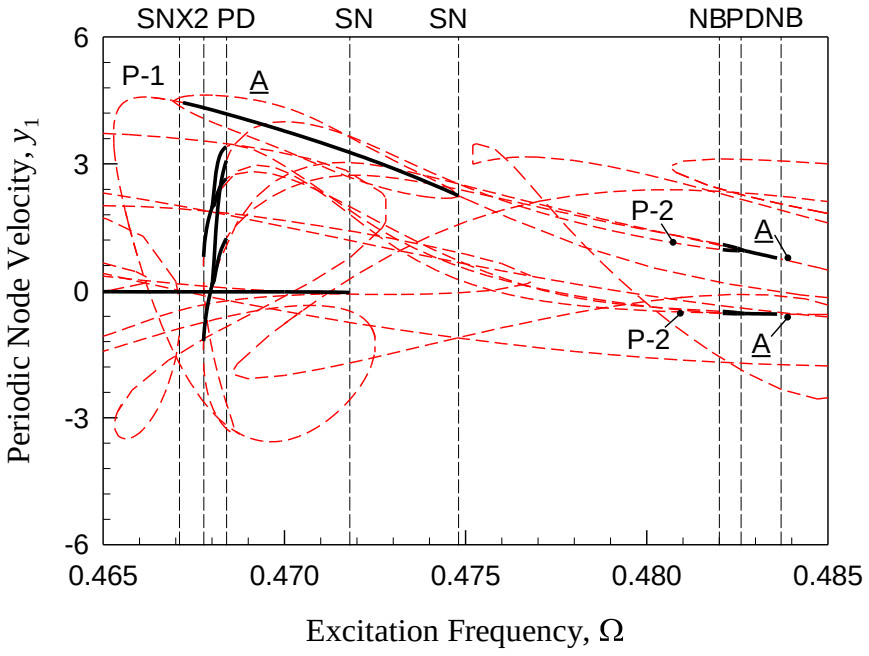

(ii)

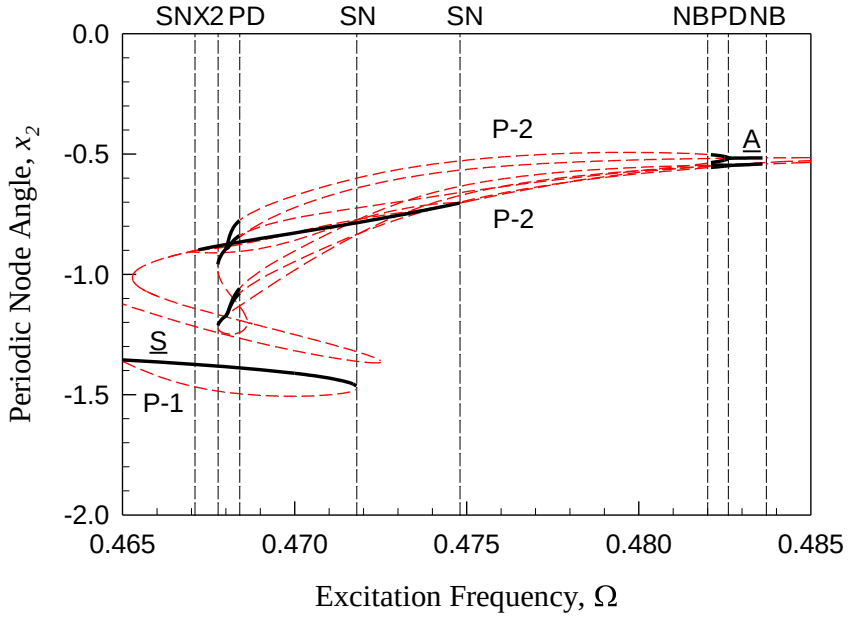

(iii)

Fig. 23. (continued)

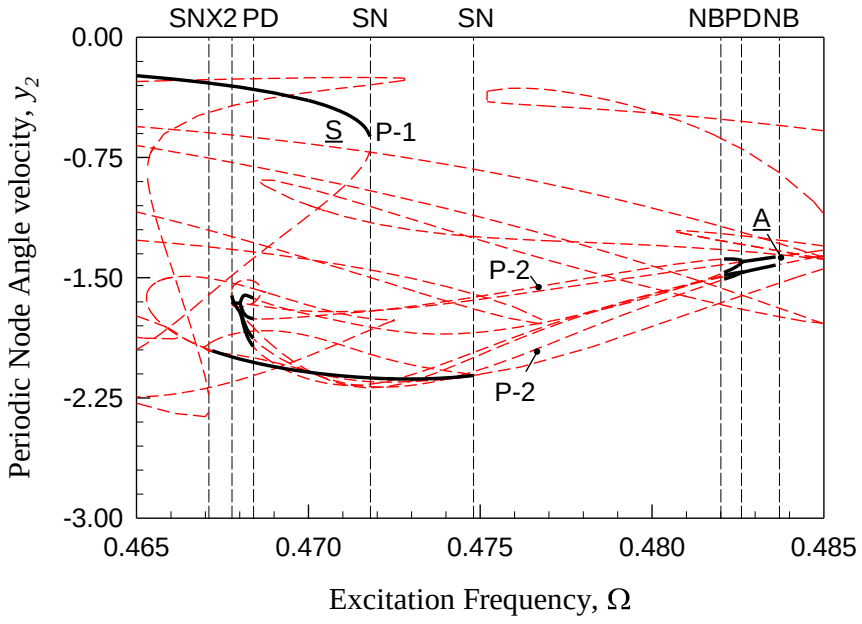

(iv)

Fig. 23. (continued)

Table 1

BIFURCATIONS FOR SYMMETRIC PERIOD-1 MOTIONS

($k_1 = 5, \quad k_2 = 100, \quad c = 0.1, \quad Q_0 = 20.0, \quad L = 2, \; T = 2\pi / \Omega$)

	Ω	Bifurcations
1st bifurcation tree	4.744	SN (A)
	7.17	SN (A)
	7.51	SN (A)
	4.61	SN (A)
	4.589	SN (J)
	9.03	NB
	10.29	NB
2nd bifurcation tree	3.8	PD
3rd bifurcation tree	1.755	SN(A)
	1.58	NB
	1.63	NB
	1.4565	SN(J)
	1.851	SN(A)
	1.91	NB
4th bifurcation tree	1.139	SN(A)
	1.233	SN(A)
	1.23	SN(A)
	1.266	SN(J)
	1.133	SN(J)
	1.1463	SN(A)
	1.229	SN(A)
	1.621	SN(J)
	1.3159	SN(J)
	1.3187	NB
	0.937	SN(A)
	0.9244	SN(A)
	0.902	SN(A)
	0.9556	SN(A)
	0.9522	NB
	0.9435	SN(J)
	0.762	SN(A)
	0.704	SN(A)
	0.7023	SN(J)

Note: J-Jumping phenomena, A- from symmetric to asymmetric period-1 motions. NB-Neimark Bifurcation, SN-saddle-node bifurcation between stable and unstable symmetric period-1 motion.

Table 1 (continue)
($k_1 = 5, \quad k_2 = 100, \quad c = 0.1, \quad Q_0 = 20.0, \quad L = 2, \; T = 2\pi / \Omega$)

	Ω	Bifurcations
4st bifurcation tree	0.6993	SN(J)
	0.6954	NB
	0.6942	SN(A)
	0.6872	SN(A)
	0.6857	SN(J)
	0.695	SN(J)
	0.7471	SN(A)
	0.7428	NB
	0.6667	SN(A)
	0.6657	NB
	0.7313	SN(J)
	0.488	SN(A)
	0.4748	SN(A)
	0.467	SN(A)
	0.4725	SN(J)
	0.4644	SN(J)
	0.4718	SN(J)
	0.4605	SN(J)

Note: J-Jumping phenomena, A- from symmetric to asymmetric period-1 motions. NB-Neimark Bifurcation, SN-saddle-node bifurcation between stable and unstable symmetric period-1 motion.

Table 2

BIFURCATIONS FOR ASYMMETRIC PERIOD-1 MOTION

($k_1 = 5, \quad k_2 = 100, \quad c = 0.1, \quad Q_0 = 20.0, \quad L = 2, T = 2\pi / \Omega$)

	Ω	Bifurcations
1st bifurcation tree	4.49	SN(J)
	4.486	PD
	6.14	SN(J)
	5.66	PD
	9.93	PD
	11.03	PD
2nd bifurcation tree	3.807	PD
3rd bifurcation tree	1.774	PD
	1.8495	PD
4th bifurcation tree	1.1032	NB
	1.1036	PD
	1.0861	NB
	1.0866	NB
	1.0882	NB
	1.0901	PD
	1.1502	PD
	1.1649	SN(J)
	1.1354	SN(J)
	1.1389	PD
	1.1502	PD
	1.1036	PD
	1.2044	PD
	1.099	PD
	0.4862	NB
	0.4837	NB
	0.4826	PD
	0.4681	PD
	0.4679	SN(A)
	0.46777	SN(J)
	0.931	NB
	0.7546	PD
	0.706	PD
	0.7472	PD
	0.6914	PD
	0.6882	PD
	0.9017	PD
	0.6668	PD

Note: J-Jumping phenomena, A- from symmetric to asymmetric period-1 motions. PD-period-doubling from period-1 to period-2 motion. SN-saddle-node bifurcation for onset of asymmetric period-1 motion.

Table 3

BIFURCATIONS FOR PERIOD-2 MOTIONS

$(\alpha_1 = 10.0,\ \alpha_2 = 5.0,\ \beta = 10.0,\ \delta = 0.5, Q_0 = 200, T = 2\pi/\Omega)$

	Ω	Bifurcations
1st bifurcation tree	11.031	SN
	8.69	NB
	11.83	NB
	14.85	PD
	14.3	PD
	13.311	NB
	13.9	SN
2nd bifurcation tree	3.807	SN
	3.8037	PD
	3.7765	PD
	3.7245	NB
	3.4025	SN
3rd bifurcation tree	1.774	SN
	1.777	NB
	1.849	SN
4th bifurcation tree	0.482	NB
	0.4684	PD
	1.1036	PD
	1.1167	NB
	1.0898	PD
	1.0828	PD
	1.1758	PD
	1.1782	SN
	0.6668	PD
	0.6893	PD
	0.6907	PD
	0.7535	PD
	0.7052	PD
	0.7472	NB
	0.9016	NB

Note: SN - for onset of asymmetric period-2 motions. PD-period-doubling from period-2 to period-4 motion. SN-saddle-node bifurcation between unstable and stable period-1 motions.

If the period-doubling bifurcation occurs on the period-1 motion, then the period-2 motion exits on the bifurcation tree. In fact, there are 11 branches of bifurcation trees which period-2 motion can be observed on them, as shown in Fig.5-23. On The first bifurcation trees in the frequency range of $\Omega \in (4.59,18)$, three period-2 motions exit in one branch of bifurcation tree. The period-2 motion lie in the frequency interval of $\Omega \in (4.486,5.66)$, $(5.6,9.93)$, $(11.031,17.536)$, which are presented in Fig.5-10. The period-2 motion in the frequency range of $\Omega \in (4.486,5.66)$ are all unstable, as shown in Fig.5. The period-doubling bifurcation of asymmetric period-1 motion is at $\Omega = 5.66$, and the period-2 motion end in close-loop at $\Omega = 4.486$. For the period-2 motion in the frequency range of $\Omega \in (5.6,9.93)$, $(11.031,17.536)$. The stable period-2 motion is in the frequency range of $\Omega \in (8.7,9.93)$, $(11.031,11.821)$, $(13.321,14.291)$ and $(14.861,17.511)$. The two period-doubling bifurcation of asymmetric period-1 motion are at $\Omega = 9.93$ and $\Omega = 11.031$. The period-2 motion end in close-loop at $\Omega = 5.6$ and $\Omega = 13.9$. Which are shown in Fig.5-10. In the frequency range of $\Omega \in (0,4.59)$. The second bifurcation trees contain one period-2 motion coexist with the asymmetric period-1 motion in the frequency interval of $\Omega \in (3.3844,3.8037)$ as shown in Fig.11. The stable period-2 motion is in the frequency range of $\Omega \in (3.8037,3.8064)$, $(3.776,3.725)$. The period-doubling bifurcation of asymmetric period-1 motion is at $\Omega = 3.8037$, and the period-2 motion end in close-loop at $\Omega = 3.401$. The last two bifurcation trees are shown in Fig.12, and the zoom views of Fig.12 are presented in Fig.13-23. The third bifurcation trees possess one period-2 motion in the frequency range of $\Omega \in (1.774,1.851)$. The stable period-2 motion is in $\Omega \in (1.774,1.776)$ and $(1.85,1.851)$. The unstable period-2 motion is in $\Omega \in (1.776,1.85)$. The two period-

doubling bifurcations of asymmetric period-1 motion are $\Omega = 1.774$ and 1.851. Which are shown in Fig.13. The last bifurcation tree possess 12 period-2 motions. One among them contains four period-2 motions occur in the same bifurcation branch in the frequency range of $\Omega \in (1.04, 1.3732)$. As shown in Fig14-17. The period-2 motions lie in the frequency range of $\Omega \in (1.1675, 1.2102), (1.0401, 1.1782)$, $(1.1389, 1.1502)$ and $(1.1035, 1.1167)$. For the period-2 motion in $\Omega \in (1.1035, 1.1167)$ and $(1.1389, 1.1502)$. The stable period-2 motion is in $\Omega \in (1.1035, 1.1036)$, $(1.1165, 1.1167)$, $(1.1389, 1.139)$ and $(1.1501, 1.1502)$. The unstable period-2 motion is in $\Omega \in (1.1036, 1.1165)$, $(1.139, 1.1501)$, $(1.1389, 1.139)$ and $(1.1501, 1.1502)$. The four period-doubling bifurcation of asymmetric period-1 motion are at $\Omega = 1.1035$, 1.1167, 1.1389 and 1.1502. For the period-2 motion in $\Omega \in (1.1675, 1.2102)$ and $(1.0401, 1.1782)$. The stable period-2 motion is in $\Omega \in (1.1675, 1.2102)$, $(1.0824, 1.099)$, $(1.1781, 1.1782)$ and $(1.1758, 1.1781)$. The period-doubling bifurcation of asymmetric period-1 motion are at $\Omega = 1.2044$ and 1.099. The period-2 motion end in close-loop at $\Omega = 1.1675$ and 1.1782. The zoom view presented in Fig.17 shows the period-2 motion in the frequency interval of $\Omega \in (1.0843, 1.09006)$, which is all unstable. The period-doubling bifurcation of asymmetric period-1 motion is at $\Omega = 1.09006$. The period-2 motion end in close-loop at $\Omega = 1.0861$. The Fig.18 presented the zoom view of the fourth bifurcation trees in $\Omega \in (0.85, 1)$. The period-2 motion in the lie in the frequency interval of $\Omega \in (0.9002, 0.913)$. The stable period-2 motion is in $\Omega \in (0.9017, 0.90172)$. The period-doubling bifurcation of asymmetric period-1 motion is at $\Omega = 0.9017$. The period-2 motion end in close-loop at $\Omega = 0.913$. The period-2 motion in in the frequency range of $\Omega \in (0.74717, 0.9111)$ can be observed in Fig.18-21, Fig.18-21

present the zoom view of the fourth bifurcation in $\Omega \in (0.6,1)$ Fig.20 and Fig.21 are the zoom view of Fig.19 as well. The stable period-2 motion is in $\Omega \in (0.74717, 0.74719)$. The period-doubling bifurcation of asymmetric period-1 motion is at $\Omega = 0.74717$. The period-2 motion end in close-loop at $\Omega = 0.7824$. The period-2 motion in the frequency interval of $\Omega \in (0.704, 0.7546)$ can be obtained in Fig.19-21. The stable period-2 motion is in $\Omega \in (0.704, 0.7051)$ and $(0.7536, 0.7546)$. The unstable period-2 motion is in $\Omega \in (0.7051, 0.7536)$. The two period-doubling bifurcation of asymmetric period-1 motion are at $\Omega = 0.704$ and 0.75460. The period-2 motion in the frequency range of $\Omega \in (0.6882, 0.6914)$ are presented in Fig.20. The stable period-2 motion is in $\Omega \in (0.6882, 0.6892)$ and (0.6908, 0.6914). The unstable period-2 motion is in $\Omega \in (0.6892, 0.6908)$. The two period-doubling bifurcation of asymmetric period-1 motion are at $\Omega = 0.6882$ and 0.6914. The period-2 motions in the frequency range of $\Omega \in (0.66676, 0.7059)$ are shown in the Fig.19-21. The stable period-2 motion is in $\Omega \in (0.66676, 0.66679)$. The period-doubling bifurcation of asymmetric period-1 motion is at $\Omega = 0.66676$, and the period-2 motion end in close-loop at $\Omega = 0.6996$. The period-2 motion in the frequency interval of $(0.468, 0.4827)$ are presented in Fig.22-23. For a better look on the asymmetric period-1 and period-2 motions, Fig.23 is given as a zoom view of Fig.22 The stable period-2 motion is in $\Omega \in (0.468, 0.4684)$, $(0.4821, 0.4827)$. The unstable period-2 motion is in $\Omega \in (0.4684, 0.4821)$. The two period-doubling of asymmetric period-1 motion are at $\Omega = 0.468$ and 0.4827. For clarity, the bifurcation points for asymmetric period-1 motions and period-2 motions are tabulated in Table 2 and Table 3.

Frequency-amplitude Characteristics

The calculation of the discrete nodes of period-1 and period-2 motions of this nonlinear spring pendulum, are completed by the corresponding mapping structures. Based on that, applying the discrete Fourier series, the nonlinear frequency-amplitude characteristics of period-1 and period-2 motions can be found. Then the harmonic amplitudes and phase angles of period-1 and period-2 motions can be computed as well. In order to avoid the abundant illustrations, the frequency-harmonic amplitude curves for several order harmonics are presented in Fig.9-10. The presented frequency-harmonic amplitudes are constant term $a_{(i)0}^{(m)}$ ($i=1,2,\ m=1,2$) and the harmonic amplitudes $A_{(i)k/m}$ ($i=1,2\quad m=2,$ $k=1,2,3,4,6,8,10,12,30,32$). The saddle-node, period-doubling bifurcation and Neimark bifurcation points of period-1 and period-2 motions are listed in Tables 1-3.

The constant terms versus excitation frequency is presented in Fig.24(i)-(ix) and Fig.25(i)-(ix). The Fig.24(i) and Fig.25(i) are the global views for the bifurcation trees of the constant terms, two windows of zoom view for the constant term of period-2 motion in the frequency interval of $\Omega\in(3.2,4)$ are presented respectively as well. Fig.24(ii)-(ix) and Fig.25(ii)-(ix) are also the zoom views for the Fig.24(i) and Fig.25(i) respectively. The bifurcation trees of constant term in the frequency interval of $\Omega\in(3.6,18)$ are shown in Fig.24(ii) and Fig.25(ii). They contain the First bifurcation trees and part of the second bifurcation trees. Fig.24(iii) and Fig.25(iii) are the zoom views for Fig.24(ii) and Fig.25(ii). The constant term for frequency range of $\Omega\in(0,2.25)$ can be observed in Fig.24(iv) and Fig.25(iv), Fig.(v)-(ix)and Fig.(v)-(ix) are zoom views of them as they bifurcation conditions are complex in this range. For symmetric period-1 motion, $a_{(1)0}^{(1)}=a_{(1)0}\neq 0,\ a_{(2)0}^{(1)}=a_{(2)0}=0$.

For the asymmetric period-1 motion, $a^{(1)}_{(1)0} = a_{(1)0} \neq 0$, $a^{(1)}_{(2)0} = a_{(2)0} \neq 0$. For the asymmetric period-2 motion, $a^{(2)}_{(1)0} \neq 0$ and $a^{(2)}_{(2)0} \neq 0$, which can be easily observed on the bifurcation tree. Meanwhile, clearly that the $a^{(1)}_{(1)0}$ and $a^{(1)}_{(2)0}$ does not share the same pattern. Which provide that the spring perform different dynamical behavior from the pendulum. This specific behavior can be explain as there are periodical forces before the parameter θ in eq.(30), so this nonlinear spring pendulum is also a parametric system and this is a parametric dynamical behavior. In fact, it is obviously that the even turns of the Harmonic-Amplitude of displacement x_1 show a similar pattern with the odd turns of the Harmonic-Amplitude of angle x_2. The maximum quantity level of the constant term is about $|a^{(m)}_{(1)0}|(m=1,2) \approx 2.8$. And $|a^{(m)}_{(2)0}|(m=1,2) \approx 1.5$. From the symmetric period-1 motion, the symmetric to asymmetric period-1 motion occur, and the asymmetric period-1 to period-2 motions. Which are more easily to observed in Fig.24(ii)-(ix) and Fig.25(ii)-(ix). There are 17 asymmetric bifurcation trees, 11 of them possess asymmetric period-1 to period-2 bifurcation trees, and the rest 6 of them only possess asymmetric period-1 motions.

Harmonic amplitude $A_{(i)1/2}(i=1,2)$ varying with excitation frequency are presented in Fig.24(x)-(xii) and Fig.25(x)-(xiii) for a better observe of the period-2 motions, as the Harmonic amplitude $A_{(i)1/2}(i=1,2)$ only occur in period-2 motion. four windows of zoom view for $A_{(i)1/2}(i=1,2)$ in $\Omega \in (1.76,1.86)$ and $(0.688,0.692)$ are given on Fig.24(x),(xii) and Fig.25(x),(xiii) for a better look on the bifurcation condition as well. The $A_{(4)1/2}$ presented in Fig.25(xi) is the harmonic amplitude of the angular velocity. The maximum quantity level of harmonic amplitude $A_{(i)1/2}(i=1,2)$ are about $A_{(1)1/2} \sim 0.19$ and

$A_{(2)1/2} \sim 3.7$. Harmonic amplitude $A_{(i)1}(i=1,2)$ varying with excitation frequency are presented in Fig.24(xiii)-(xxiv) and Fig.25(xiv)-(xxv) for period-1 to period-2 motions. The maximum quantity level of the primary harmonic amplitude are about $A_{(1)1} \sim 1.9$ and $A_{(2)1} \sim 3.9$. The Fig.24(xiii) and Fig.25(xiv) are the global view of harmonic amplitude $A_{(i)1}(i=1,2)$, two windows of zoom views for $A_{(i)1}(i=1,2)$ in the frequency interval of $\Omega \in (3.2, 4.0)$ are presented in Fig.24(xiii) and Fig.25(xiv) as well. For $\Omega \in (4.9,18)$ and $(0, 2.25)$, the frequency-amplitude curves of are very crowded as shown in Fig.24(xiii) and Fig.25(xiv). For clear illustration, several zoomed views are given in Fig.24(xiv)-(xxiv) and Fig.25(xv)-(xxv), and proper labels are placed for bifurcations as well. A small window is given in Fig.24(xix) to show the periodical doubling bifurcation points. Fig.24(xx)-(xxiv) and Fig.25(xxi)-(xxv) are zoom view for Fig.24(xix) and Fig.25(xx). Harmonic amplitude $A_{(i)3/2}(i=1,2)$ versus excitation frequency are presented in Fig.24(xxii)-(xxiv) and Fig.25(xxiii)-(xxvi) for period-2 motions, which are similar to the harmonic amplitude $A_{(i)1/2}(i=1,2)$ respectively. Four windows of zoom view for $A_{(i)3/2}(i=1,2)$ in the frequency range of $\Omega \in (1.76,1.86),(0.688, 0.692)$ are shown in Fig.24(xxii),(xxiv) and Fig.25(xxiii),(xxvi) as well. The bifurcation branch for $A_{(4)3/2}$ in the frequency range of $\Omega \in (3.36, 3.90)$ is presented in Fig.25 (xxiv). The maximum quantity level of harmonic amplitude $A_{(i)3/2}(i=1,2)$ are about $A_{(1)3/2} \sim 0.25$ and $A_{(2)3/2} \sim 3.4$ Harmonic amplitude $A_{(i)2}(i=1,2)$ varying with excitation frequency are presented in Fig.24(xxv)-(xxxiii) and Fig.25(xxvii)-(xxxv) for period-1 to period-2 motions. It is obvious that $A_{(2)2}$

has a similar skeleton structure to $A_{(1)1}$. The maximum quantity level of harmonic amplitude $A_{(i)2}(i=1,2)$ are about $A_{(1)2} \sim 2.3$ and $A_{(2)2} \sim 1.6$. In $A_{(2)2}$ some bifurcation branches can be observed more clearly, just like $A_{(1)1}$. Similarly the general view of the Harmonic amplitude in the frequency range of $\Omega \in (0,18)$ are shown in Fig.24(xxv) and Fig.25(xxvii). Two windows of zoom view for $A_{(i)2}(i=1,2)$ in the frequency interval of $\Omega \in (3.2,4)$ are also presented on Fig.24(xxv) and Fig.25(xxvii). For clear illustration, several zoomed views are given in Fig.24(xxvi)-(xxxiii) and Fig.25(xxviii)-(xxxv), and the proper labels are given for bifurcations. Among them Fig.24(xxvii) and Fig.25(xxix) are zoom view of Fig.24(xxvi) and Fig.25(xxviii), Fig.24(xxix)-(xxxiii) and Fig.25(xxxi)-(xxxv) are zoom view of Fig.24(xxviii) and Fig.25(xxx). Harmonic amplitude $A_{(i)3}(i=1,2)$ varying with excitation frequency are presented in Fig.24(xxxiv)-(xlii) and Fig.25(xxxvi)-(xliv) for period-1 to period-2 motions. Some bifurcation branches of $A_{(1)3}$ can be easily observed. The maximum quantity level of the primary harmonic amplitude is about $A_{(1)3} \sim 0.44$. The bifurcation branches of $A_{(2)3}$ is more complex, the corresponding quantity level is about $A_{(2)3} \sim 1.75$. For clear illustration, several zoomed views are given in Fig.24(xxxv)-(xlii) and Fig.25(xxxvi)-(xliv), the proper labels are given for the bifurcations conditions as well. Similarly the zoom views for $A_{(i)3}(i=1,2)$ in $\Omega \in (3.2,4)$ are given in Fig.24(xxxv) and Fig.25(xxxvi), Fig.24(xxxix)-(xlii) and Fig.25(xl)-(xliv) are the zoom view for Fig.24(xxxviii) and Fig.25(xxxix) as well. Harmonic amplitude $A_{(i)4}(i=1,2)$ varying with excitation frequency are presented in Fig.24(xliii)-(li) and Fig.25(xlv)-(liii) for period-1 to period-2 motions. In the frequency range of $\Omega \in (0,2.25)$ and $(4.49,18)$. The bifurcation

branches are very crowded, and the quantity level of asymmetric period-1 and period-2 motion in $\Omega \in (4.49,18)$ is getting very small. The maximum quantity level of the primary harmonic amplitude is about $A_{(1)4} \sim 0.422$ and $A_{(2)4} \sim 0.86$. Several zoomed views with proper labels for bifurcations are given in Fig.24(xliv)-(li) and Fig.25(xlvi)-(liv) to clear illustration. Harmonic amplitude $A_{(i)5}(i = 1,2)$ varying with excitation frequency are presented in Fig.24(lii)-(lx) and Fig.25(liv)-(lxii) for period-1 to period-2 motions. Two windows of zoom view for $A_{(i)5}(i = 1,2)$ in $\Omega \in (3.2,4)$ are given in Fig.24(lii) and Fig.25(liv). The maximum quantity level of the primary harmonic amplitude are about $A_{(1)5} \sim 0.61$ and $A_{(2)5} \sim 0.9$. The bifurcation branches in the frequency interval of $\Omega \in (0,2.25)$ and $(4.49,18)$ are very crowded. To clear illustration, several zoomed views with proper labels for bifurcations are given in Fig.24(xliii)-(lx) and Fig.25(lv)-(lxii). Among them the Fig.24(lvi)-(lx) and Fig.25(lviii)-(lxii) are the zoom view for Fig.24(lv) and Fig.25(lvii). Harmonic amplitude $A_{(i)6}(i = 1,2)$ varying with excitation frequency are presented in Fig.24(lxi)-(lxix) and Fig.25(lxiii)-(lxxi) for period-1 to period-2 motions. The maximum quantity level of the primary harmonic amplitude are about $A_{(1)6} \sim 0.68$ and $A_{(2)6} \sim 0.47$. As the bifurcation branches are very complex in the frequency interval of $\Omega \in (0,2.25)$ and $(4.49,18)$. To clear illustration, several zoomed views with proper labels for bifurcations are given in Fig.24(lxii)-(lxix) and Fig.25(lxiv)-(lxxi). Two windows of zoom view for $\Omega \in (3.2,4)$ are in Fig.24(lxii) and Fig.25(lxiv) for a clear look on the bifurcation tree. Fig.24(lxv)-(lxix) and Fig.25(lxvii)-(lxxi) are the zoom view for Fig.24(lxiv) and Fig.25(lxvi). The last four sets of harmonic frequency-amplitudes are presented to avoid

abundant illustrations. Harmonic amplitude $A_{(i)15}(i=1,2)$ are shown in Fig.24(lxx)-(lxxvii) and Fig.25(lxxii)-(lxxix) for period-1 to period-2 motions. The maximum quantity level of the primary harmonic amplitude is about $A_{(1)15} \sim 0.38$ and $A_{(2)15} \sim 0.16$. As the harmonic amplitude for asymmetric bifurcation branches are getting very small, more zoomed views are given in Fig.24(lxxi)-(lxxvii) and Fig.25(lxxiii)-(lxxix) with proper labels for bifurcations. Similarly Fig.24(lxxiv)-(lxxvii) and Fig.25(lxxv)-(lxxix) are zoom views for Fig.24(lxxiii) and Fig.25(lxxii). Harmonic amplitude $A_{(i)16}(i=1,2)$ are shown in Fig.24(lxxviii)-(lxxxv) and Fig.25(lxxx)-(lxxxvii) for period-1 to period-2 motions. The maximum quantity level of the primary harmonic amplitude are about $A_{(1)16} \sim 0.56$ and $A_{(2)16} \sim 0.145$. As the harmonic amplitude for asymmetric bifurcation branches are getting very small, more zoomed views are given in Fig.24(lxxviii)-(lxxxv) and Fig.25(lxxxi)-(lxxxvii) with proper labels for bifurcations. Among them Fig.24(lxxxi)-(lxxxv) and Fig.25(lxxxiii)-(lxxxvii) are zoom view for Fig.24(lxxx) and Fig.25(lxxxii).

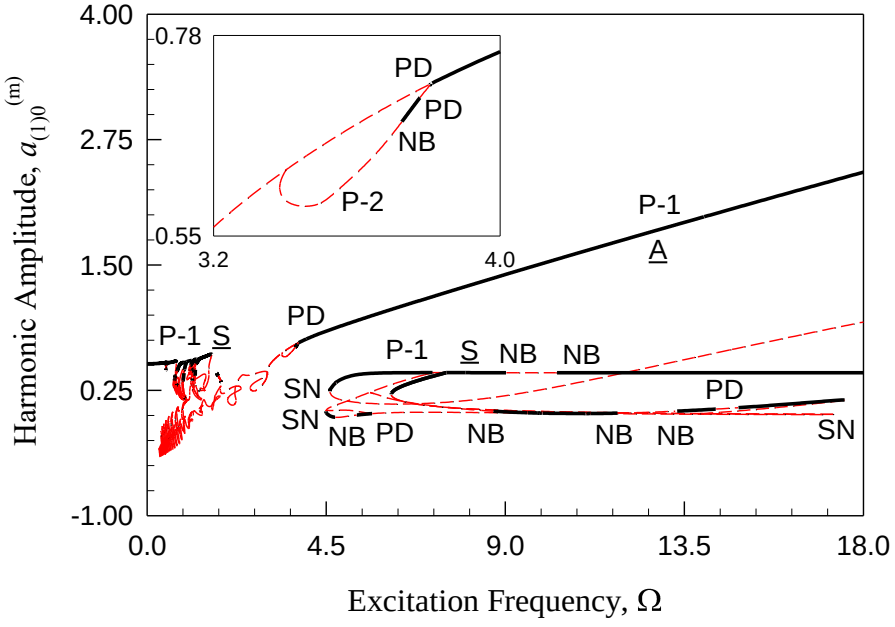

(i)

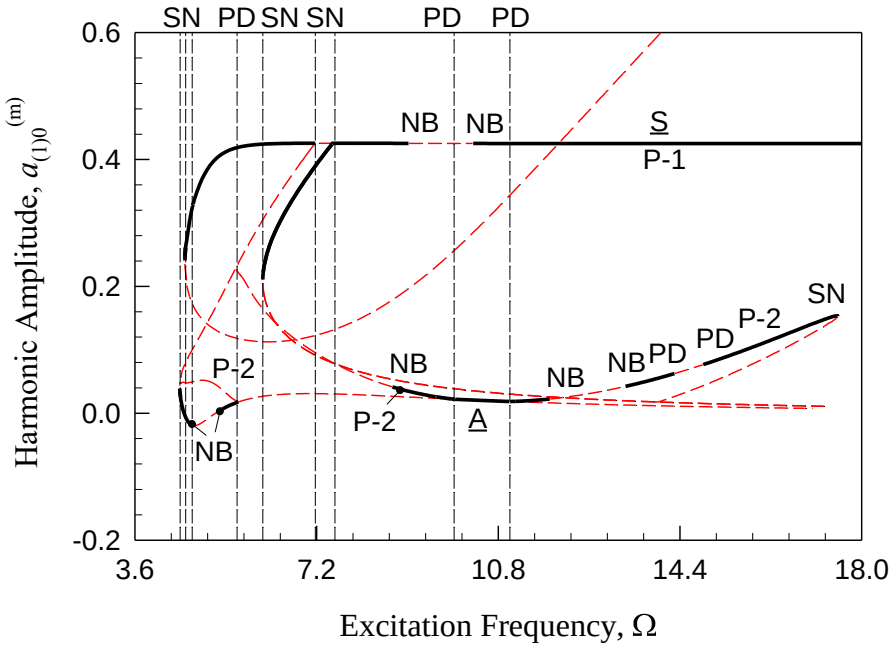

(ii)

Fig. 24. The frequency-amplitude characteristics of bifurcation tree of period-1 to period-2 motions varying with excitation frequency ($\Omega \in (0,18)$) for the displacement x_1,. (i)-(ix) $a_{(1)0}^{(m)}$ ($m = 1, 2$), (x)-(lxxxv) $A_{(1)k/m}$ ($k = 1,2,3,4,6,8,10,12,30,32$) ($m = 2$, $k_1 = 5$, $k_2 = 100$, $c = 0.1$, $Q_0 = 20.0$, $L = 2$, $T = 2\pi / \Omega$).

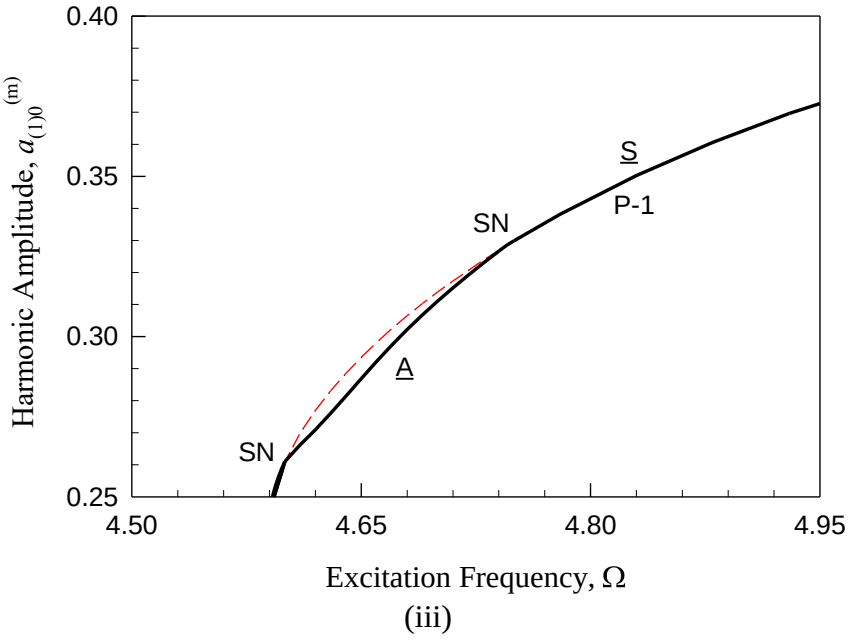

(iii)

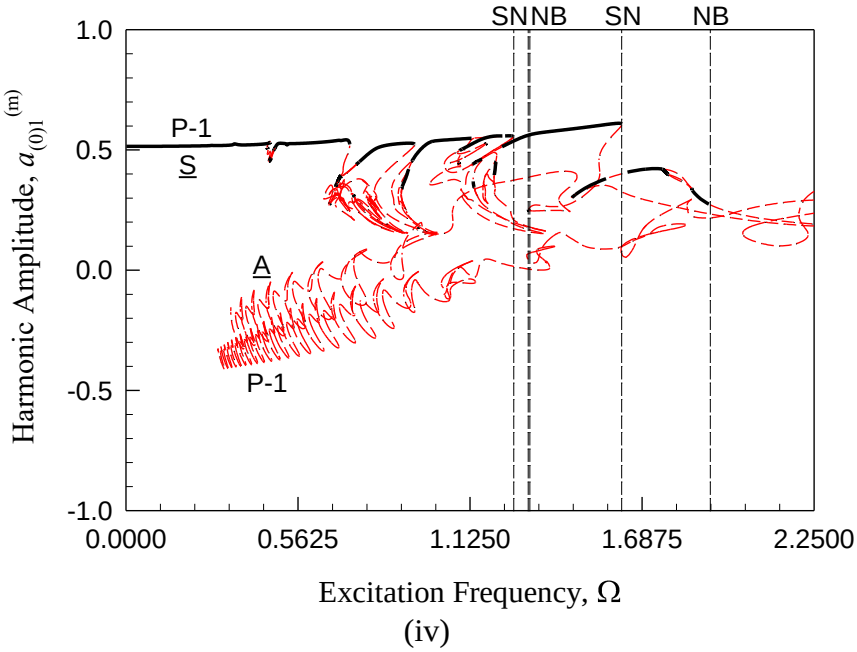

(iv)

Fig. 24. (Continued).

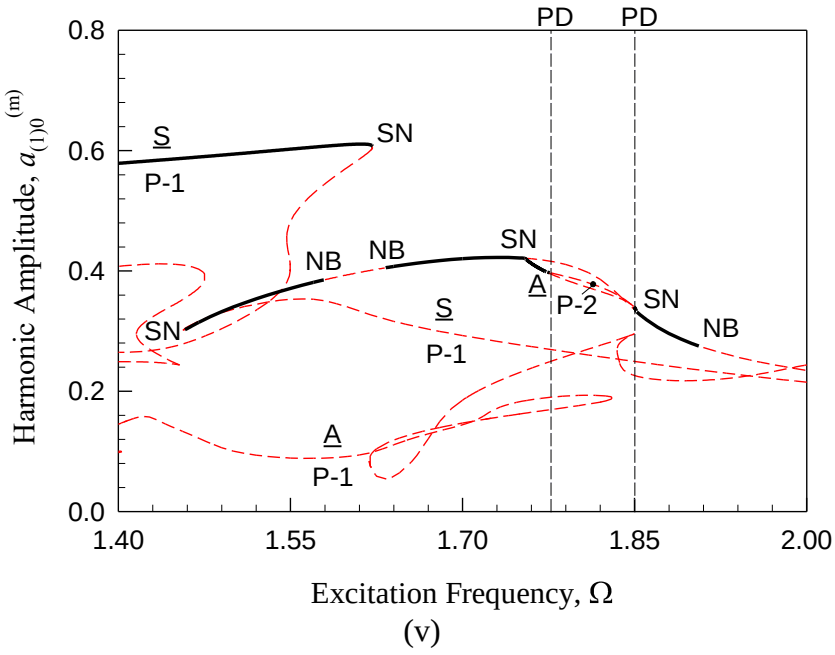

(v)

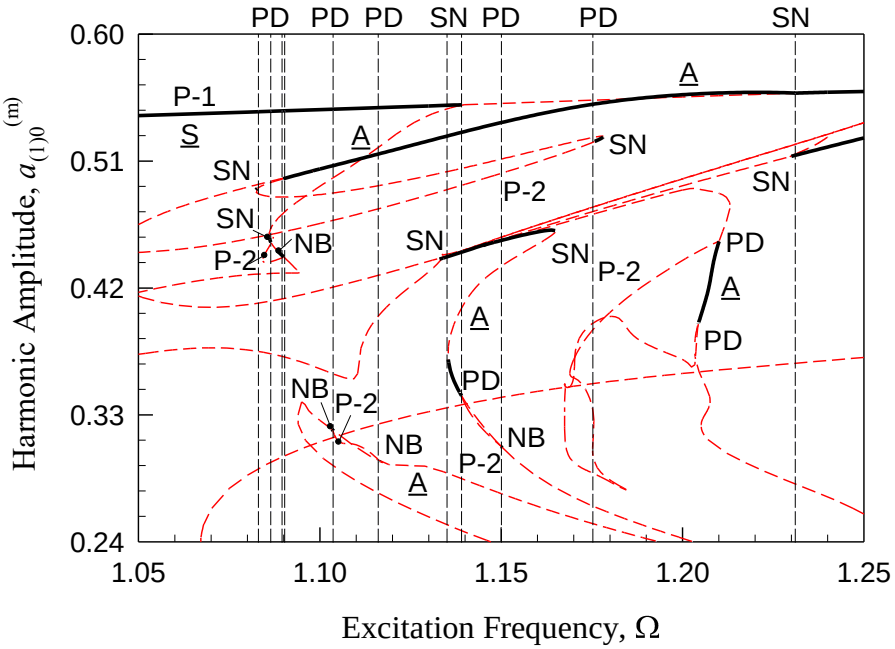

(vi)

Fig. 24. (Continued).

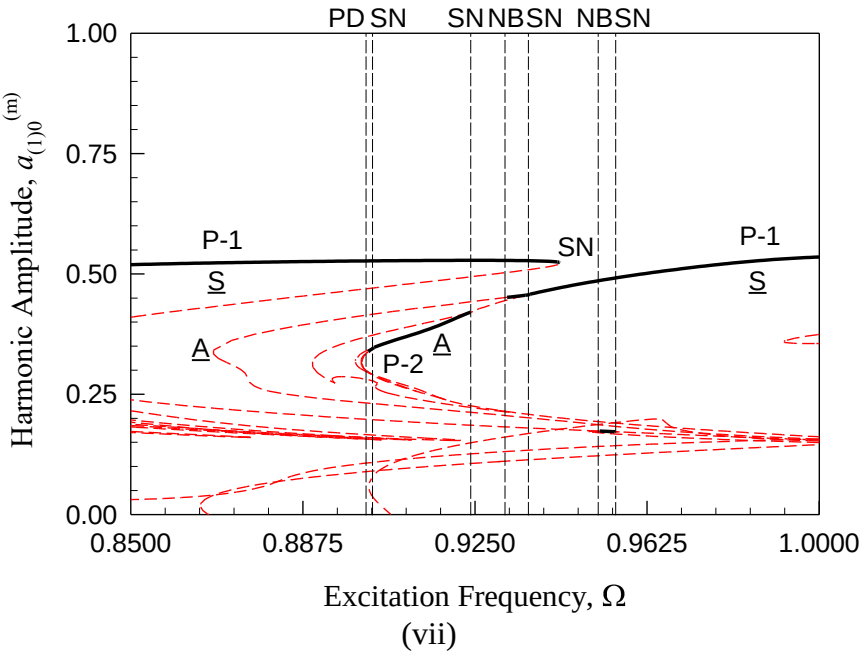

(vii)

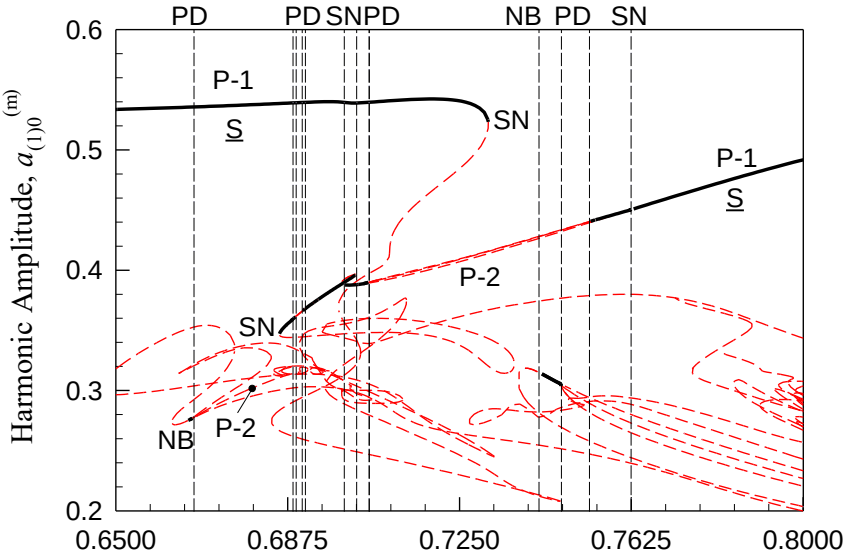

(viii)

Fig. 24. (Continued).

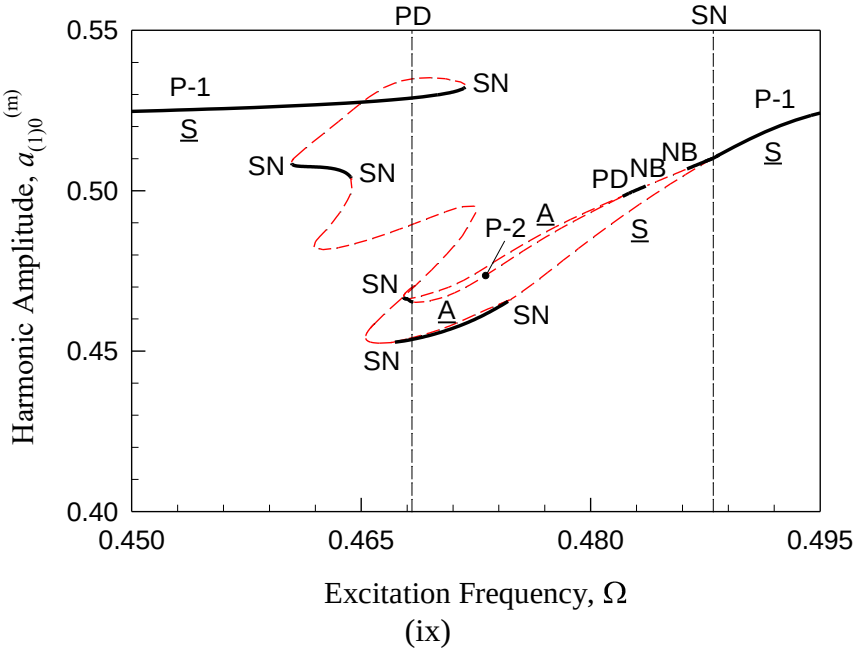

(ix)

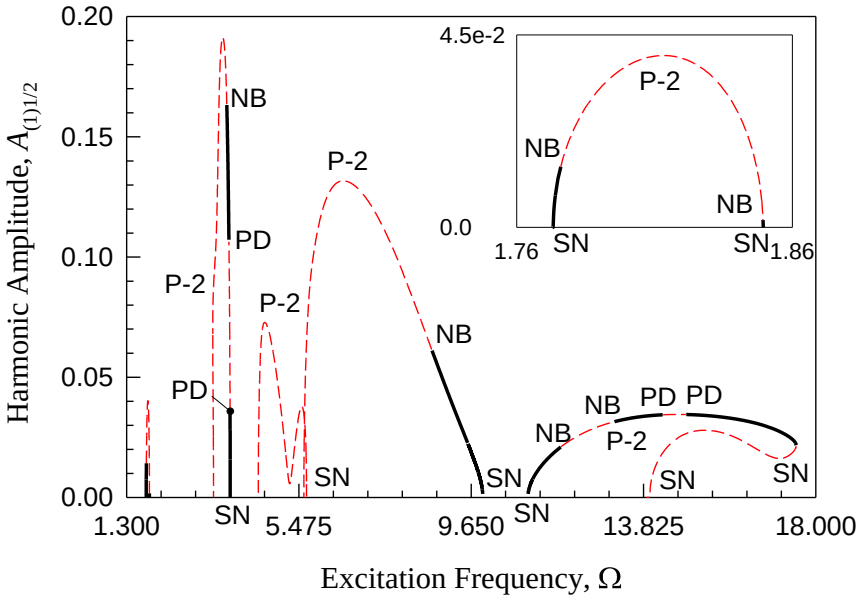

(x)

Fig. 24. (Continued).

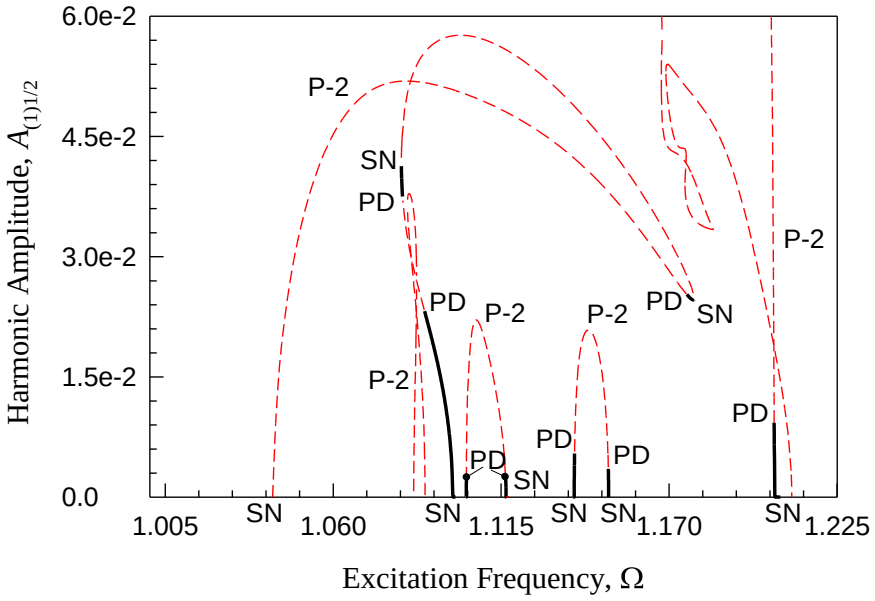

(xi)

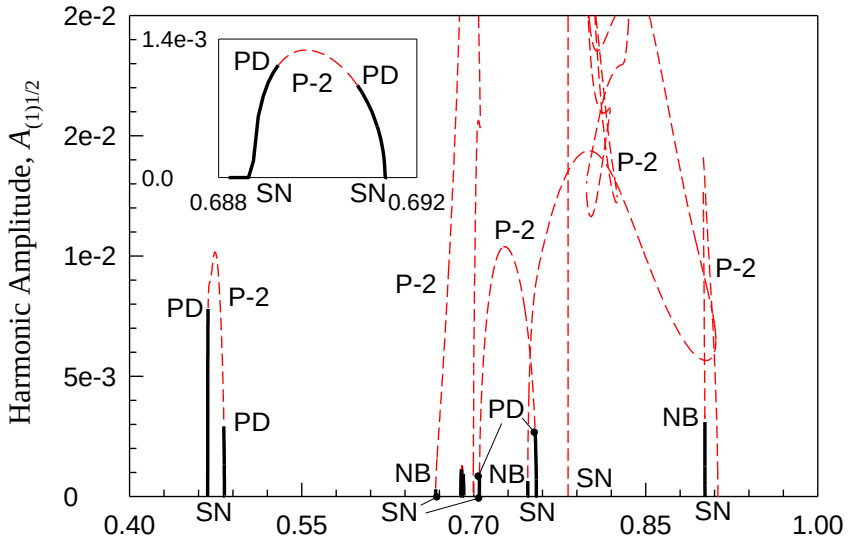

(xii)

Fig. 24. (Continued).

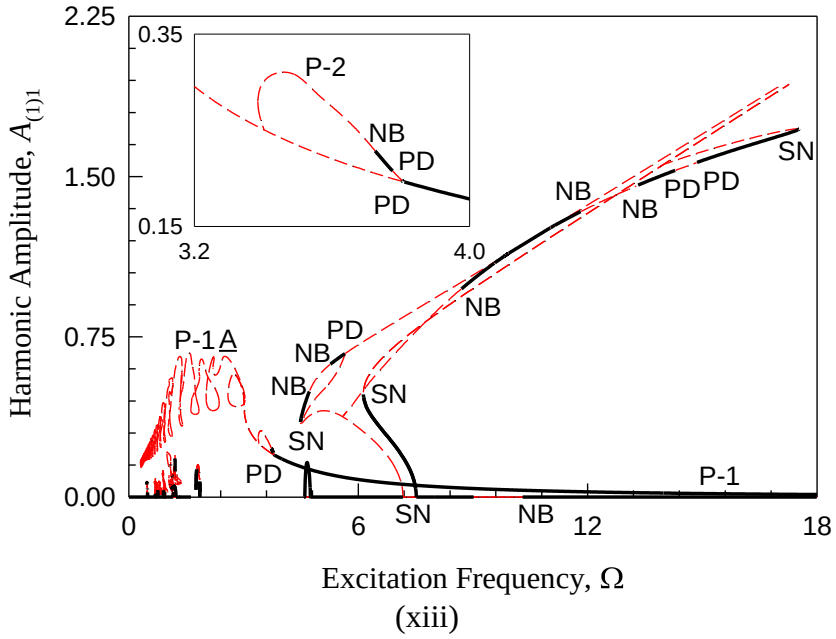

(xiii)

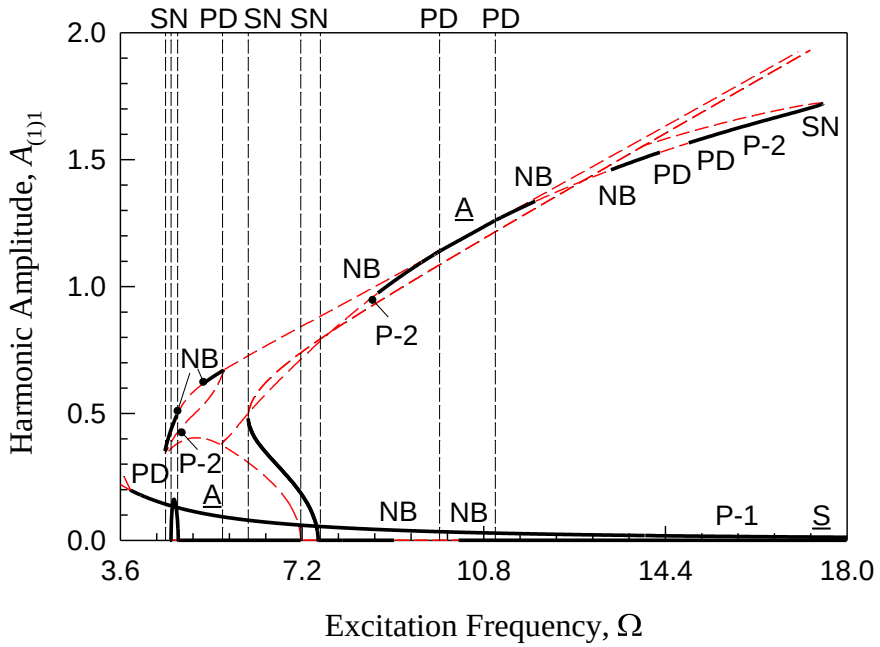

(xiv)

Fig. 24. (Continued).

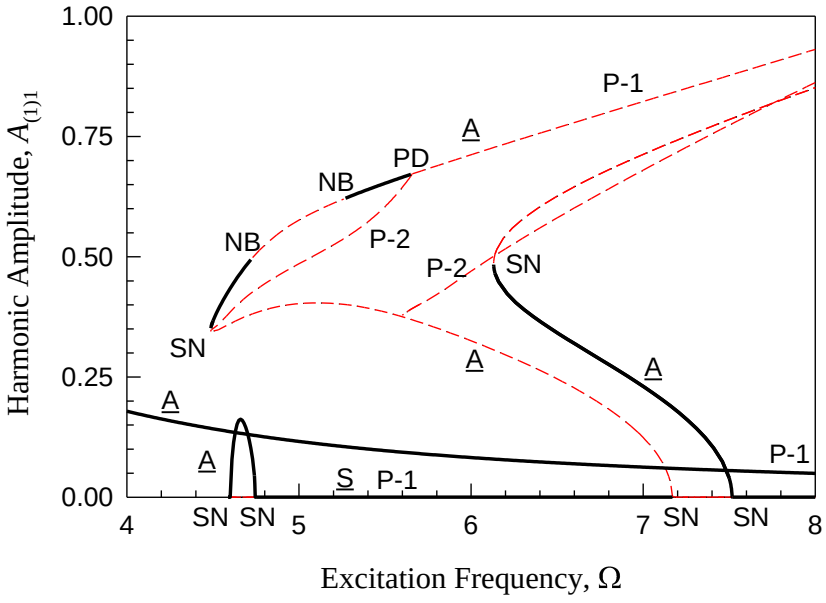

(xv)

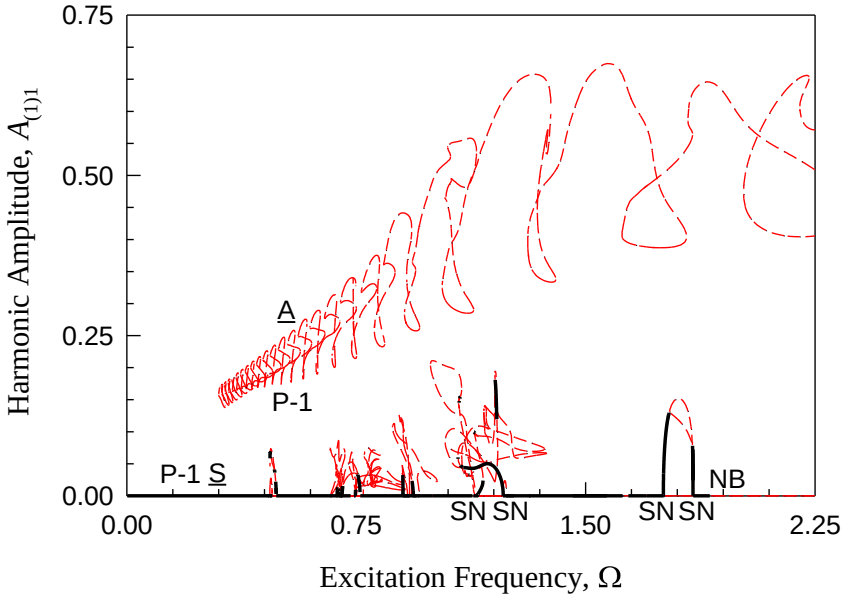

(xvi)

Fig. 24. (Continued).

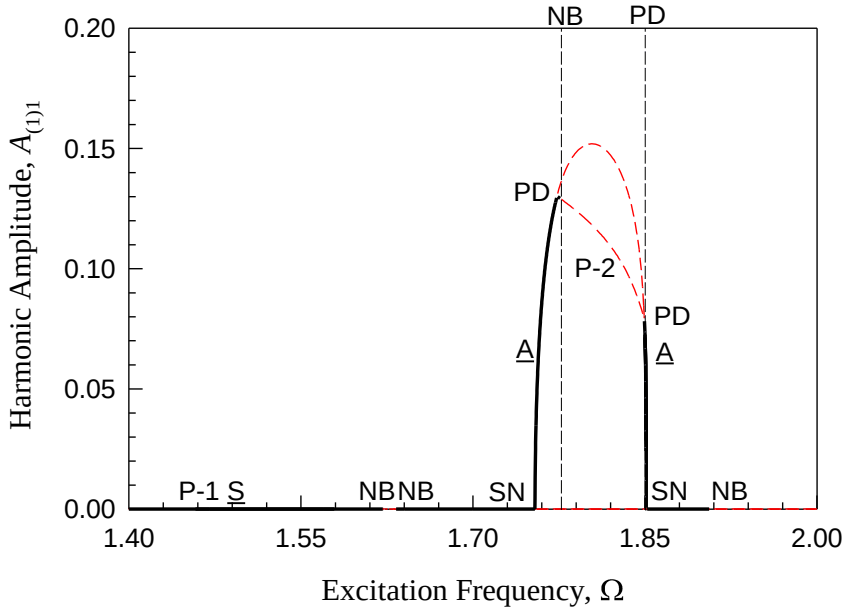

(xvii)

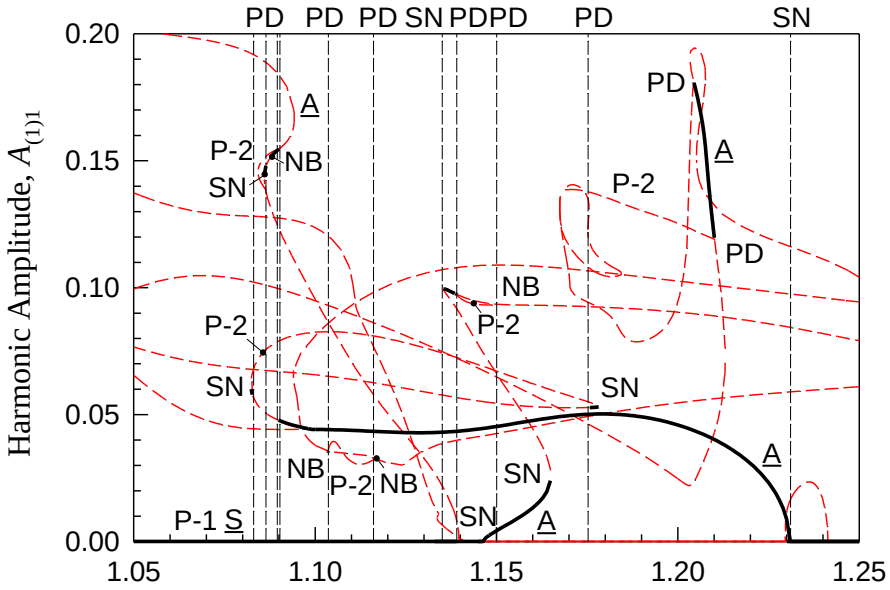

(xviii)

Fig. 24. (Continued).

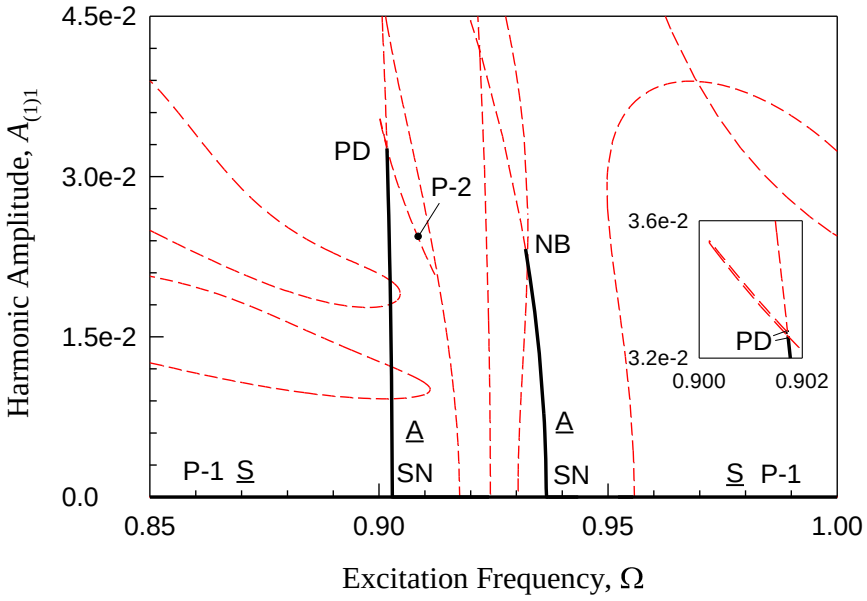

(xix)

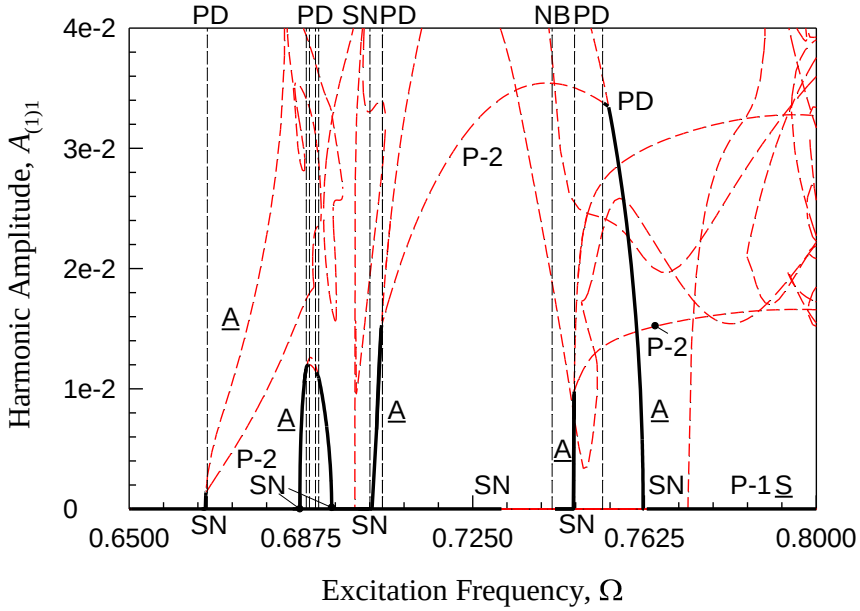

(xx)

Fig. 24. (Continued).

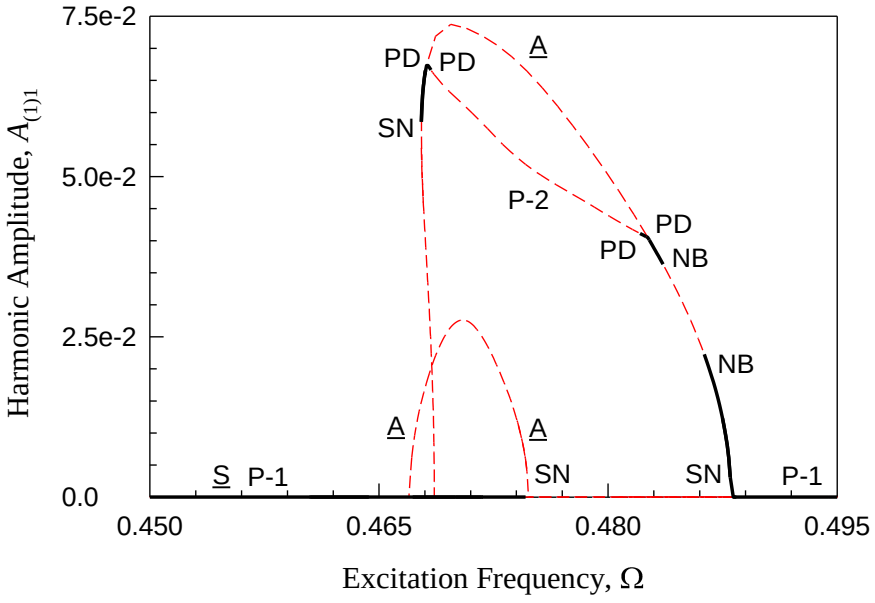

(xxi)

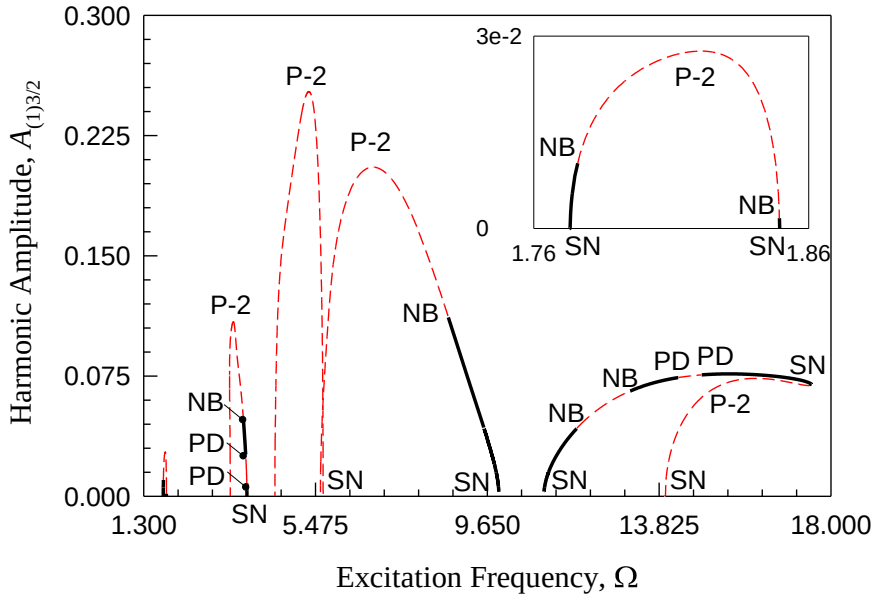

(xxii)

Fig. 24. (Continued).

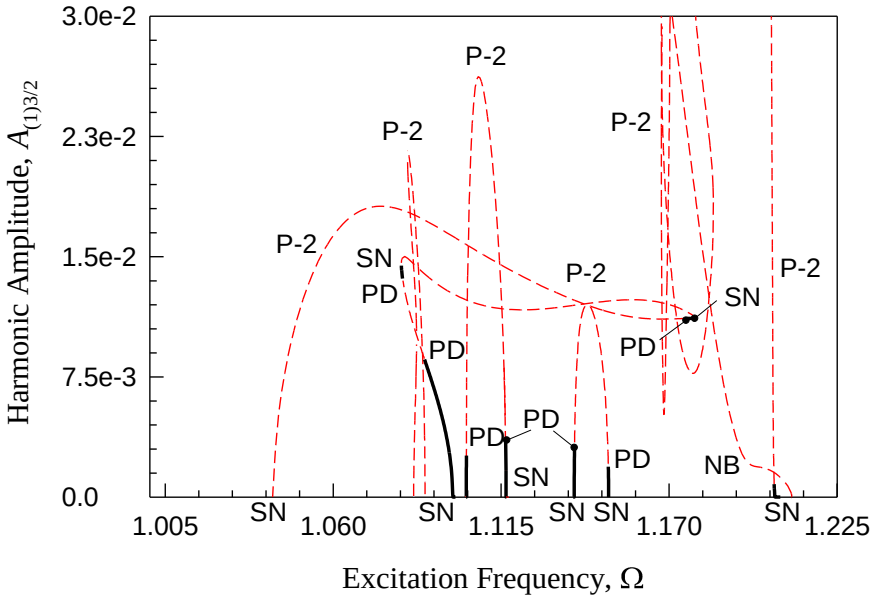

(xxiii)

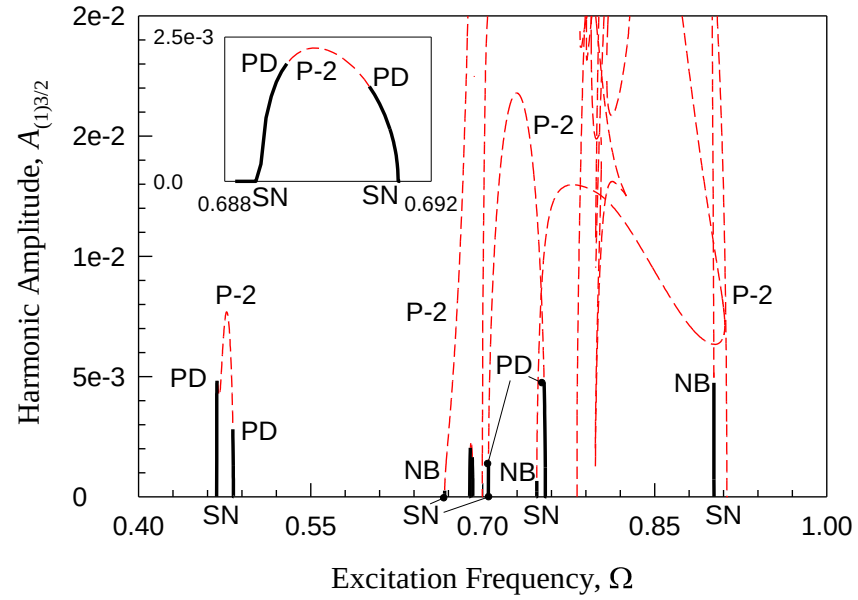

(xxiv)

Fig. 24. (Continued).

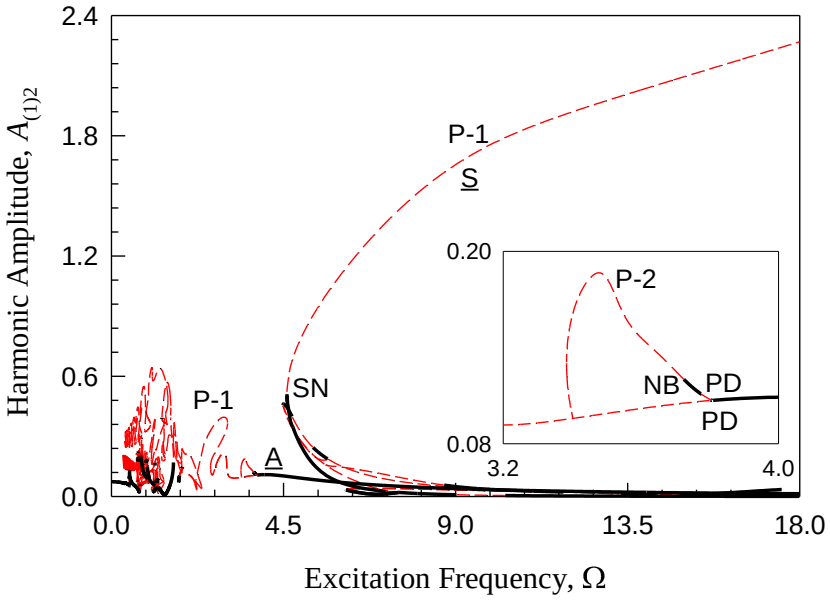

(xxv)

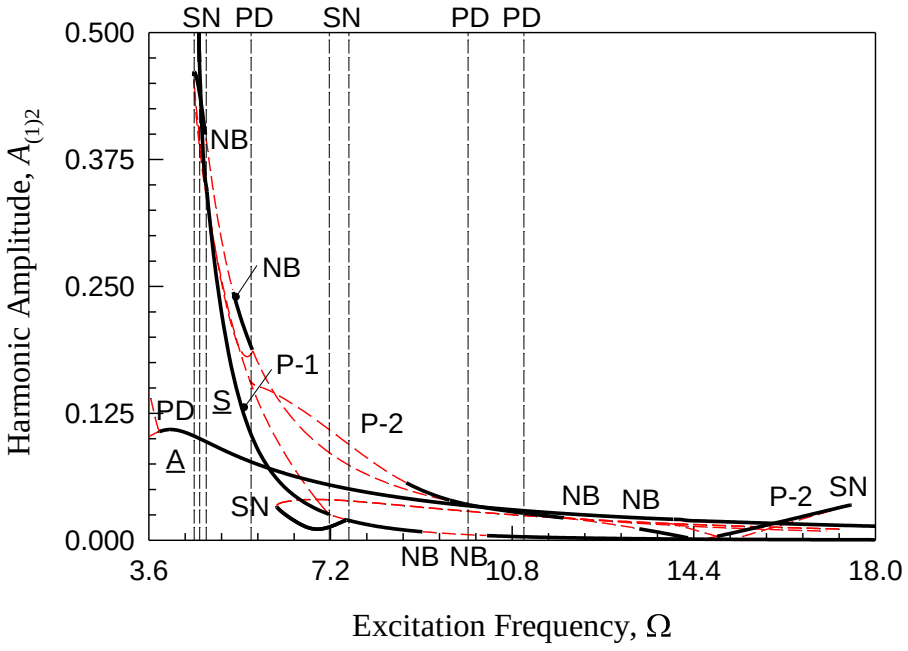

(xxvi)

Fig. 24. (Continued).

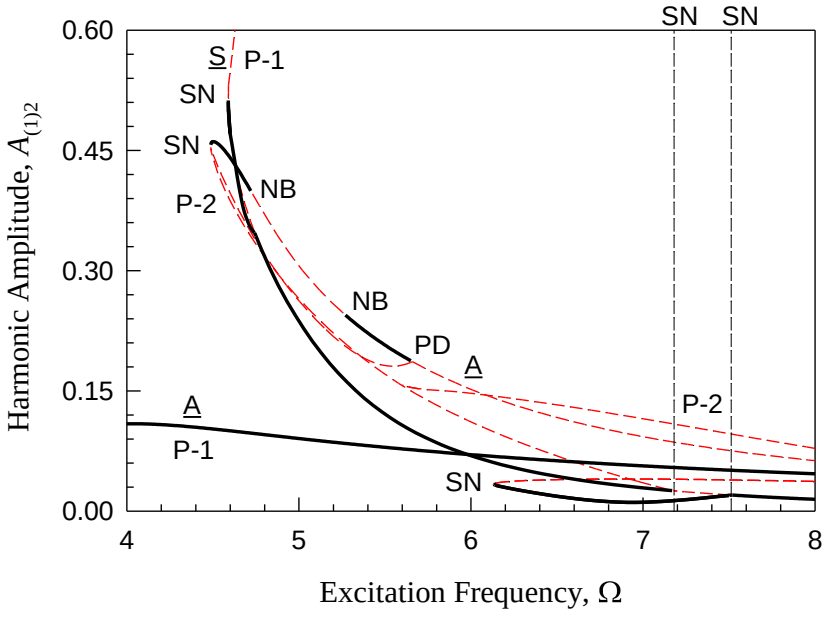

(xxvii)

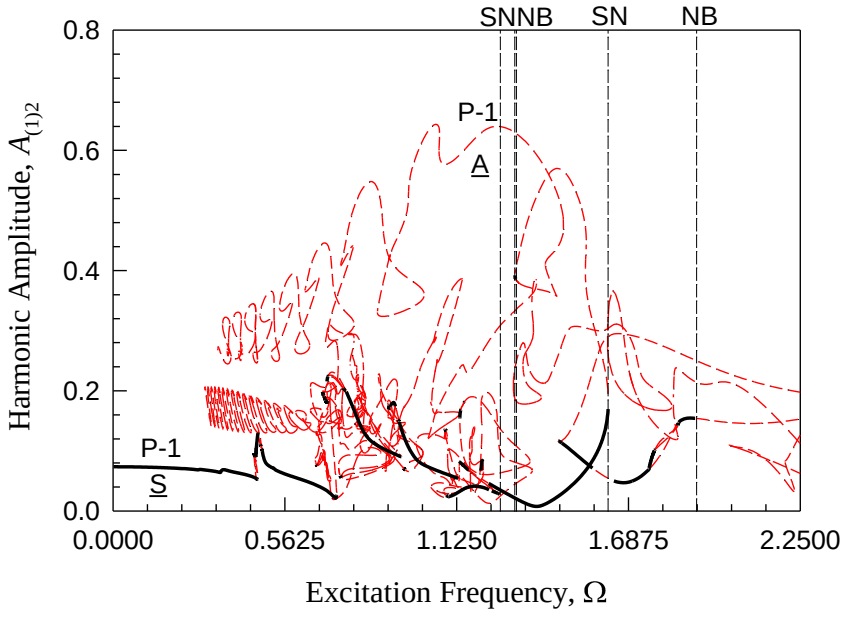

(xxviii)

Fig. 24. (Continued).

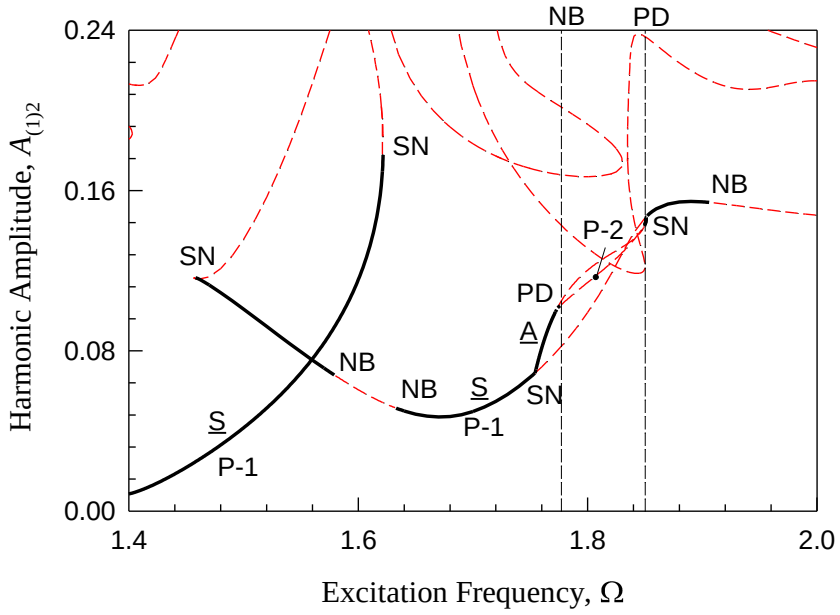

(xxix)

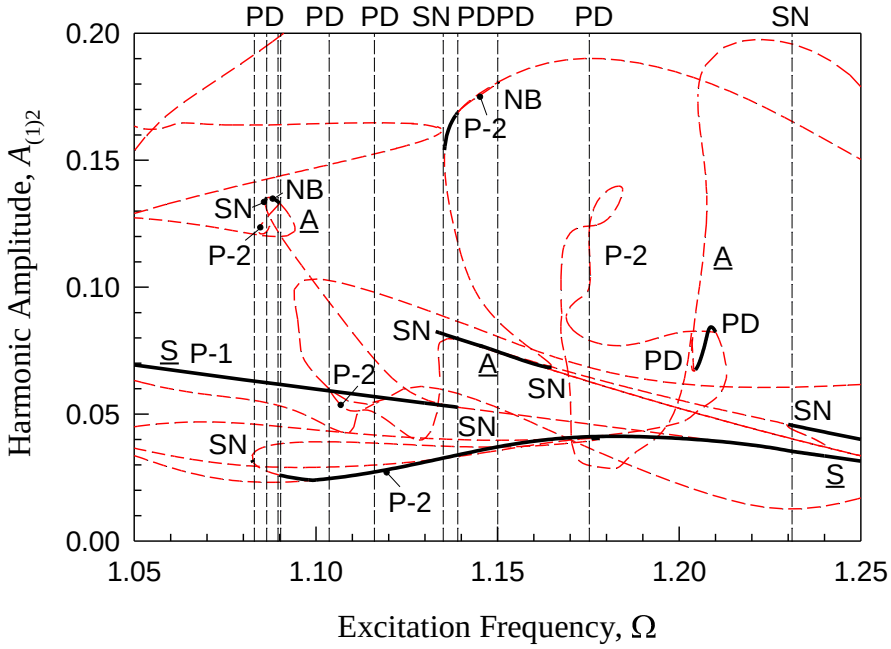

(xxx)

Fig. 24. (Continued).

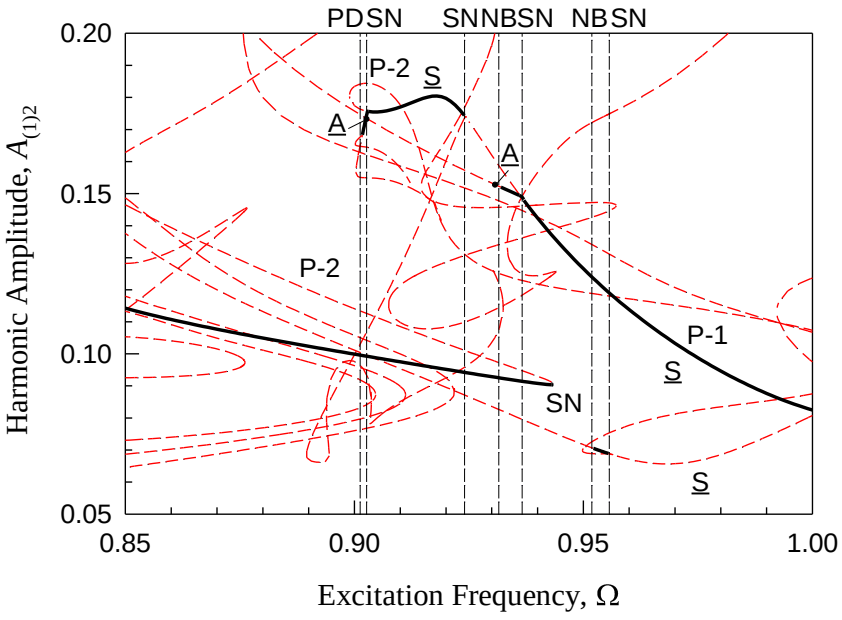

(xxxi)

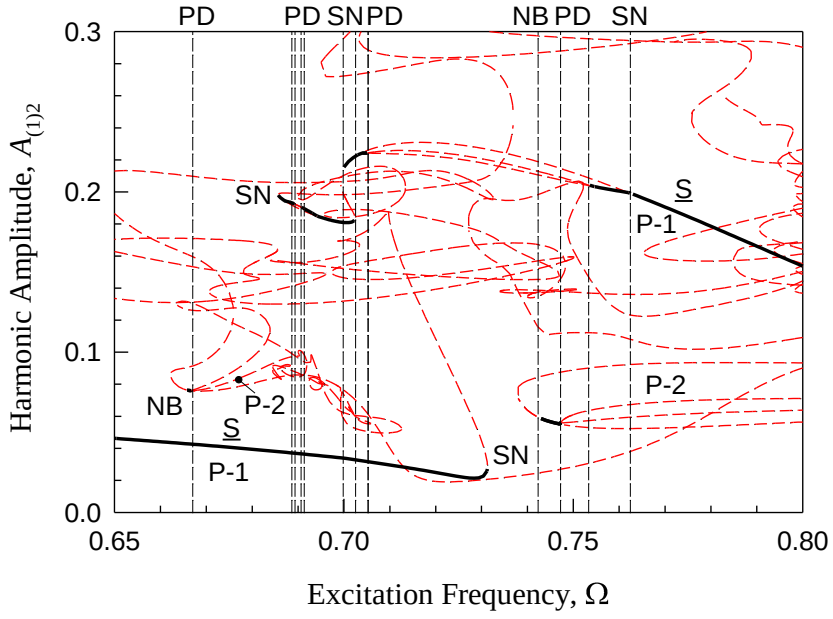

(xxxii)

Fig. 24. (Continued).

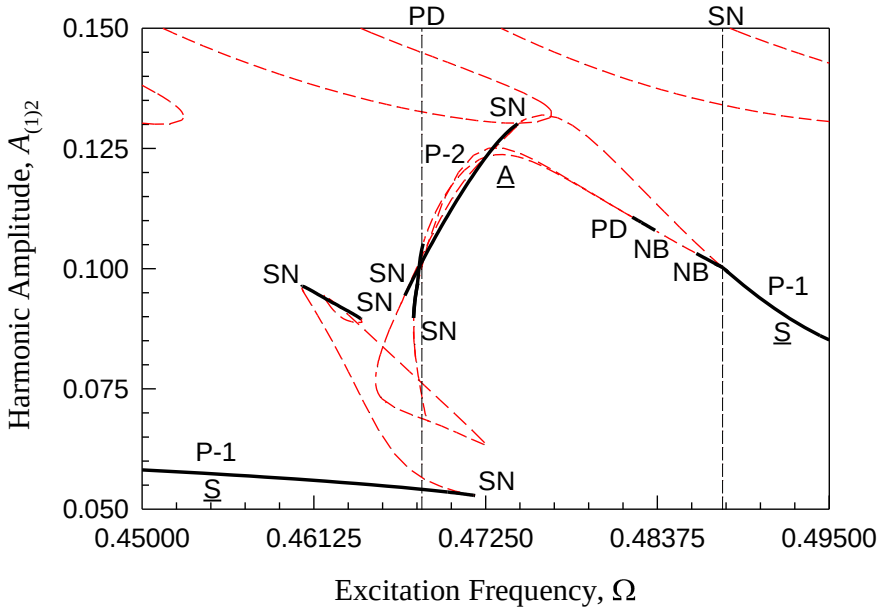

(xxxiii)

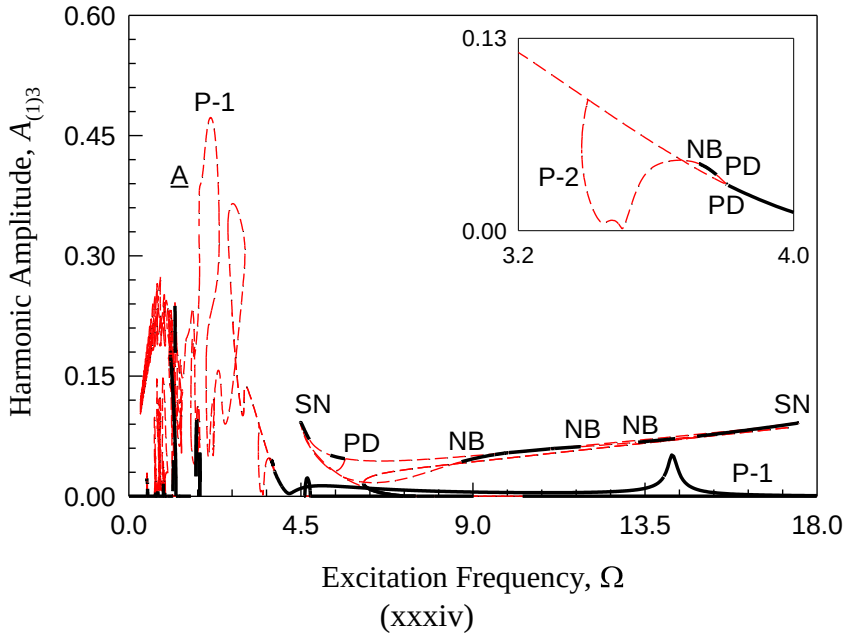

(xxxiv)

Fig. 24. (Continued).

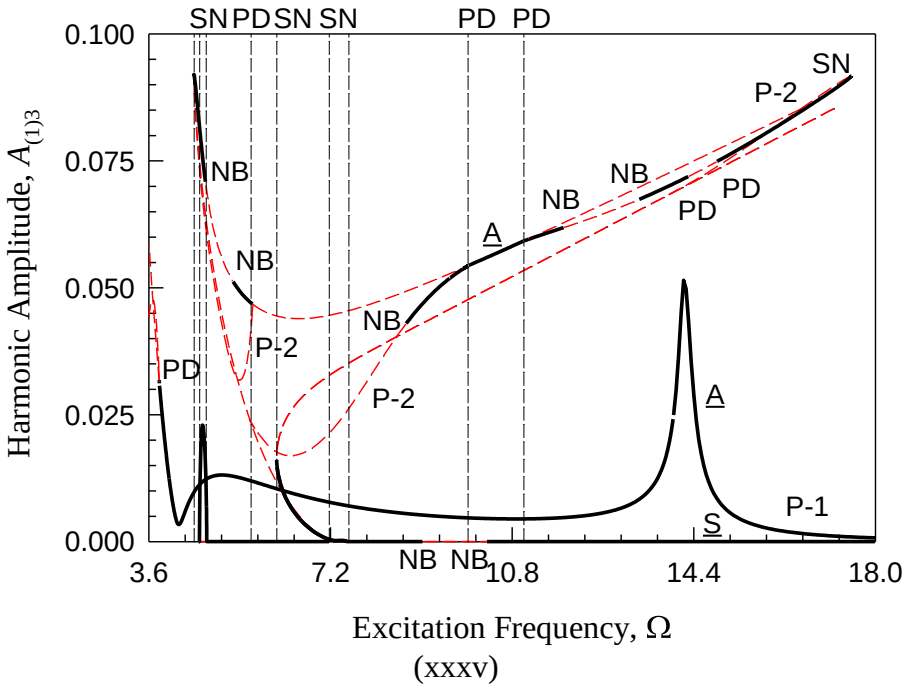

(xxxv)

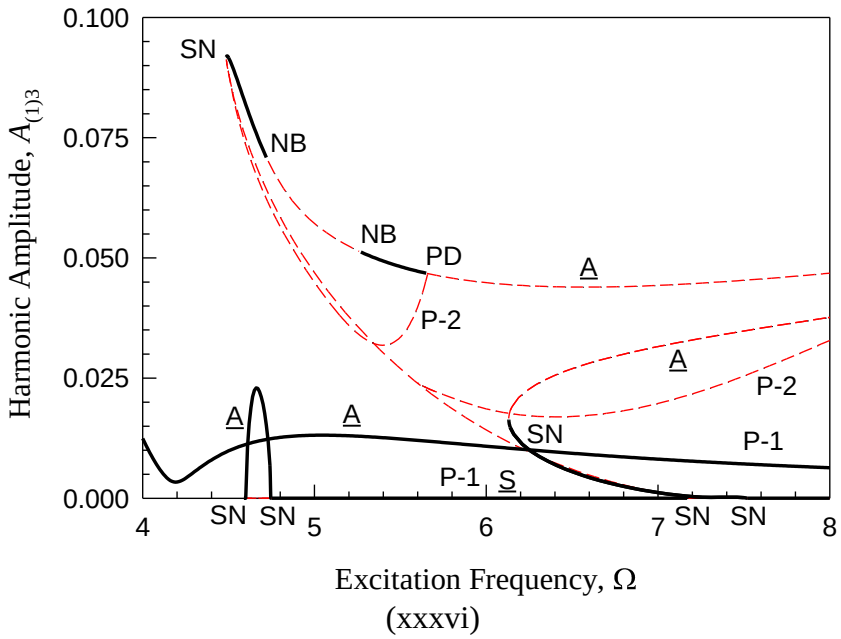

(xxxvi)

Fig. 24. (Continued).

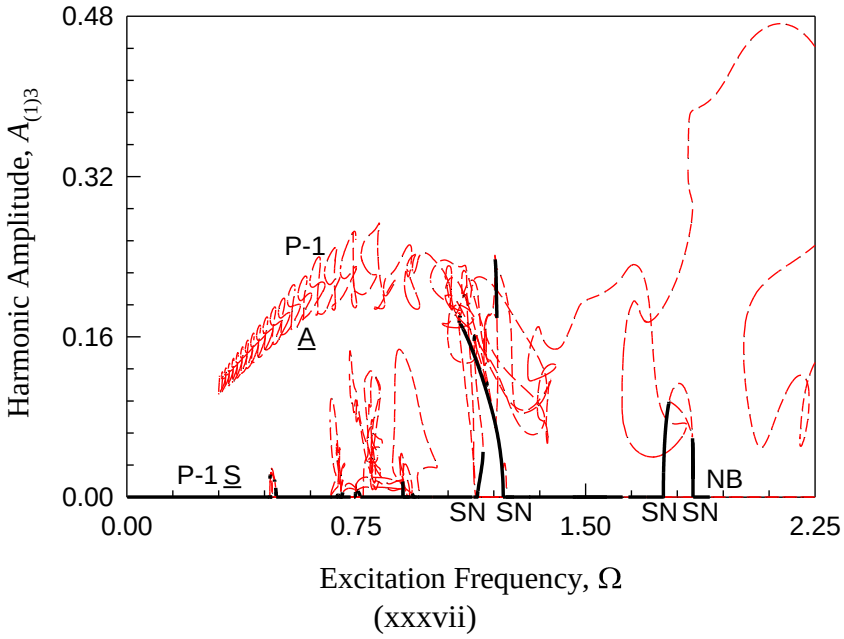

(xxxvii)

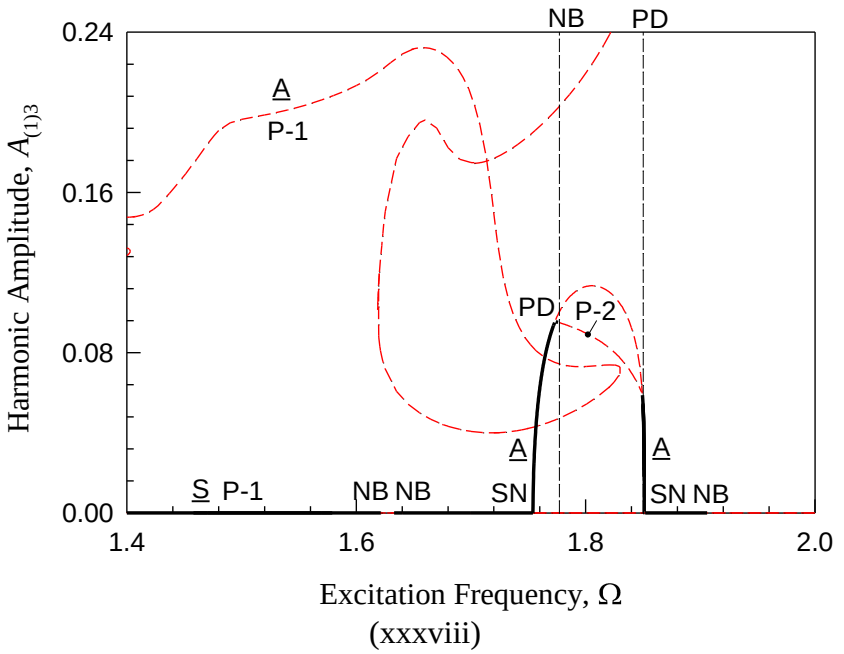

(xxxviii)

Fig. 24. (Continued).

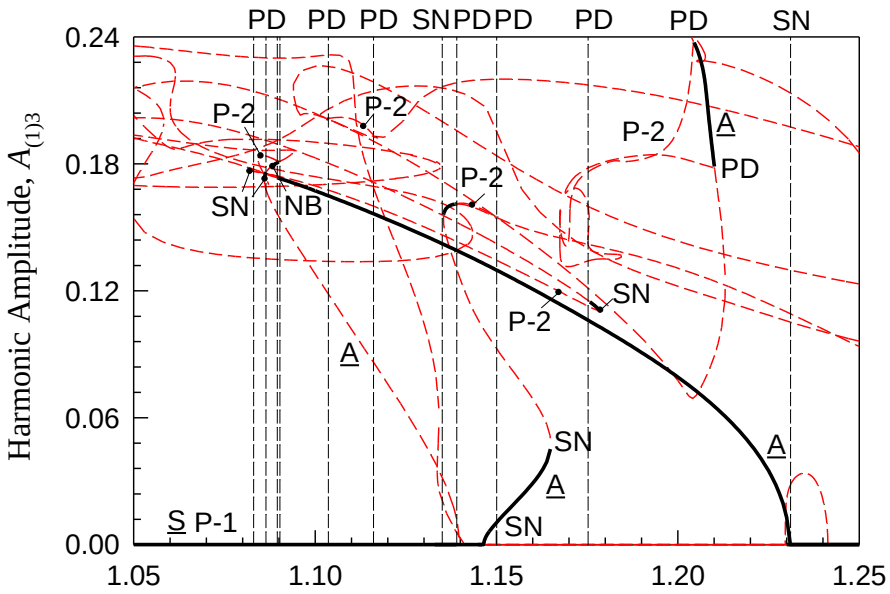

(xxxix)

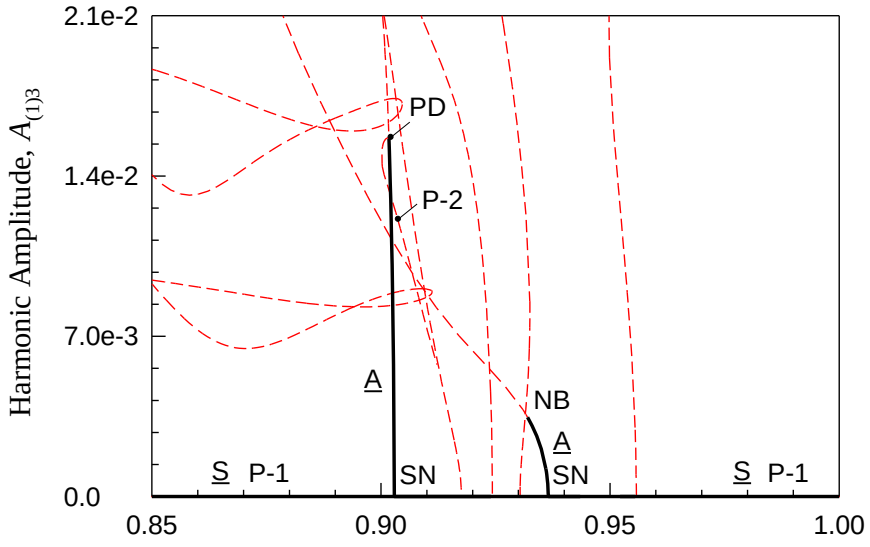

(xl)

Fig. 24. (Continued).

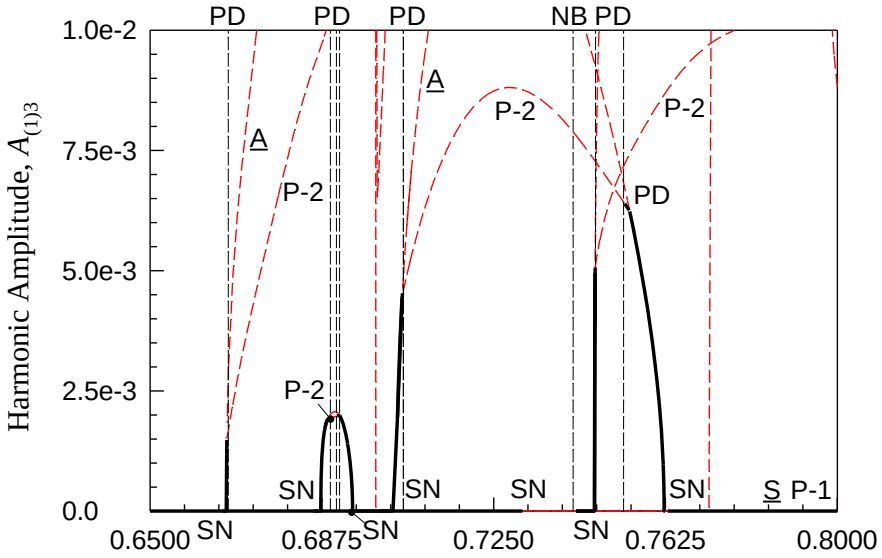

(xli)

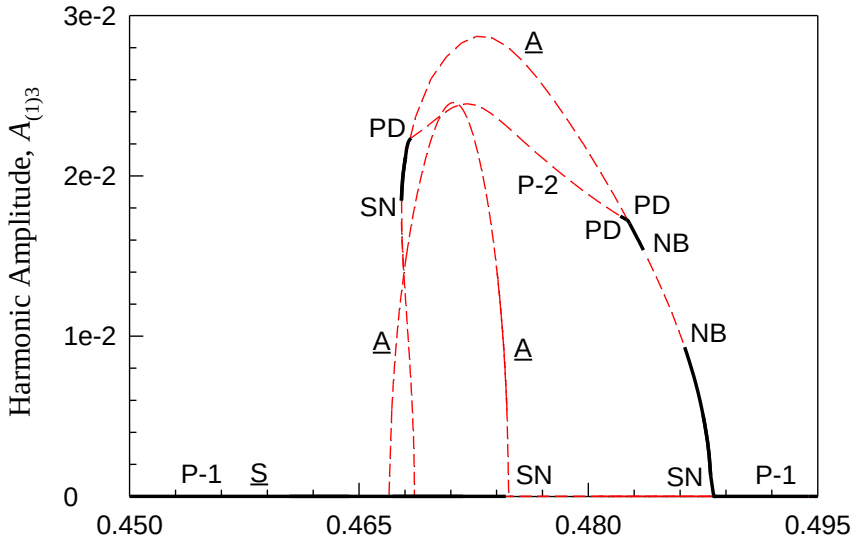

(xlii)

Fig. 24. (Continued).

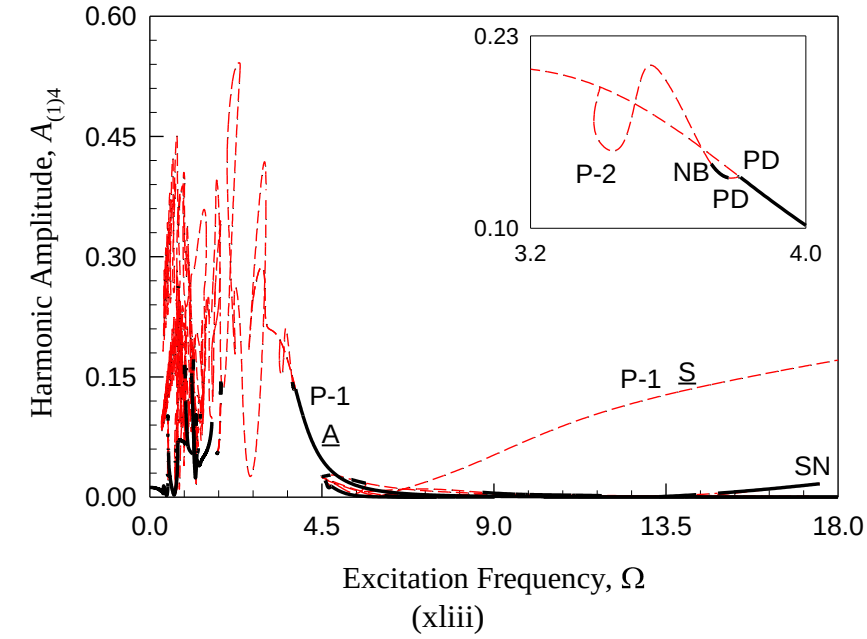

(xliii)

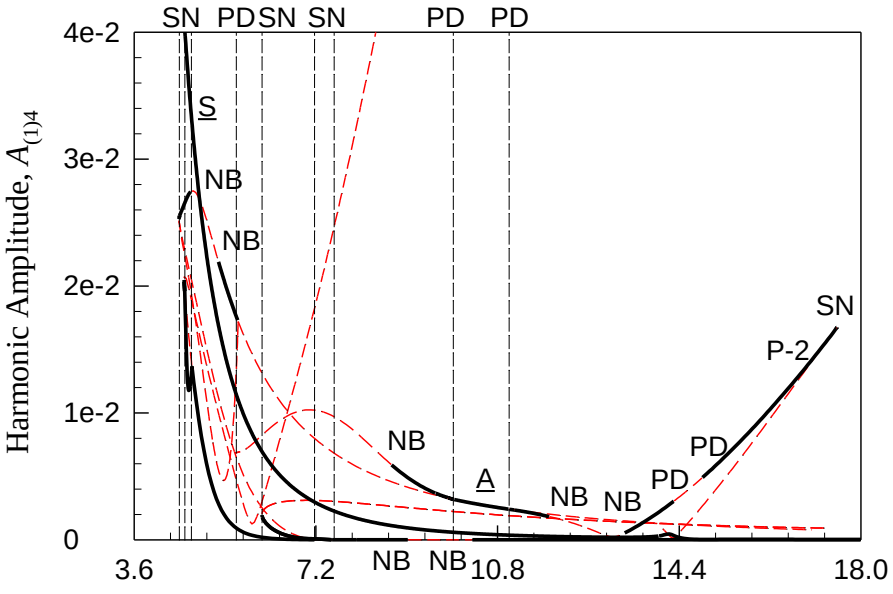

(xliv)

Fig. 24. (Continued).

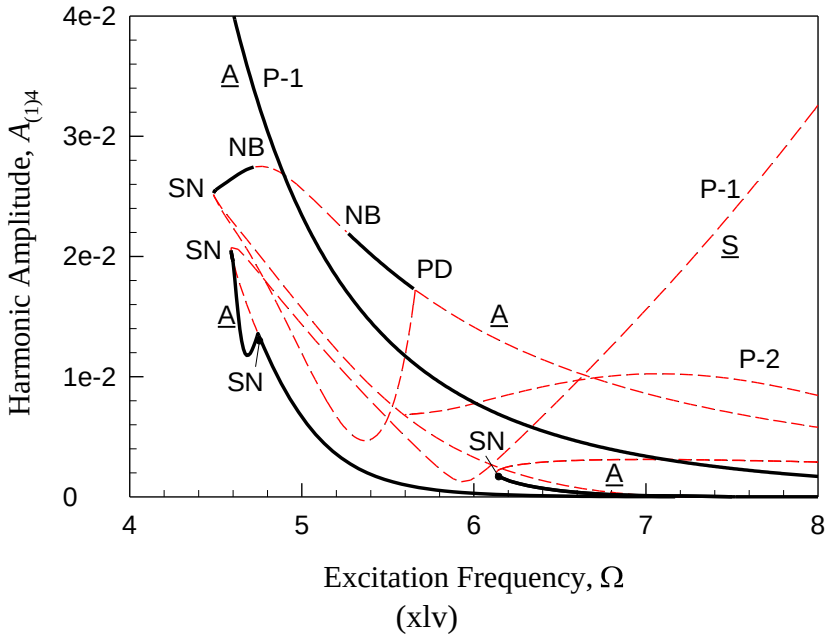

(xlv)

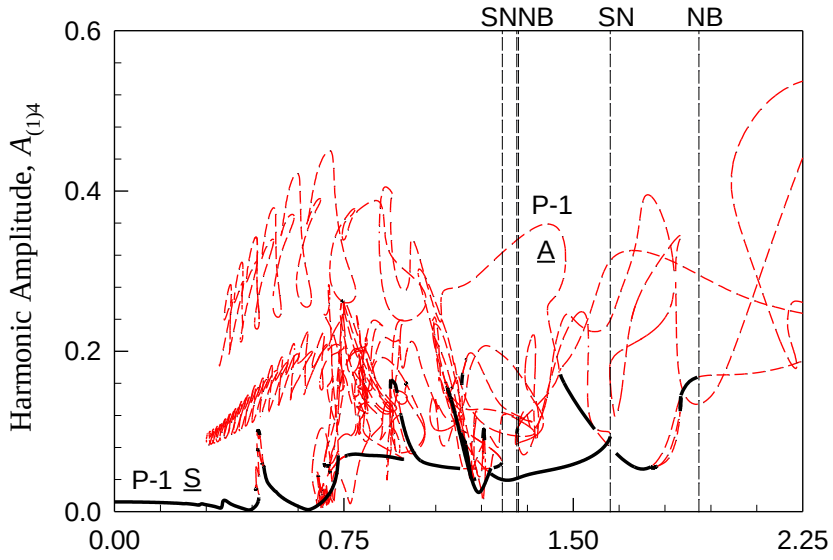

(xlvi)

Fig. 24. (Continued).

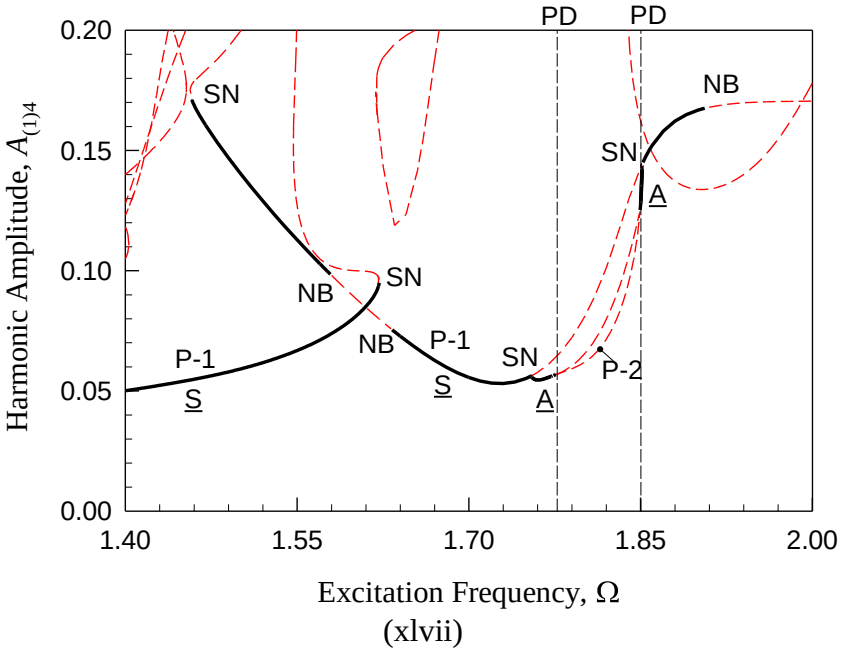

(xlvii)

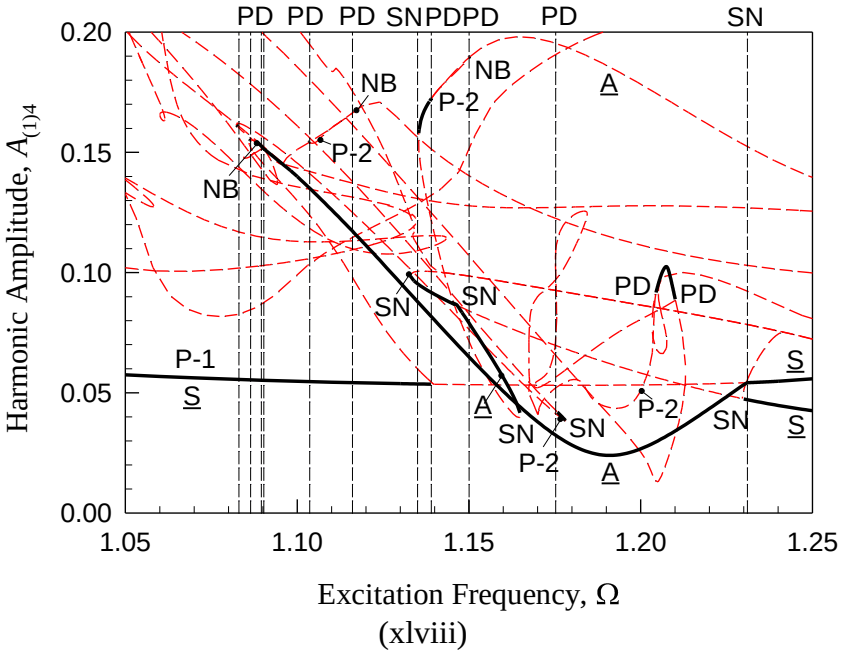

(xlviii)

Fig. 24. (Continued).

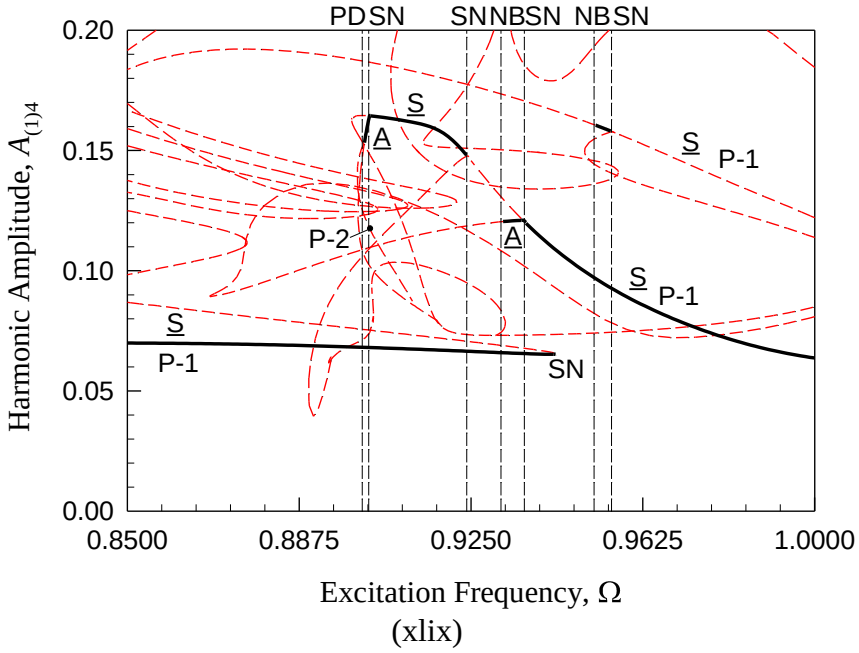

(xlix)

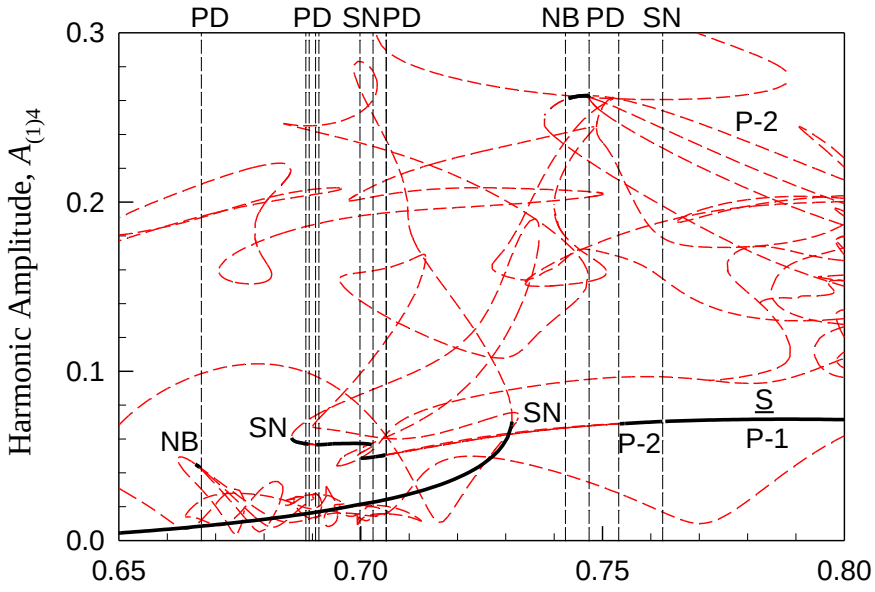

(l)

Fig. 24. (Continued).

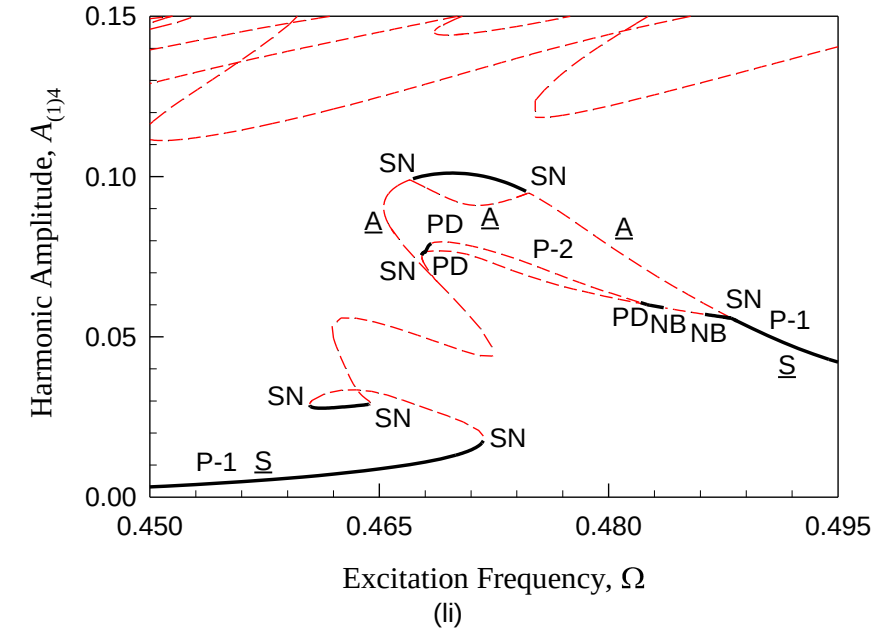

(li)

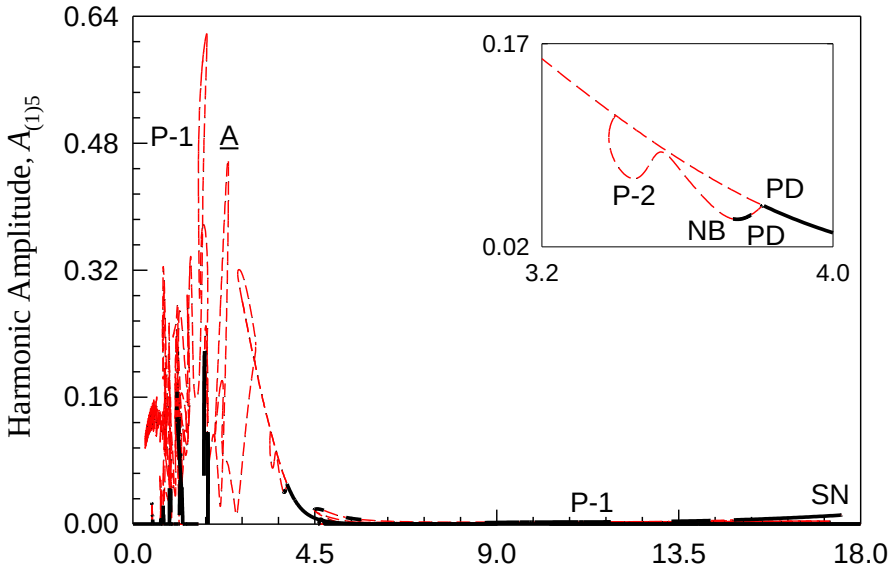

(lii)

Fig. 24. (Continued).

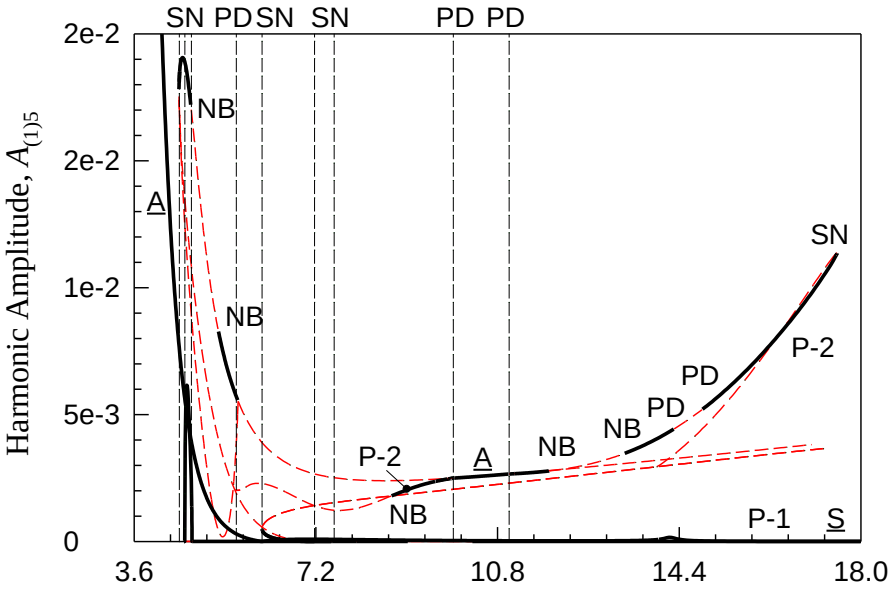

(liii)

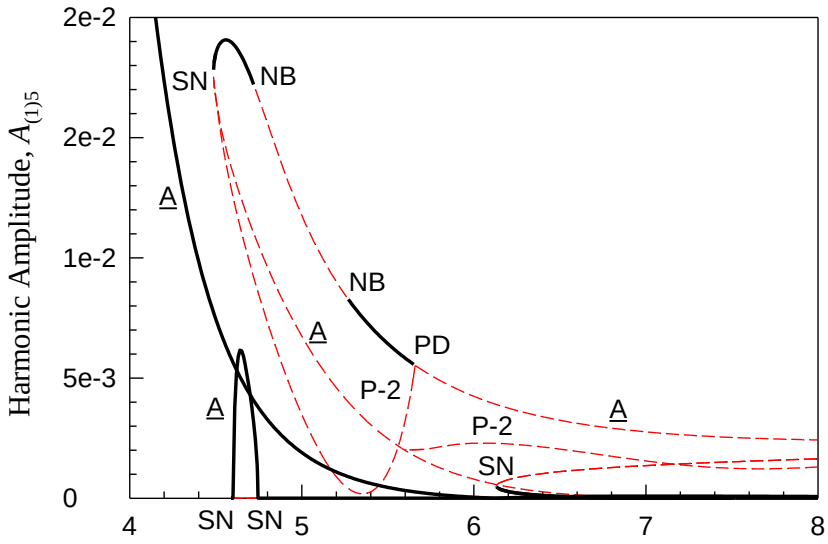

(liv)

Fig. 24. (Continued).

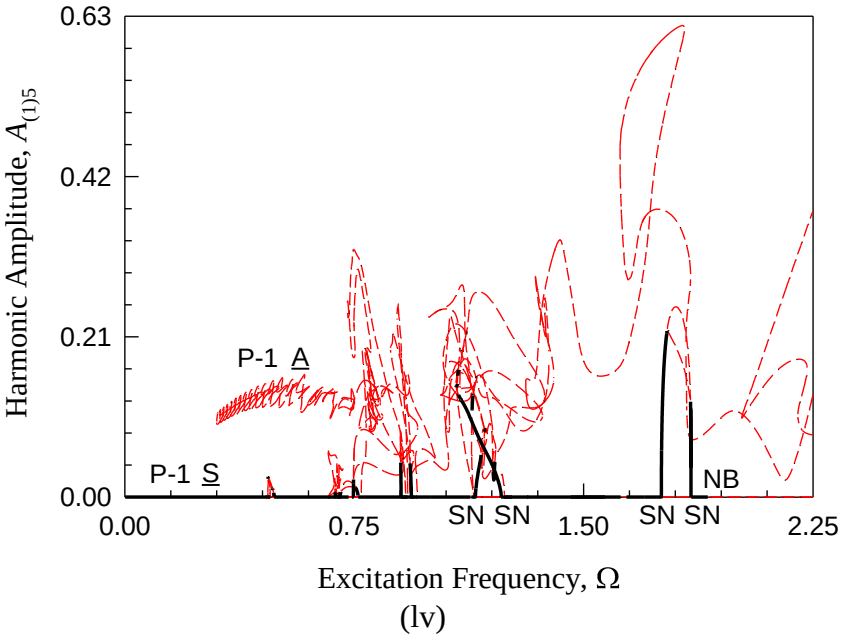

(lv)

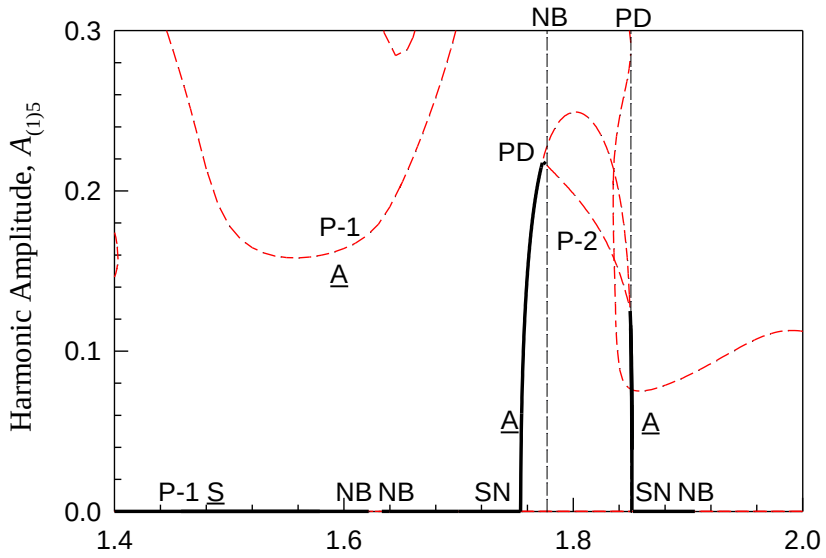

(lvi)

Fig. 24. (Continued).

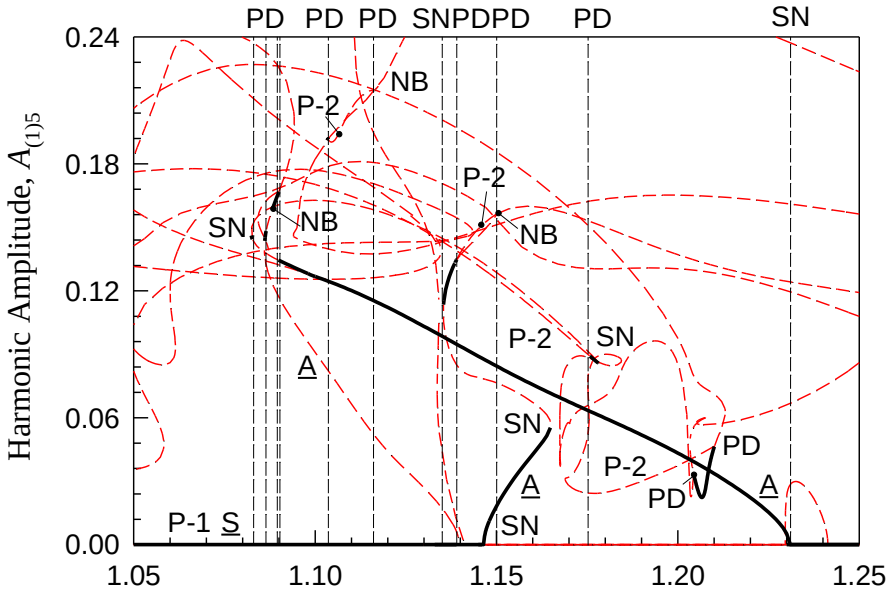

(lvii)

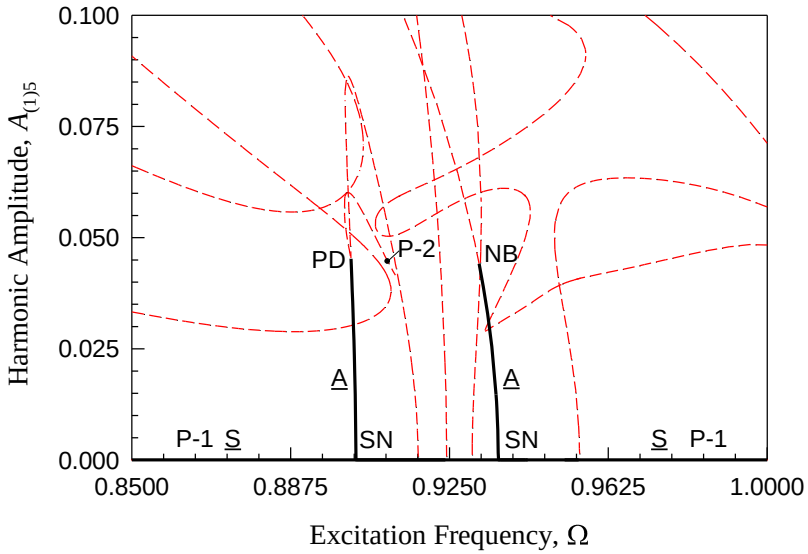

(lviii)

Fig. 24. (Continued).

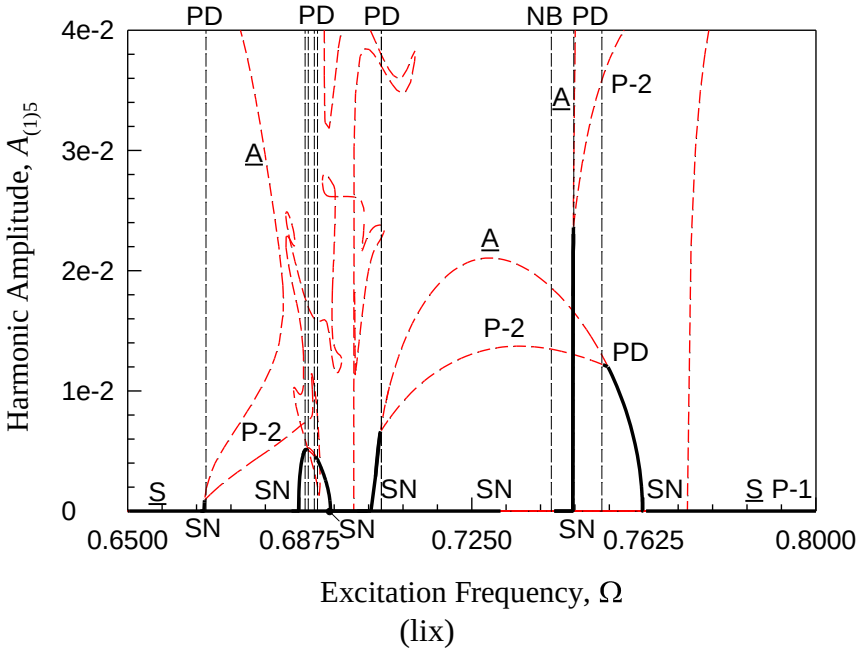

(lix)

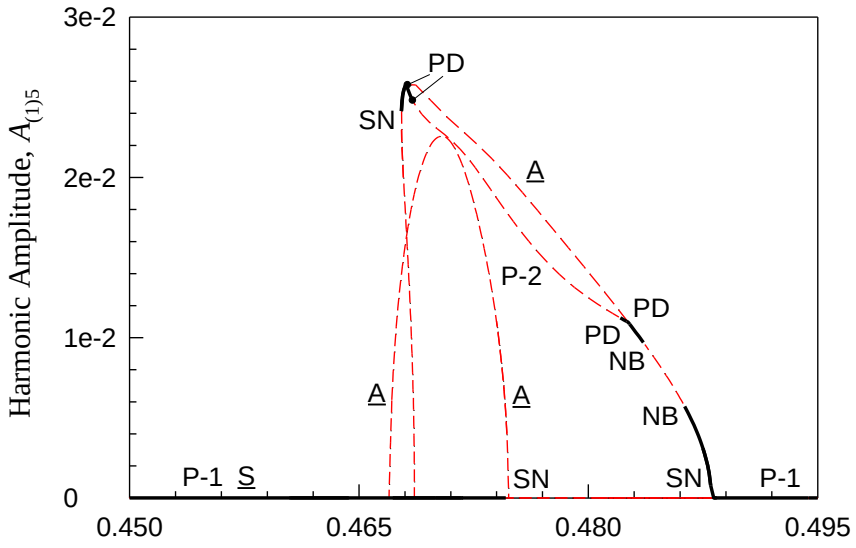

(lx)

Fig. 24. (Continued).

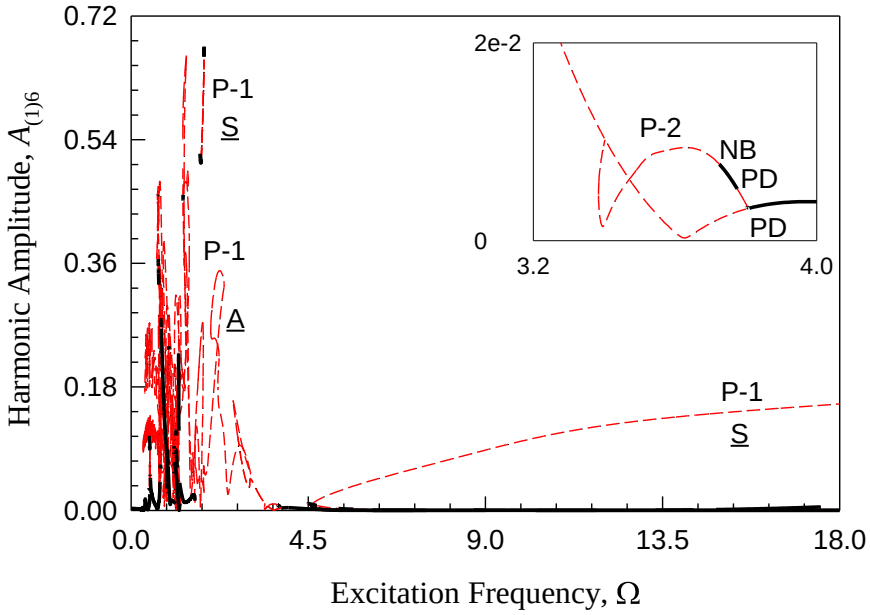

(lxi)

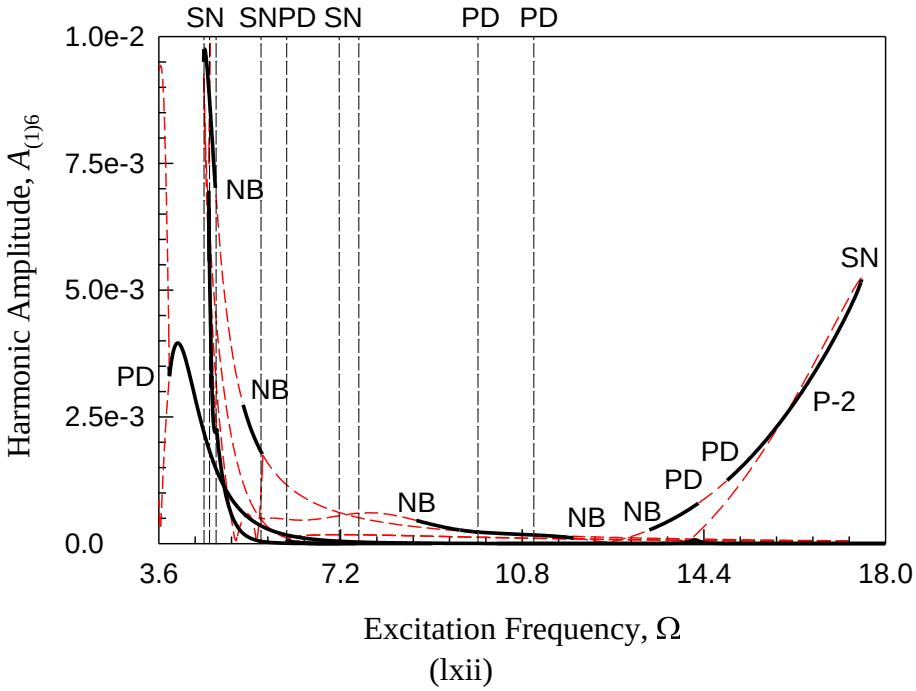

(lxii)

Fig. 24. (Continued).

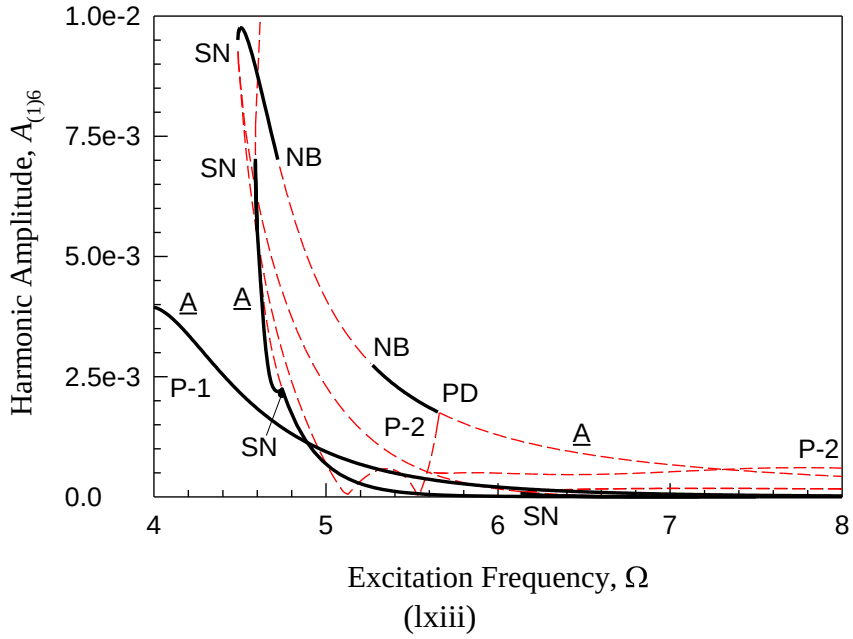

(lxiii)

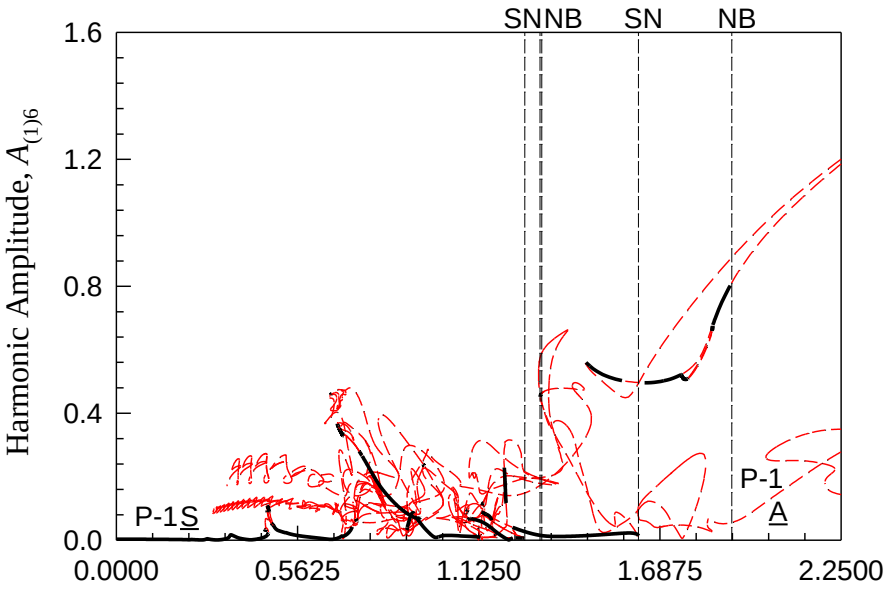

(lxiv)

Fig. 24. (Continued).

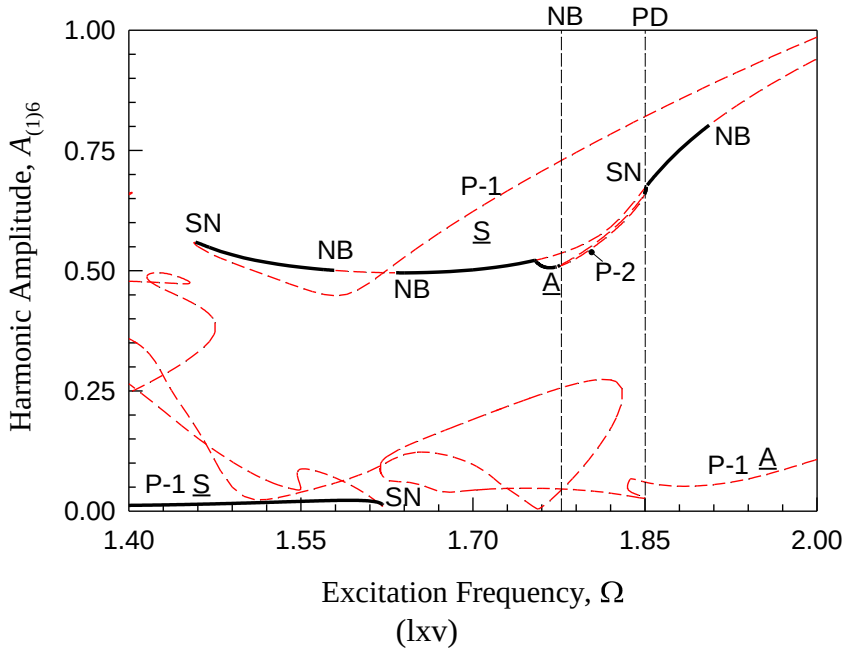

(lxv)

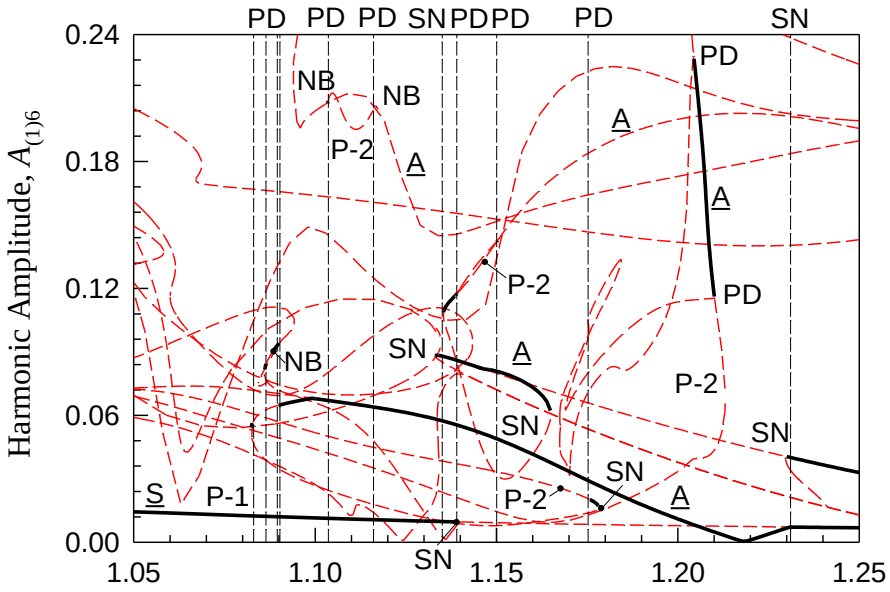

(lxvi)

Fig. 24. (Continued).

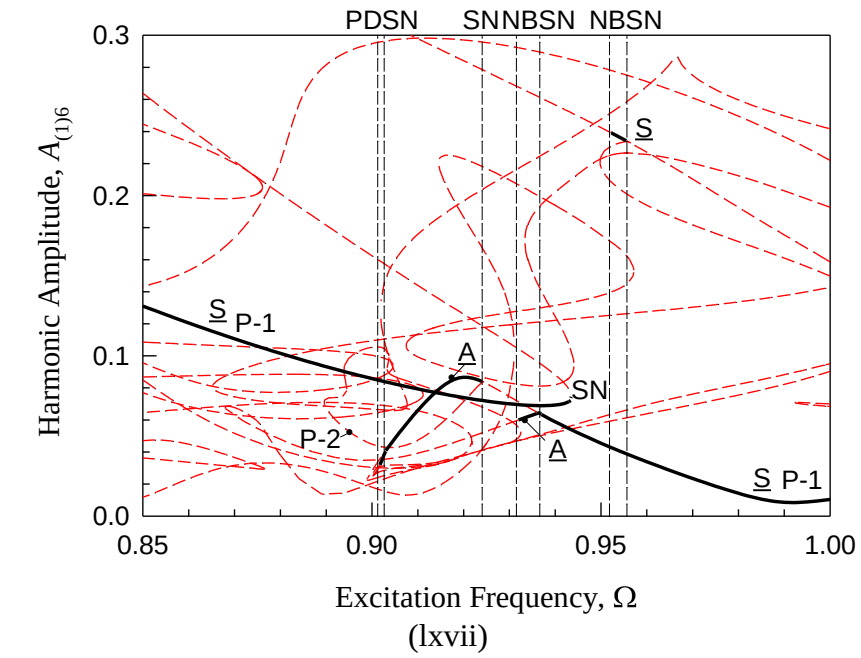

(lxvii)

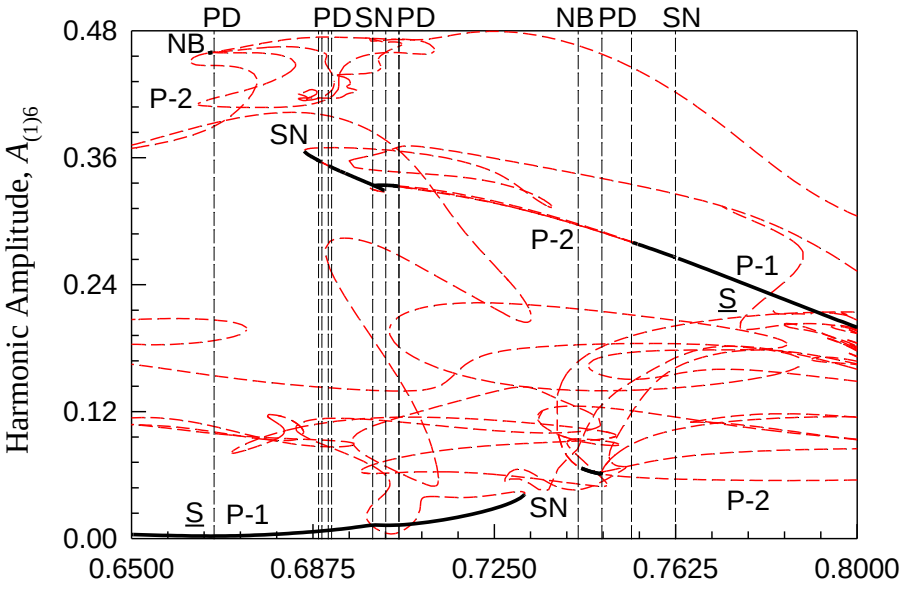

(lxviii)

Fig. 24. (Continued).

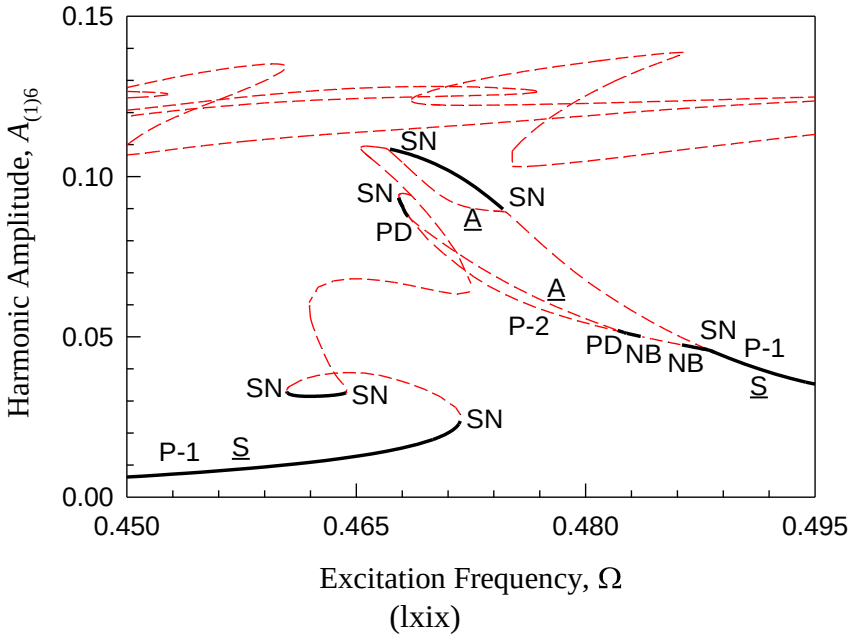

(lxix)

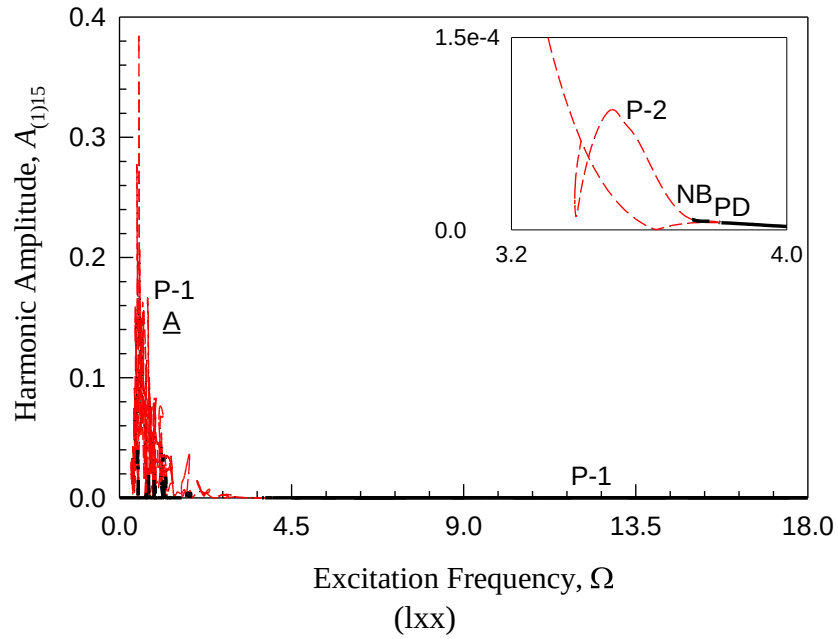

(lxx)

Fig. 24. (Continued).

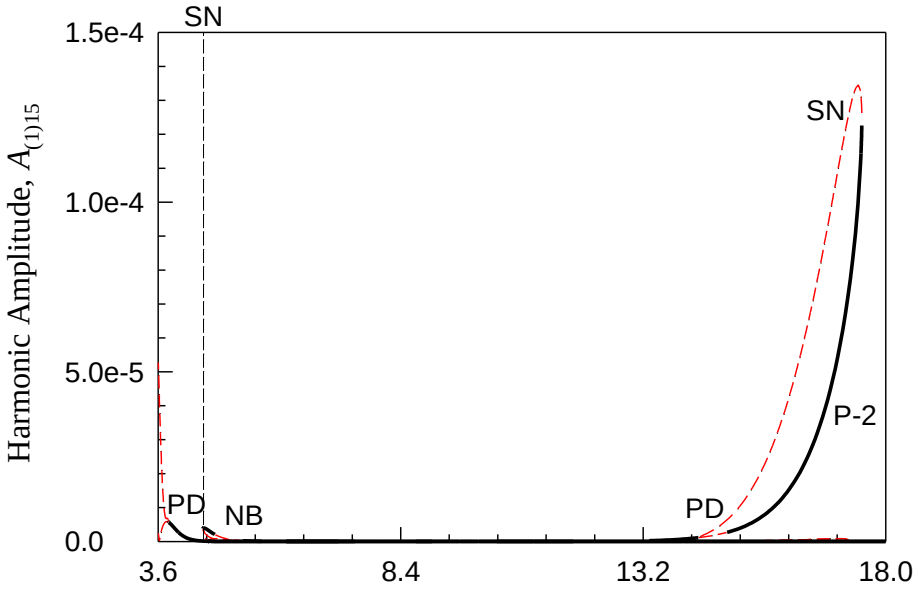

(lxxi)

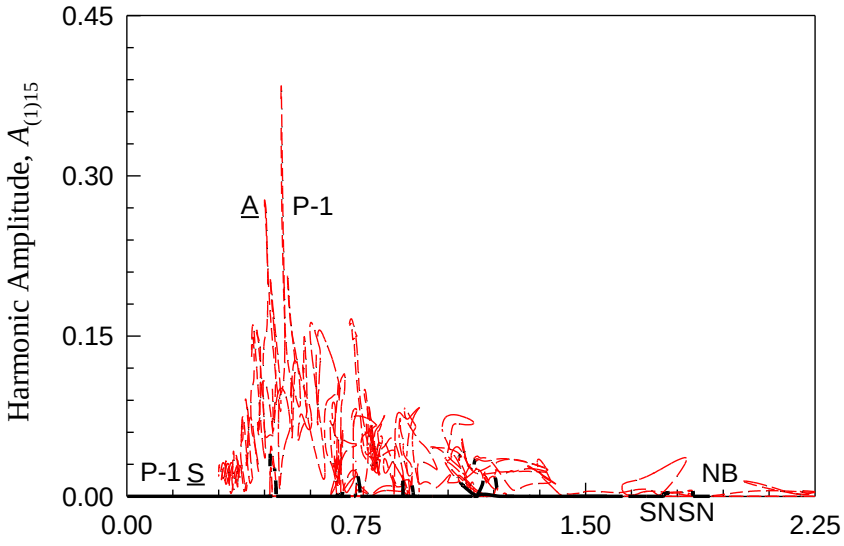

(lxxii)

Fig. 24. (Continued).

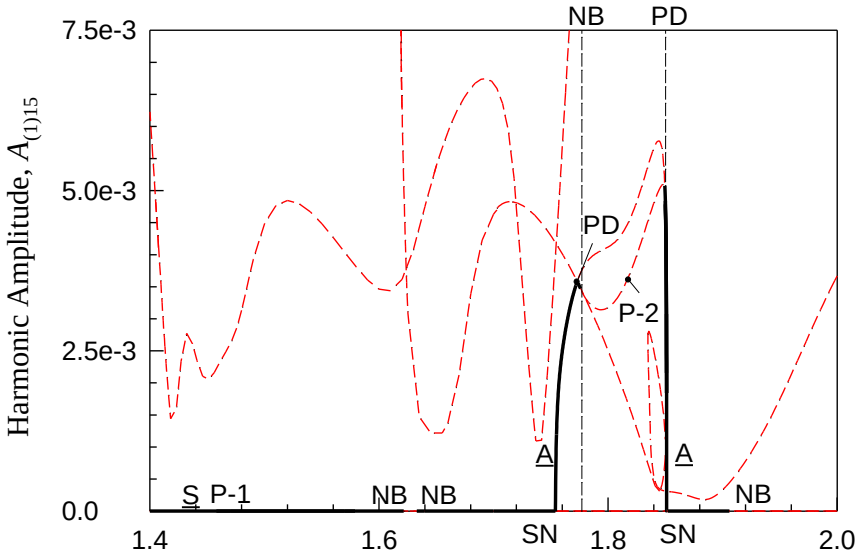

(lxxiii)

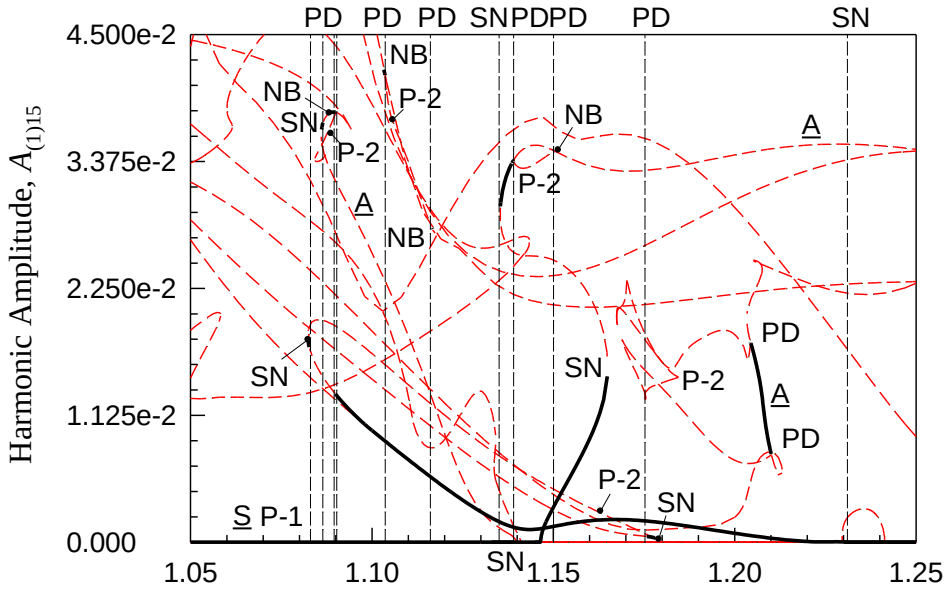

(lxxiv)

Fig. 24. (Continued).

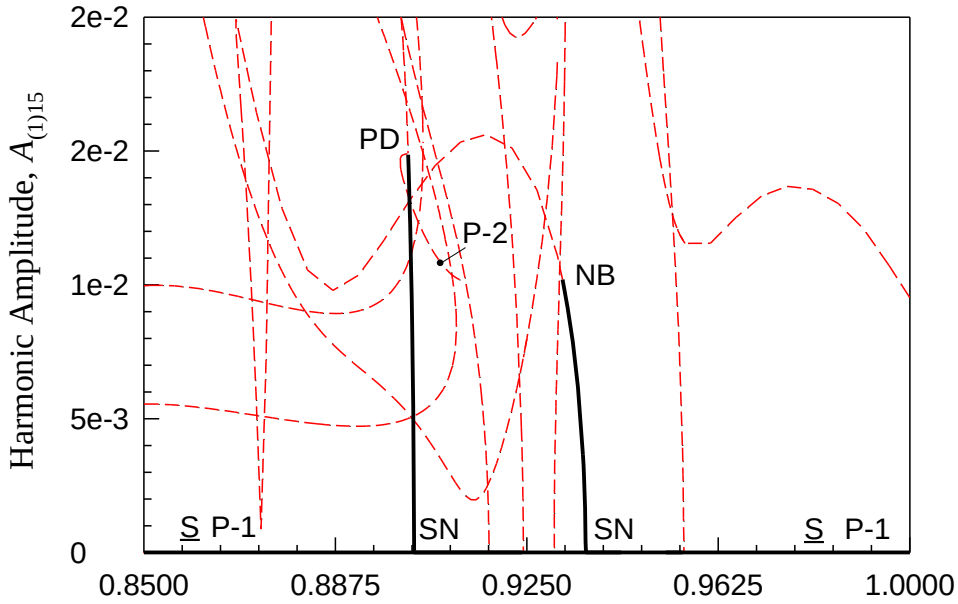

(lxxv)

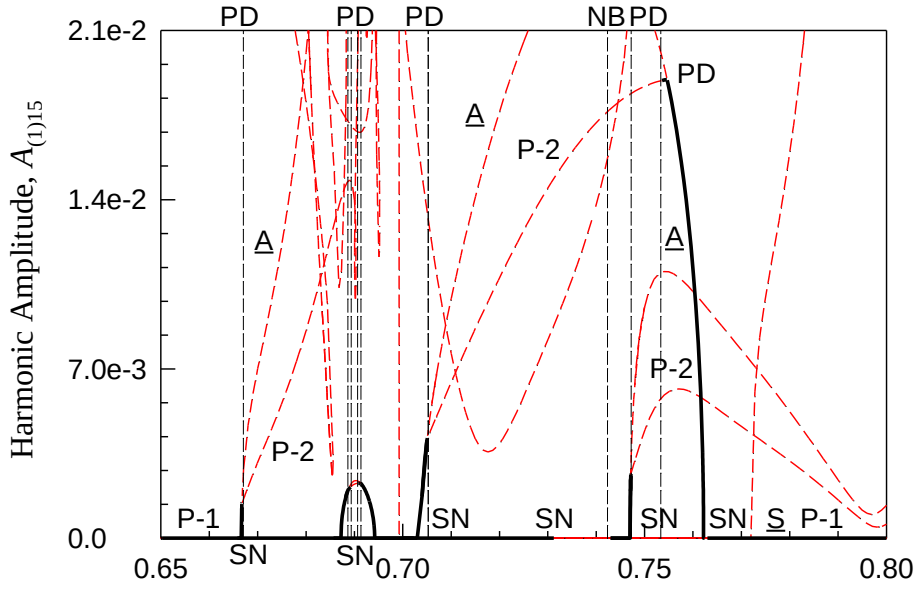

(lxxvi)

Fig. 24. (Continued).

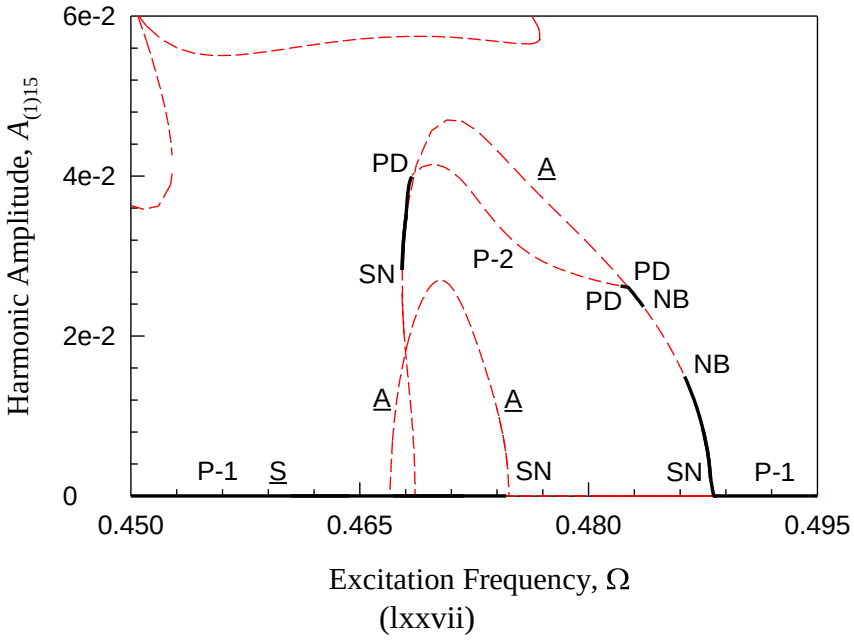

(lxxvii)

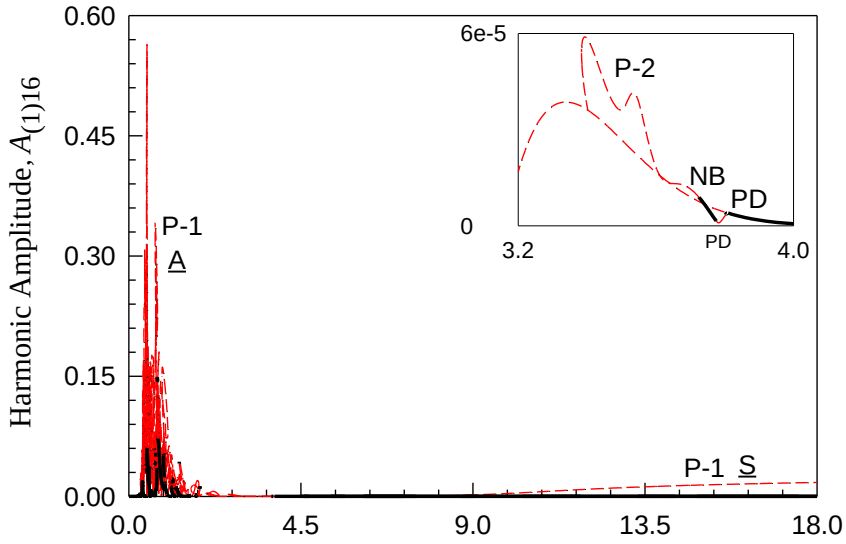

(lxxviii)

Fig. 24. (Continued).

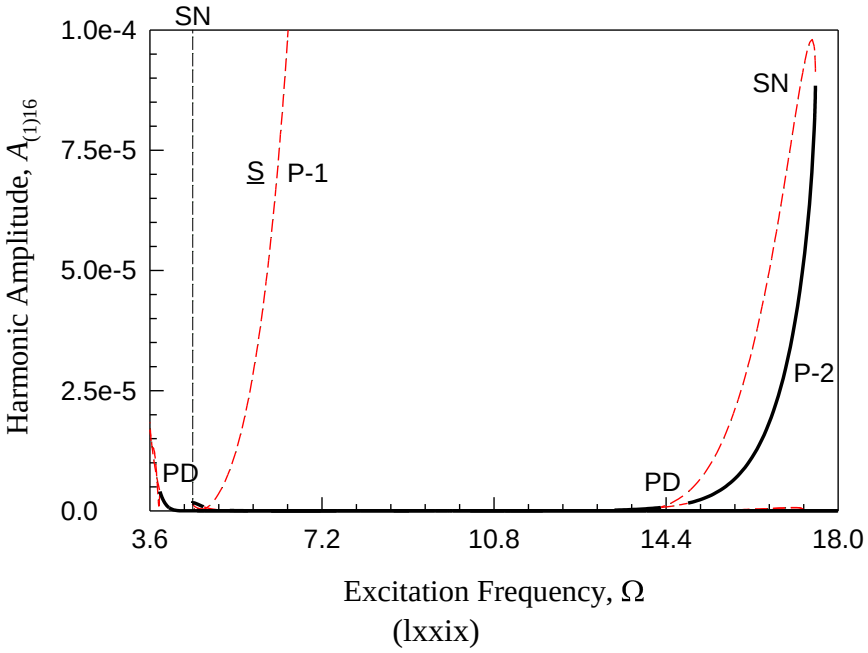

(lxxix)

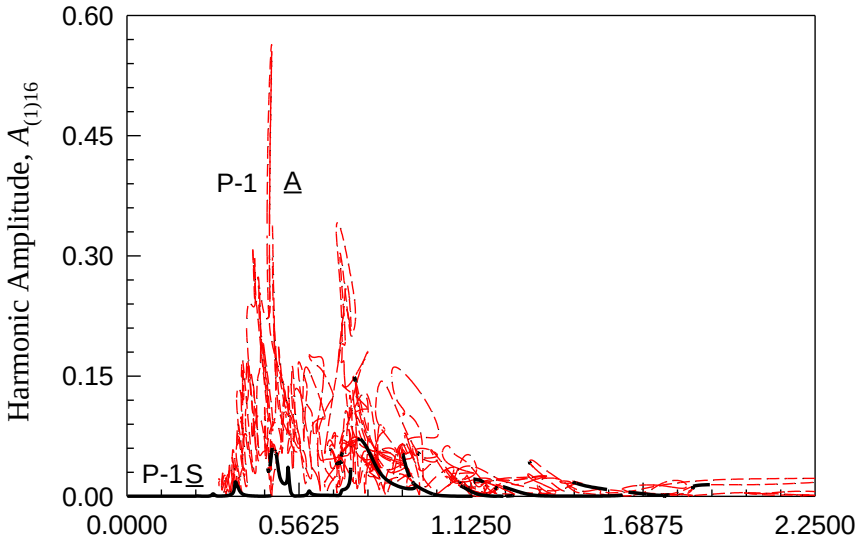

(lxxx)

Fig. 24. (Continued).

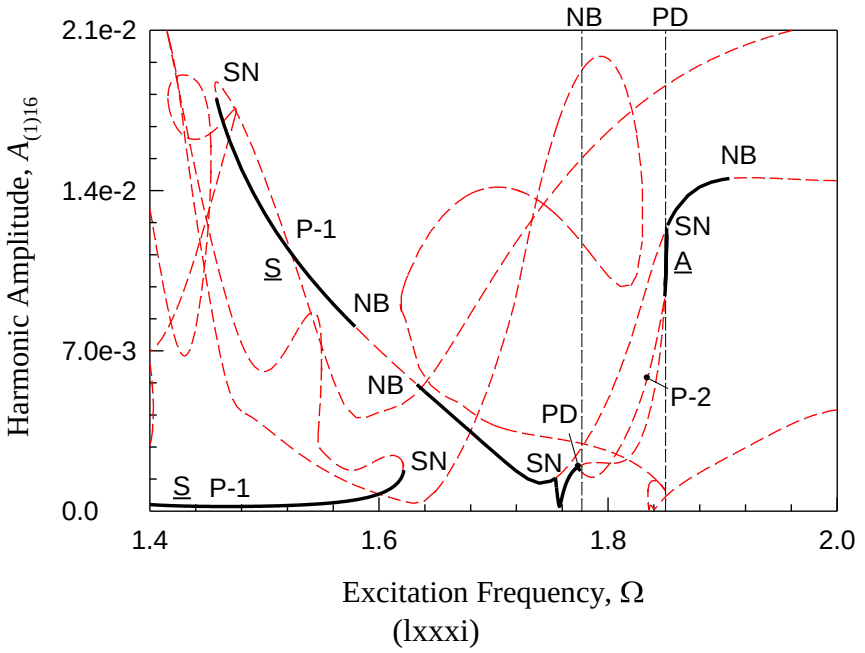

(lxxxi)

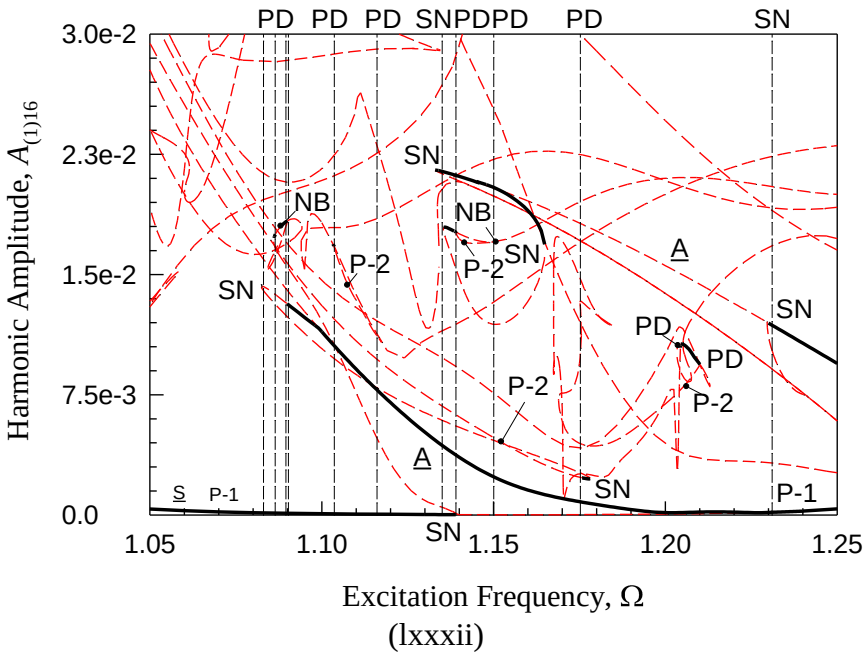

(lxxxii)

Fig. 24. (Continued).

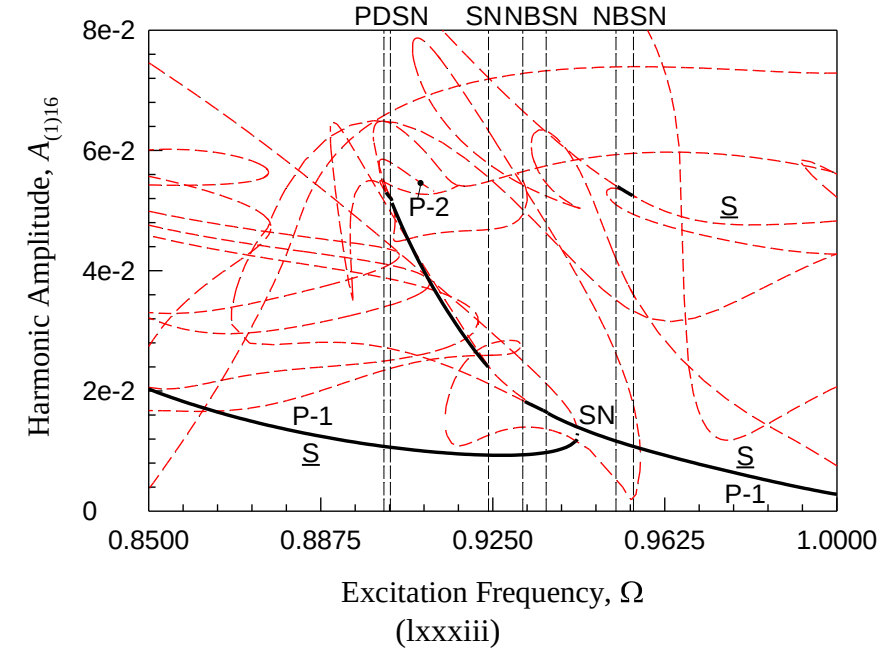

(lxxxiii)

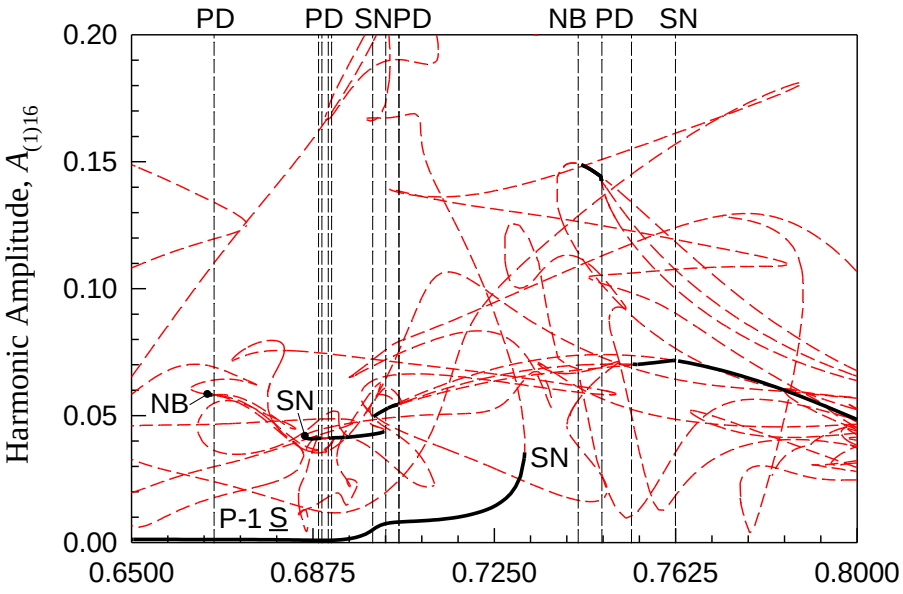

(lxxxiv)

Fig. 24. (Continued).

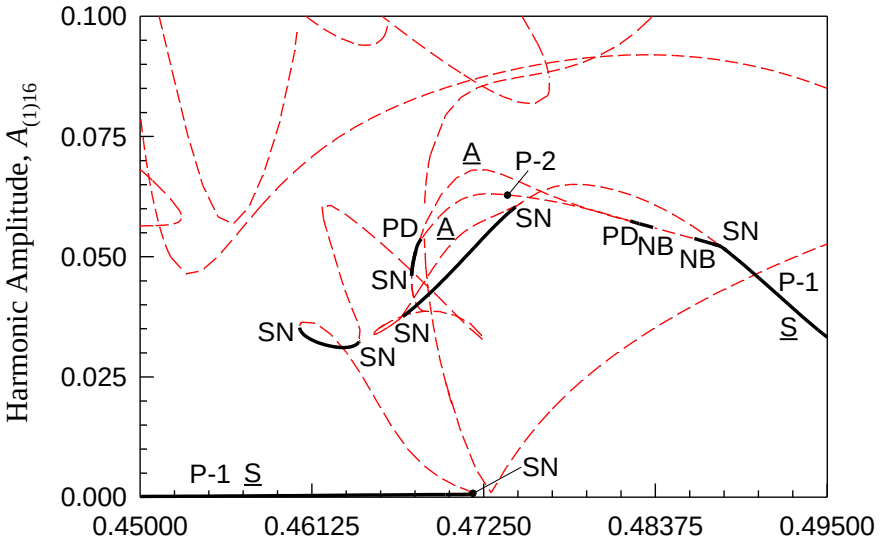

(lxxxv)

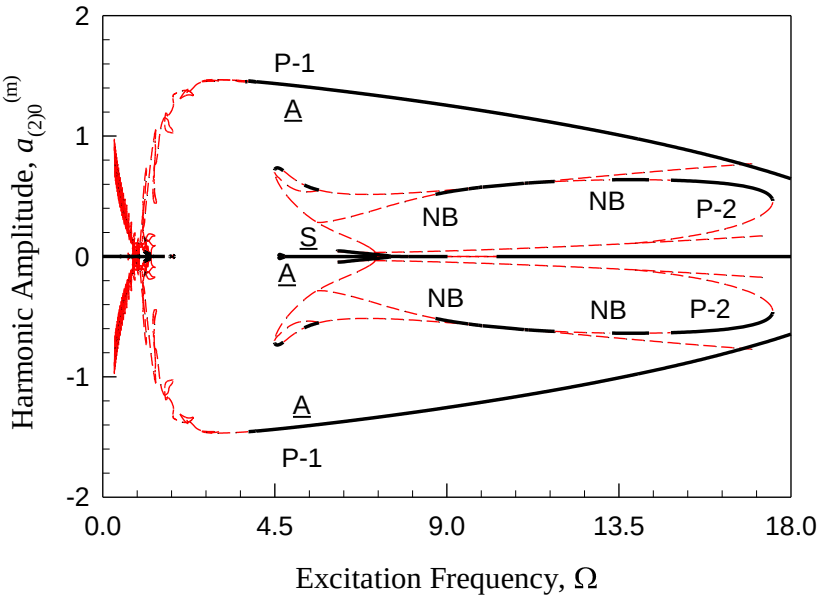

(i)

Fig. 25. The frequency-amplitude characteristics of bifurcation tree of period-1 to period-2 motions varying with excitation frequency ($\Omega \in (0,18)$) for the angle x_2 . (i)-(ix) $a_{(2)0}^{(m)}$ ($m = 1,2$), (x)-(lxxxvii) $A_{(2)k/m}$ ($k = 1,2,3,4,6,8,10,12,30,32$) ($m = 2$, $k_1 = 5$, $k_2 = 100$, $c = 0.1$, $Q_0 = 20.0$, $L = 2$, $T = 2\pi / \Omega$).

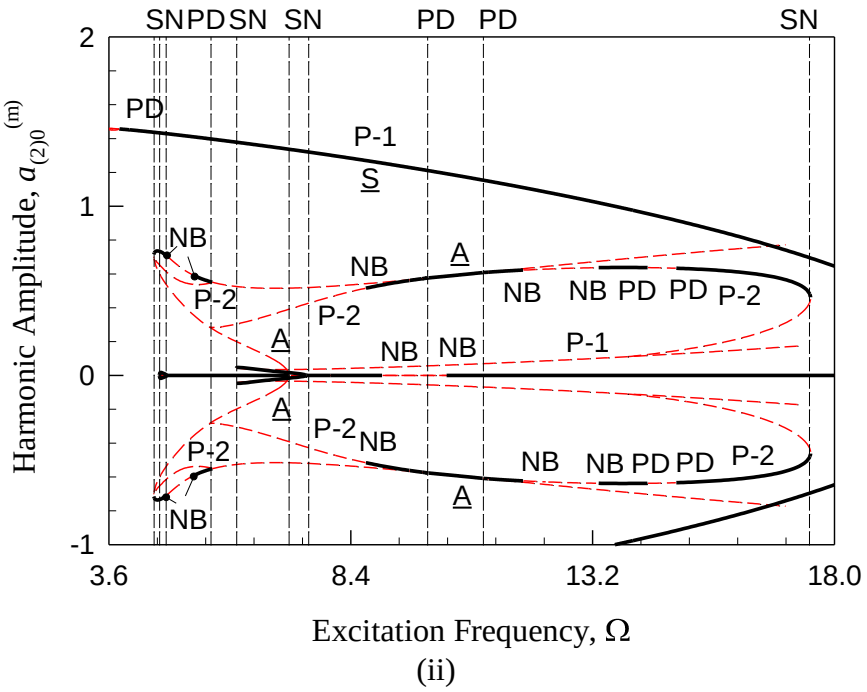

(ii)

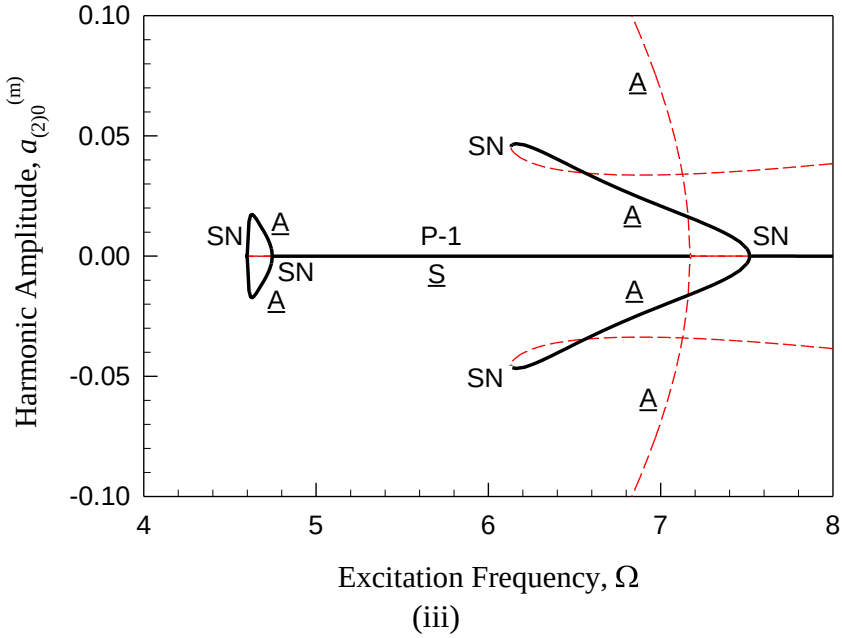

(iii)

Fig. 25. (Continued).

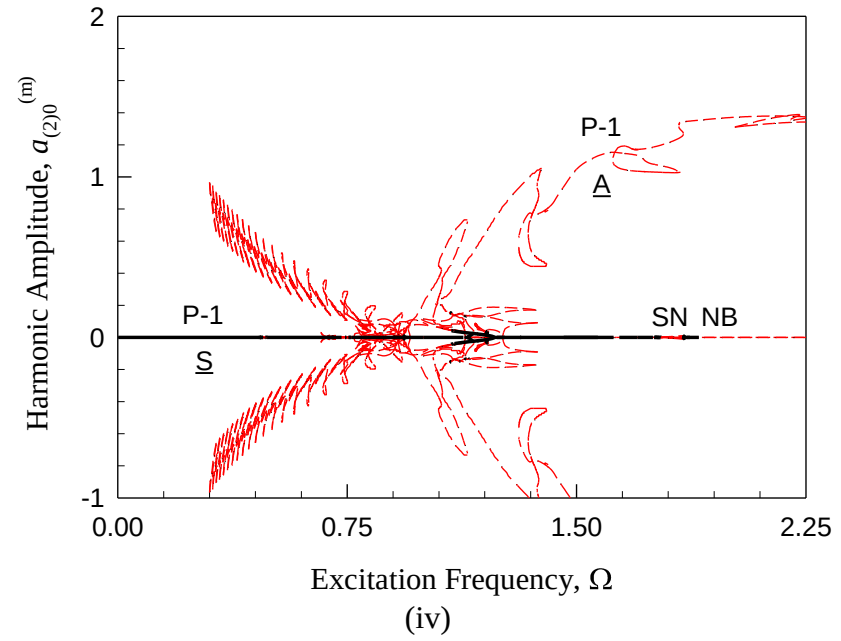

(iv)

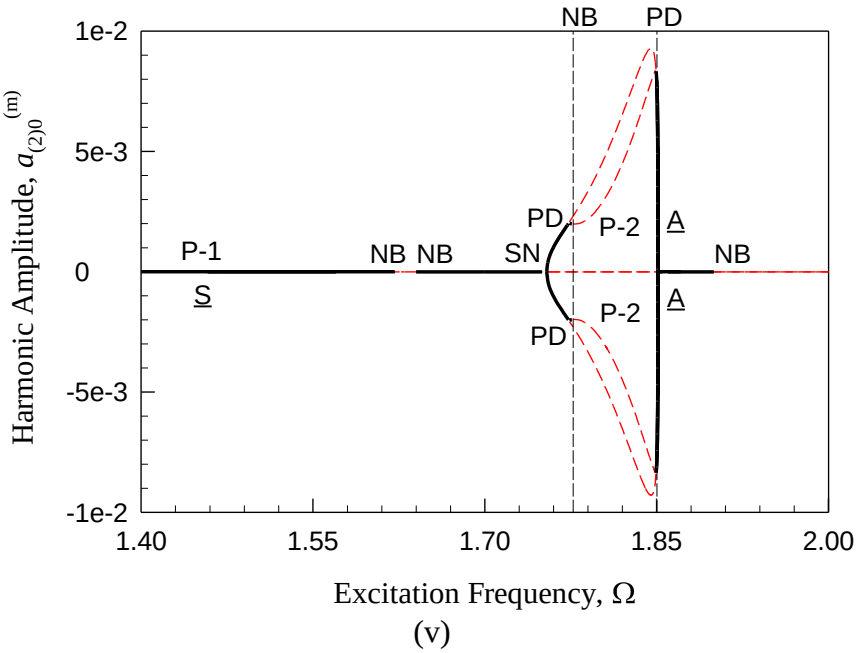

(v)

Fig. 25. (Continued).

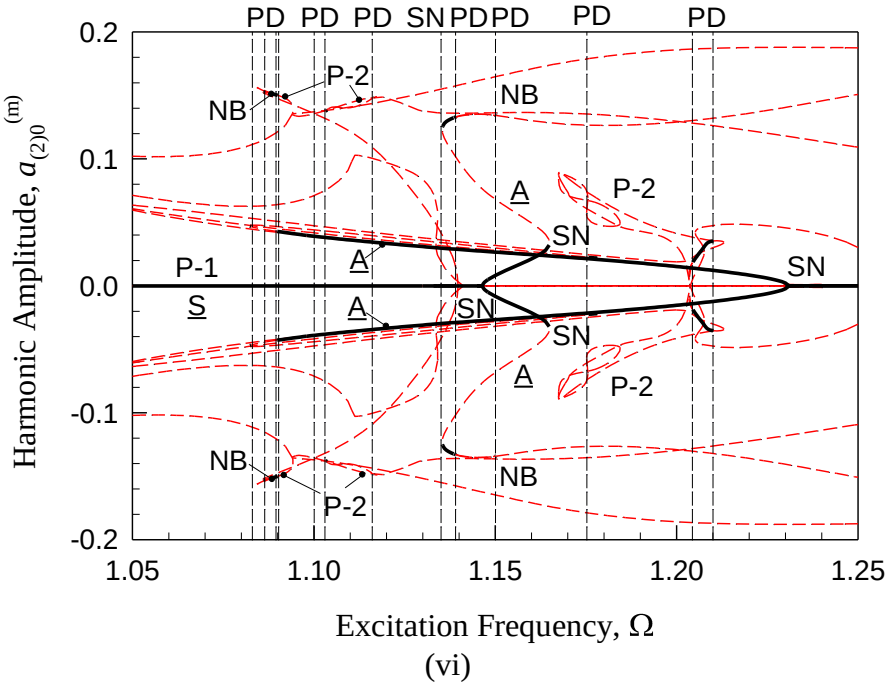

(vi)

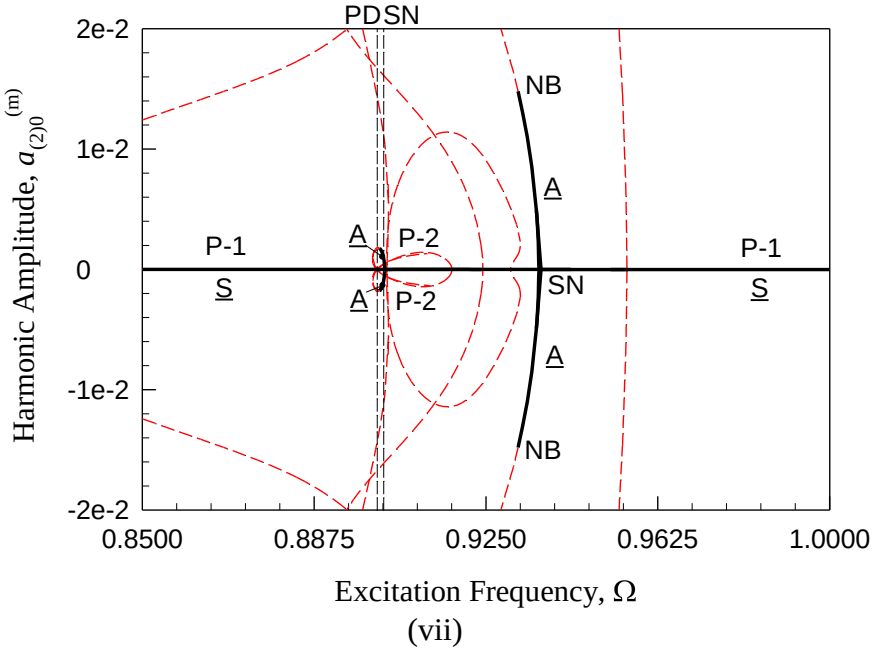

(vii)

Fig. 25. (Continued).

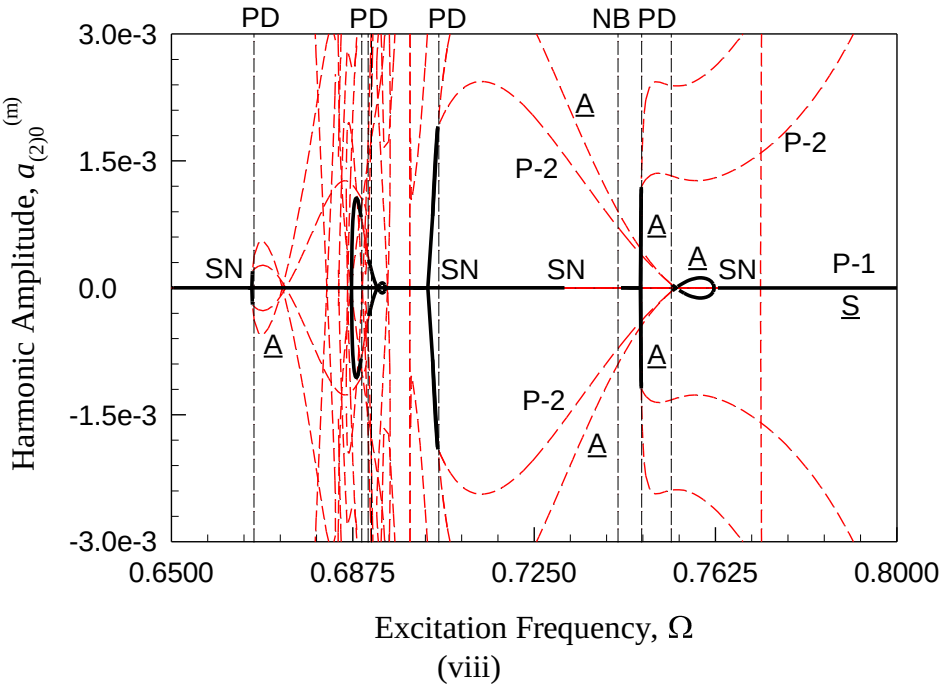

(viii)

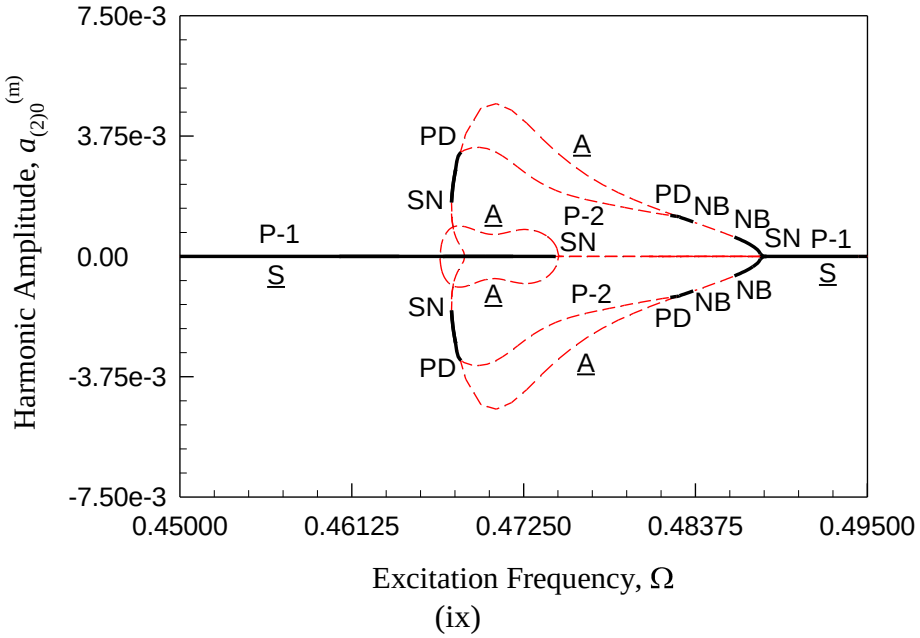

(ix)

Fig. 25. (Continued).

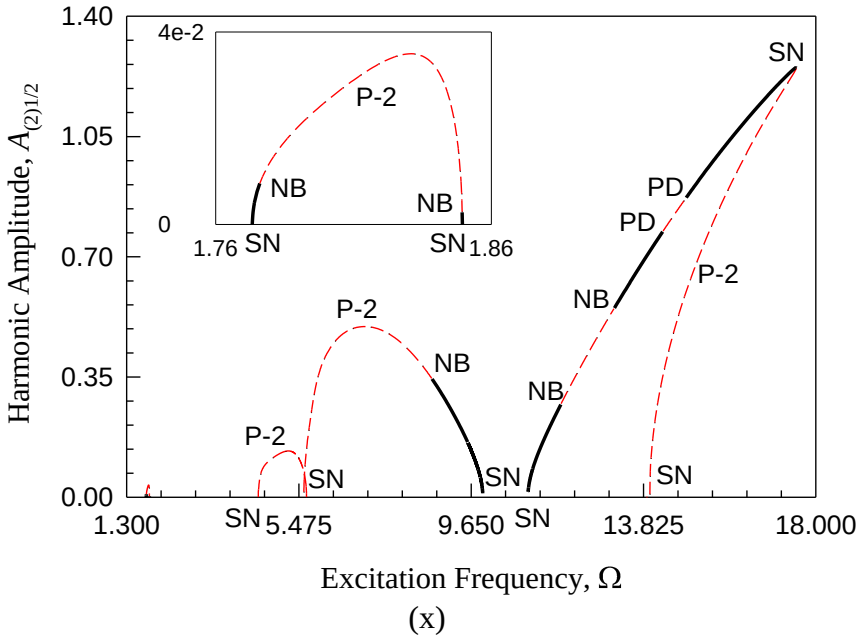

(x)

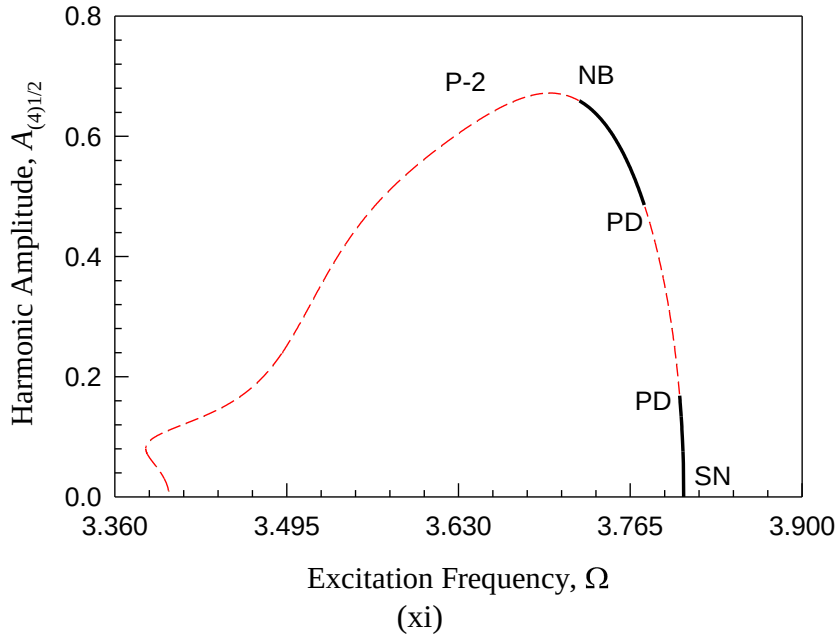

(xi)

Fig. 25. (Continued).

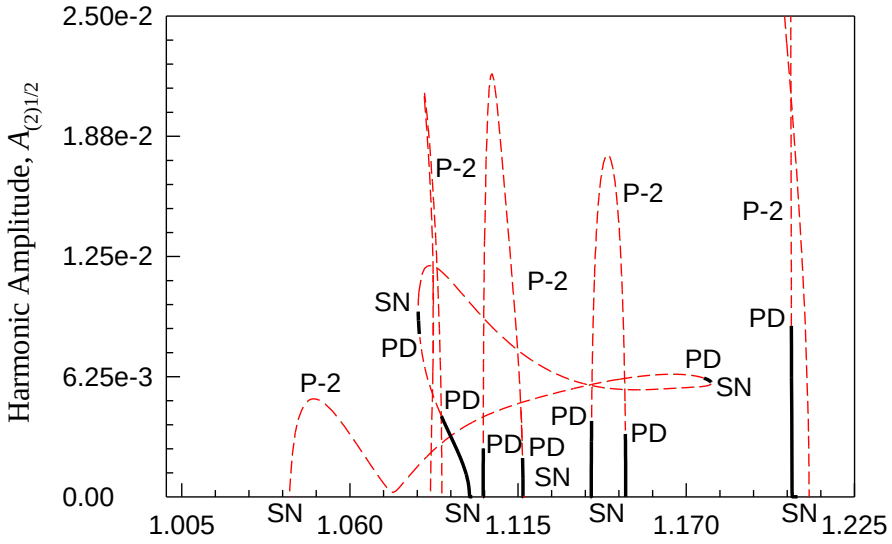

(xii)

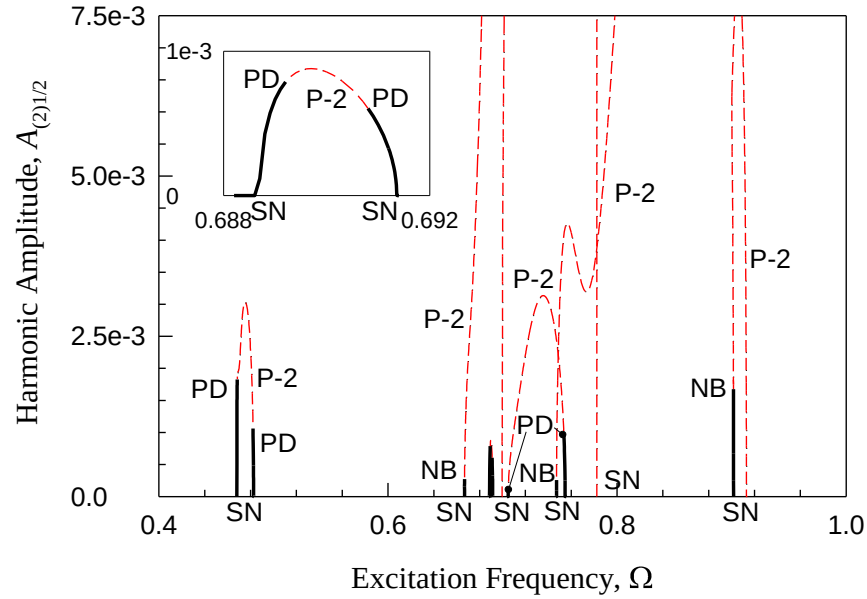

(xiii)

Fig. 25. (Continued).

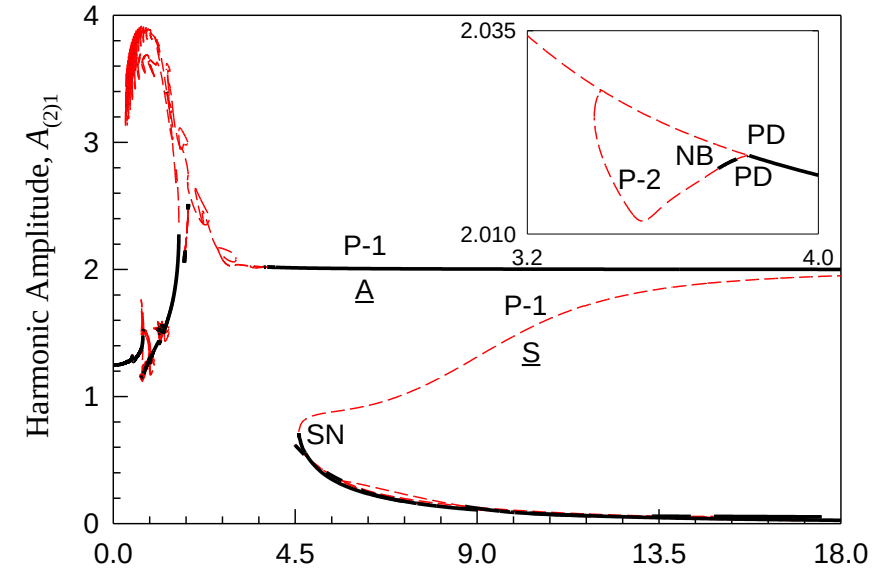

(xiv)

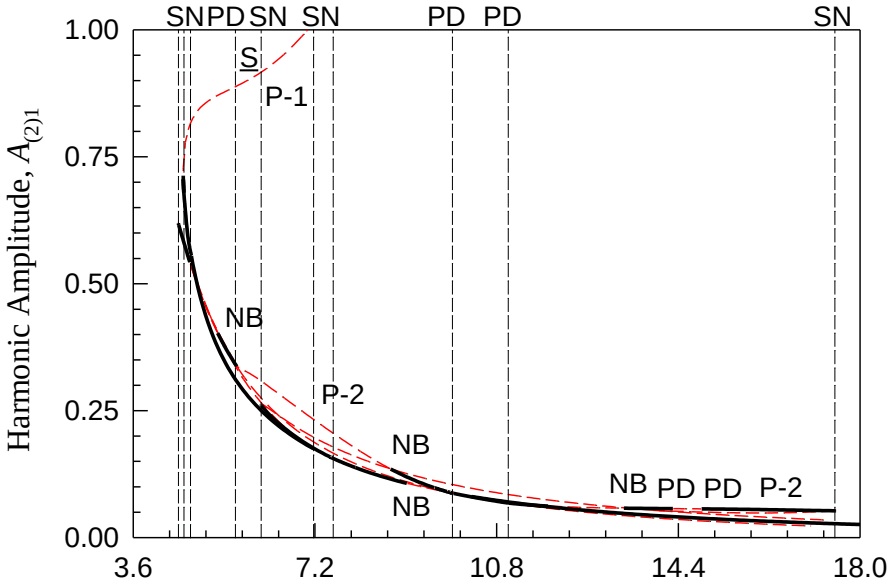

(xv)

Fig. 25. (Continued).

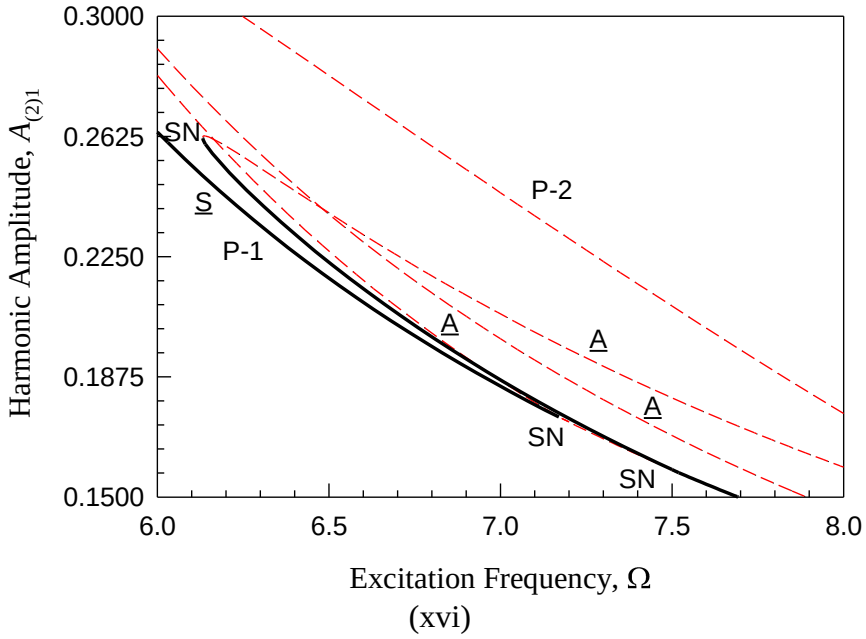

(xvi)

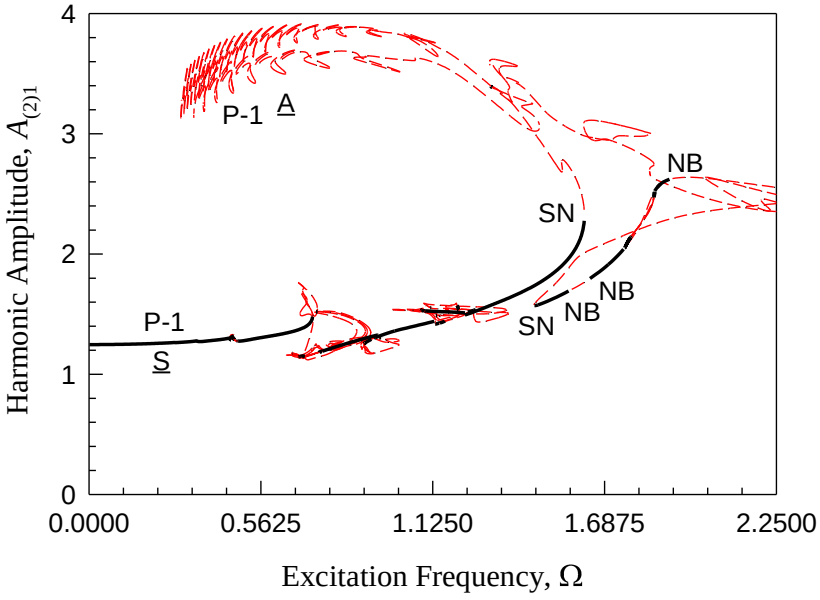

(xvii)

Fig. 25. (Continued).

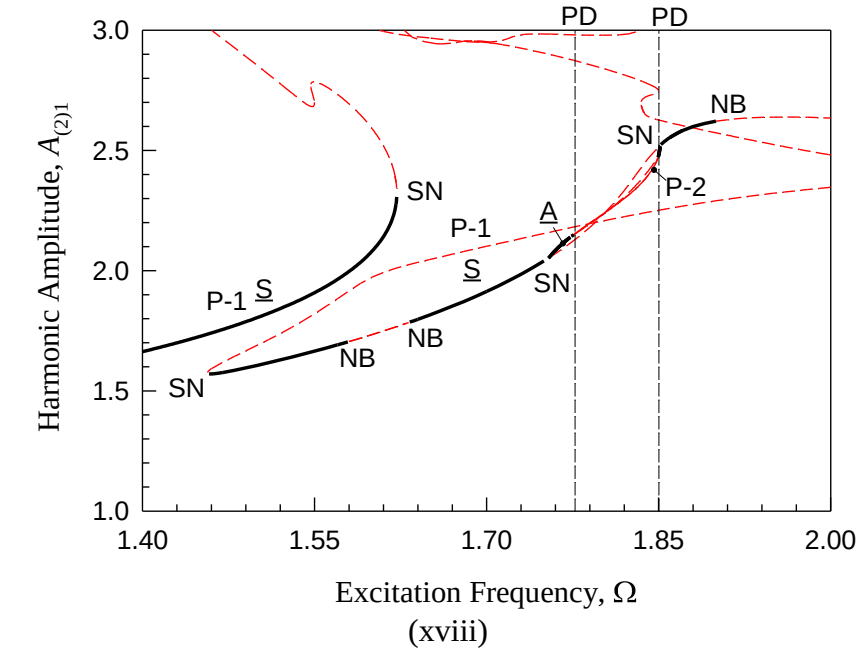

(xviii)

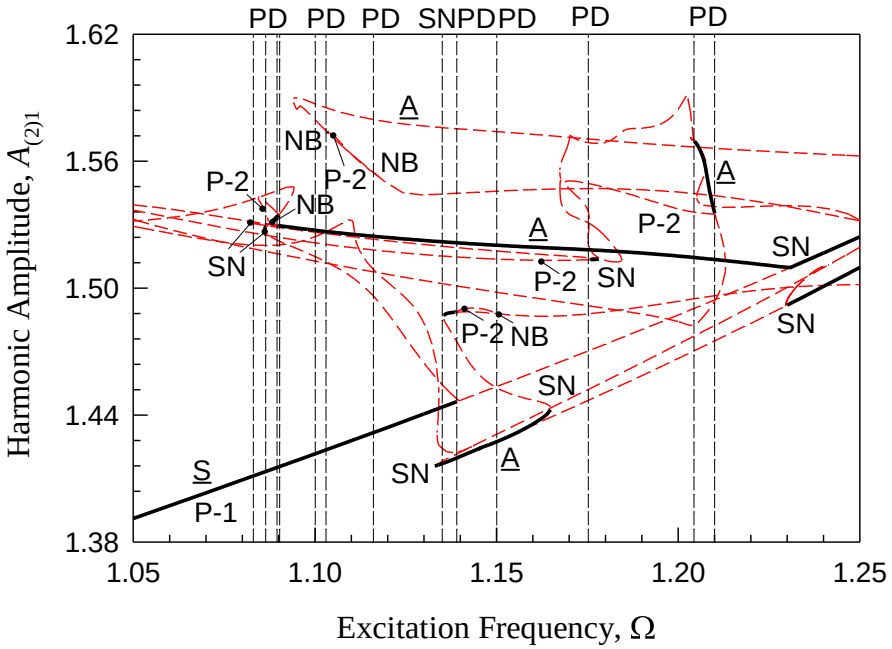

(xix)

Fig. 25. (Continued).

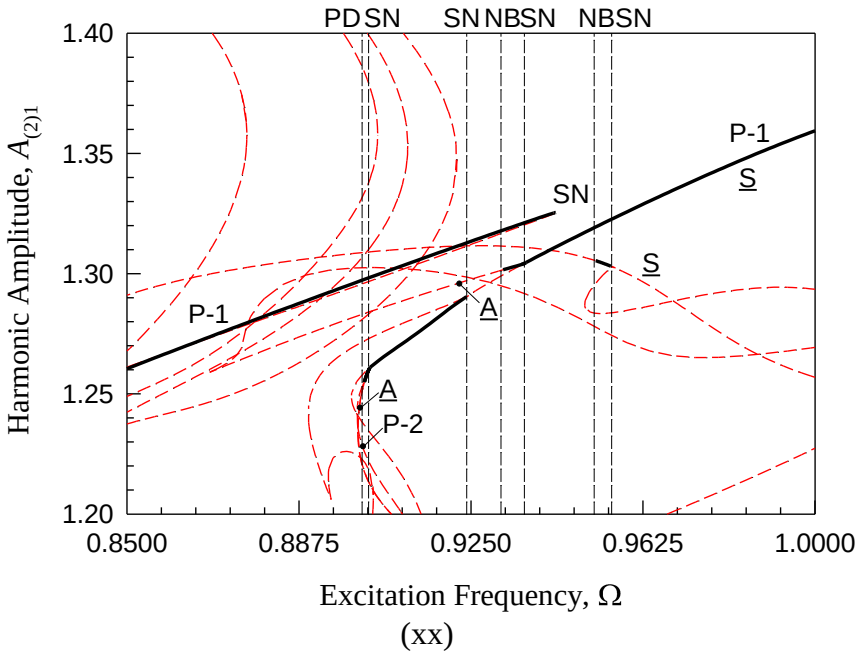

(xx)

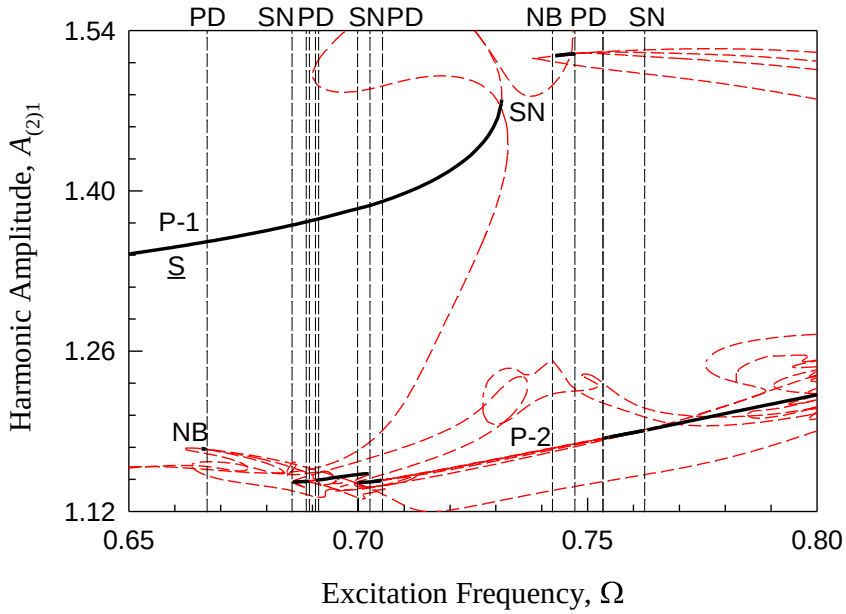

(xxi)

Fig. 25. (Continued).

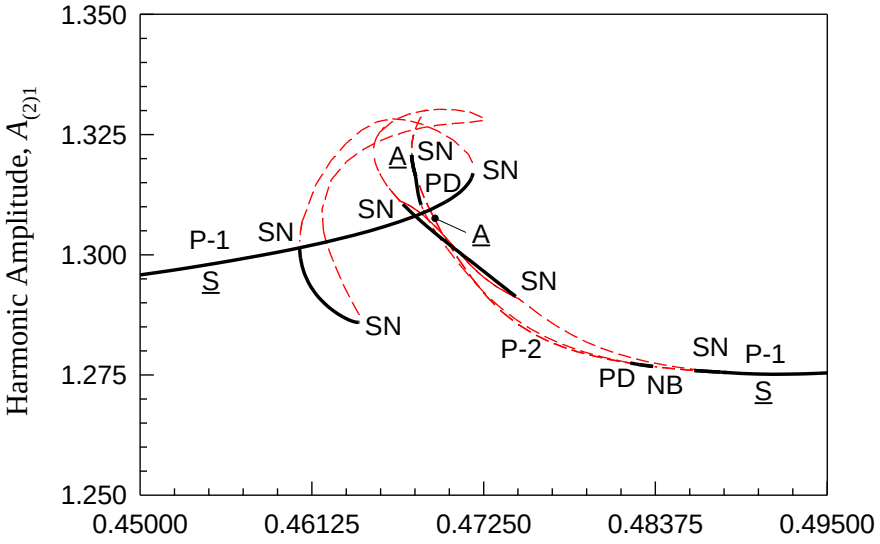

(xxii)

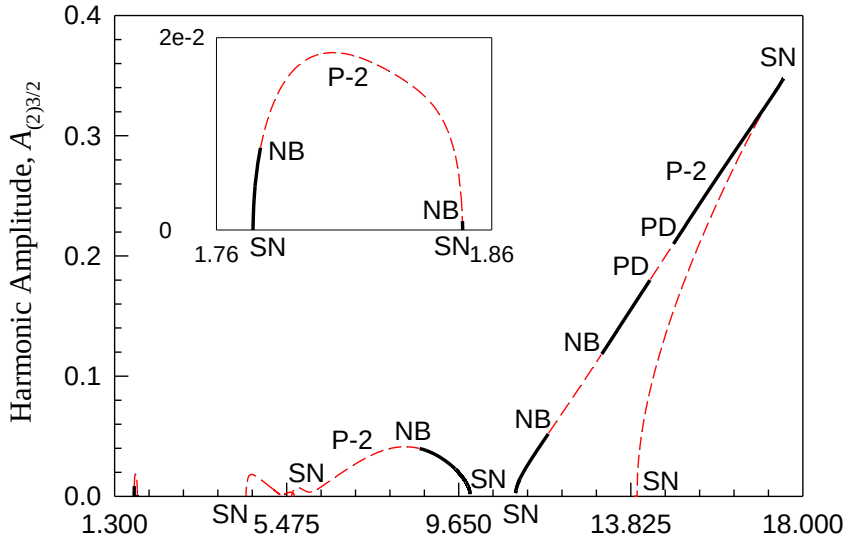

(xxiii)

Fig. 25. (Continued).

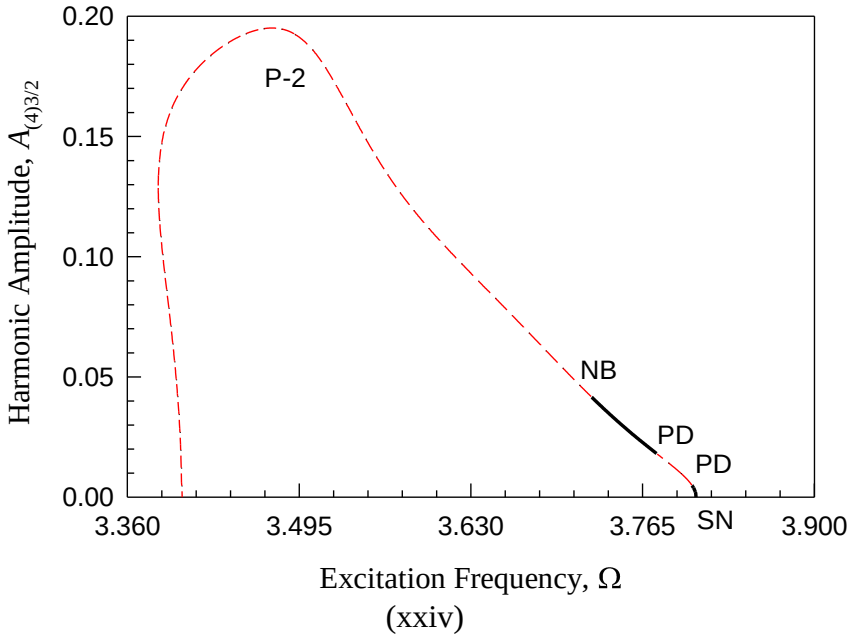

(xxiv)

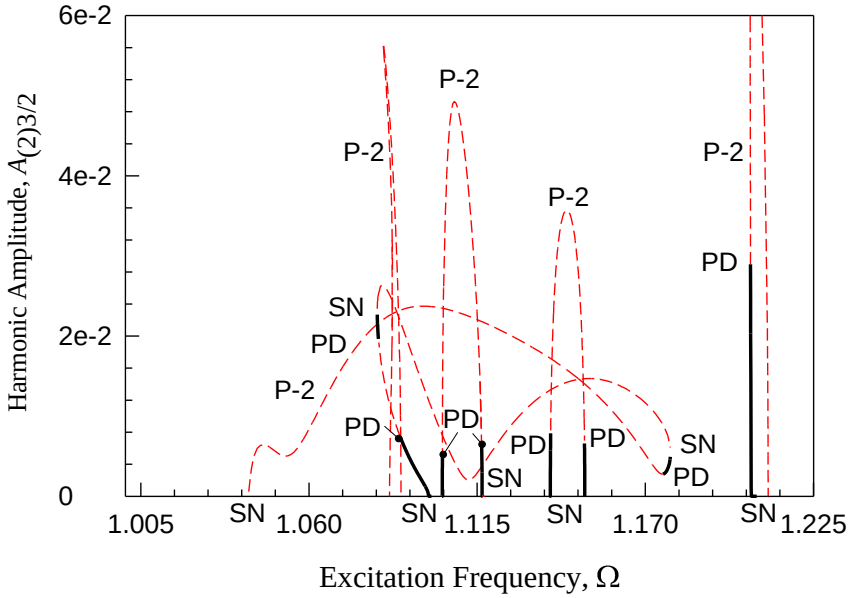

(xxv)

Fig. 25. (Continued).

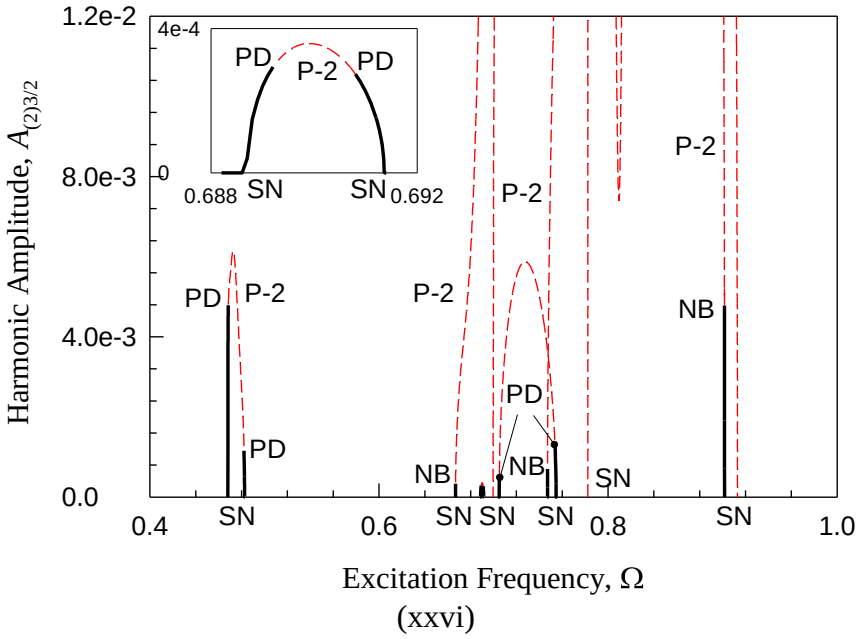

(xxvi)

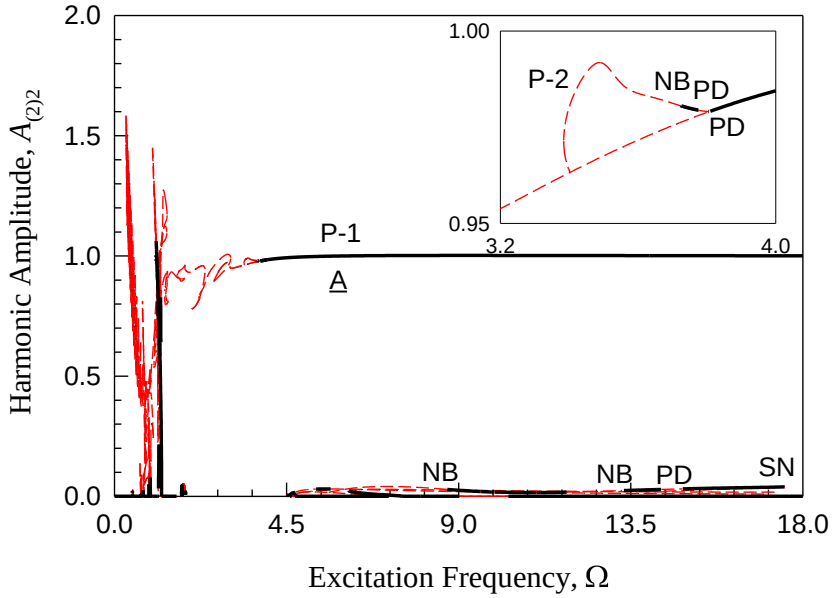

(xxvii)

Fig. 25. (Continued).

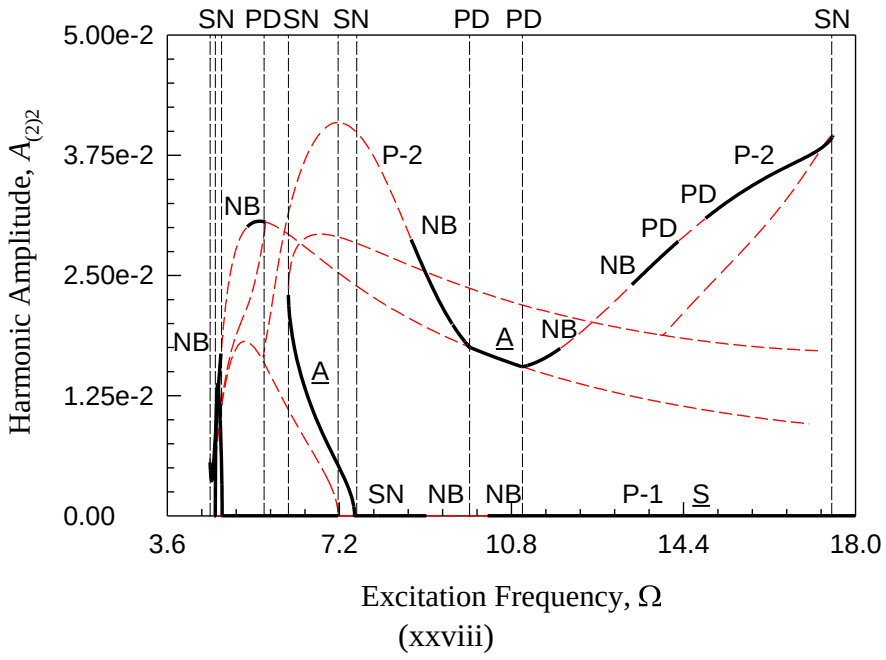

(xxviii)

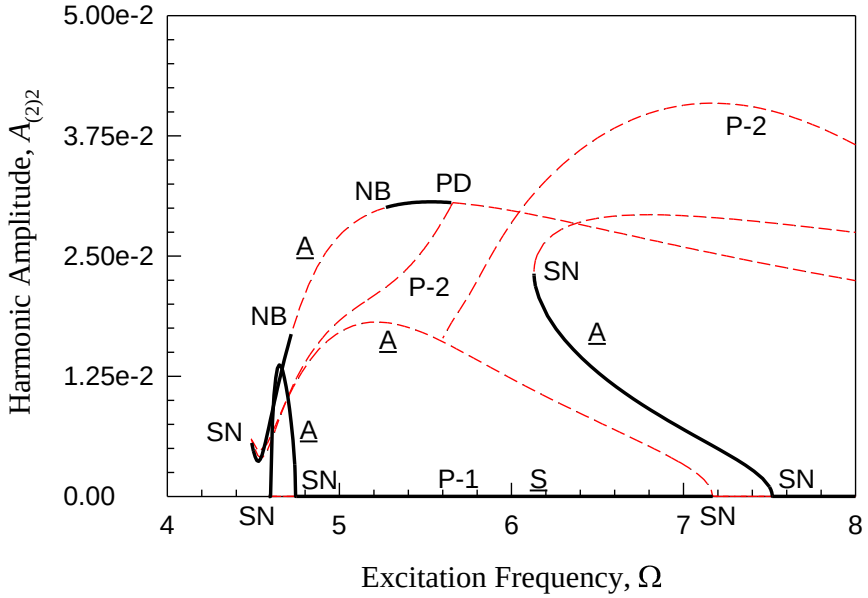

(xxix)

Fig. 25. (Continued).

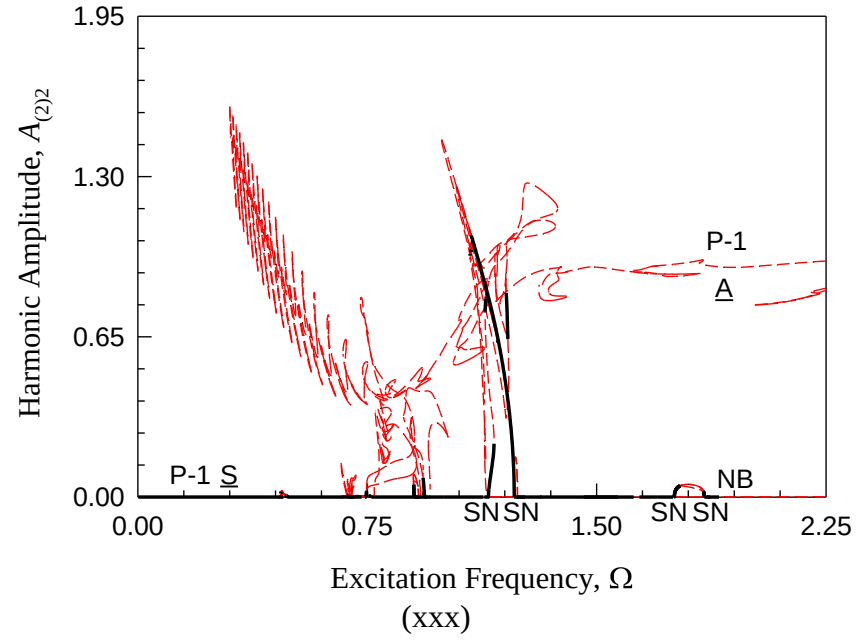

(xxx)

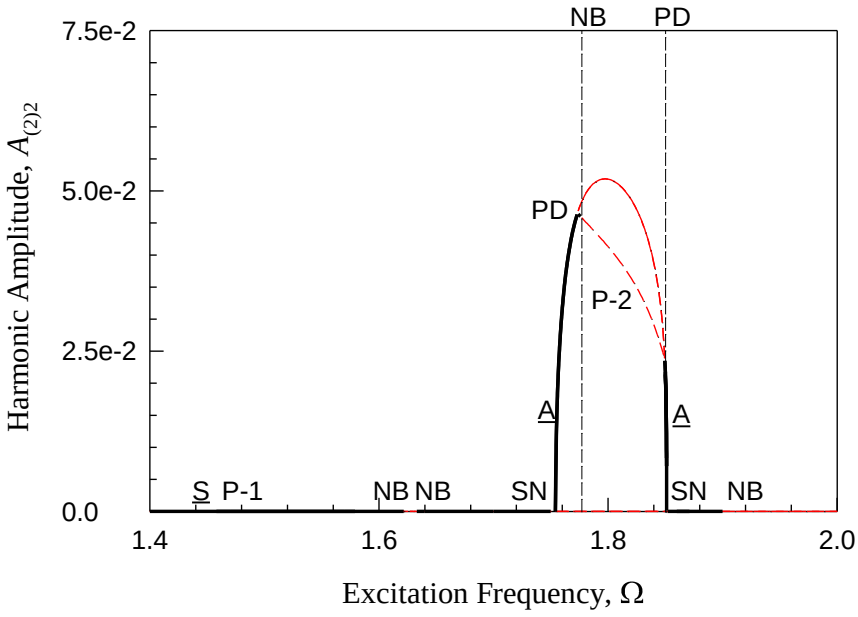

(xxxi)

Fig. 25. (Continued).

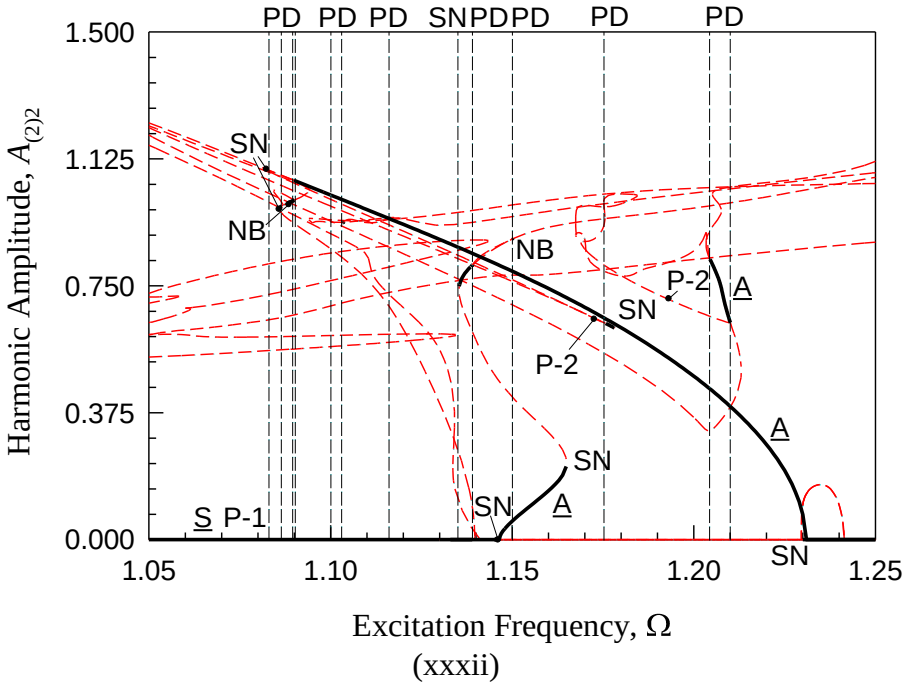

(xxxii)

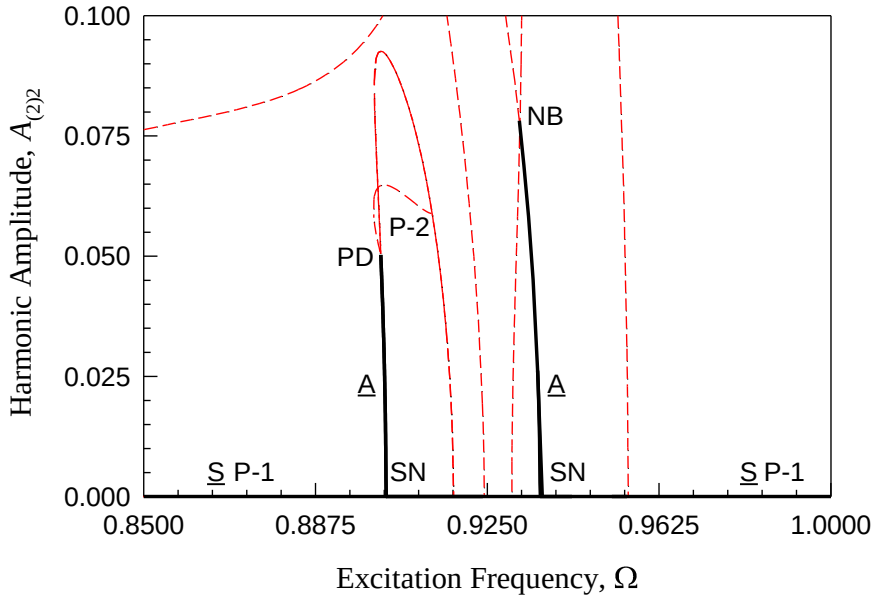

(xxxiii)

Fig. 25. (Continued).

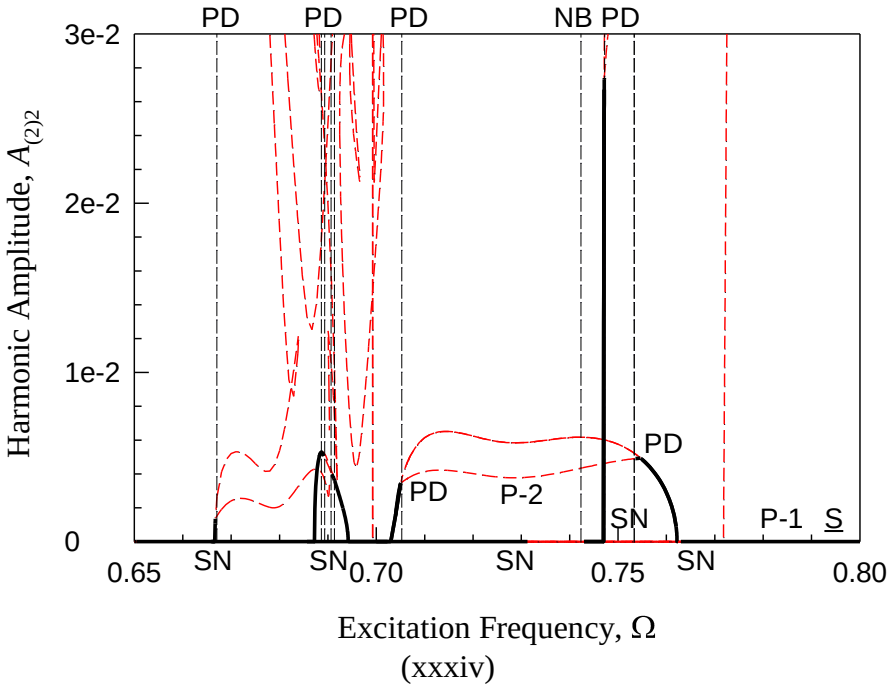

(xxxiv)

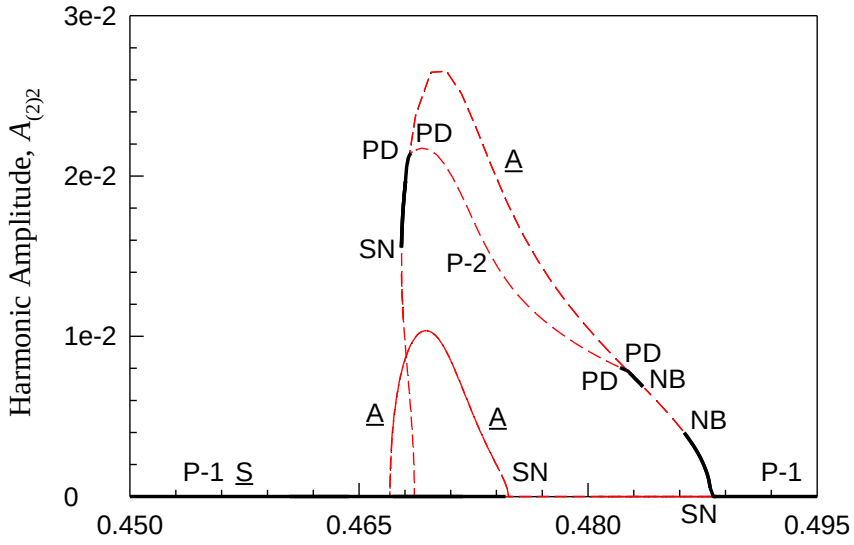

(xxxv)

Fig. 25. (Continued).

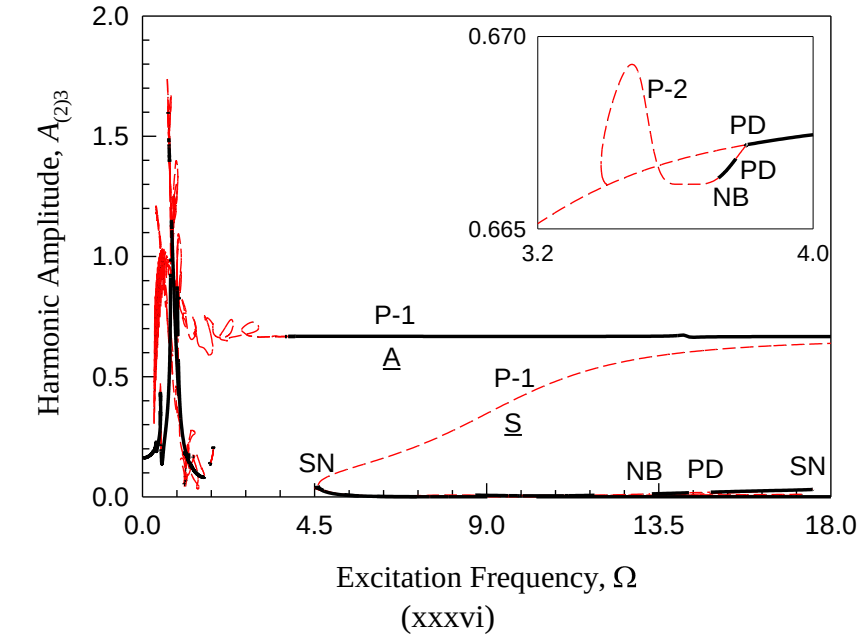

(xxxvi)

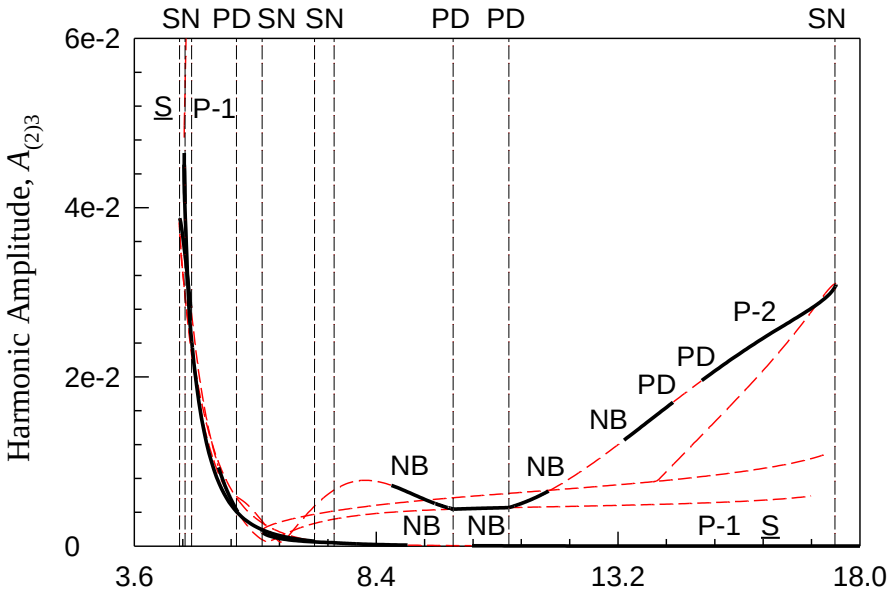

(xxxvii)

Fig. 25. (Continued).

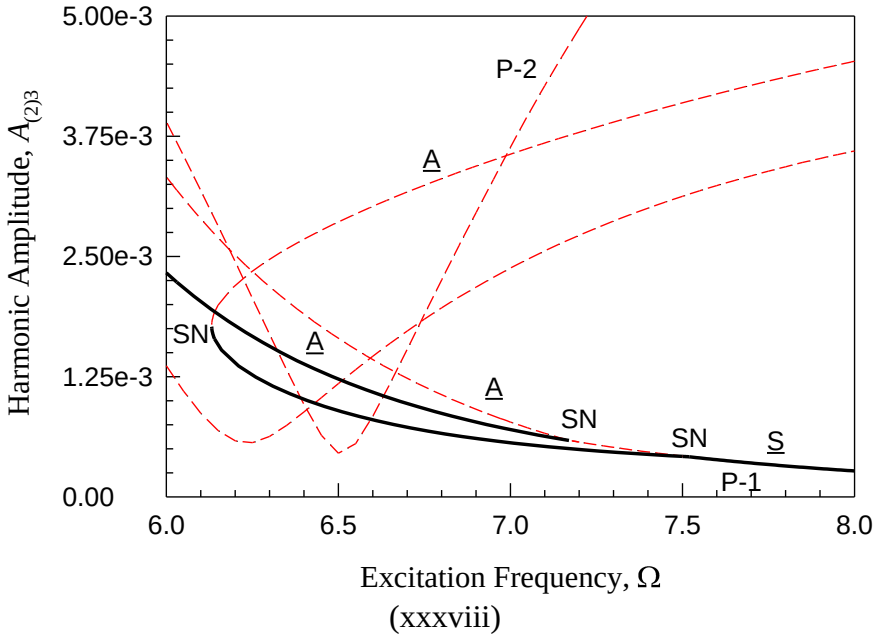

(xxxviii)

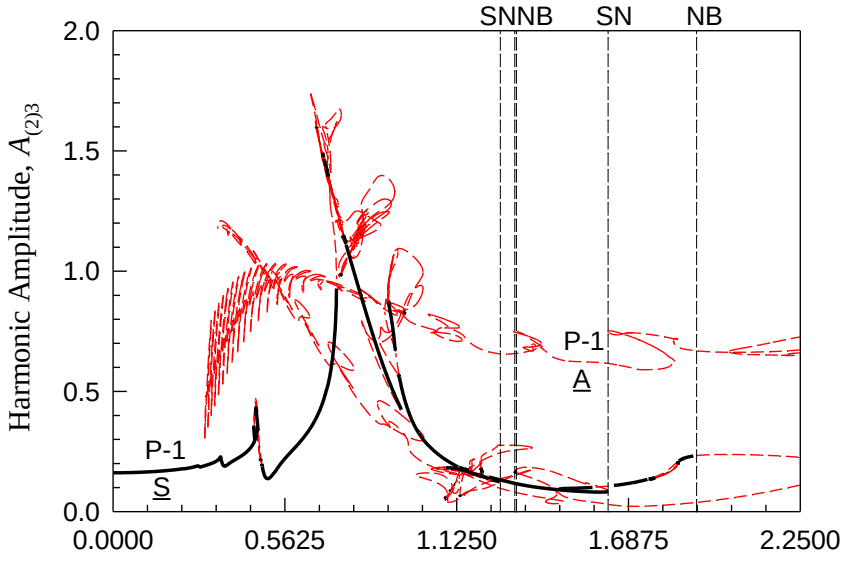

(xxxix)

Fig. 25. (Continued).

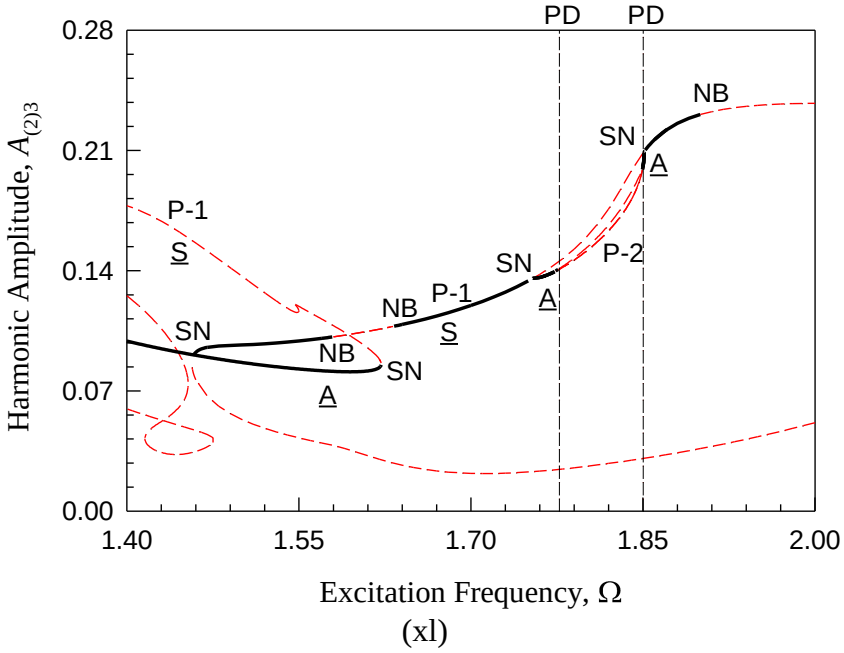

(xl)

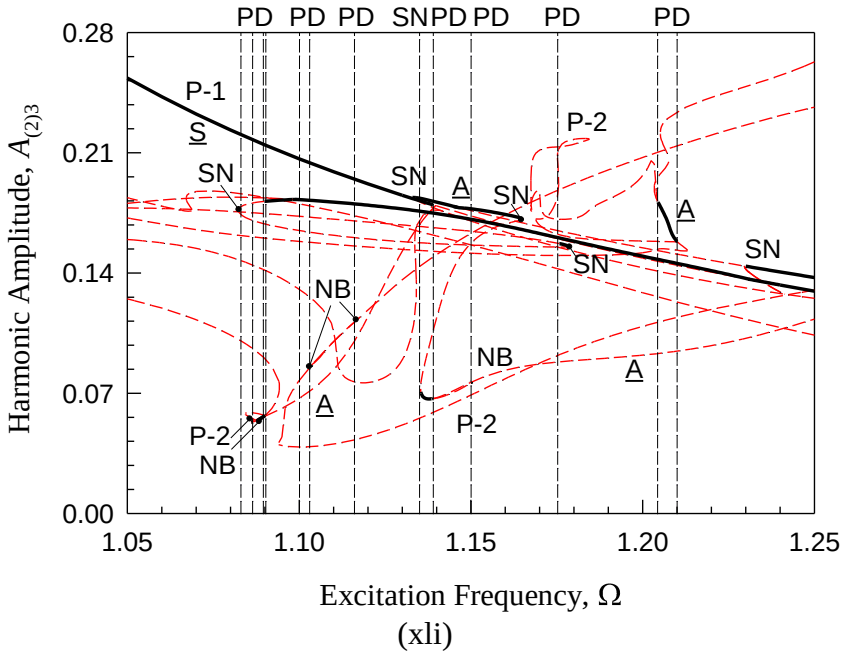

(xli)

Fig. 25. (Continued).

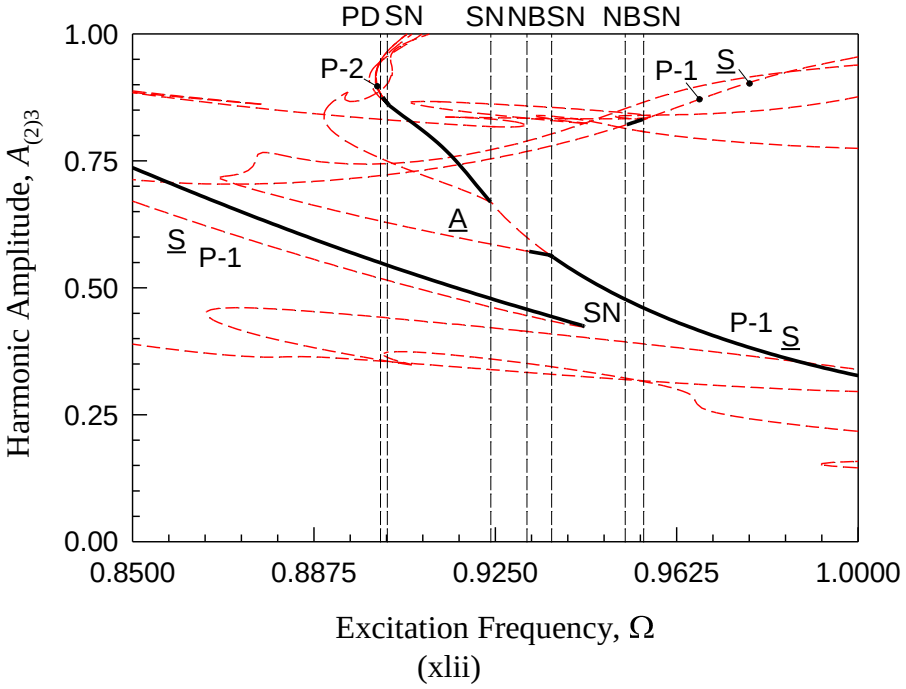

(xlii)

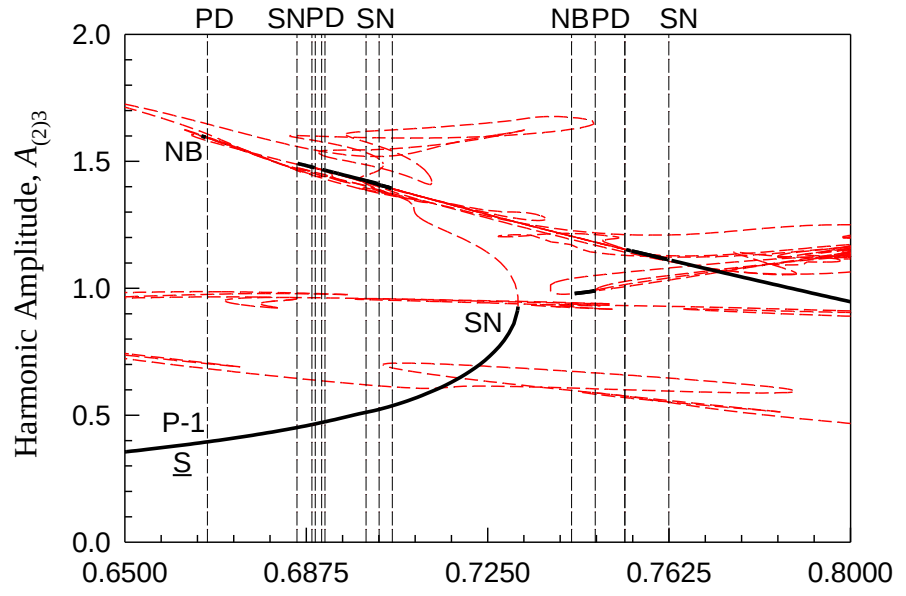

(xliii)

Fig. 25. (Continued).

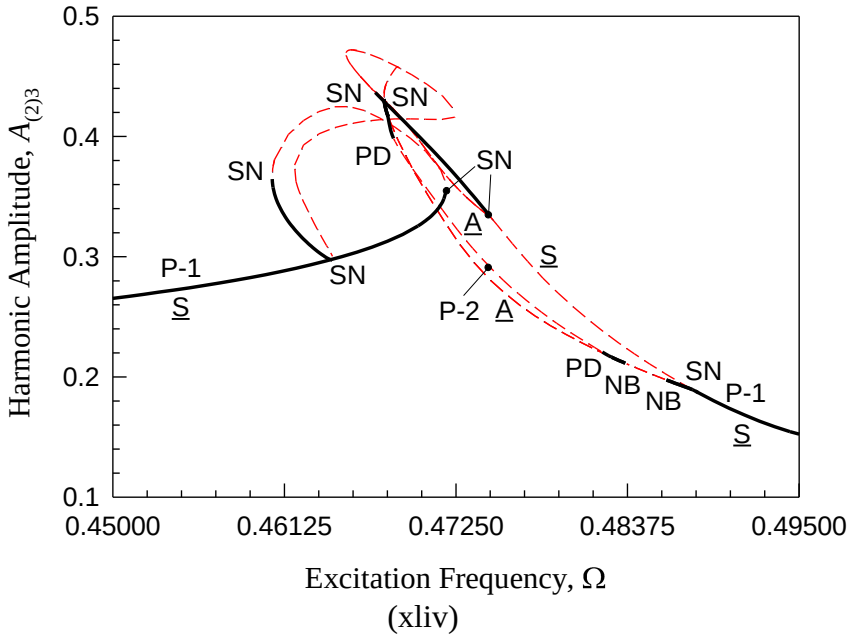

(xliv)

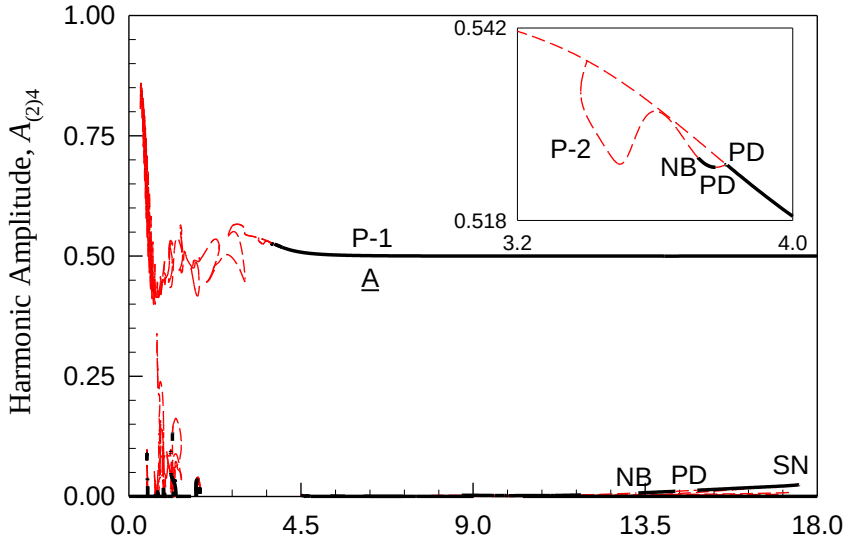

(xliv)

Fig. 25. (Continued).

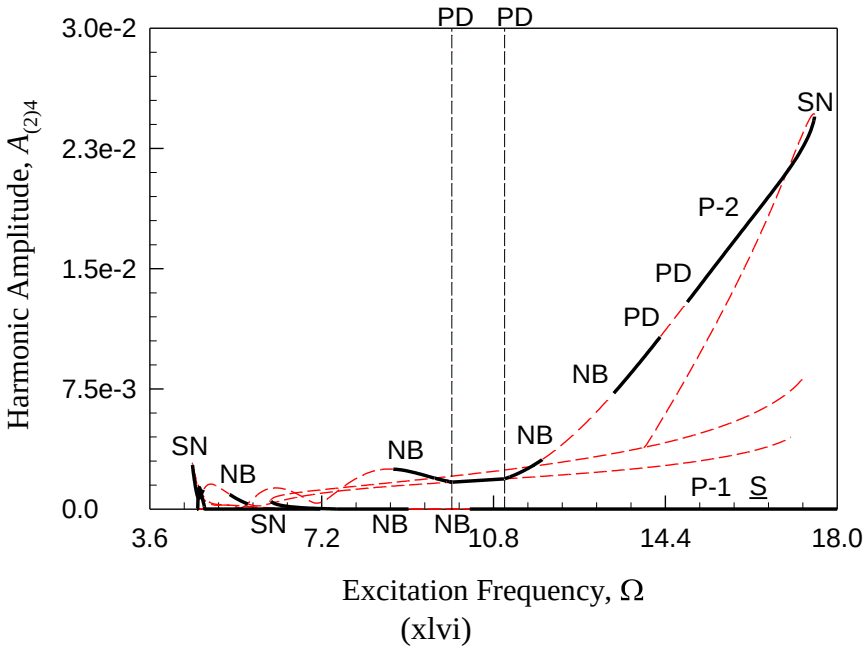

(xlvi)

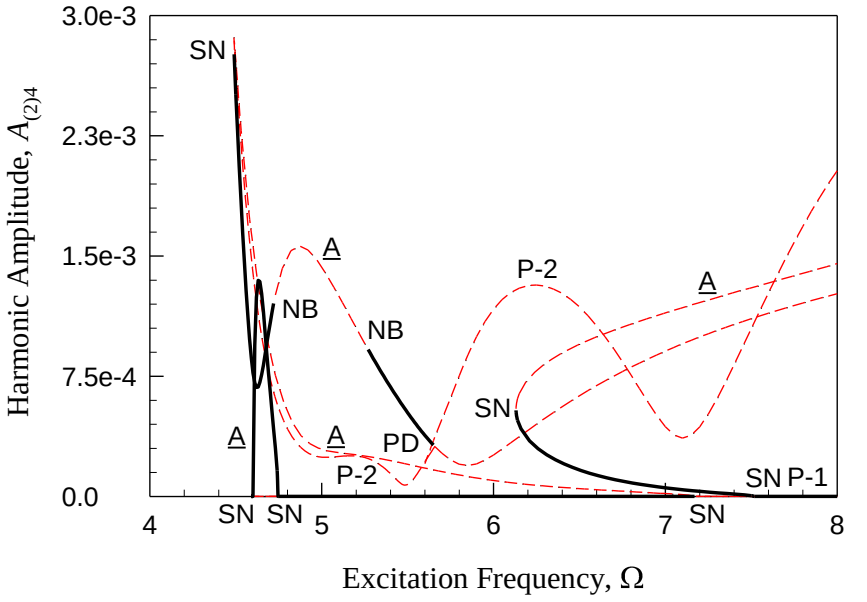

(xlvii)

Fig.25. (Continued).

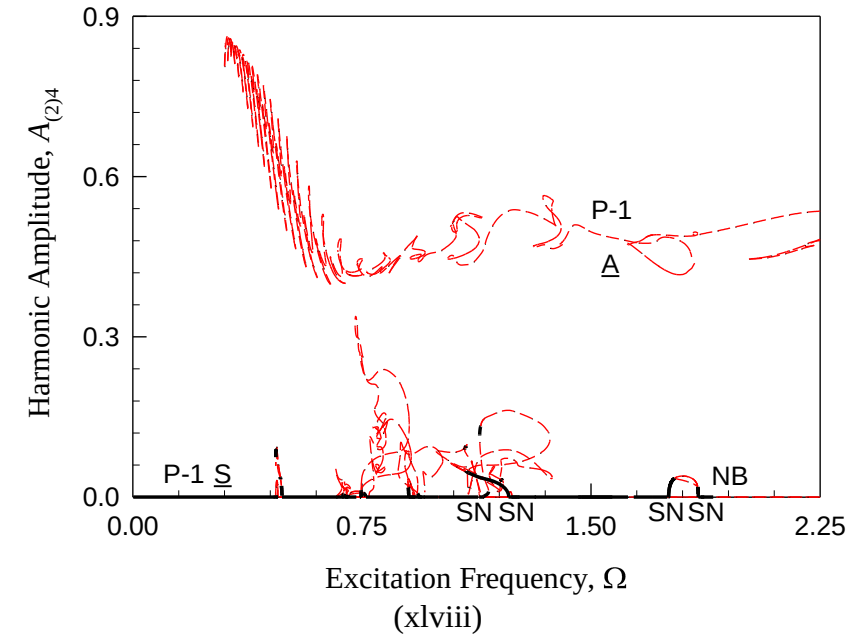

(xlviii)

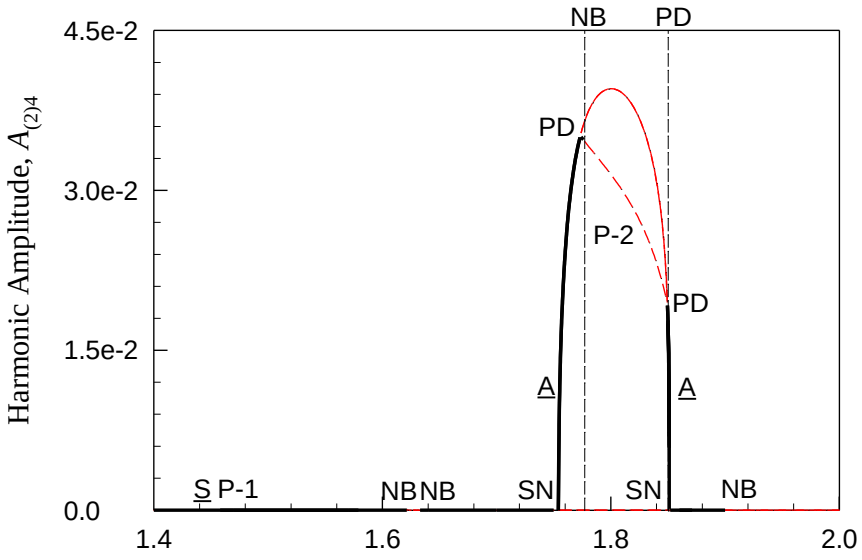

(xlix)

Fig.25. (Continued).

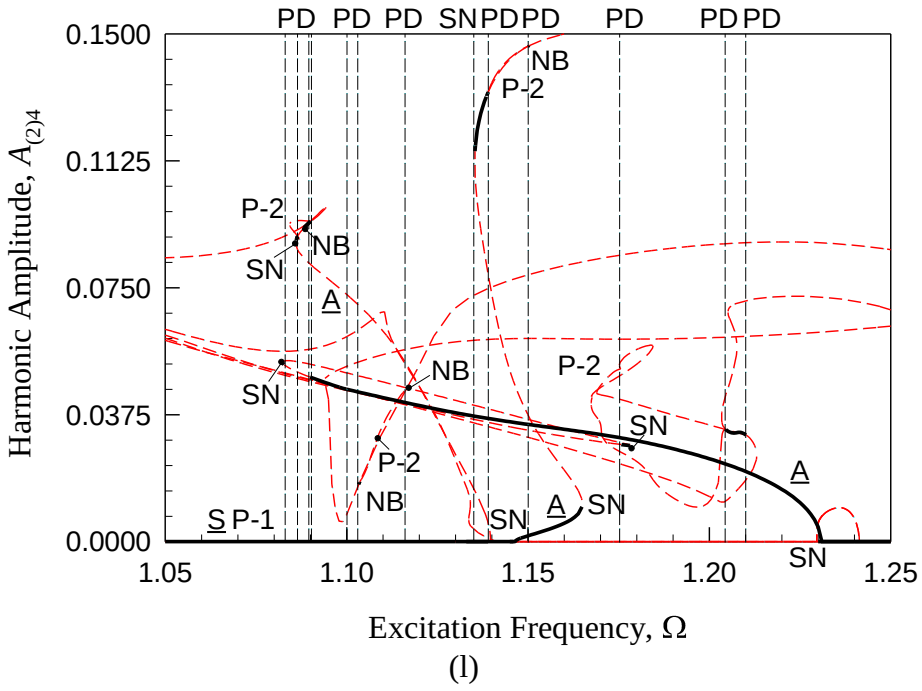

(l)

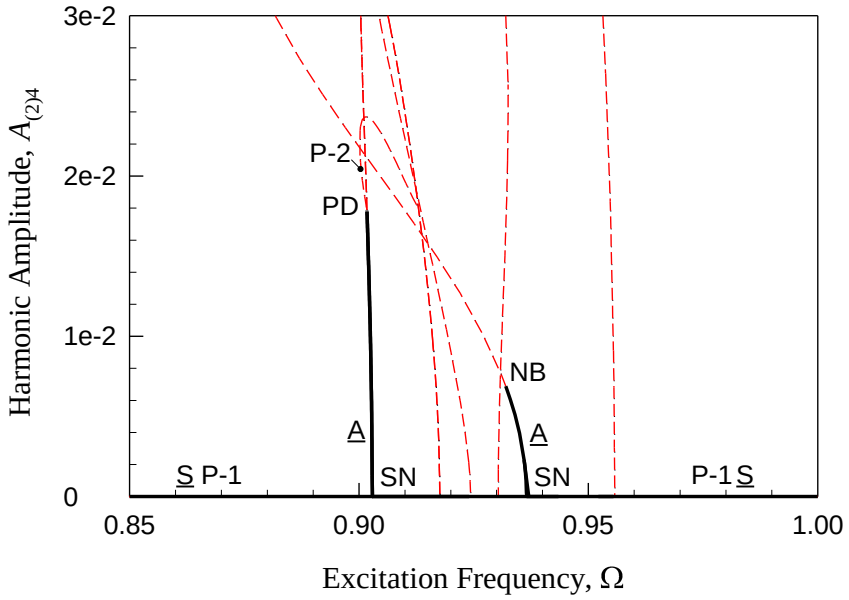

(li)

Fig.25. (Continued).

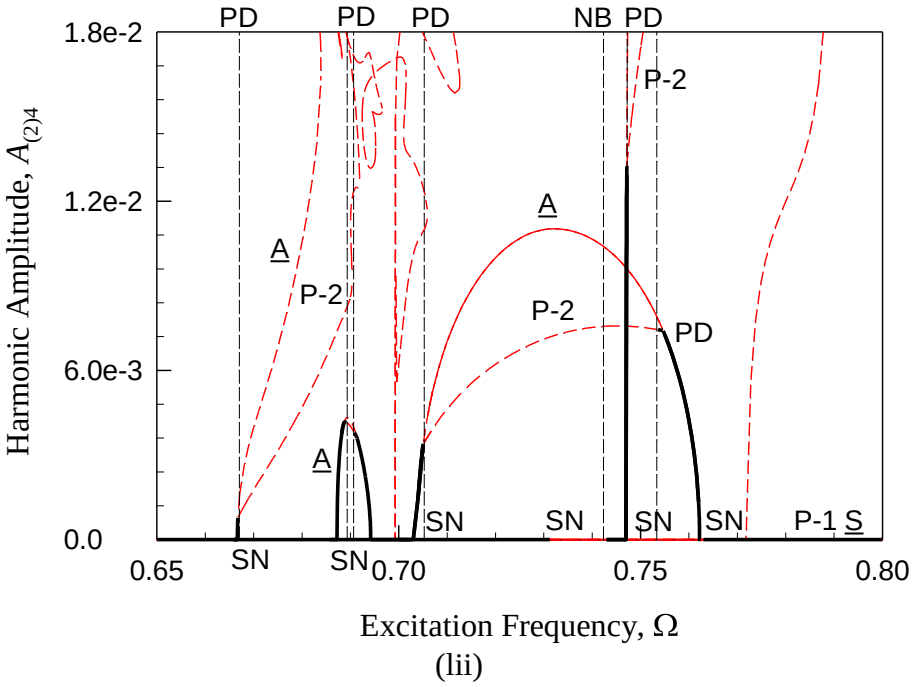

(lii)

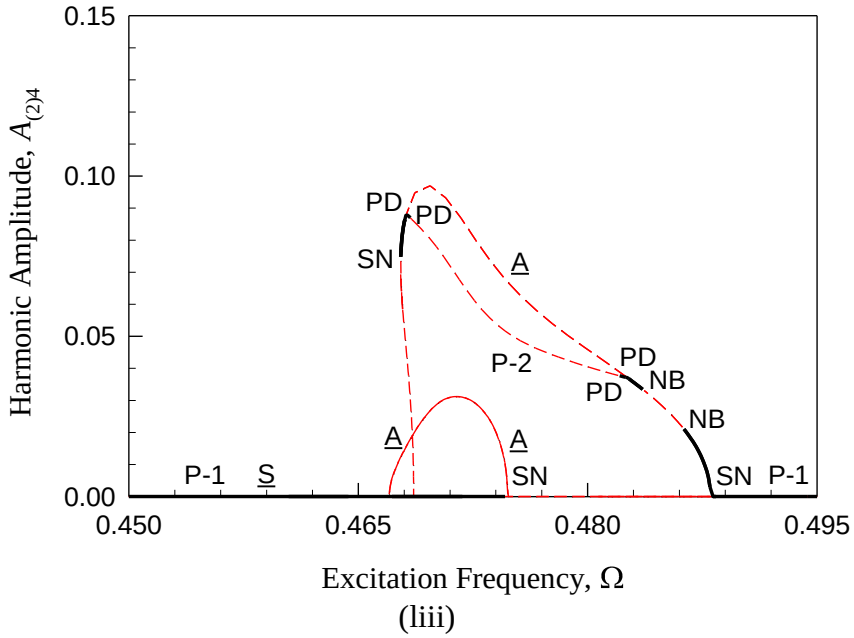

(liii)

Fig.25. (Continued).

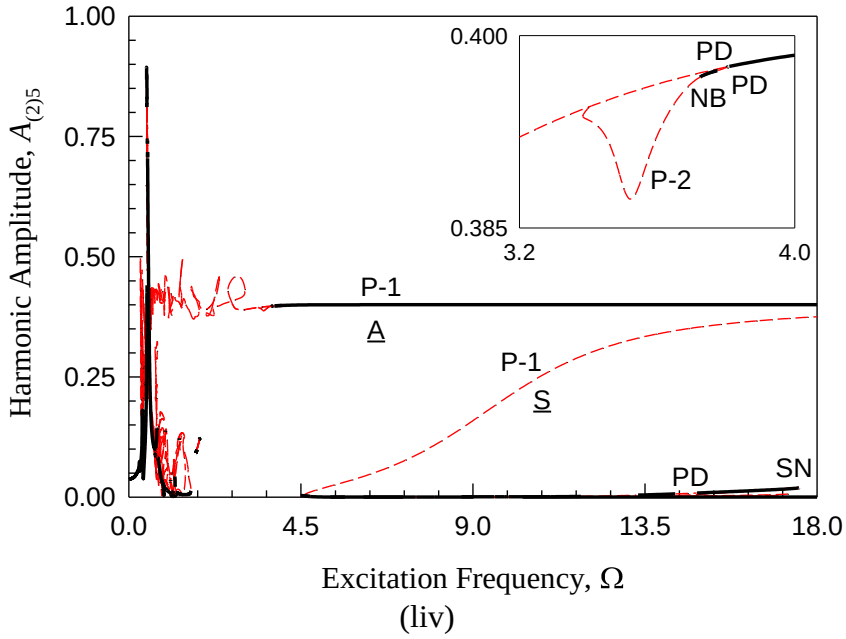

(liv)

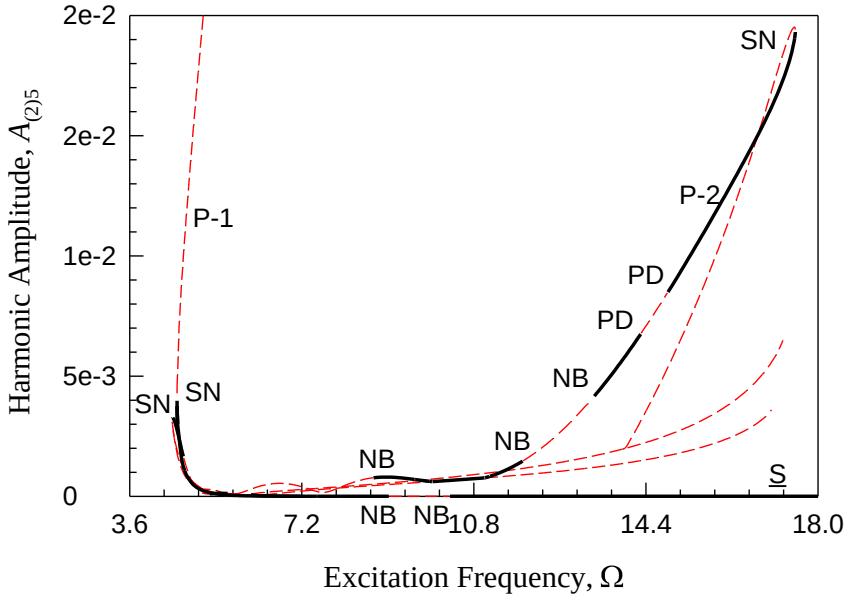

(lv)

Fig.25. (Continued).

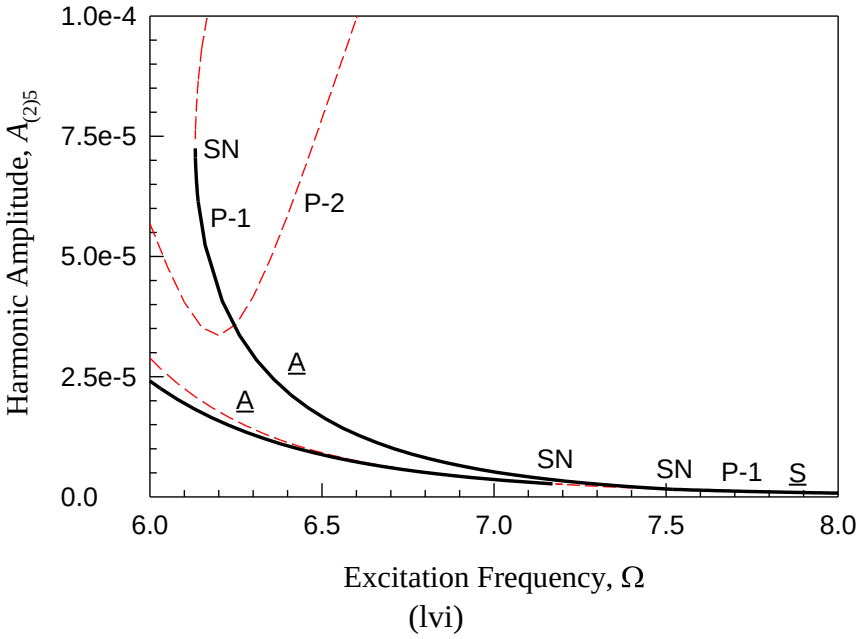

(lvi)

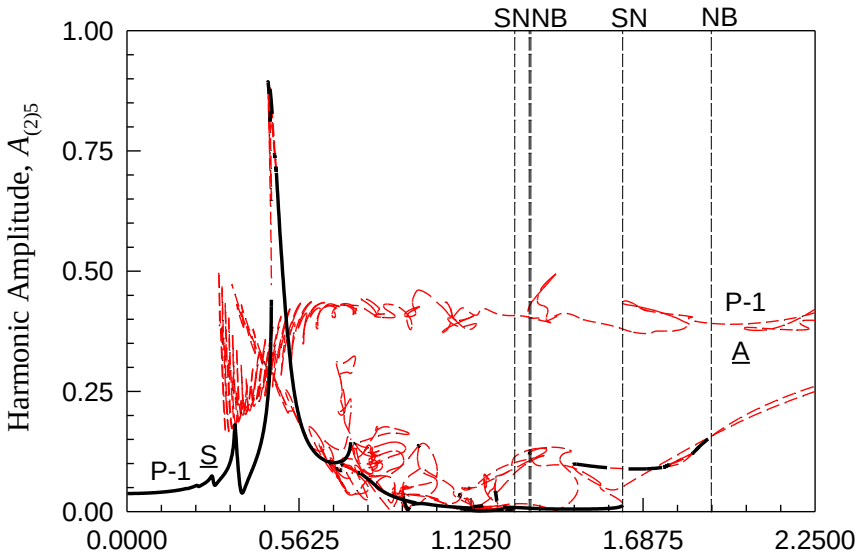

(lvii)

Fig.25. (Continued).

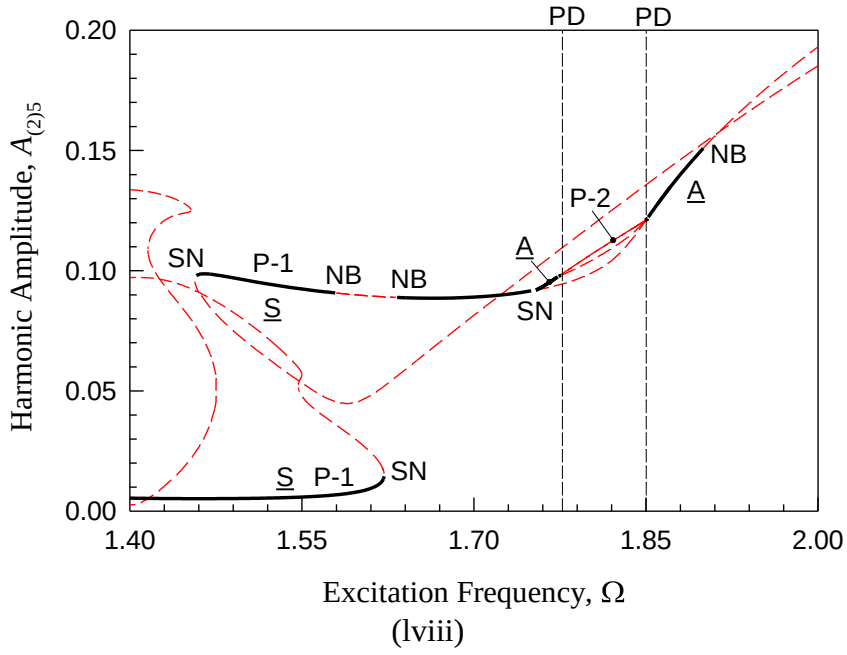

(lviii)

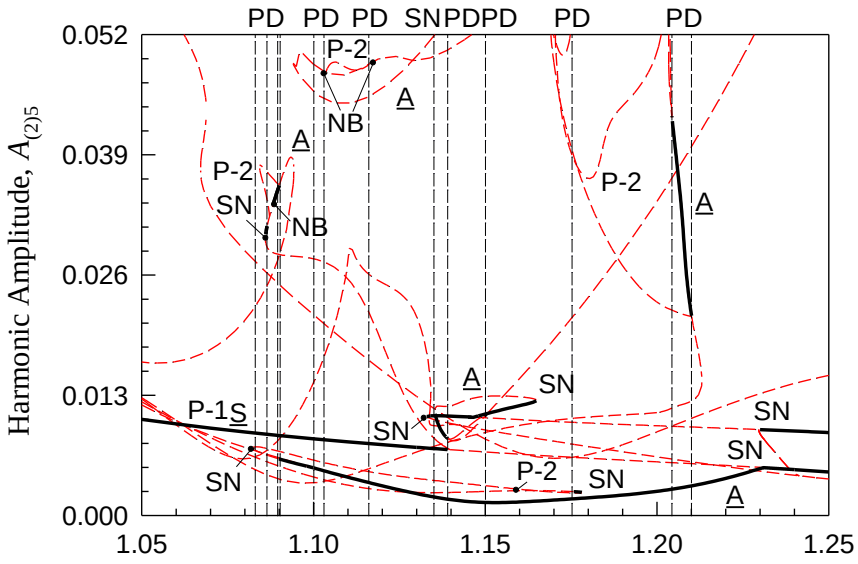

(lix)

Fig.25. (Continued).

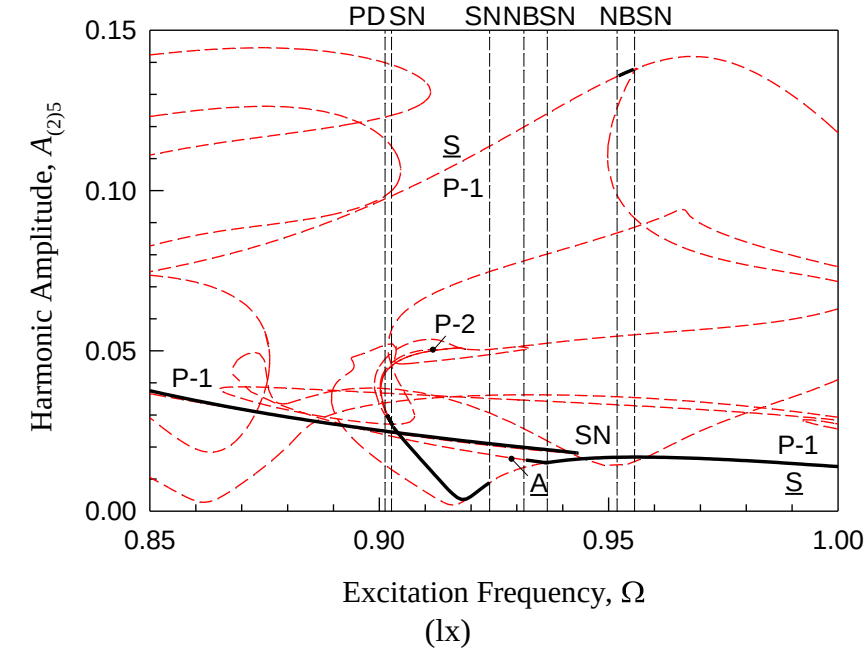

(lx)

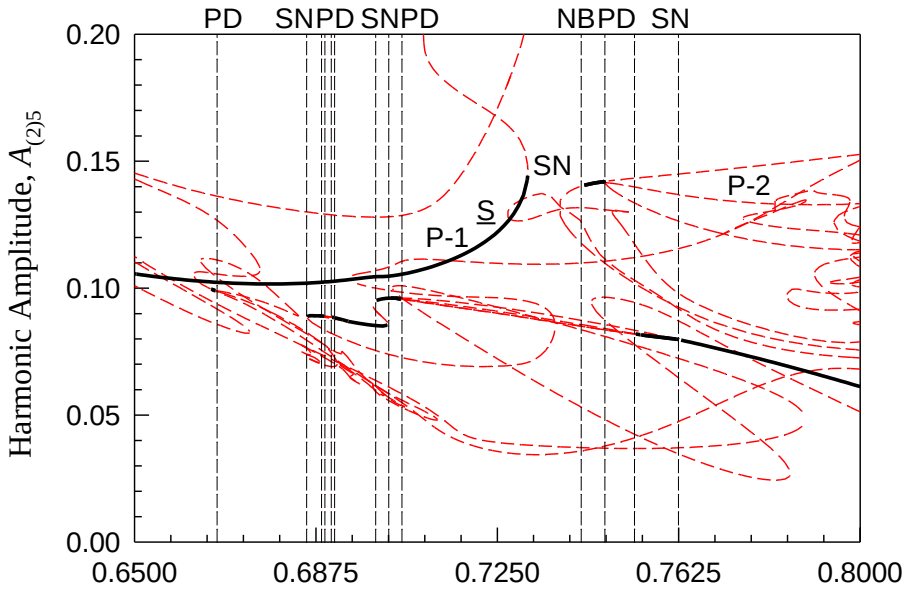

(lxi)

Fig.25. (Continued).

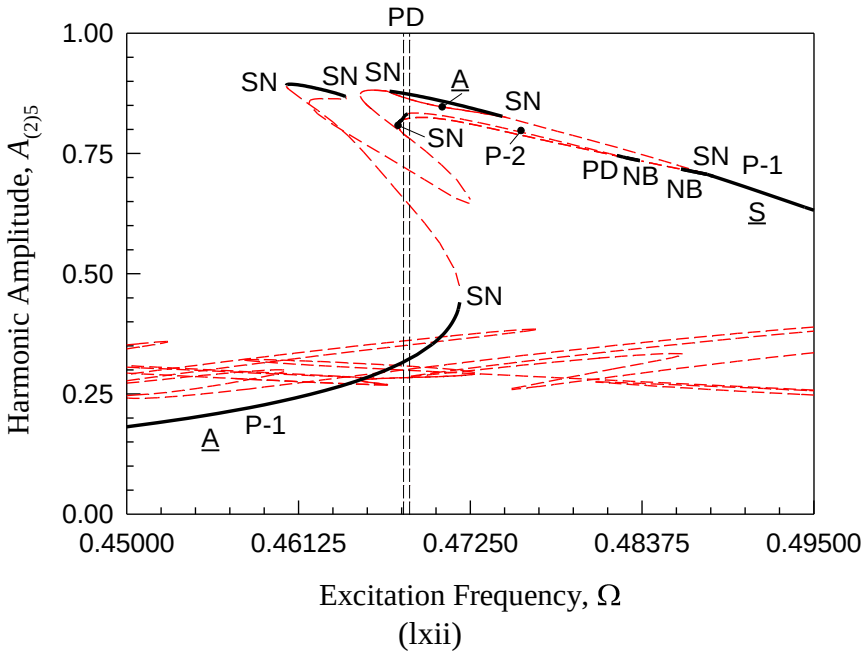

(lxii)

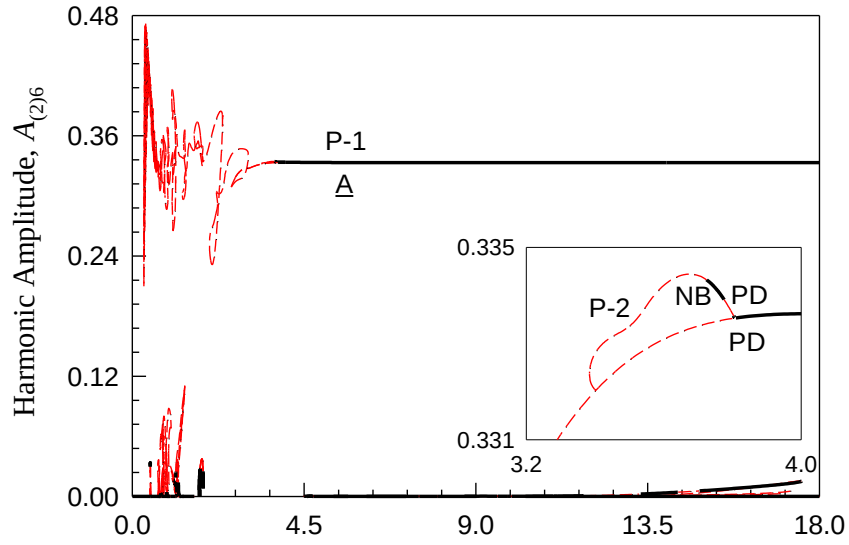

(lxiii)

Fig.25. (Continued).

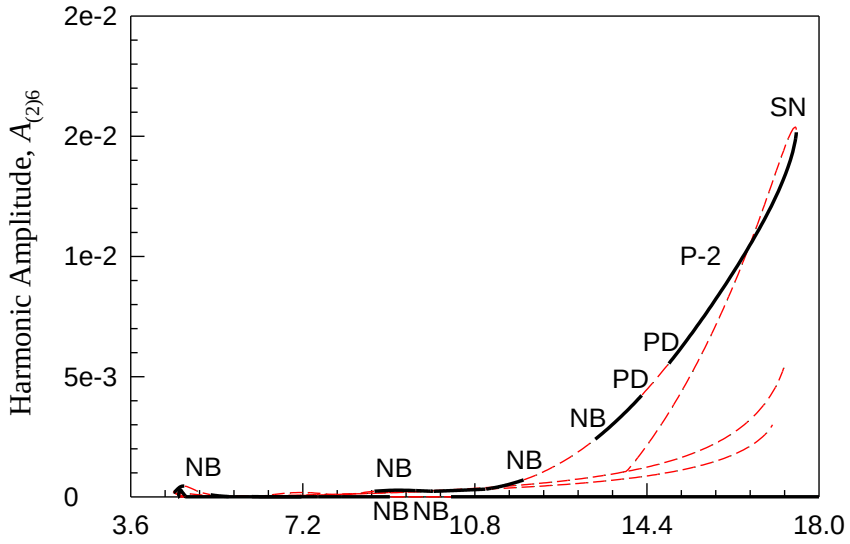

(lxiv)

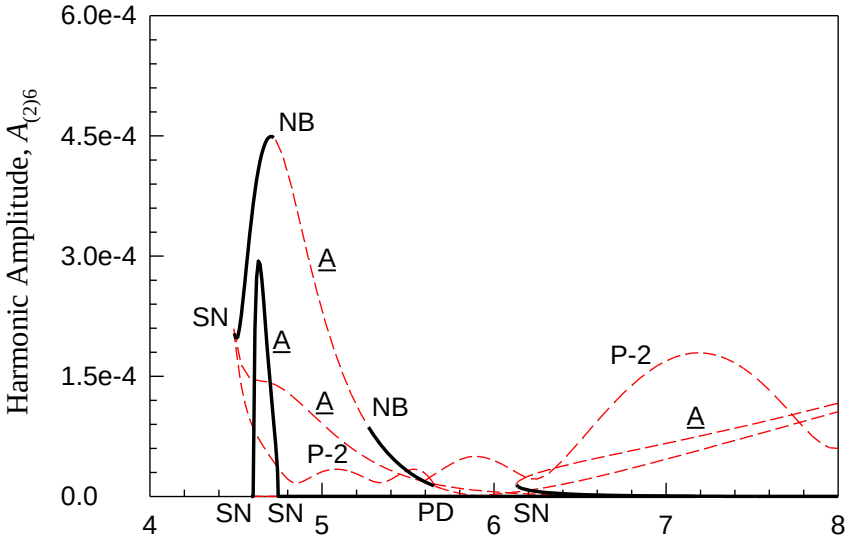

(lxv)

Fig.25. (Continued).

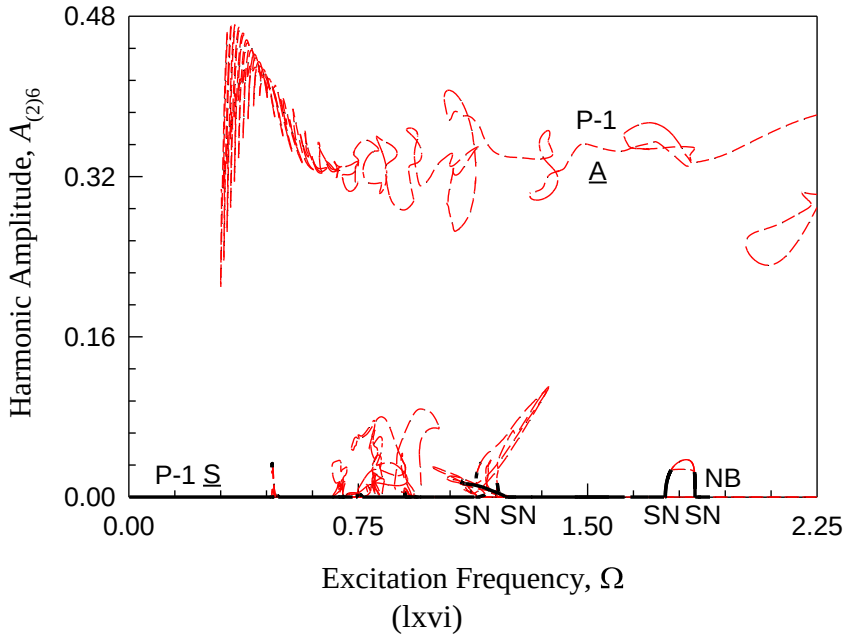

(lxvi)

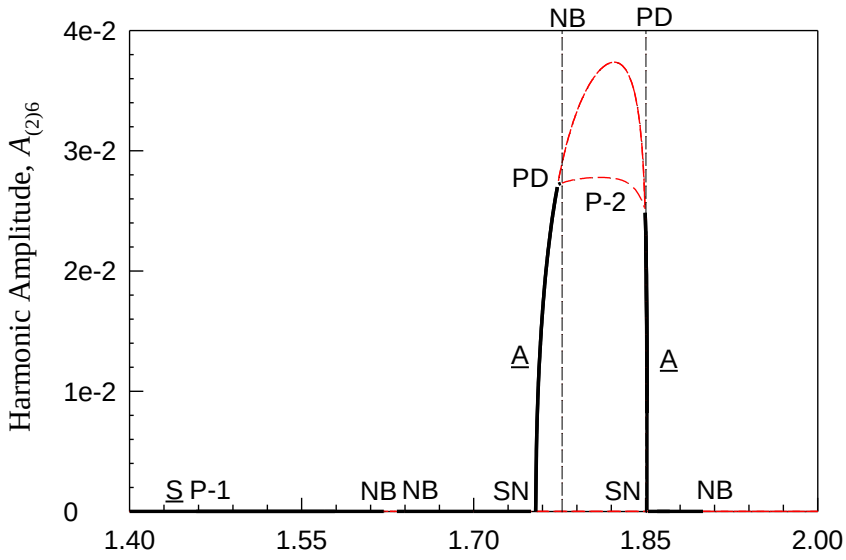

(lxvii)

Fig.25. (Continued).

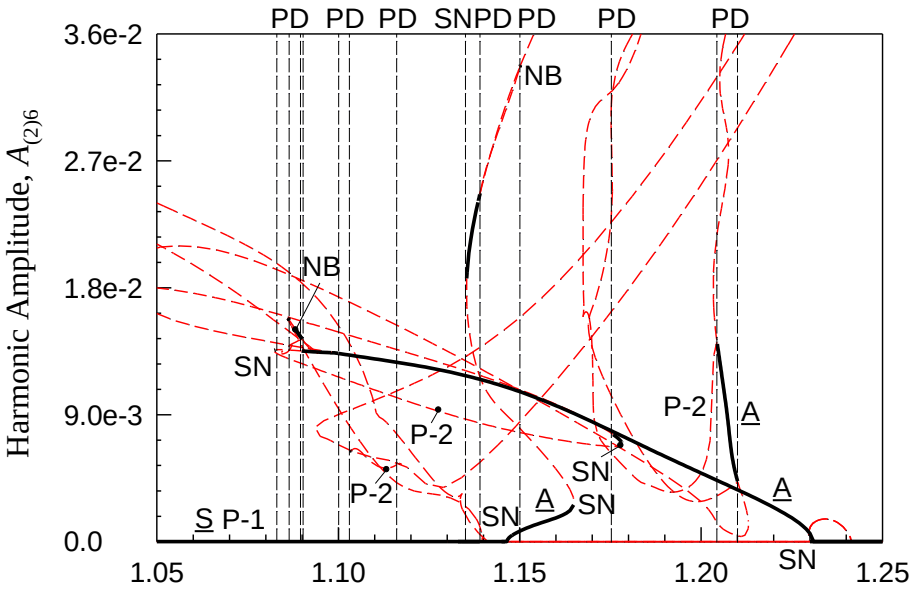

(lxviii)

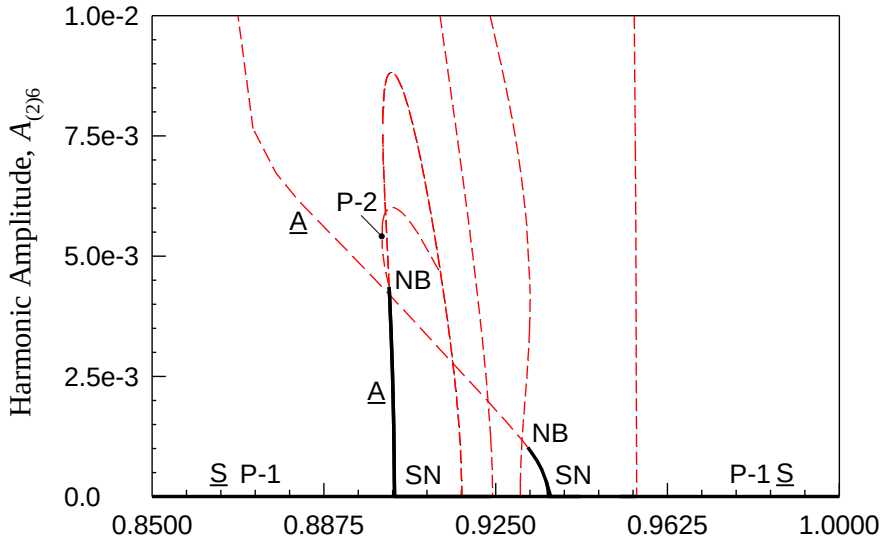

(lxix)

Fig.25. (Continued).

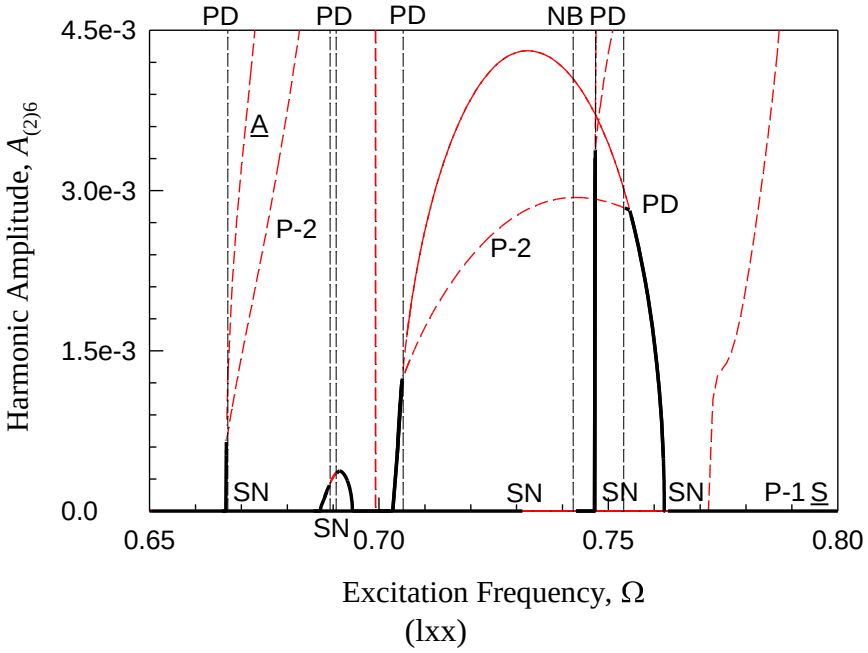

(lxx)

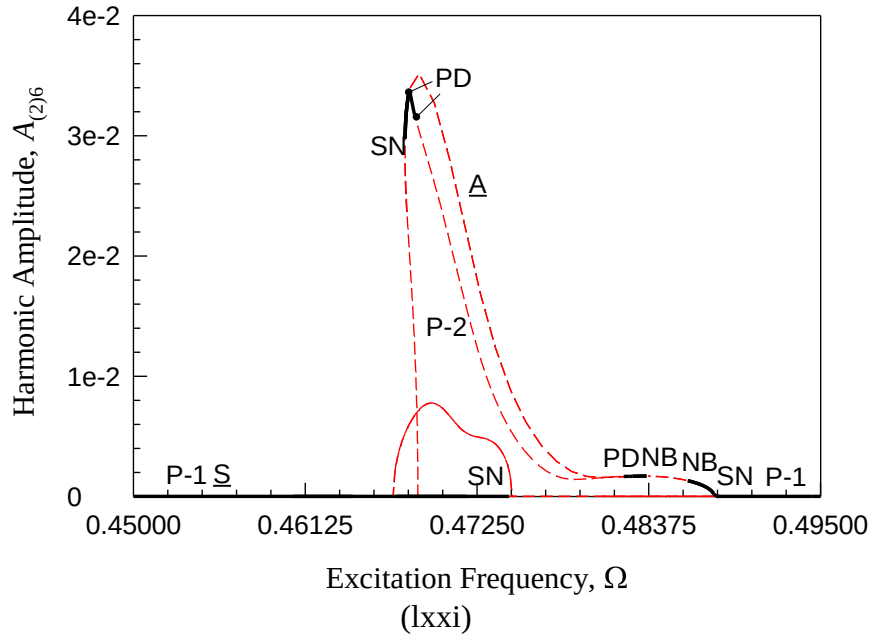

(lxxi)

Fig.25. (Continued).

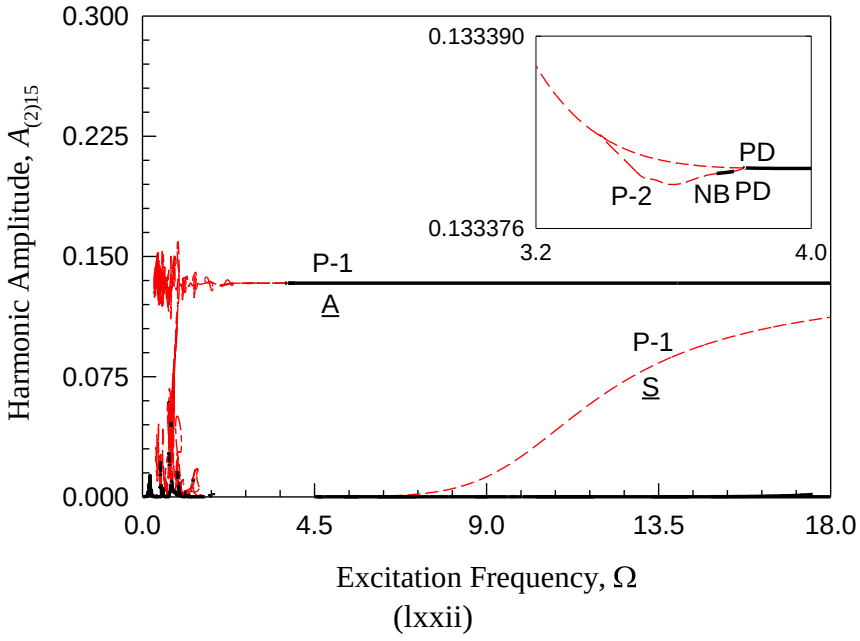

(lxxii)

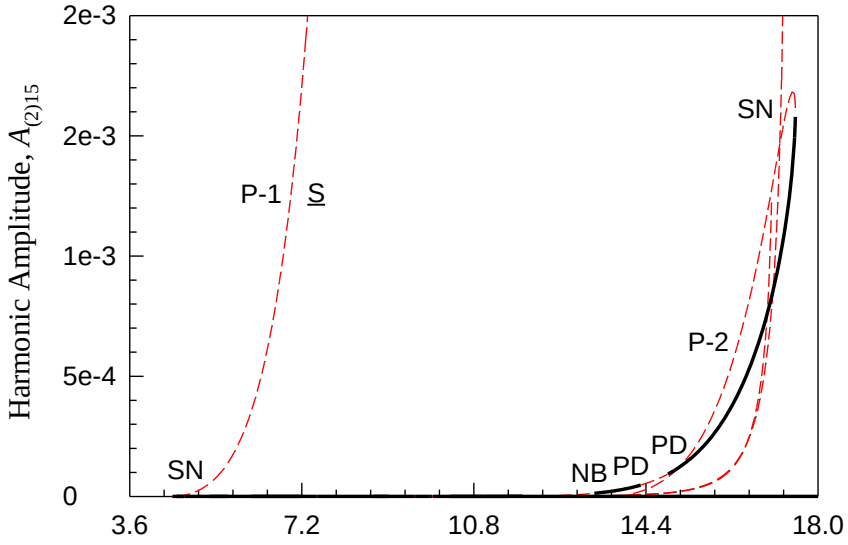

(lxxiii)

Fig.25. (Continued).

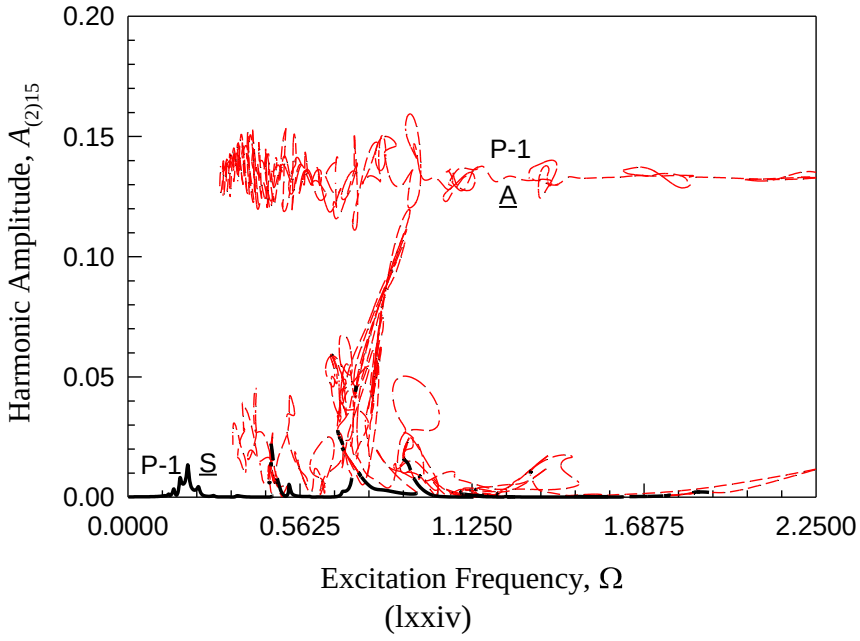

(lxxiv)

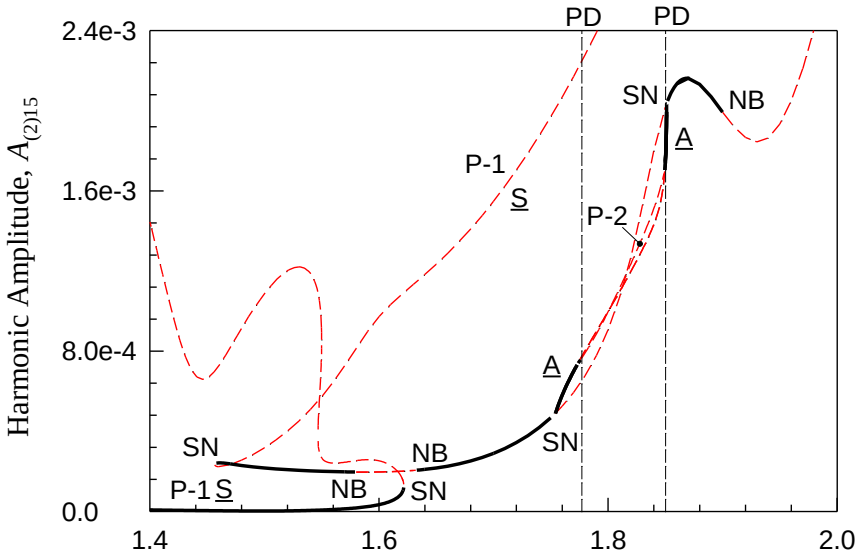

(lxxv)

Fig.25. (Continued).

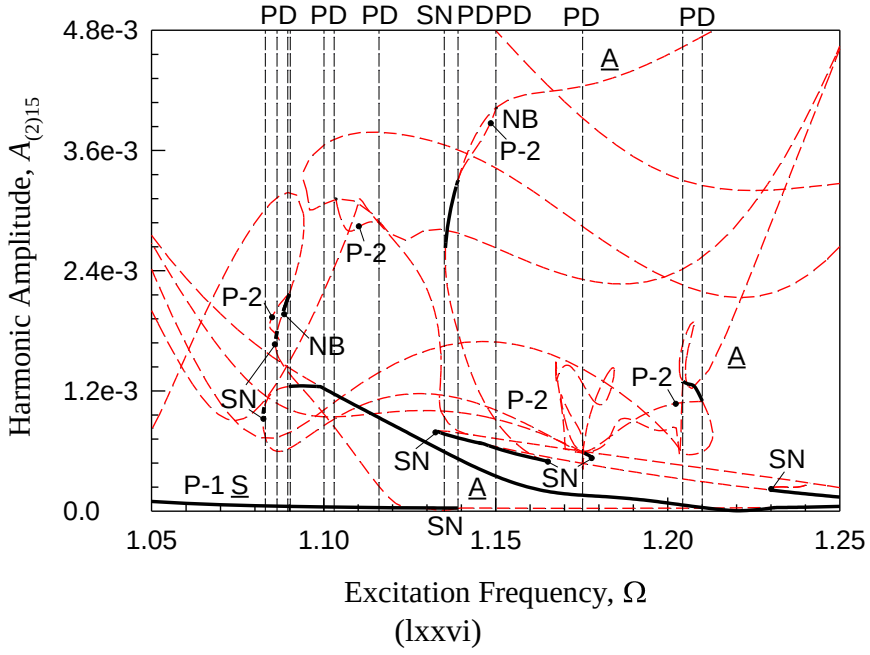

(lxxvi)

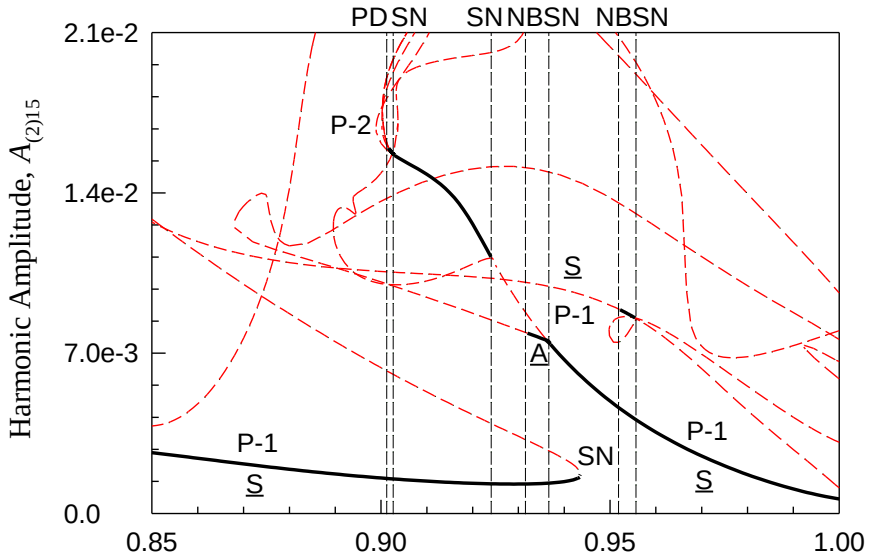

(lxxvii)

Fig.25. (Continued).

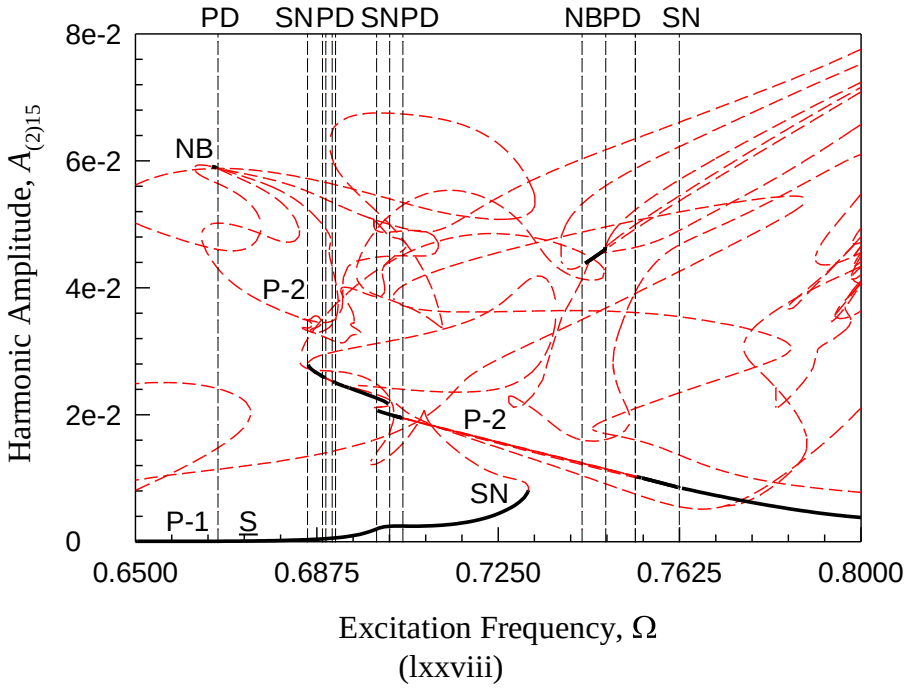

(lxxviii)

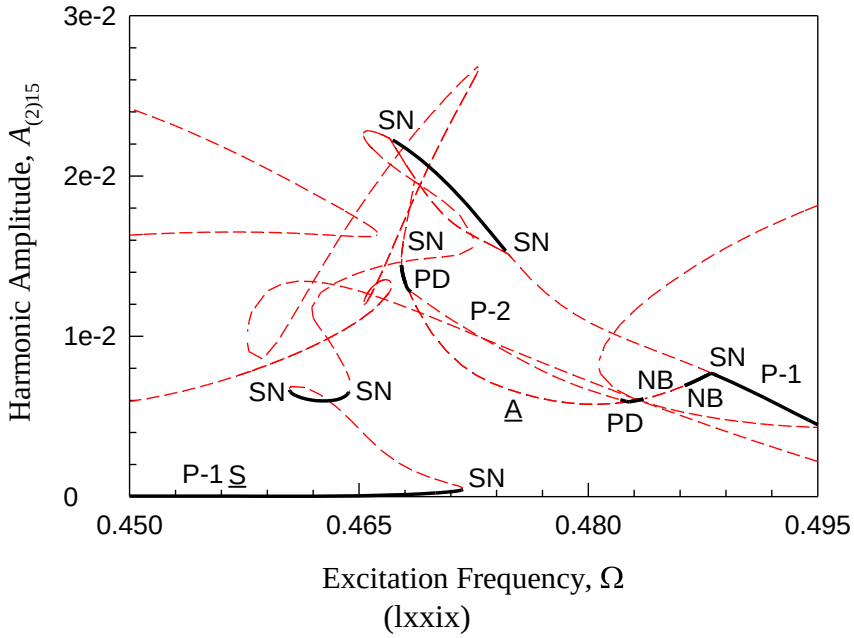

(lxxix)

Fig.25. (Continued).

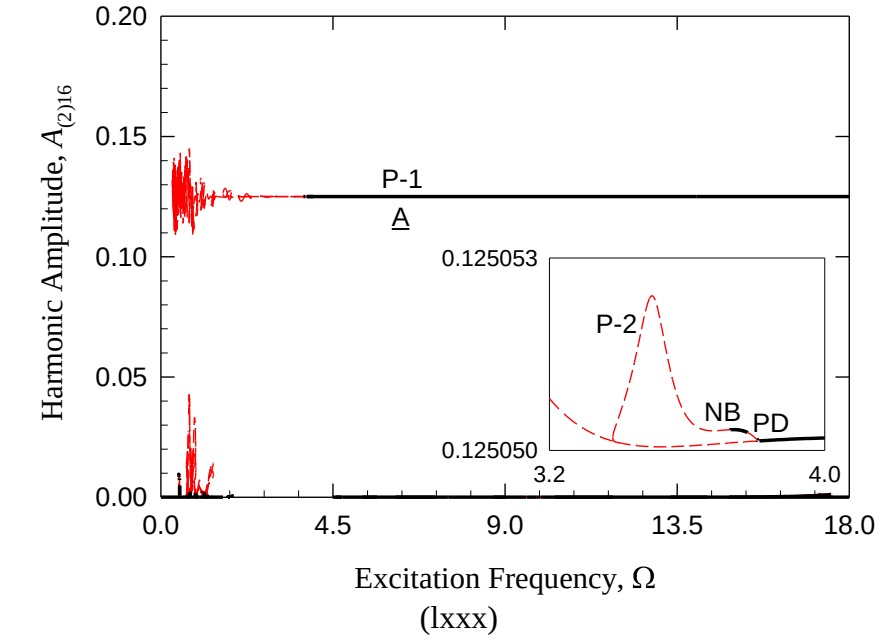

(lxxx)

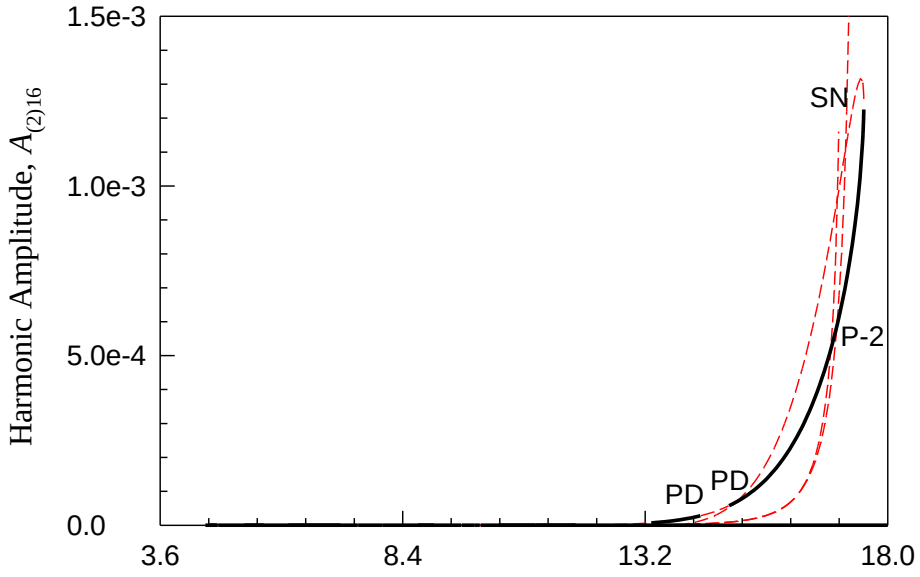

(lxxxi)

Fig.25. (Continued).

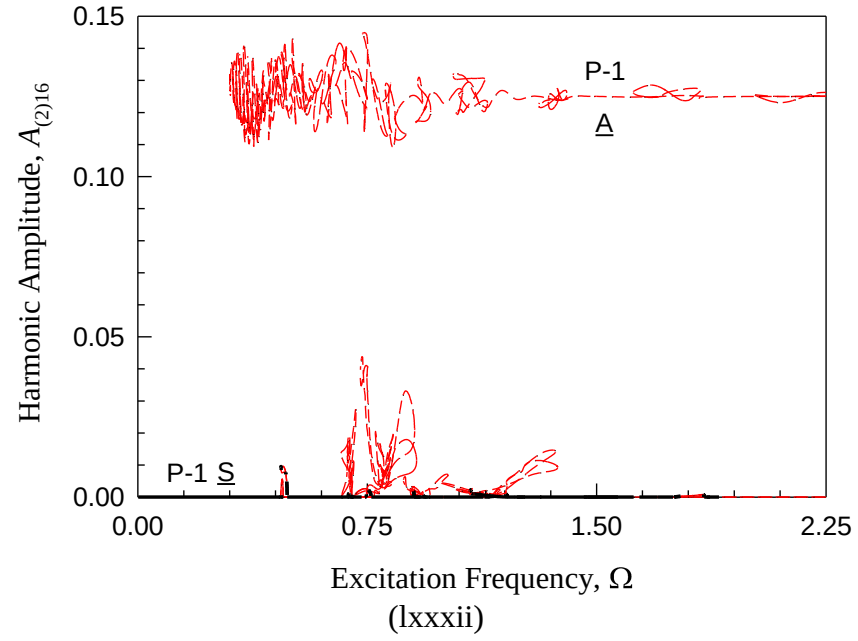

(lxxxii)

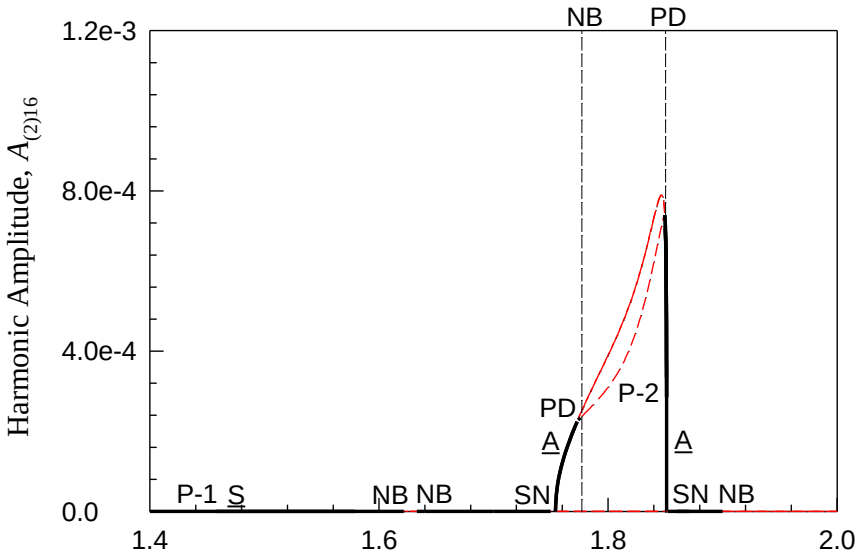

(lxxxiii)

Fig.25. (Continued).

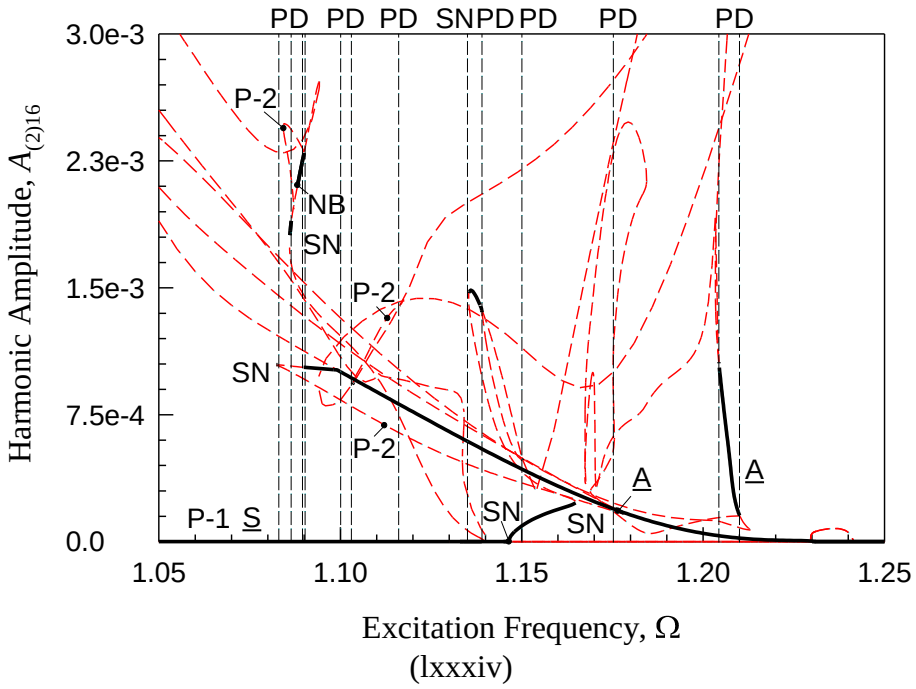

(lxxxiv)

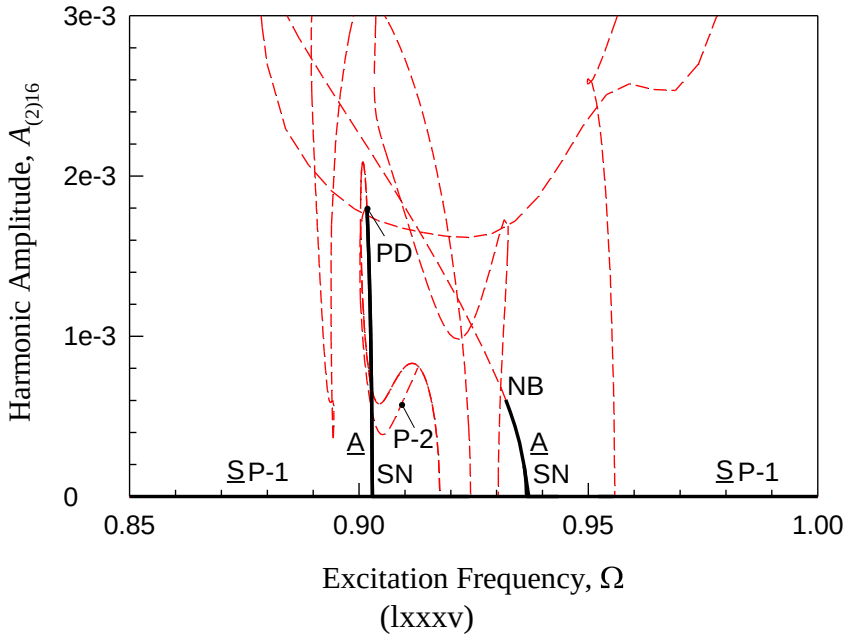

(lxxxv)

Fig.25. (Continued).

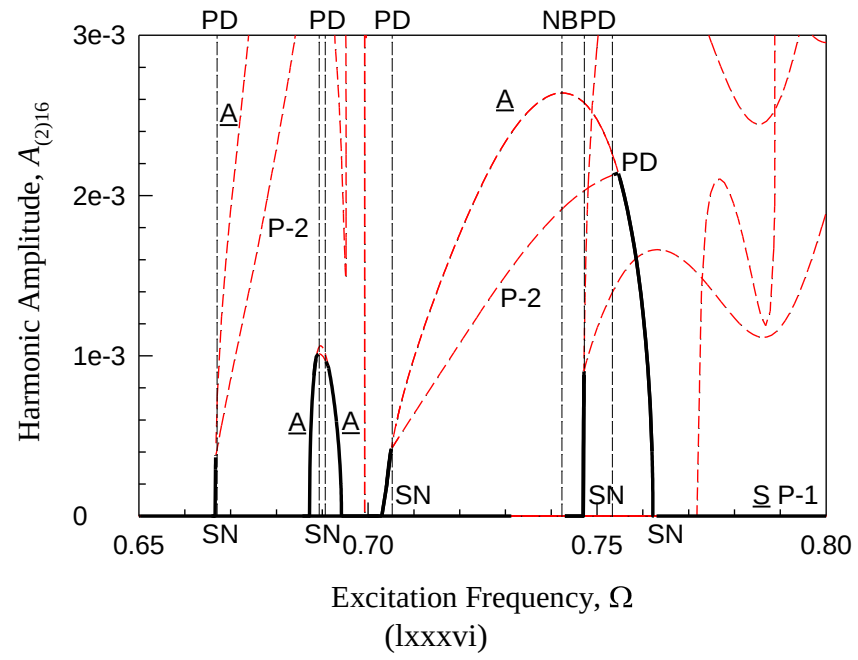

(lxxxvi)

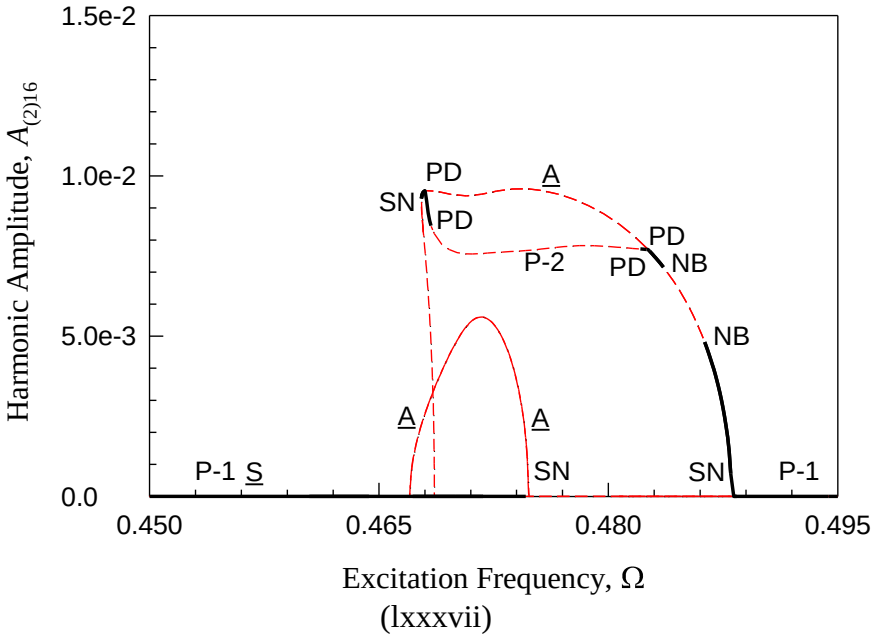

(lxxxvii)

Fig.25. (Continued).

CHAPTER VIII

NUMERICAL SIMULATIONS AND COMPARISON

The analytical prediction of period-1 to period-2 motions was predicted by the semi-analytical method. From the predicted results, the corresponding nonlinear frequency-amplitude characteristics were completed. The numerical simulation of period-1 to period-2 motions are completed for the verification with the semi-analytical prediction., The Numerical simulations are carried out by symplectic method. The initial conditions are from analytical predictions. The Harmonic frequency-amplitude and frequency-phase correspondences are analyzed for a bettering understanding of the complexity of periodic motions. The numerical results are presented by solid curves and the analytical results are presented by circle symbols.

Symmetric Period-1 Motions

A simulation of symmetric period-1 motions at excitation frequency $\Omega = 1.4565$ is presented in Fig.26. The initial conditions for the period-1 motion are $x_{10} \approx 0.4526$. $\dot{x}_{10} \approx -5.1271$, $x_{20} \approx 4.600$ and $\dot{x}_{20} \approx -0.1075$. The trajectory, displacement, velocity, harmonic amplitude spectrum and phase spectrum of such a period-1 motion of the oscillators are presented in Fig.26(a)-(j), respectively. The circular symbols are for semi-analytical results of the period-1 motions, and the solid curves are for numerical results. The red symbols are for the initial points. The analytical and numerical solutions match very well. In Fig.26(a), the trajectory of the spring oscillator is off the origin with three cycles. In Fig.26(b), the trajectory of the pendulum period-1 motion is near zero or 2π. Thus, the time-histories of displacement and velocity waves of the period-1 motion of the spring

oscillator in are with a few waves, as shown in Fig.26(c) and (d). However, the time-histories of angular displacement and angular velocity for the period-1 motions of pendulum oscillator are only one sinusoidal wave, as shown in Fig.26(e) and (f). To understand the harmonic effects on periodic motions, the harmonic amplitudes of the period-1 motion of the spring pendulum are presented in Fig.26(g) and (h). In Fig.26(g), the harmonic spectrum of the spring oscillator is presented. Only oven term harmonics exist. The constant term is $a_{(1)0} \approx 0.3012$. The main harmonic terms are $A_{(1)2} \approx 0.1166$, $A_{(1)4} \approx 0.1740$, $A_{(1)6} \approx 0.5596$, $A_{(1)8} \approx 0.0582$, $A_{(1)10} \approx 0.0612$, $A_{(1)12} \approx 0.0544$, $A_{(1)14} \approx 0.0117$, $A_{(1)16} \approx 0.0185$. Other harmonic amplitudes are $A_{(1)k} \in (10^{-11}, 10^{-3})$ for $k = 18, 20, \cdots, 90$ with $A_{(1)90} \approx 1.7560\text{E-}11$. In Fig.26(h), the harmonic amplitude of the pendulum is presented. The constant term is $a_{(2)0} \approx 6.28319$, which is equivalent to $a_{(2)0} \approx 0$. The main harmonic terms are $A_{(2)1} \approx 1.5738$, $A_{(2)3} \approx 0.0869$, $A_{(2)5} \approx 0.0965$, $A_{(2)7} \approx 0.0525$. Other harmonic amplitudes are $A_{(2)k} \in (10^{-11}, 10^{-3})$ for $k = 9, 11, \cdots, 79$ with $A_{(2)79} \approx 1.4503\text{E-}13$. To understand the complexity of period-1 motion in the spring pendulum, harmonic phases of the spring oscillator and pendulum oscillator are presented in Fig.26(i) and (j).

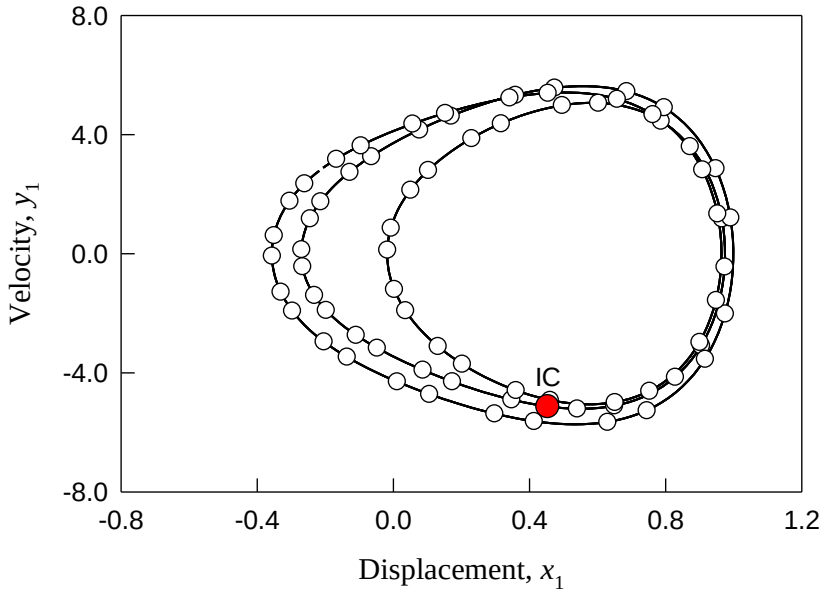

(a)

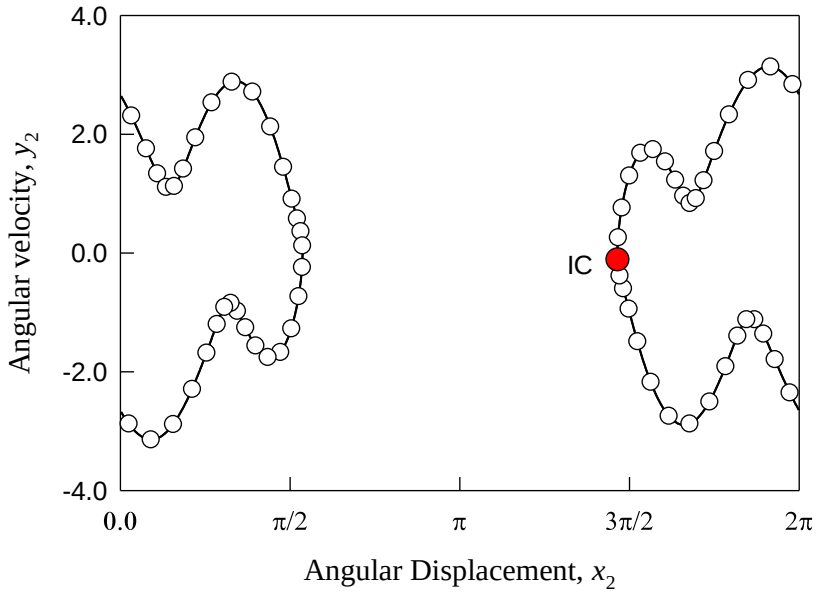

(b)

Fig.26 stable symmetric period-1 motion ($\Omega = 1.4565$): (a) spring trajectory (b) pendulum trajectory, (c) displacement, (d) velocity, (e) angular displacement, (f) angular velocity, (g) spring harmonic amplitude, (h) pendulum harmonic amplitude, (i) spring harmonic phase, (j) pendulum harmonic phase. Parameters: ($k_1 = 5.0$, $k_2 = 100.0$, $c = 0.1$, $m = 1.0$, $L = 2$, $Q_0 = 20$). $(x_{10}, \dot{x}_{10}, x_{20}, \dot{x}_{20}) \approx (0.4526, -5.1271, 4.600, -0.1075)$.

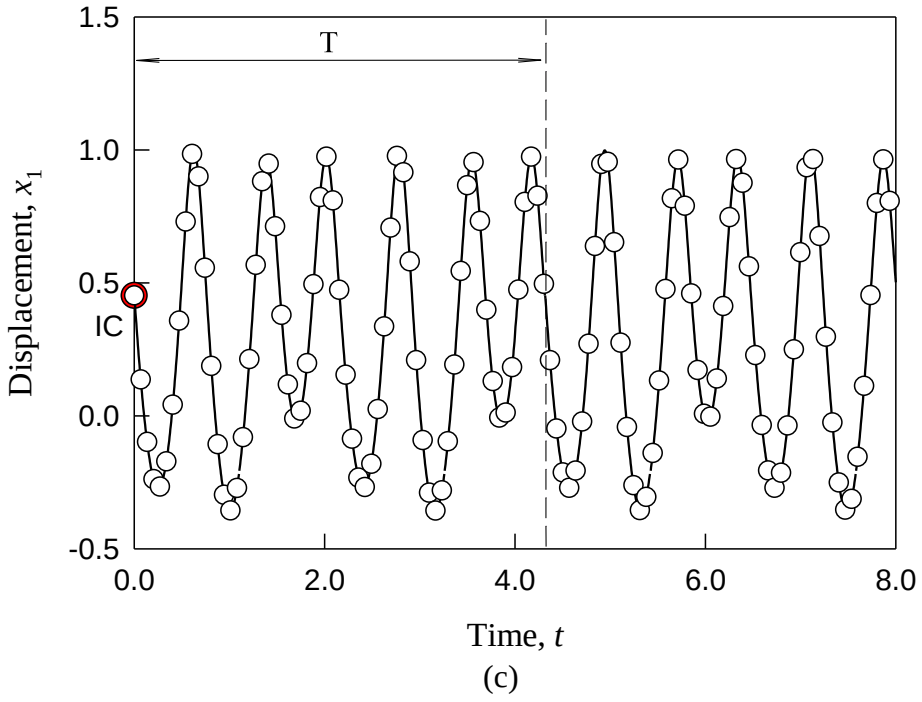

(c)

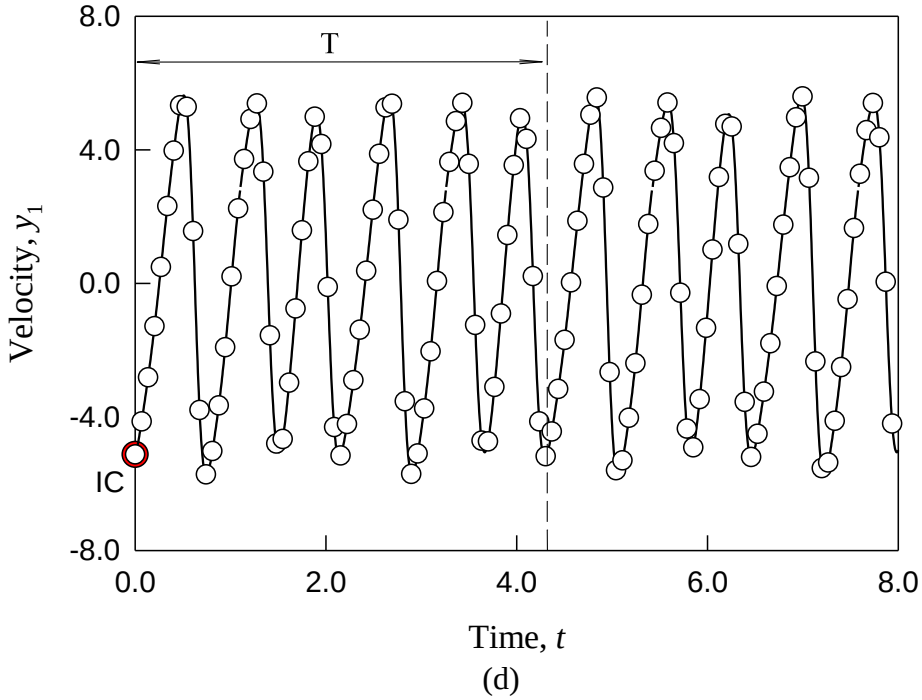

(d)

Fig.26.(Continued).

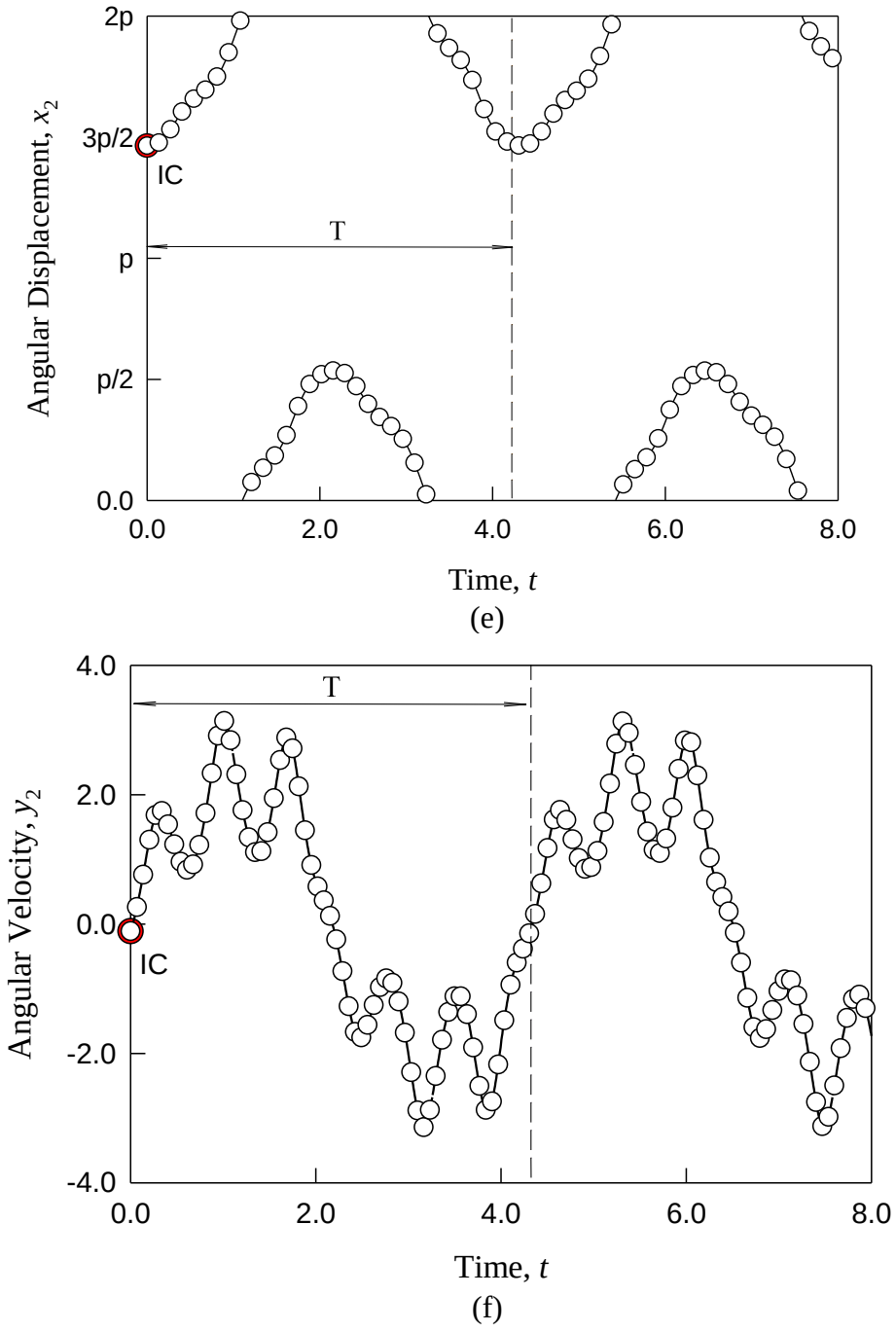

Fig.26. (Continued).

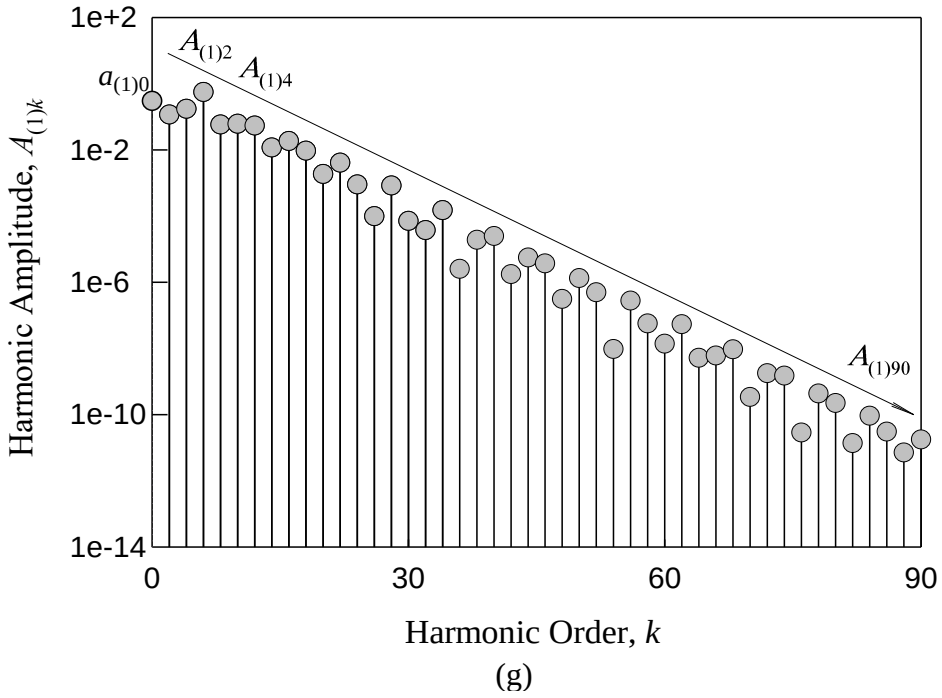

(g)

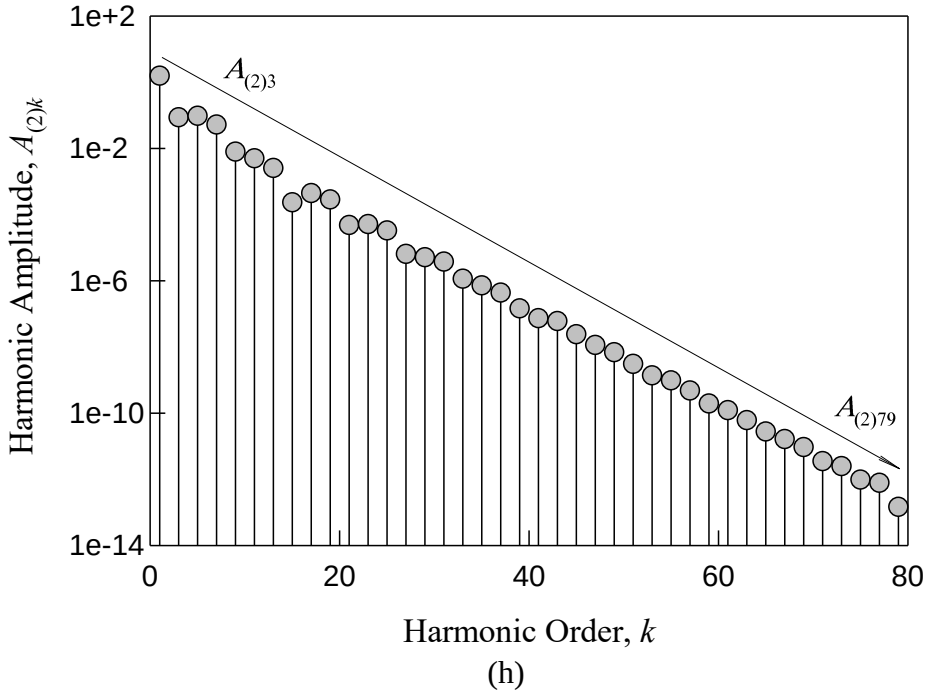

(h)

Fig.26. (Continued).

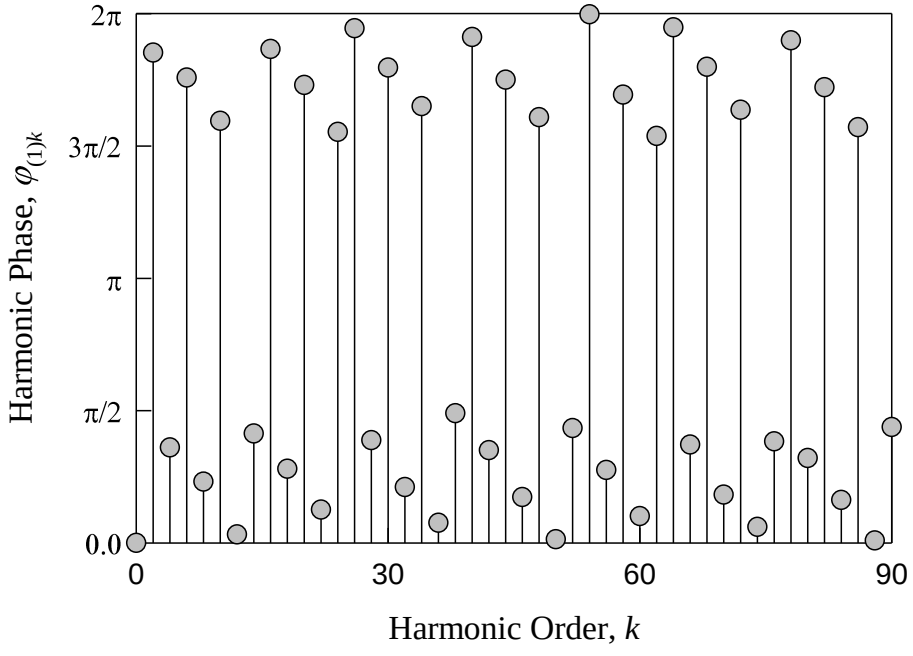

(i)

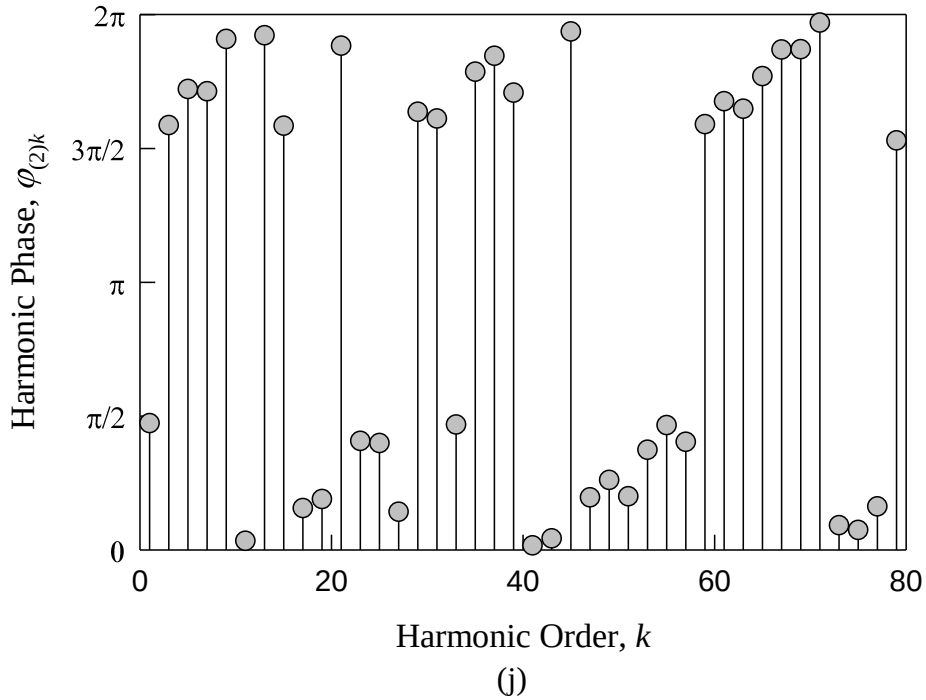

(j)

Fig.26. (Continued).

Asymmetric Period-1 Motions

A simulation of asymmetric period-1 motions at excitation frequency $\Omega = 4$ is presented in Fig.27. The initial conditions for the period-1 motion are $x_{10} \approx 0.9467$. $\dot{x}_{10} \approx 2.0098$, $x_{20} \approx 4.4589$ and $\dot{x}_{20} \approx 3.8007$. The trajectory, displacement, velocity, harmonic amplitude spectrum and phase spectrum of such a period-1 motion of the oscillators are presented in Fig.27(a)-(j), respectively. The circular symbols are for semi-analytical results of the period-1 motions, and the solid curves are for numerical results. The red symbols are for the initial points. The analytical and numerical solutions match very well. In Fig.27(a), the trajectory of the spring oscillator is off the origin. In Fig.27(b), the angle of the pendulum at this frequency keep increasing with time, as presented in the trajectory of the pendulum. It looks more clearly in the time-histories of angular displacement and angular velocity for the period-1 motions of pendulum oscillator as shown in Fig.27(e) and (f). And the time-histories of displacement and velocity waves of the period-1 motion of the spring oscillator in are with a few waves, as shown in Fig.27(c) and (d). To understand the harmonic effects on periodic motions, the harmonic amplitudes of the period-1 motion of the spring pendulum are presented in Fig.27(g) and (h). In Fig.27(g), the harmonic spectrum of the spring oscillator is presented. The constant term is $a_{(1)0} \approx 0.7615$. The main harmonic terms are $A_{(1)1} \approx 0.1787$, $A_{(1)2} \approx 0.1090$, $A_{(1)3} \approx 0.0124$, $A_{(1)4} \approx 0.102$, $A_{(1)5} \approx 0.0305$, $A_{(1)6} \approx 3.944\text{E-}03$, $A_{(1)7} \approx 2.5277\text{E-}03$, $A_{(1)8} \approx 1.2494\text{E-}03$. Other harmonic amplitudes are $A_{(1)k} \in (10^{-12}, 10^{-3})$ for $k = 9,10,\cdots,32$ with $A_{(1)32} \approx 8.6399\text{E-}13$. In Fig.27(h), the harmonic amplitude of the angular velocity is presented as $A_{(4)k}$. The main harmonic terms

are $A_{(4)1} \approx 0.5927$, $A_{(4)2} \approx 0.1242$, $A_{(4)3} \approx 0.0189$, $A_{(4)4} \approx 0.3058$, $A_{(4)5} \approx 0.0979$, $A_{(4)6} \approx 6.5356\text{E-}03$, $A_{(4)7} \approx 5.2958\text{E-}03$, $A_{(4)8} \approx 4.537\text{E-}03$, Other harmonic amplitudes are $A_{(4)k} \in (10^{-12}, 10^{-3})$ for $k = 9,10,\cdots,32$ with $A_{(4)32} \approx 5.8037\text{E-}13$. To understand the complexity of period-1 motion in the spring pendulum, harmonic phases of the spring oscillator and pendulum oscillator are presented in Fig.27(i) and (j). In Fig.27(j) $\varphi_{4(k)}$ are the harmonic phases of the angular velocity.

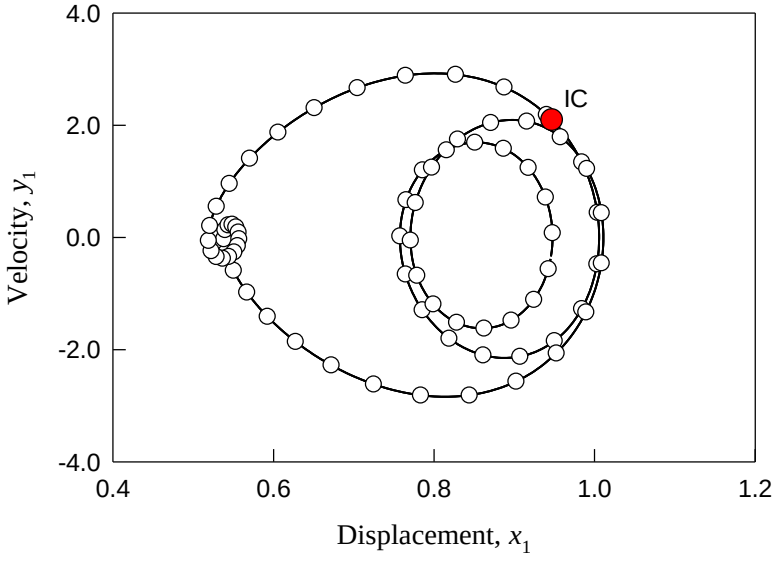

(a)

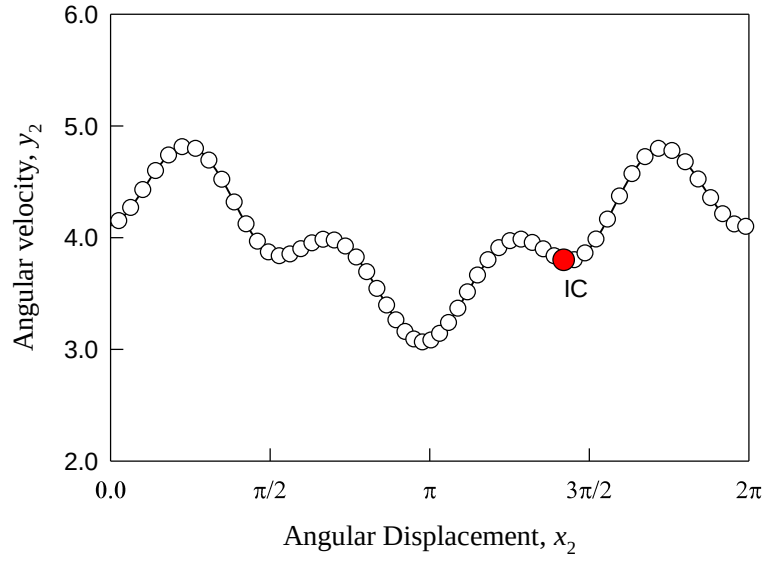

(b)

Fig.27. stable asymmetric period-1 motion ($\Omega = 4$): (a) spring trajectory (b) pendulum trajectory, (c) displacement, (d) velocity, (e) angular displacement, (f) angular velocity, (g) spring harmonic amplitude, (h) pendulum harmonic amplitude, (i) spring harmonic phase, (j) pendulum harmonic phase. Parameters: ($k_1 = 5.0$, $k_2 = 100.0$, $c = 0.1$, $m = 1.0$, $L = 2$, $Q_0 = 20.0$). $(x_{10}, \dot{x}_{10}, x_{20}, \dot{x}_{20}) \approx (0.9467,\ 2.0998, 4.4589, 3.8007)$.

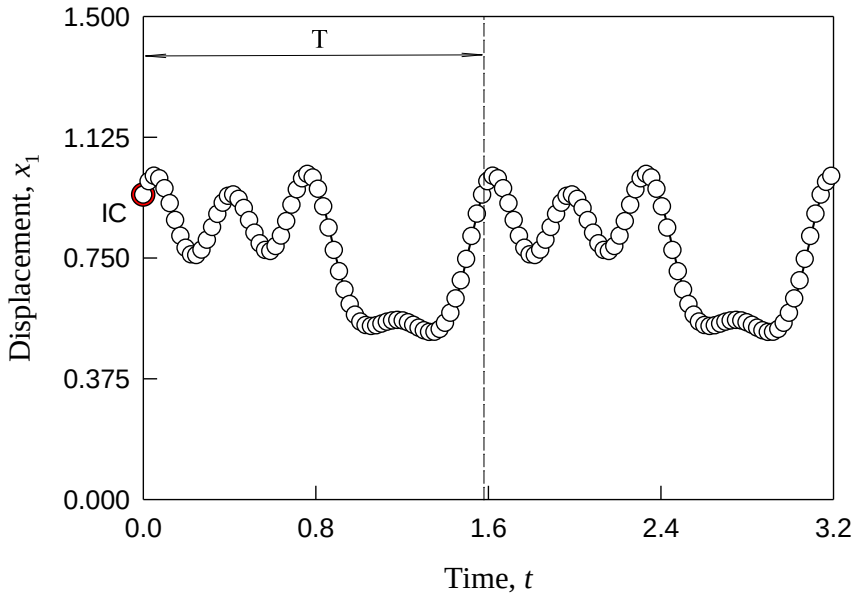

(c)

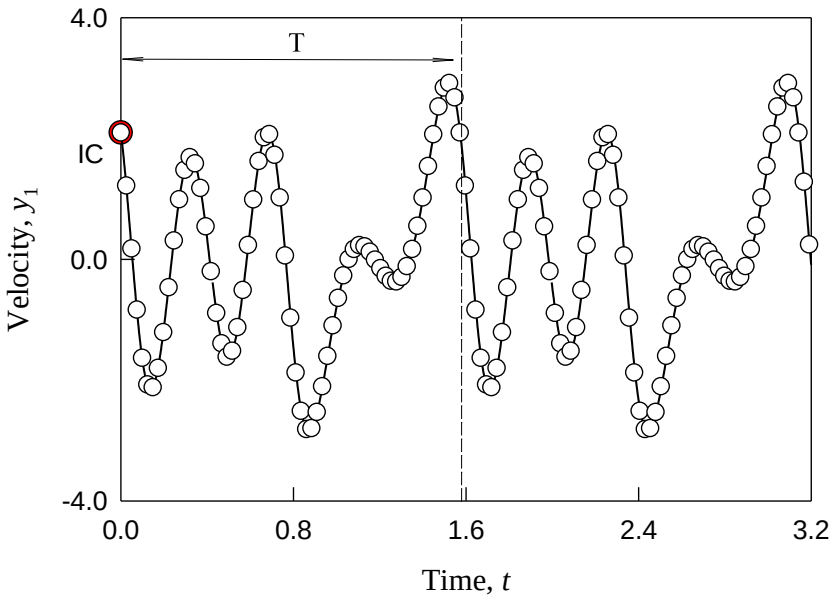

(d)

Fig.27. (Continue).

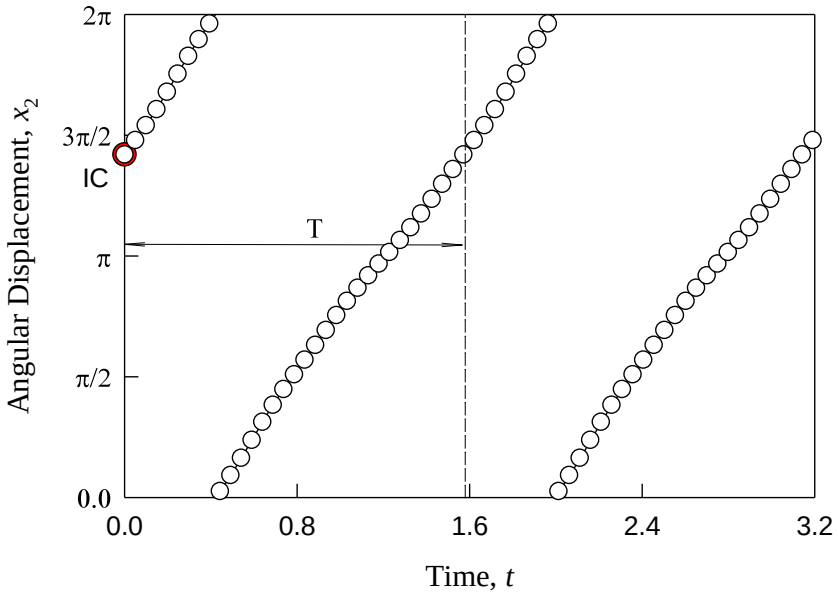

(e)

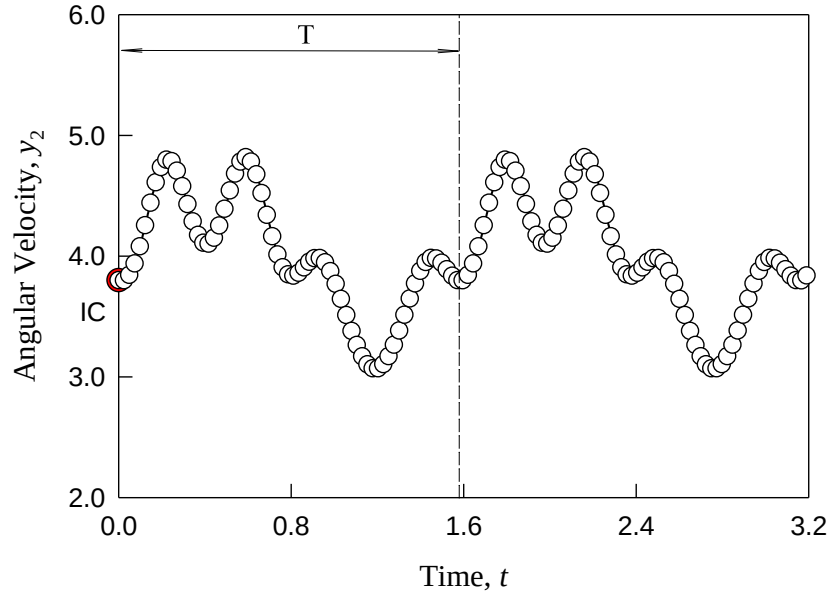

(f)

Fig.27. (Continue).

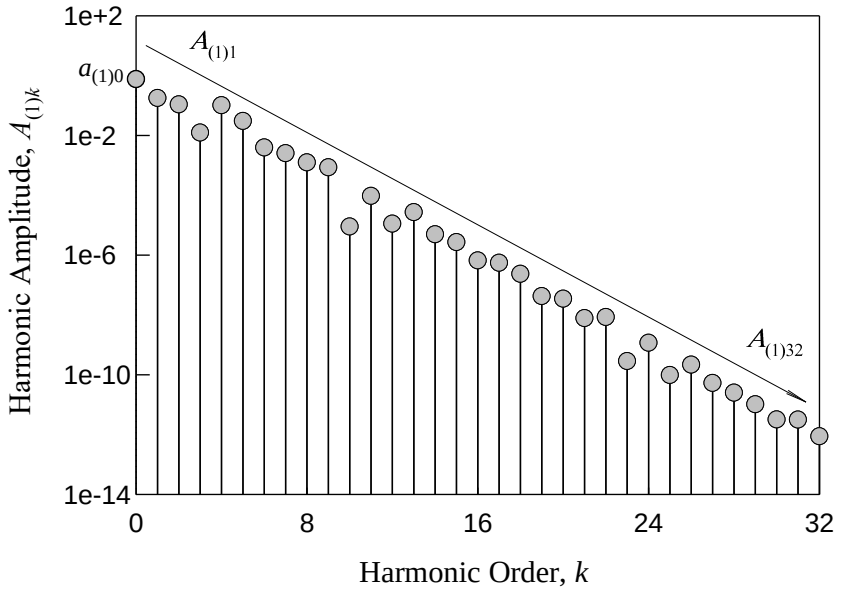

(g)

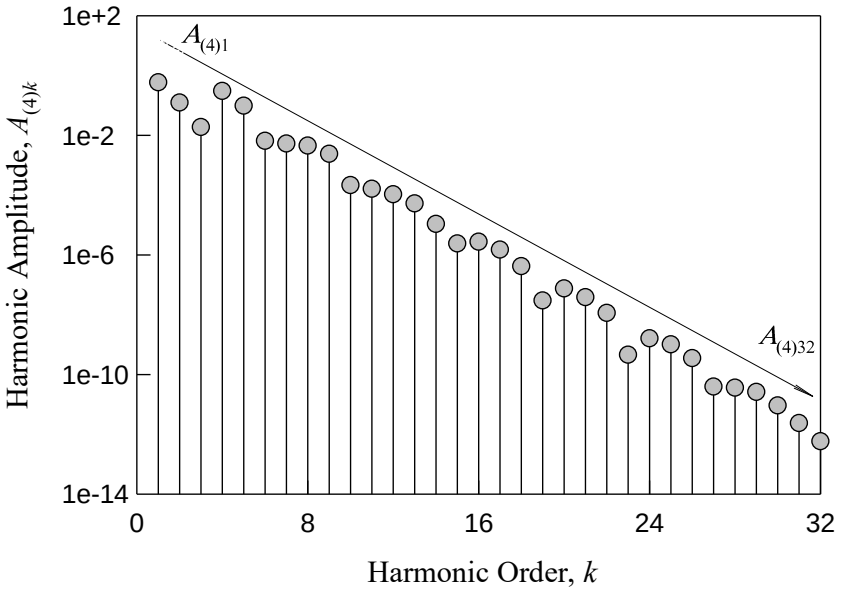

(h)

Fig.27. (Continue).

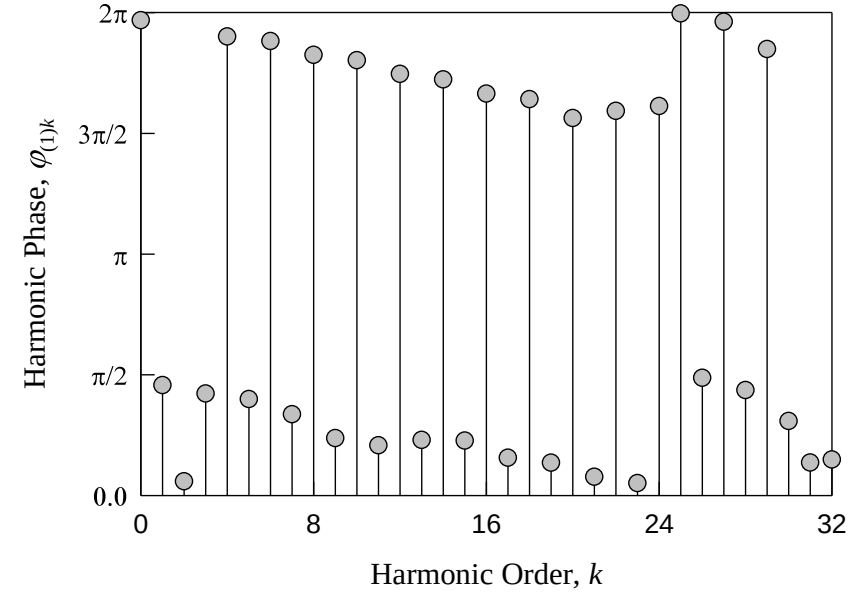

(i)

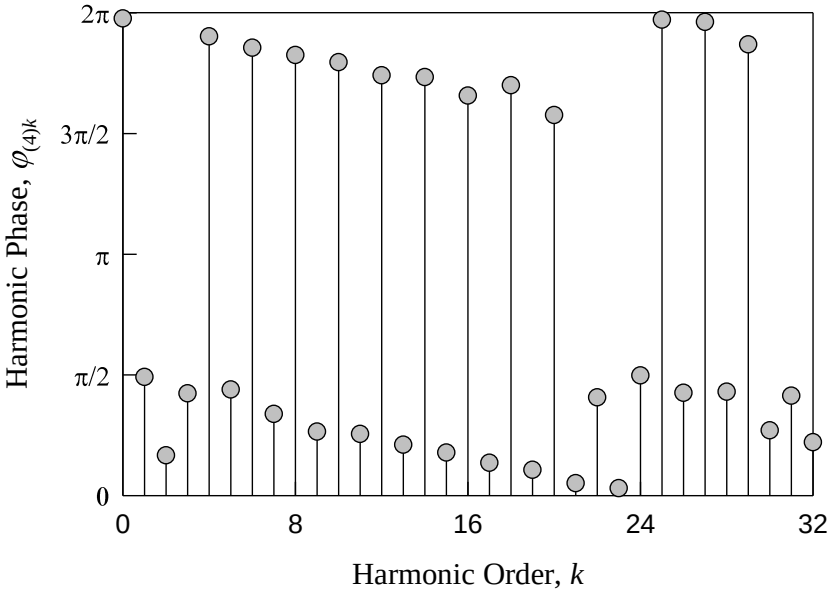

(j)

Fig.27. (Continue).

Period-2 Motions

A simulation of period-2 motions at excitation frequency $\Omega = 1.776$ is presented in Fig.28. The initial conditions for the period-2 motion are $x_{10} \approx 0.8857$. $\dot{x}_{10} \approx -0.8859$, $x_{20} \approx 3.9885$ and $\dot{x}_{20} \approx -0.5079$. The trajectory, displacement, velocity, harmonic amplitude spectrum and phase spectrum of such a period-2 motion of the oscillators are presented in Fig.28(a)-(j), respectively. The semi-analytical results of the period-2 motions are presented by circular symbols, and the solid curves represent the numerical results. The red symbols are for the initial points and the blue symbols are for the points at time $t = nT (n = 1, 2, 3)$. The analytical and numerical solutions match very well as the figures show. In Fig.28(a), the trajectory of the spring oscillator is off the origin points. In Fig.28(b), the trajectory of the pendulum is near 0 or 2π. Thus, the time-histories of displacement and velocity waves of the period-2 motion of the spring oscillator in are with a few waves, as shown in Fig.28(c) and (d). However, the time-histories of angular displacement and angular velocity for the period-2 motions of pendulum oscillator are only two sinusoidal wave, as shown in Fig.28(e) and (f). To understand the harmonic effects on periodic motions, the harmonic amplitudes of the period-2 motion of the spring pendulum are presented in Fig.28(g) and (h). In Fig.28(g), the harmonic spectrum of the spring oscillator is presented. Only oven term harmonics exist. The constant term is $a_{(1)0} \approx 0.3972$. The main harmonic terms are

$A_{(1)1/2} \approx 0.0142$, $A_{(1)1} \approx 0.1293$, $A_{(1)3/2} \approx 0.0102$, $A_{(1)2} \approx 0.1025$, $A_{(1)5/2} \approx 7.9145\text{E-}3$,

$A_{(1)3} \approx 0.0951$, $A_{(1)7/2} \approx 0.0110$, $A_{(1)4} \approx 0.0568$, $A_{(1)9/2} \approx 0.0176$, $A_{(1)5} \approx 0.2167$,

$A_{(1)11/2} \approx 0.0217$, $A_{(1)6} \approx 0.5115$, $A_{(1)13/2} \approx 0.0160$, $A_{(1)7} \approx 0.0527$, $A_{(1)15/2} \approx 7.0320\text{E-}03$,

$A_{(1)8} \approx 0.1295$, $A_{(1)17/2} \approx 4.4121\text{E-}03$, $A_{(1)9} \approx 0.0117$, $A_{(1)19/2} \approx 2.4873\text{E-}03$, $A_{(1)10} \approx 0.0114$,

$A_{(1)21/2} \approx 2.7256\text{E-}03$, $A_{(1)11} \approx 0.0287$, $A_{(1)23/2} \approx 8.0148\text{E-}3$, $A_{(1)12} \approx 0.0357$, $A_{(1)25/2} \approx 2.7505\text{E-}03$, $A_{(1)13} \approx 6.8491\text{E-}03$, $A_{(1)27/2} \approx 2.1326\text{E-}03$, $A_{(1)14} \approx 0.0210$. Other Harmonic amplitudes are $A_{(1)k/2} \in (10^{-11}, 10^{-3})$ for $k = 29, 30, \cdots, 160$. with $A_{(1)80} \approx 2.8484\text{E-}12$. In Fig.27(h), the harmonic amplitude of the pendulum is presented. The constant term is $a_{(2)0} \approx 1.9955\text{E-}03$, The main harmonic terms are $A_{(2)1/2} \approx 8.5689E-03$, $A_{(2)1} \approx 2.1498$, $A_{(2)3/2} \approx 8.5514E-03$, $A_{(2)2} \approx 0.0464$, $A_{(2)5/2} \approx 4.2683E-03$, $A_{(2)3} \approx 0.1408$, $A_{(2)7/2} \approx 3.7347E-03$, $A_{(2)4} \approx 0.0348$, $A_{(2)9/2} \approx 4.0989E-03$, $A_{(2)5} \approx 0.0981$, $A_{(2)11/2} \approx 1.0047E-03$, $A_{(2)6} \approx 0.0273$, $A_{(2)13/2} \approx 3.4685E-03$, $A_{(2)7} \approx 0.0762$, $A_{(2)15/2} \approx 2.7356E-03$, $A_{(2)8} \approx 0.0121$, $A_{(2)17/2} \approx 8.3154e-03$. $A_{(2)9} \approx 5.1998E-03$. Other harmonic amplitudes are $A_{(2)k} \in (10^{-11}, 10^{-3})$ for $k = 19, 20, \cdots, 160$ with $A_{(2)80} \approx 1.6915\text{E-}12$. To understand the complexity of period-2 motion in the spring pendulum, harmonic phases of the spring oscillator and pendulum oscillator are presented in Fig.28(i) and (j).

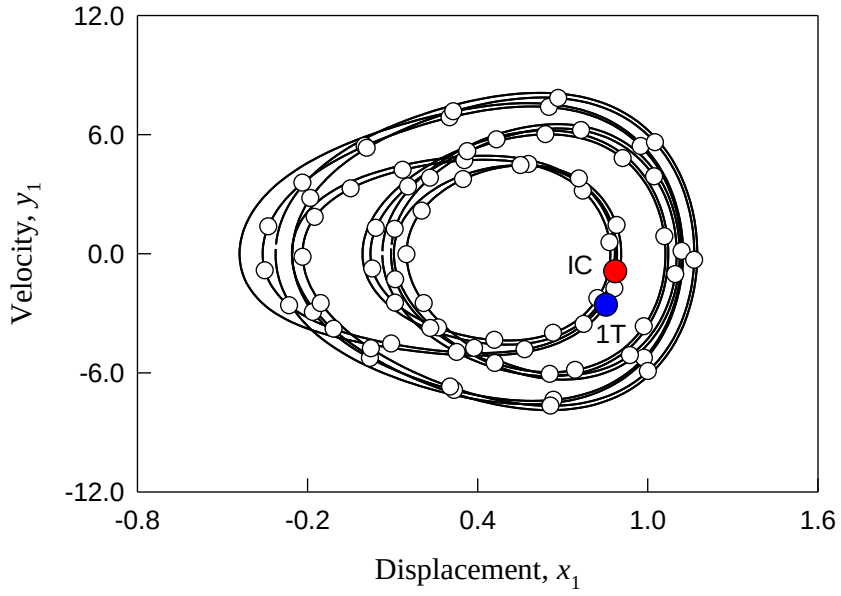

(a)

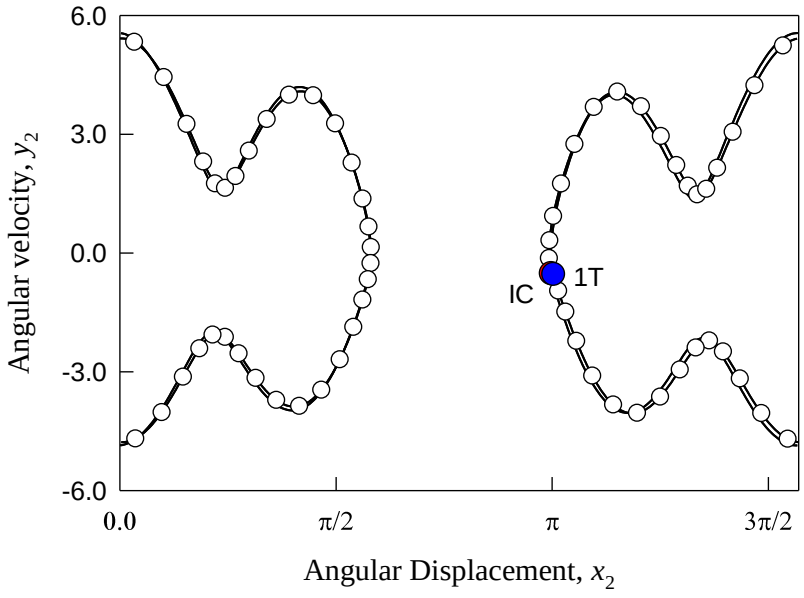

(b)

Fig.28. stable period-2 motion ($\Omega = 1.776$): (a) spring trajectory (b) pendulum trajectory, (c) displacement, (d) velocity, (e) angular displacement, (f) angular velocity, (g) spring harmonic amplitude, (h) pendulum harmonic amplitude, (i) spring harmonic phase, (j) pendulum harmonic phase. Parameters: ($k_1 = 5.0$, $k_2 = 100.0$, $c = 0.1$, $m = 1.0$, $L = 2$, $Q_0 = 20.0$). $(x_{10}, \dot{x}_{10}, x_{20}, \dot{x}_{20}) \approx (0.8857,\ -0.8859, 3.9885, -0.5079)$.

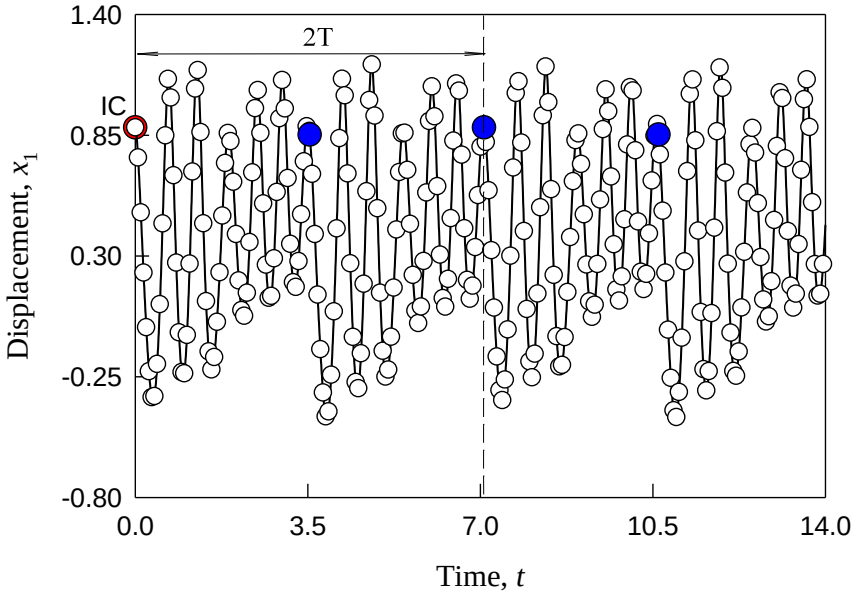

(c)

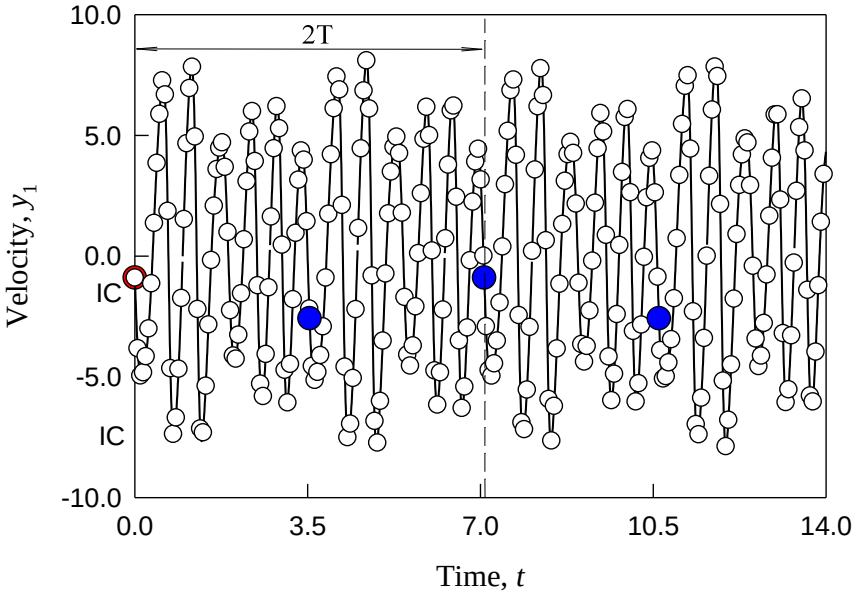

(d)

Fig.28. (Continued).

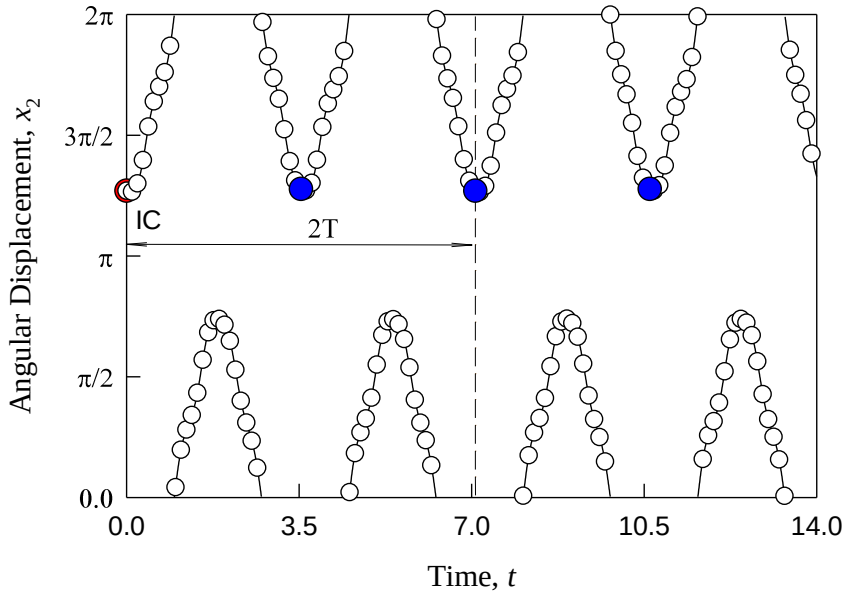

(e)

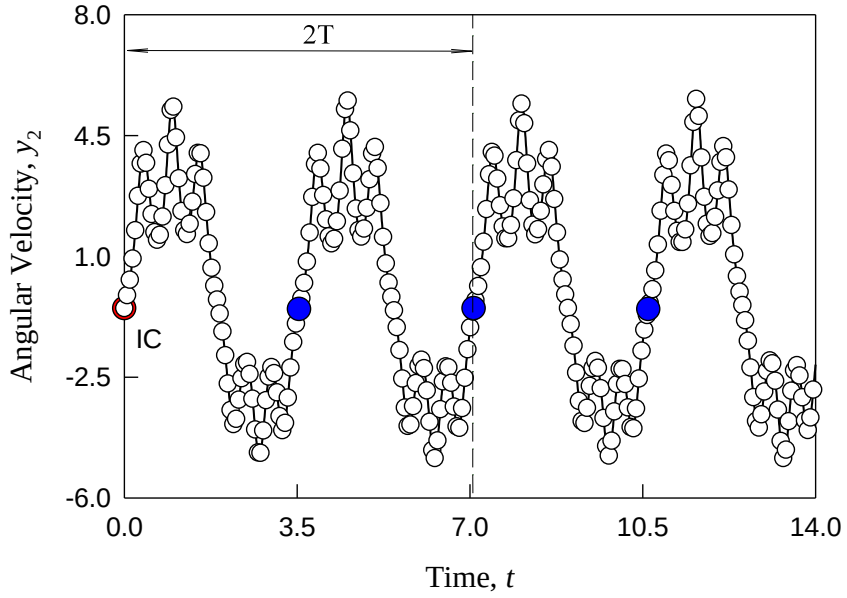

(f)

Fig.28. (Continued).

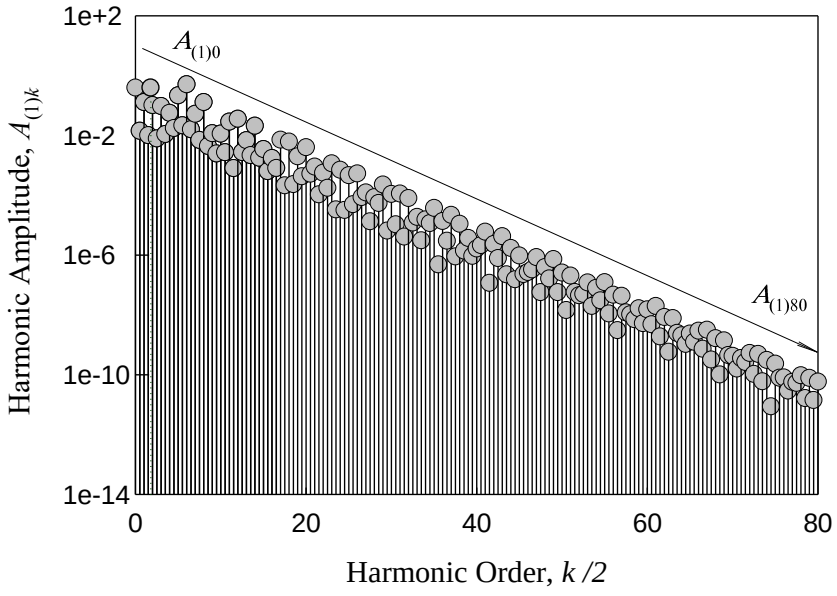

(g)

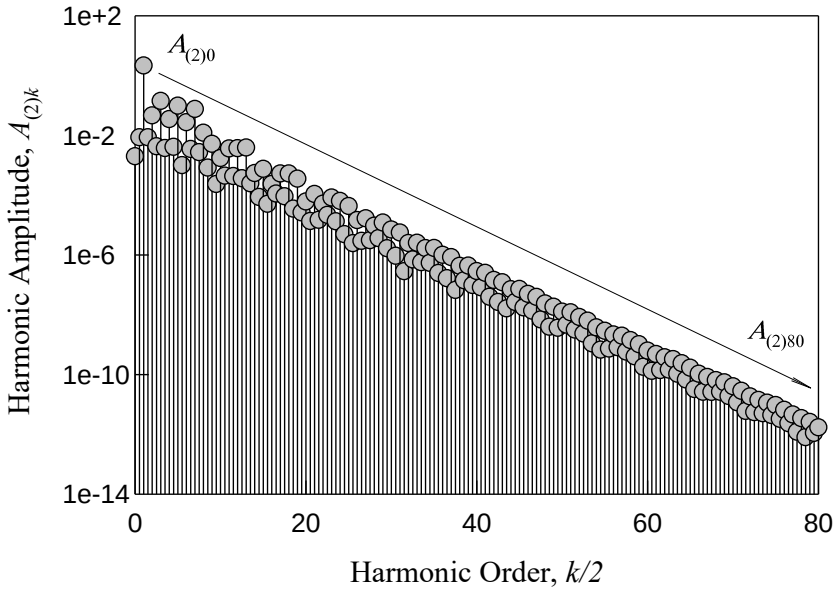

(h)

Fig.28. (Continued).

(i)

(j)

Fig.28. (Continued).

CHAPTER VII

CONCLUSIONS

In this paper, the period-1 to period-2 motions of a periodically forced, nonlinear spring pendulum were discussed through a semi-analytical method. The discrete periodic nodes of periodic motions were obtained from the implicit mappings structure. The corresponding stability analysis and bifurcation analysis of periodic motions were performed through eigenvalue analysis. The corresponding harmonic amplitude spectrum and phase angle of the period-1 to period-2 motions from the semi-analytical results, were presented for a better understanding of the periodic motions. The numerical simulations of the period-1 to period-2 motions were completed from the semi-analytical results to numerically verify with the analytical predictions. Through the numerical simulation, the nonlinear spring possess parametric dynamical behavior caused by an additive external force, which is different from the pendulum.

REFERENCES

[1] Lagrange, J. L., 1788, *Mecanique Analytique* (2 vol.)(edition Albert Balnchard: Paris, 1965).

[2] Poincare, H., 1899, *Methodes Nouvelles de la Mecanique Celeste*, Vol.3, Gauthier-Villars: Paris.

[3] van der Pol, B., 1920, A theory of the amplitude of free and forced triode vibrations, *Radio Review*, **1:** 701-710, 754-762.

[4] Fatou, P., 1928, Sur le mouvement d'un systeme soumis `a des forces a courte periode, *Bull.. Soc. Math.* **56**, 98–139

[5] Krylov, N.M. and Bogolyubov, N.N., 1935, *Methodes approchees de la mecanique non-lineaire dans leurs application a l'Aeetude de la perturbation des mouvements periodiques de divers phenomenes de resonance s'y rapportant*, Academie des Sciences d'Ukraine:Kiev. (in French).

[6] Hayashi, C., 1964, *Nonlinear oscillations in Physical Systems* (McGraw-Hill Book Company, New York).

[7] Barkham, P.G.D. and Soudack, A.C. 1969, "An extension to the method of Krylov and Bogoliubov," *International Journal of Control*, **10**, 377-392.

[8] Barkham, P.G.D. and Soudack, A.C., 1970, "Approximate solutions of nonlinear, non-autonomous second-order differential equations," *International Journal of Control*, **11**, 763-767.

[9] Rand, R.H. and Armbruster, D., 1987, *Perturbation Methods, Bifurcation Theory, and Computer Algebra*. Applied Mathematical Sciences, no. **65**, Springer-Verlag: New York.

[10] Garcia-Margallo,J. and Bejarano, J.D., 1987, "A generalization of the method of harmonic balance," *Journal of Sound and Vibration*, **116**, 591-595.

[11] Yuste, S.B. and Bejarano, J.D., 1989, "Extension and improvement to the Krylov-Bogoliubov method that use elliptic functions," *International Journal of Control*, **49**, 1127-1141.

[12] Coppola, V.T. and Rand, R.H., 1990, "Averaging using elliptic functions: Approximation of limit cycle," *Acta Mechanica*, **81**, pp.125-142.

[13] Luo, A.C.J., 2012, *Continuous Dynamical Systems*, HEP/L&H Scientific: Beijing/Glen

Carbon.

[14] Luo, A.C.J. and Huang, J.Z., 2012, "Approximate solutions of periodic motions in nonlinear systems via a generalized harmonic balance," *Journal of Vibration and Control*, **18**, 1661-1871.

[15] Luo, A.C.J. and Huang, J.Z., 2012 "Analytical dynamics of period-m flows and chaos in nonlinear systems," *International Journal of Bifurcation and Chaos*, 22, Article No. 1250093 (29 pages).

[16] Luo, A.C.J. and Huang, J.Z., 2012, "Analytical routines of period-1 motions to chaos in a periodically forced Duffing oscillator with twin-well potential," *Journal of Applied Nonlinear Dynamics,* 1, 73-108.

[17] Luo A.C.J. and Huang, J.Z., 2012, "Unstable and stable period-m motions in a twin-well potential Duffing oscillator," *Discontinuity, Nonlinearity and Complexity* 1: 113-145.

[18] Luo, A.C.J., 2015, "Periodic flows in nonlinear dynamical systems based on discrete implicit maps," *International Journal of Bifurcation and Chaos,* **25**(3), Article No.:1550044.

[19] Luo, A.C.J. and Guo, Y., 2015, "A semi-analytical prediction of periodic motions in Duffing oscillator through mappings structures," *Discontinuity, Nonlinearity, and Complexity*, **4**, pp.121–150.

[20] Guo, Y. and Luo, A.C.J., 2015, "Periodic motions in a double-well Duffing oscillator under periodic excitation through discrete implicit mappings," *International Journal of Dynamics and Control*, doi:10.1007/5.40435-015-d61-6.

[21] Luo, A.C.J. and Xing, S.Y., 2017, "Time-delay effects on periodic motions in a periodically forced, time-delayed, hardening Duffing oscillator", *Journal of Vibration Testing and System Dynamics*, 1(1), 75-93.